Comprehensive Gas Chromatography with Selective Detection Techniques for Screening of Environmental Pollutants

Weeraya Khummueng

Doctor of Philosophy

2008

RMIT

Comprehensive Gas Chromatography with Selective Detection Techniques for Screening of Environmental Pollutants

A thesis submitted in fulfilment of the requirements for the degree of Doctor of Philosophy

Weeraya Khummueng

M.Sc. (Applied Analytical and Inorganic Chemistry)
Mahidol University, Bangkok, Thailand, 2001

School of Applied Sciences
Science, Engineering and Technology Portfolio
RMIT University
July 2008

DECLARATION

I certify that except where due acknowledgement has been made, the work is that of the author alone; the work has not been submitted previously, in whole or in part, to qualify for any other academic award; the content of the thesis is the result of work which has been carried out since the official commencement date of the approved research program; and, any editorial work, paid or unpaid, carried out by a third party is acknowledged.

Weeraya Khummueng
July, 2008

ACKNOWLEDGEMENTS

First of all, I would like to express my deepest gratitude to my senior supervisor Professor Philip Marriott for giving me the opportunity to conduct my Ph.D. here in one of the most well-known GC×GC research groups in the world. Thank you for your constant guidance, support and encouragement for the past four years. Working in the RMIT ACROSS separation group under your supervision has provided a great time during my Ph.D study and experiences. ***Thank you so much Phil!***

I would like to thank my co-supervisor Dr. Craige Trenerry and his colleague Mr. Gavin Rose from The Department of Primary Industries Research, Victoria for their support through out the study.

My thanks also go out to Mr. Paul Morrison for his technical support during my years at RMIT University. Your expertise in chromatographic techniques, especially in GC and GC×GC was very helpful and always amazed me.

To all friends in the RMIT ACROSS separation group and all the guests who came across during the period of my Ph.D. study (Carin, Omar, Melanie, Prof. Marco, Zenilda, Graham, Anne etc.) thank you for your friendship. My very big thank you to Tin, Michael, Daniel, Kim, Doa, Nui, Dome and Idsaranee for your friendship and always caring in the past four years in Melbourne. Being friend with you guys here is such a memorable and enjoyable time that I will never forget. I do hope to see you guys again in Thailand and I will show you around.

To all staffs in the School of Applied Sciences, RMIT University; thank you for your helpful with all facilities whenever it has been asked.

To my beloved Mum and Dad, there are no words to express my deepest thanks to you. Thank you so much for the un-conditional love, support and encouragement. Thank you so much for believing in me. Especially Mum, you are the BEST! Thank you for becoming such a good friend. You are helping me to become a stronger girl. I hope that I am your pride and also hope that you are enjoying this moment as much as I do.

Last but not least, I would like to thank Faculty of Sciences and Technology, Prince of Songkla University, Pattani campus and Royal Thai Government for my Ph.D scholarship. Also, I would like to thank you, The Office of Educational Affair, Canberra, Australia for all the help you provided.

LITERATURE CONTRIBUTIONS

REFEREED PUBLISHED PAPERS

1.) Khummueng W., Harynuk J., Marriott P.J., "Modulation Ratio in Comprehensive Two-Dimensional Gas Chromatography". *Anal. Chem.*, 78, 4578-87 (2006).

2.) Khummueng W., Trenerry C., Rose G., Marriott P.J., "Application of Comprehensive Two-Dimensional Gas Chromatography with Nitrogen-Selective Detection for the Analysis of Fungicide Residues in Vegetable Samples". *J. Chromatogr A.*, 1131(1-2), 203-14 (2006).

3.) von Mühlen C., Khummueng W., Zini C.A., Caramão E. B., Marriott P. J., "Detector Technologies for Comprehensive Two-Dimensional Gas Chromatography". *J. Sep. Sci.*, 29, 1909-1921 (2006).

4.) Khummueng W., Morrison P., and Marriott P.J., "Dual NPD/ECD Detection in Comprehensive Two-Dimensional Gas Chromatography for Multi-class Pesticide Analysis". *J. Sep. Sci.*, 31(19), 3404 – 3415 (2008).

5.) Khummueng W., and Marriott P.J., "The Nomenclature of Comprehensive Two-Dimensional Gas Chromatography: Defining the Modulation Ratio (M_R)".
LCGC Eur., 38-45 (2008).

ORAL PRESENTATIONS

1.) Khummueng W., Harynuk J., Marriott P.J., "Modulation Ratio in Comprehensive Two-Dimensional Gas Chromatography". *13nd Annual RACI, Research and Development Topics Meeting in Analytical and Environmental Chemistry*., Toorak College, Old Mornington Road, Mt Eliza, Victoria, Australia, 10th-13th December, 2005.

2.) Khummueng W., Marriott P.J., Trenerry C., Rose G., "A Study of Fungicides by Using Comprehensive Two-Dimensional Gas Chromatography with Nitrogen Phosphorus Detector (GC×GC-NPD)". *Chromatography 2006 Advances in Separation Science Symposium*., National Measurement Institute Lehany Theatre, Bradfield Road, Lindfield, Sydney, NSW, Australia, 18th -19th July, 2006.

3.) Khummueng W., Marriott P.J., "A study of Fungicides by Using Comprehensive Two-Dimensional Gas Chromatography". *29th International Symposium on Capillary Chromatograph.*, Palazzo Dei Congressi-Riva Del Garda, Italy, 29th May – 2nd June, 2006.

POSTER PRESENTATIONS

1.) Khummueng W., Wilairat P., Marriott P.J., "Determination of Amphetamine and Related Compounds in Urine by High Performance Liquid Chromatography with 1, 2 Naphtthoquinone-4-Sulphonate (NQS) as Derivatizing Agent". *Interact 2004*., Conrad Jupiters, Gold Coast - Queensland, Australia, 4th – 8th July, 2004.

2.) Khummueng W., Marriott P.J., Trenerry C., Rose G., "Preliminary Investigation of Organophosphorus Pesticides using Multidimensional and Comprehensive Two-Dimensional Gas Chromatography". *12th Annual RACI*., Research and Development Topics Meeting in Analytical and Environmental Chemistry, Melbourne, Victoria, Australia, 5th-8th December, 2004.

3.) Khummueng W., Marriott P.J., Ryan D., Morrison P., "Targeted and Comprehensive Two-Dimensional Gas Chromatography with Time of Flight Mass Spectrometric Detection for Environmental Pollutants Analysis". *The Australian and New Zealand Society for Mass Spectrometry Inc. (ANZSMS 20) Conference.*, Glenelg, Adelaide, South Australia, Australia, between 30th January - 3rd February, 2005.

4.) Khummueng W., Marriott P.J., Trenerry C., Rose G., "Accelerated Solvent Extraction – Comprehensive Two Dimensional Gas Chromatography with micro Electron Capture Detector (GC×GC-μECD) for the Determination of Organochlorine Residues". *The 20th Conference of Residue Chemists (20th CRC 2005).*, Wellington, New Zealand, 4th -7th October, 2005.

5.) Khummueng W., Marriott P.J., "Simultaneous Quantification of Multipesticide Residue in Food Samples by Comprehensive Two Dimensional Gas Chromatography Using Dual Electron-Capture and Nitrogen-Phosphorus Detection". *14th Annual RACI Environmental and Analytical Division R&D Topics.*, University of Wollongong, NSW, Australia, 5th-8th December, 2006.

6.) Khummueng W., Marriott P.J., "Dual Detection in Comprehensive Two Dimensional Gas Chromatography for the Analysis of Multipesticide Residue in Vegetable Samples (GC×GC-NPD/μECD)". *4th GC×GC Symposium and 30th International Symposium on Capillary Chromatography*., Dalian, China, 4th-7th June, 2007.

LIST OF CONTENTS

STATEMENT OF AUTHENTICITY II
ACKNOWLEDGEMENTS III
LITERATURE CONTRIBUTIONS V
LIST OF CONTENTS VIII
LIST OF FIGURES XIV
LIST OF TABLES XX
ABBREVIATIONS XXII
THESIS ABSTRACT XXV
SYNOPSIS XXVII

CHAPTER 1: INTRODUCTION TO COMPREHENSIVE TWO-DIMENSIONAL GAS CHROMATOGRAPHY (GC×GC) 1
1.1 Introduction 2
1.2 Principles and basic concepts of GC×GC 5
1.3 Peak capacity in GC×GC 8
1.4 GC×GC nomenclature 11
1.5 GC×GC implementation 14
1.5.1 Sample introduction in GC×GC 16
1.5.1.1 Solid Phase Micro Extraction (SPME) 16
1.5.1.2 Thermal desorption in GC×GC analysis 17
1.5.1.3 Cold on-column injection in GC×GC analysis 17
1.5.1.4 Large sample volume injection (LVI) 18
1.5.2 GC×GC column combinations 18
1.5.2.1 Orthogonality in GC×GC analysis 19
1.5.2.2 Non-polar–polar (Orthogonal) column set 20
1.5.2.3 Polar–non-polar (inverse) column set 21
1.5.3 Modulator in GC×GC analysis 24
1.5.3.1 The sweeper-modulator 26
1.5.3.2 The KT 2001 27
1.5.3.3 The dual-jet CO_2 modulator 28
1.5.3.4 The semi-rotating cryogenic modulator 29
1.5.3.5 The KT 2003, CO_2 loop modulator 30
1.6 Longitudinal Modulated Cryogenic System (LMCS) 32
1.6.1 LMCS modes of separation 39

1.6.1.1 Targeted mode using LMCS modulator 39
1.6.1.2 Comprehensive mode using LMCS modulator 41
1.6.1.3 Micro-switching valve mode using LMCS modulator 43
1.7 Detector technologies for GC×GC analysis 44
1.8 GC×GC data handing and visualisation 45
1.9 GC×GC optimisation parameters 47
1.10 Wrap around phenomena in GC×GC 50
References 51

CHAPTER 2: OVERVIEW OF DETECTOR TECHNOLOGIES FOR COMPREHENSIVE TWO-DIMENSIONAL GAS CHROMATOGRAPHY 57
Abstract 58
2.1 Introduction 59
2.2 GC×GC detectors 62
2.2.1 Flame Ionization Detector (FID) 62
2.2.2 Thermionic Detector (TID) 65
2.2.3 Electron Capture Detector (ECD) 68
2.2.4 Micro-Electron Capture Detector (μECD) 70
2.2.5 Sulfur Chemiluminescence Detector (SCD) 73
2.2.6 Nitrogen Chemiluminescence Detector (NCD) 77
2.2.7 Atomic Emission Detector (AED) 79
2.2.8 Olfactometry Detection in GC×GC 81
2.3 Case studies of GC×GC-selective detection 86
2.4 Conclusion 89
References 90

CHAPTER 3: MODULATION RATIO IN COMPREHENSIVE TWO-DIMENSIONAL GAS CHROMATOGRAPHY 95
Abstract 96
3.1 Introduction 97
3.2 Experiment 100
3.2.1 Chromatographic conditions 100
3.2.2 Column sets 100
3.2.3 Standards 100
3.2.4 Data analysis 101
3.2.5 Modulation period study 101

3.2.6 Modulation phase study 101
3.3 Results and Discussion 102
3.3.1 Theoretical study of the modulation ratio 102
3.3.2 Experimental testing of the modulation ratio 116
3.4 Conclusion 128
References 130

CHAPTER 4: TARGETED AND COMPREHENSIVE TWO-DIMENSIONAL GAS CHROMATOGRAPHY WITH MULTI-PASS LOOP CRYOGENIC MODULATION 131
Abstract 132
4.1 Introduction 133
4.2 Experimental 138
4.2.1 Gas Chromatographic system 138
4.2.2 Column sets 138
4.2.3 Standards 138
4.2.4 Multi-pass loop geometries 139
4.3 Results and Discussion 140
4.3.1 General concept and multi-pass loop arrangements 140
4.3.2 The multi-pass loop operation 142
4.3.3 Regular targeted mode of LMCS 146
4.3.4 Multi-pass loop type 1 operation 152
4.3.5 Multi-pass loop type 2 operation 158
4.3.6 Comprehensive mode in GC×GC using multi-pass loop modulation 163
4.4 Further study of LMCS multi-pass loop modulation 165
4.5 Conclusion 166
References 167

CHAPTER 5: APPLICATION OF COMPREHENSIVE TWO-DIMENSIONAL GAS CHROMATOGRAPHY WITH SELECTIVE DETECTION FOR THE ANALYSIS OF FUNGICIDES RESIDUES IN VEGETABLE SAMPLES 169
Abstract 170
5.1 Introduction 171
5.2 Experimental 177
5.2.1 Instrumentation 177
5.2.2 Chromatographic conditions 178

5.2.3 Mass spectrometric detection 178
5.2.4 Data analysis 178
5.2.5 Standards and calibration solutions 180
5.2.6 Repeatability and reproducibility 180
5.2.7 Limits of detection (LOD) and quantitation (LOQ) 180
5.2.8 Sample extraction 181
5.3 Results and Discussion 182
5.3.1 Optimization of NPD detector gas flow for fungicides analysis 182
5.3.2 GC×GC column sets for fungicide analysis 185
5.3.3 Identification and on-column degradation of fungicides 189
5.3.4 GC-NPD, GC×GC-NPD and validation study 192
5.3.4.1 Repeatability and reproducibility 192
5.3.4.2 Limit of detection and limit of quantitation 193
5.3.4.3 Calibration curves of standard fungicides 194
5.3.5 Application of GC×GC-NPD in vegetable samples 197
5.4 Conclusion 201
References 202

CHAPTER 6: DUAL DETECTION IN COMPREHENSIVE TWO-DIMENSIONAL GAS CHROMATOGRAPHY FOR MULTI-CLASS PESTICIDES ANALYSIS (GC×GC-NPD/ECD) 204
Abstract 205
6.1 Introduction 206
6.2 Experimental 210
6.2.1 GC×GC system 210
6.2.2 Column sets 210
6.2.3 Chromatographic conditions 211
6.2.4 Analytical characteristics of the dual detection system 211
6.2.5 Data analysis 212
6.2.6 Standard pesticides 212
6.2.7 Sample preparation 213
6.3 Results and Discussion 214
6.3.1 GC×GC-dual detection (GC×GC-NPD/ECD) instrumental set-up and feature 214
6.3.2 The efficiency of NPD and ECD detectors for multi-class pesticides analysis 219
6.3.3 The effect of changing ECD detector make-up gas flow 221

6.3.4 Wrap around observation in GC×GC-dual detection system 224
6.3.5 Dual detection repeatability and area ratio measurements 227
6.3.6 Analytical characteristic of GC×GC-dual detection 232
6.3.7 GC×GC-dual detection method development for multi-class pesticide analysis 235
6.3.8 The application of dual detection to analysis of pesticides in vegetable samples 238
6.4 Conclusion 241
References 242

CHAPTER 7: COMPREHENSIVE TWO-DIMENSIONAL GAS CHROMATOGRAPHY FOR THE ANALYSIS OF POLYCHLORINATED BIPHENYLS AND RELATED COMPOUNDS IN ENVIRONMENTAL SAMPLES 245
Abstract 246
7.1 Introduction to Polychorinated Biphenyls (PCBs) 247
7.2 The analytical methods for the determination of PCBs in environmental samples 251
7.3 Group-types separation concept for PCBs analysis 255
7.4 Experimental; Aroclor 1248 analysis 258
7.4.1 Gas Chromatographic system 258
7.4.2 Column sets 258
7.4.3 Standards 258
7.4.4 Chromatographic conditions 258
7.5 Experimental; Aroclor 1260 analysis 259
7.5.1 Instrumentation 259
7.5.2 Column sets 259
7.5.3 Chromatographic conditions 260
7.5.4 Data analysis 260
7.5.5 Standards 260
7.6 Results and Discussion 261
7.6.1 The separation of Aroclor 1248 using GC×GC-FID 261
7.6.2 The separation of Aroclor 1260 by using GC×GC-μECD 266
7.6.3 Application of GC×GC-μECD for the analysis of PCBs congeners in contaminated soil. 271
7.7 Conclusion 273
References 274

CHAPTER 8: THESIS CONCLUSION AND RECOMMENDATION FOR FUTURE RESEARCH DIRECTIONS 277
8.1 Thesis conclusion 278
8.2 Recommended future research directions 282
References 285

LIST OF FIGURES

Figure 1.1: Schematic of Multi-dimensional gas chromatography (MDGC) system. 4

Figure 1.2: Schematic diagram of GC×GC and GC-MS instrumentation. 7

Figure 1.3: The general focus and re-mobilise process of the modulator used in a GC×GC system, based upon the longitudinal modulation process. 7

Figure 1.4: Diagram of peak capacity in 1D-GC, MDGC with two heart cutting events and GC×GC, respectively. 10

Figure 1.5: Chromatogram of in-phase and out-of-phase (almost 180° out of phase) modulation. 12

Figure 1.6: General schematic of GC×GC implementation. 15

Figure 1.7: Diagram illustrating the general use of the two-dimensional separation space. 20

Figure 1.8: Diagram of a contour plot map when a non-polar–polar column set was employed. 21

Figure 1.9: Diagram of a contour plot map when the polar–non-polar column set was used. 22

Figure 1.10: Colour plot obtained from GC×GC-FID used for diesel oil sample analysed on DB1-BP20 and BP21-BPX35. 23

Figure 1.11: Schematic of GC×GC system with sweeper modulator. 26

Figure 1.12: Schematic GC×GC system with the KT 2001 modulator. 27

Figure 1.13: Schematic of GC×GC system with the dual-jets CO_2 modulator. 28

Figure 1.14: Cryogenic modulation with the dual jets CO_2 modulator. 29

Figure 1.15: Schematic of GC×GC system with the semi-rotating cryogenic modulator. 30

Figure 1.16: Schematic of a GC×GC system with the KT 2003, CO_2 loop modulator. 32

Figure 1.17: Schematic diagram of a GC×GC system with the LMCS modulator. 33

Figure 1.18: The LMCS modulator showing the essential part of this modulator. 34

Figure 1.19: Schematic of the LMCS modulator. 35

Figure 1.20: Schematic of the cryogenic region of LMCS modulator. 37

Figure 1.21: Photograph of cryogenic trap movement in vertical direction of LMCS modulator. 38

Figure 1.22: Example the raw 1D-GC and 2D-GC chromatograms obtained from targeted operational mode. 41

Figure 1.23: Results obtained from GC×GC comprehensive mode. 42

Figure 1.24: Results obtained from switching valve operational mode using LMCS modulator. 44

Figure 1.25: Raw 2D chromatogram and contour plot generation of a compound obtained from GC×GC analysis. 46

Figure 1.26: Presents visualization of data obtained from GC×GC analysis. 47

Figure 1.27: Optimisation steps to reduce wrap around phenomena in GC×GC. 49

Figure 2.1: Schematic diagram of the GC×GC instrument, showing use of a short, fast elution second dimension column which produces very narrow peaks at the detector. 60

Figure 2.2: Schematic diagram of a Flame Ionization Detector. 65

Figure 2.3: Schematic diagram of Thermionic Detector. 67

Figure 2.4: Schematic diagram of the Agilent 6890 Series micro-Electron Capture Detector (μECD). 71

Figure 2.5: Schematic diagram of dual plasma SCD detector. 75

Figure 2.6: Schematic diagram of dual plasma burner in NCD detector. 78

Figure 2.7: Schematic diagram of an Atomic Emission Detection system (AED). 80

Figure 2.8: Internal design of the sniffer port of GC-O system. 82

Figure 2.9: GC system coupled with olfactory detector (ODO II) and MS detector. 83

Figure 2.10: Schematic diagram of an olfactometry detection for GC×GC system (GC×GC-O). 85

Figure 2.11: (A) GC-FID and GC-NPD chromatograms for a N- and P-containing compound mixture, **(B)** GC×GC-FID and GC×GC-NPD modulated peaks for ethion, under similar conditions. 87

Figure 2.12: (A) GC×GC-FID and **(B)** GC×GC-NPD chromatograms for a N- and P containing compound mixture, under similar chromatographic conditions. 88

Figure 3.1: Models of primary dimension peaks having half-height widths of 4.7 s and retention times of 16s. 103

Figure 3.2: Models of the modulated peaks from **Figure 3.1** using a modulation period of 2.6667 s, (M_R of 3.0). 105

Figure 3.3: Effect of peak intensity on the number of observed modulation pulses. 107

Figure 3.4: Cumulative peak areas for different values of M_R and modulation phase from the models of Gaussian peaks. 114

Figure 3.5: Cumulative peak areas for different values of M_R and modulation phase from the models of tailing peaks (As = 2.0). 115

Figure 3.6: 1D-GC chromatogram of the 17 compounds standard mixture. 116

Figure 3.7: Experimental data from the modulation of a symmetric peak (tridecane) using modulation periods of 2, 3, 5, 7 and 9s. 117

Figure 3.8: Experimental data from the modulation of a tailing peak (Nonan-1-ol) using modulation periods of 2, 3, 5, 7 and 9s. 118

Figure 3.9: GC×GC chromatogram of tridecane using different modulation phase with modulation period of 6 s. 121

Figure 3.10: GC×GC chromatogram of nonan-1-ol using different modulation phase with modulation period of 6 s. 122

Figure 3.11: Cumulative peak areas plot of symmetric peak and tailing peak from experimental data. 126

Figure 4.1: The multi-pass loop cryogenic modulation gas chromatography system. 141

Figure 4.2: Illustration of the operational modes of the cryogenic trap when solute from ^{1}D was introduced into the regular and multi-pass loop modulator and was remobilised to ^{2}D. 144

Figure 4.3: 1D-GC chromatogram of 17 organochlorine pesticide standards. The cryofluid (liquid CO_2) was not applied during the analysis. 145

Figure 4.4: (A) 1D-GC chromatogram of 17 OCs pesticides. Solid line show selected regions (labelled in **a** to **h**) which will be trapped by the straight through type LMCS. **(B)** Raw 2D-GC chromatogram of the selected region from **a** to **h** when targeted mode was performed. 148

Figure 4.5: Expanded regions of **a** to **d** as shown in **Fig 4.4 (B)**, when targeted mode of the straight through type cryogenic LMCS was performed. 149

Figure 4.6: Expanded regions of **e** to **h** as shown in **Fig 4.4 (B)**, when targeted mode of the straight through type cryogenic LMCS was performed. 150

Figure 4.7: (A) 1D-GC chromatogram of 17 OCs pesticides. Solid line show the region (labelled in **a** to **g**) which will be trapped by the multi-pass cryogenic loop type 1. **(B)** Raw 2D-GC chromatogram of the selected region from **a** to **g** when targeted mode using multi-pass loop type 1 was performed. 154

Figure 4.8: Expanded regions of **a** to **d** as shown in **Fig 4.7 (B)**, when the targeted MDGC using multi-pass loop type 1 was performed. 155

Figure 4.9: Expanded regions of **e** to **g** as shown in **Fig 4.7 (B)**, when the targeted MDGC using multi-pass loop type 1 was performed. 156

Figure 4.10: (A) 1D-GC chromatogram of 17 OCs pesticides. Solid line show the region (labelled in **a** to **h**) which will be trapped by the multi-pass loop type 2. **(B)** Raw 2D-GC chromatogram of the selected region from **a** to **h** when targeted mode was performed. 159

Figure 4.11: Expanded regions of **a** to **d** as shown in **Fig 4.10 (B)**, when targeted mode using multi-pass loop type 2 was performed. 160

Figure 4.12: Expanded regions of **e** to **h** as shown in **Fig 4.10 (B)**, when targeted mode using multi-pass loop type 2 was performed. 161

Figure 4.13: Contour plot of the analysis of 17 organochlorine pesticides in comprehensive mode using regular and loop types. 164

Figure 4.14: Suggested diagrams of multi-pass loop cryogenic modulation. 165

Figure 5.1: Mechanism of hydrolysis of iprodione. 174

Figure 5.2: Degradation of iprodione under UV wavelength in plants and soil. 175

Figure 5.3: Thermal degradation scheme of iprodione. 176

Figure 5.4: Names and structures of the nine standard fungicides. 179

Figure 5.5: Effect of selected conditions of detector gas flows on NPD peak response and peak shape. 184

Figure 5.6: GC×GC-NPD contour plots with different column sets listed in **Table 5.1** 186

Figure 5.7: Chromatogram of nine fungicide standards with the final detector gas flows and chromatographic condition. 187

Figure 5.8: Mass spectra of selected fungicides. 191

Figure 5.9: Calibration curves of selected fungicide standards using conditions as in **Figure 5.7**. 195

Figure 5.10: Chromatogram of single dimension GC-NPD using conditions as in **Figure 5.7**. 198

Figure 5.11: Contour plot of GC×GC-NPD using conditions as in **Figure 5.7**. 199

Figure 5.12: Contour plots of GC×GC-μECD using conditions as in **Figure 5.7**. 200

Figure 6.1: Schematic of the GC×GC-NPD/ECD system used throughout this study. 215

Figure 6.2: Colour plot of selected pesticides for dual detection in GC×GC. The chromatographic condition used in this study was the fast temperature program described in **Section 6.2.3.** 216

Figure 6.3: 1D-GC and GC×GC chromatograms obtained from single and dual detection. 220

Figure 6.4: Colour plot of selected pesticides as described in **Figure 6.2** from NPD detector with fast chromatographic condition stated in **Section 6.2.3** when different P_M were used. 225

Figure 6.5: Chemical structure of pesticides standard used for comparison of signal ratio of ECD:NPD detector. N, P, S and Cl in each molecule correspond to ratio of ECD:NPD. 231

Figure 6.6: Flow diagram of progress role of ^1t_R, ^2t_R and DRR 232

Figure 6.7: Colour plot of fungicides, OP and OC pesticides obtained from GC×GC dual detection when ~ optimum chromatographic condition described in **Section 6.2.3** and P_M = 6s were used. 236

Figure 6.8: Colour plot of multi-class pesticide standard mixture from GC×GC dual detection when ~ optimum chromatographic condition described in **Section 6.2.3** and P_M = 6s were used. 237

Figure 6.9: Colour plot of blank spinach extract and blank spinach extract spiked with pesticide standard mixture using GC×GC dual detection when optimum chromatographic condition described in **Section 6.2.3** and P_M = 6s were used. 240

Figure 7.1: General formula and structure of PCBs. 247

Figure 7.2: Plot of congener number *vs* relative mass abundance of Aroclor 1248 and 1260 composition. 250

Figure 7.3: Contour plot of PCB congener separation by using GC×GC-μECD. 257

Figure 7.4: Chromatogram of 1D-GC-FID and GC×GC-FID of Aroclor 1248. 262

Figure 7.5: Raw 2D-GC chromatogram of expanded region of area **X** in **Figure 7.4.** 263

Figure 7.6: (A) raw 2D-GC chromatogram of the analysis of Aroclor 1248. **(B)** Contour plot of the Aroclor 1248. 265

Figure 7.7: 1D-GC chromatogram and colour plot of Aroclor 1260 mixture, when a non-polar–polar column set and chromatographic condition #2 shown in **Table 7.3** was used. 268

Figure 7.8: 1D-GC chromatogram and colour plot of Aroclor 1260 mixture, when a non-polar–polar column set and chromatographic condition #5 shown in **Table 7.3** was used. 269

Figure 7.9: 1D-GC chromatogram and colour plot of Aroclor 1260 mixture, when a non-polar–polar column set was used. The optimum chromatographic condition (condition #7) shown in **Table 7.3** and P_M = 5 s were performed. 270

Figure 7.10: 1D-GC chromatogram and contour plot of PCBs congener contaminated in soil samples. 272

LIST OF TABLES

Table 2.1: Applications of comprehensive two-dimensional gas chromatography with element-selective detectors. 61

Table 3.1: Results of modelling study of symmetrical peak for different M_R and phase. 109

Table 3.2: Results of modelling study of asymmetrical peak for different M_R and phase. 110

Table 3.3: Reproducibility of retention time, peak area, and peak width at half height for the 17 compounds standard mixture using normal GC. 120

Table 3.4: Number of observed modulation pulses for modulated and tailing peaks in the experimental study compared to the values expected from the model. 124

Table 3.5: Modulation ratios (M_R) of all 17 compounds in the standard mixture for modulation periods of 2, 3, 5, 7 and 9 s. 125

Table 4.1: Results obtained from targeted mode using regular straight through type operation, including heart cutting events. 151

Table 4.2: Results obtained from targeted mode using multi-pass loop type 1operation including heart cutting events. 157

Table 4.3: Results obtained from targeted operation using multi-pass loop type 2 operation. 162

Table 5.1: GC×GC-NPD column sets used in preliminary study. 177

Table 5.2: The optimization conditions and results for the NPD detector gas flows (H_2, air and N_2), bead voltage of NPD detector, peak response (area and height) of procymidone (2.5 $mg.L^{-1}$) in each condition. 183

Table 5.3: Data analysis of GC-NPD and GC×GC-NPD (n=3) 188

Table 5.4: Validation parameters of GC×GC-NPD developed method for fungicides analysis with concentration at 0.5 $mg.L^{-1}$. 193

Table 5.5: Equations of peak area and peak height, R^2, LOD and LOQ of selected fungicide standards. 196

Table 6.1: List of compound names based on elution order and CAS number of pesticide standards used in this study. 213

Table 6.2: The elution temperature of selected pesticides when a typical, and a short, column set were used. 218

Table 6.3: The summation of peak area and peak height of selected pesticides in NPD channel when make-up gas flow in ECD detector was varied from 25 to 150 mL.min^{-1}. 223

Table 6.4: Apparent and absolute $^{2}t_{R}$ of selected pesticides when different modulation periods (P_M) were used in GC×GC-NPD/ECD system. 226

Table 6.5: Repeatability and reproducibility of the GC×GC-NPD/μECD system. 229

Table 6.6: Repeatability of area ratio from ECD and NPD channels (n=5). 230

Table 6.7: Linear regression and R^2 of the selected pesticides using GC×GC-dual detection. 234

Table 6.8: DRR value of selected pesticides in spinach extract sample matrix. 239

Table 7.1: Number of congeners in each PCB homolog group. 249

Table 7.2: Applications of PCBs and related compounds using GC×GC technique. 254

Table 7.3: Chromatographic and detection conditions for the separation of PCB 1260 used in this study. 267

ABBREVIATIONS

List of abbreviations

1D-GC	Conventional or one-dimensional gas chromatography
2D-GC	Two-dimensional gas chromatography
^{1}D	First-dimension
^{2}D	Second- dimension
GC-MS	Gas chromatography with mass spectrometric detection
MDGC	Multidimensional gas chromatography
GC×GC	Comprehensive two-dimensional gas chromatography
M_R	Modulation ratio
P_M	Modulation period
LMCS	Longitudinal modulated cryogenic system
NPD	Nitrogen-phosphorus detector
μECD	Micro-electron capture detector
OCs	Organochlorine pesticides
OPs	Organophosphate pesticides
FCs	Fungicides
PCBs	Polychlorinated biphenyls
FID	Flame ionisation detector
TID	Thermionic detector
NCD	Nitrogen chemiluminescence detector
SCD	Sulfur chemiluminescence detector
AED	Atomic emission detector
GC-O	Gas chromatography with olfactometry detection
PIONA	Paraffins, iso-paraffins, olefins, naphthenes, aromatics
FPD	Flame photometric detector
PFPD	Pulsed flame photometric detector
TL	Transfer line
s	Second

ms	Millisecond
$^{1}t_R$	First dimension retention time (min)
$^{2}t_R$	Second dimension retention time (s)
n_c	Total peak capacity
n_1	First dimension peak capacity
n_2	Second dimension peak capacity
qMS	Quadrupole mass spectrometry
TOFMS	Time of flight mass spectrometry
PM	Particulate matter
HS-SPME	Head space-solid phase micro extraction
TD	Thermal desorption
DTD	Direct thermal desorption
COC	Cold on column injection
LVI	Large volume injection
SVE	Solvent vapor exit
PTV	Programmed temperature vaporisation
PAHs	Polynuclear aromatic hydrocabons
CSR	Concurrent solvent re-condensation
FAME	Fatty acid methyl ester
DCSI	Double cool-strand interface
ppb	Part per billion
BPX5	5% phenyl polysilphenylene-siloxane phase
BP20	Polyethylene glycol
BPX35	35% phenyl polysilphenylene-siloxane phase
BPX50	50% phenyl polysilphenylene-siloxane phase
BPX80	80% phenyl polysilphenylene-siloxane phase
AUX	Auxiliary
TMDGC	Targeted multidimensional gas chromatography
3D plot	Three dimensions plot
σ	Standard deviation
PCDDs	Polychlorinated dibenzo-p-dioxins

PCDFs	Polychlorinated dibenzofurans
R_s	Resolution
w_1	Primary peak width
w_2	Secondary peak width
n_M	Modulation number
F_M	Modulation phase
w_b	Peak width at base
w_h	Peak width at half height
T_e	Elution temperature
$ng.L^{-1}$	Nanogram per littre
NIST	National institute of standards and technology
$mL.min^{-1}$	Millilitter per minute
$mg.L^{-1}$	Milligram per litter
$pg.s^{-1}$	Picogram per second
$°C.s^{-1}$	Degree celsius per second
RSD	Relative standard deviation
i.d.	Internal diameter
d_f	Film thickness
S/N	Signal to noise ratio
LOQ	Limit of quantification
LOD	Limit of detection
^1A_S	First dimension peak asymmetry
^2A_S	Second dimension peak asymmetry
DRR	Detector response ratio
ASE	Accelerated solvent extraction
$^2t_{Rabs}$	Absolute ^2t_R
$^2t_{Rapp}$	Apparent ^2t_R
POPs	Persistent organic pollutants
UNEP	United nations environment programme
2378-TCDD	2,3,7,8-Tetrachlorodibenzo-p-dioxin

THESIS ABSTRACT

Comprehensive two-dimensional gas chromatography (GC×GC) is a relatively new technique, being about sixteen years since it was introduced by Phillips and Lui in 1991. Since it was introduced to the GC community, it has become a technique of choice for complex samples analysis at least in selected research laboratories. Like other novel techniques, the fundamentals of this technique are going for more understanding as well as the establish of applications in a wide range of samples such as petroleum products, food flavour and perfume, drugs and environmental samples, etc. Several research groups have attempted to study and understand the key elements of GC×GC (the modulator for instance) to explain the modulation process and modes of operation. New nomenclatures and definitions comprise one aspect of knowledge in GC×GC fundamental relationships. In this thesis, a new terminology called Modulation Ratio (M_R) has been added to the list of GC×GC nomenclature. M_R has been proposed to explain the modulation process and provides chromatographers with the appropriate modulation period (P_M) choice when GC×GC experiments are carried out. The results show that M_R value of 3 to 4 is the preferred value in a GC×GC experiment in order to preserve the separation of solutes achieved in the ^{1}D dimension. However, following the initial M_R study, it was further demonstrated that it is possible to optimise the M_R for different regions of a chromatogram, through adjustment of the modulation period (P_M).

The new operational methods of targeted and comprehensive modes of GC by using multi-pass loop modulation were investigated. The normal set up, and two looped segments of the capillary column passing through the LMCS modulator were compared in performance. Both targeted and comprehensive GC×GC modes, the straight through column segment type, and the two different loop type modulators, were contrasted in the manner in which they permit isolation of regions of the chromatographic band.

Additionally, two selective detectors (Nitrogen Phosphorus Detector (NPD) and micro-Electron Capture Detector (μECD)) were coupled to the GC×GC system for the analysis of environmental pollutants. In this present work, NPD is the detector

of choice for the analysis of nitrogen and phosphorus containing compounds. Thus, the analysis of fungicide residues in vegetable samples using GC×GC-NPD was carried out. The unique capability of the GC×GC presentation to show the degradation of a fungicide (iprodione) was demonstrated in this study. The dual detection arrangement which employed both NPD and ECD as parallel detectors (GC×GC-NPD/μECD) for the analysis of multi-class pesticides containing organochlorine pesticides (OCs), organophosphorus pesticdes (OPs) and fungicides (FCs) was conducted. Two 15 cm long deactivated fused silica transfer lines connected the output of the second dimension column (^{2}D) to the parallel detectors via a microfluidic-splitting valve, with an equal split ratio, resulting in two simultaneous contour plots to be visualized from this system. In this context, an opportunity is shown for assigning a detector response ratio (DRR) with the simultaneous response of a solute in the two detectors, as an additional confirmation of solute identity.

Finally, the application of GC×GC-μECD system for the analysis of PCB congeners was performed. The group separation of PCB congeners was achieved with the optimum GC×GC condition. To illustrate the potential of GC×GC- μECD technique as a powerful tool for conducting a group separation of PCB congeners, highly contaminated soil samples were investigated.

SYNOPSIS

This research study is aimed at developing the fundamentals and applications of multidimensional gas chromatography (MDGC) and comprehensive two-dimensional gas chromatography (GC×GC) techniques using the Longitudinal Modulated Cryogenic System (LMCS, the modulator) for environmental pollutants analysis. This thesis comprises 8 chapters. Four chapters contained herein have been published, the titles of which are reflected in the refereed published papers. The thesis will present a range of technical innovations in GC×GC, with application to pesticides analysis and a new conceptual development in GC×GC. Details of each chapter in this thesis are summarized below.

Chapter 1: This provides fundamentals, instrumentation and applications of GC×GC using selective detectors for the analysis of environmental samples. The chapter contains principles of GC×GC and MDGC, GC×GC instrumentation and optimisation, details of six cryogenic modulators that have been used in GC×GC research world-wide, especially focussing on the features of the Longitudinal Modulated Cryogenic System (LMCS) technology as a thermal modulator, which will be used through out this study. The principle of LMCS modes of separation and its applications will be presented.

Chapter 2: The overview of detector technologies that have been used for GC×GC is presented. The principles of seven detectors (FID, TID, ECD, NPD, NCD, SCD, AED and Olfactometry) and their applications when coupled with GC×GC are included. A chapter has been published in Journal of Separation Science in 2006 titled "Overview of detector technologies for comprehensive two-dimensional gas chromatography" as a contribution from von Mühlen and colleagues. As a second author in this publication, I (Khummueng W.) would like to clarify my contribution in this work as well as in this thesis. The ECD, NCD, SCD and Olfactometry detectors were contributed by me, contributing approximately 50% on this paper. For this reason, I decided to include this work in my thesis. Due to this thesis focused on

GC×GC with selective detection for the environmental pollutants analysis, especially NPD and ECD detector. The review in JSS specifically was in specific detection (the FID was included because of its universality of response as a comparison). It was decided to keep this focus on specific detection in Chapter 2, rather than include MS. The MS is powerful, but was not included within this thesis as a detection tool for GC×GC. Basically, we aimed to review both fundamentals and applications of GC×GC coupled with MS technique as a future publication. However, the review of GC×GC coupled with MS titled "Comprehensive two-dimensional gas chromatography-mass spectrometry: A review" has been published by Mondello and his colleagues in 2008. Identification of all standards and samples used in this research work using MS techniques were to be a further study.

Chapter 3: The new terminology and concept in GC×GC named the Modulation Ratio (M_R) is described in this chapter. The M_R concept was applied to the investigation of both symmetric and asymmetric peaks. The theoretical and experimental results showed the agreement in both types of GC×GC primary peak shapes. The formula for the calculation of M_R values and the advantages are also provided. The ramification of the M_R concept for quantitative analysis will be highlighted.

Chapter 4: A novel set-up for the modulation process in GC×GC analysis by using the LMCS modulator was tested. The set up was referred to as multi-pass loop modulation. The modulator comprised a thin film and smaller o.d. capillary column inserted and passed through the LMCS modulator in a loop arrangement. Two types of multi-pass loop modulation were carried out and the results were compared to the straight through type which is the basic mode used in most systems. The approach was applied for the analysis of organochlorine pesticide standards in order to illustrate the effectiveness of the technique for environmental analysis. Peak broadening in this study was explained in term of the characteristic of the LMCS modulator with slower movement up-stream (trap position) and faster in the down stroke (release position), thus a further set up which is suitable for LMCS movement may be suggested for

future study. However, the most recent LMCS device has fast movement in both strokes, which is believed will make multi-pass modulation more effective.

Chapter 5: The application of GC×GC-NPD for the analysis of fungicides in vegetable samples is presented. Nine fungicides used in this study are all nitrogen containing compounds. The results show the symmetry of peak shape for these compounds compared to phosphorus containing compounds. The optimisation of detector gas flows was carried out for best performance of the NPD detector. The separation of the fungicides from each other and from the sample matrix was achieved. The method was applied to the analysis of spiked fungicides in vegetable samples with GC-qMS performed for fungicides identification. An unexpected observation on iprodione degradation was investigated in the 2D GC×GC presentation, with both injector-based and column thermal degradation proposed.

Chapter 6: Dual detection using NPD and ECD detectors coupled with GC×GC was conducted. 15 cm lengths of un-coated fused silica were connected at the end of the second dimension column via a micro-fluidic stream splitting valve. The results from this set-up provide two channels of chromatographic results; one from NPD and the other from ECD detector. Multi-class pesticides (17 organochlorine pesticides, 15 organophosphate insecticides and 9 fungicides) were used as an example to illustrate the potential of this approach. The separation of the individual pesticides from the matrix sample was also achieved. The results show that NPD detection is more selective compared to ECD detection due to all pesticides used in this study responding to the ECD channel while just the N- and P-containing compounds were presented in the NPD detector channel. Exact matching of peak position in both detector 2D plots is a useful identification tool, as is the ratio of ECD:NPD response which is proposed as an identification tool for pesticides residue analysis in GC×GC, called the Detection Response Ratio (DRR).

Chapter 7: A review of literature of polychlorinated biphenyl (PCBs) analysis by using GC×GC with selective detection, and a case study of the analysis of PCB

standards and PCB congeners in contaminated soil samples, are included in this chapter. In this study, varied temperature programs of GC×GC-μECD for the separation of PCBs in the soil extract was carried out. Group separation of PCB standards and PCB contaminated soil extracts was achieved.

Chapter 8: Thesis conclusions and recommendation for further study are presented in this chapter.

Chapter

1

INTRODUCTION TO COMPREHENSIVE TWO-DIMENSIONAL GAS CHROMATOGRAPHY (GC×GC)

1.1 Introduction

Gas chromatography (1D-GC) is one of the most important techniques for the separation, characterisation and/or determination of semi-volatile to volatile organic compounds. The technique is normally used as a monitor tool of industrial products such as food, drugs, pharmaceuticals, cosmetics, and petrochemicals samples, etc for volatile compounds and also for natural products. Additionally, it is a technique of choice for toxicants analysis for instance, PCBs and related compounds, PAHs, and pesticide residues in environmental samples. The separation of compounds from each other and from the sample matrix may be a challenging task in gas chromatography. More often, an insufficiency of column efficiency of the technique preventing achievement of the best separation is the major problem in the analysis of complex samples. For example, there is no conventional GC method with a single separation column that provides resolution of all 209 PCBs congeners from each other [1], and also there is no 1D-GC system capable of separating all substances obtained in oil samples. Since the limitation of 1D-GC as stated above was of concern, an attempt to seek, and develop a more powerful technique to accomplish this disadvantage must be encouraged.

Multi-dimensional gas chromatography (MDGC) is an extended technique of conventional GC especially designed to increase peak capacity. An extension of peak capacity seems to be a key factor for the development of MDGC systems that can provide better separation. The higher peak capacity, the more individual peaks are separated from each other and from the matrix background. MDGC has been developed since early after the invention of GC, with much interest in the 1970s and 1980s [2]. Giddings and his colleagues [3,4] pointed out that all complex samples require more than one column or separation mechanism to separate the compounds contained in the mixture. They reported the theoretical concepts of MDGC as a technique for the separation of complex samples by employing another dimension. Further MDGC theories and conceptual studies by Giddings were reported in the literature [5-7].

Generally in an MDGC system, two columns are located in two different GC ovens, permitting individual chromatographic conditions to be established. The target peaks or regions will be transferred into the second dimension column (^{2}D) using an interface which is located between the two GC ovens or is at the end of ^{1}D in the first oven. Normally, a switching valve such as a Deans' switch is employed as a transfer device. The transfer process is normally performed as an online process called "heart cutting" technique, in which selected peaks or regions eluted from the first dimension column (^{1}D) are transferred to ^{2}D for further separation. The heart cutting process in MDGC has been reported in the literature [8-10] and will be described in the next section. The separation improvement offered by the MDGC approach is limited to a few regions of the chromatogram, while other regions will be diverted to pass through only the first columns and/or a transfer line and are detected by the monitor detector. This made MDGC generally an inappropriate method to be applied to complex sample analysis, where the entire sample needs to be analysed for characterisation and identification proposes.

A numbers of limitations in MDGC such as the requirement of careful time selection and interpretation of specific regions to be heart-cut, the complicated instrument set-up, leak of effluent, and cold spots in the system which may be caused by the valve itself resulted in MDGC not being widely used in routine laboratories. **Figure 1.1** shows a schematic diagram of MDGC system using either two or one GC ovens. Begnaud et al. [11] pointed out the drawback of the MDGC technique using a switching valve and the other transfer devices, and proposed a double cool-strand interface for the MDGC method, to overcome the disadvantages. Using the double cool-strand interface allows heart-cut to be performed without any switching valves and transfer devices. However, the operation and data interpretation are still relatively difficult to deal with. Drawbacks of the MDGC approach makes it desirable to establish and develop a generation of chromatographic techniques where the entire sample can be subjected to further separation by use of a second separation mechanism.

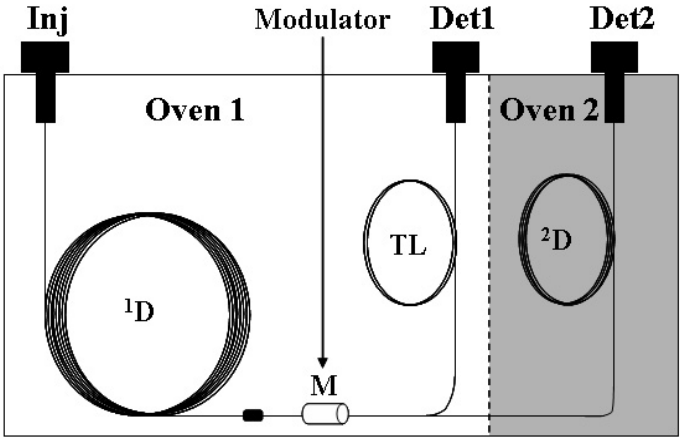

Figure 1.1: Schematic of Multi-dimensional gas chromatography (MDGC) system shows an interface/modulator located between ^{1}D and ^{2}D columns (M). Both columns are in different ovens but it is possible to have both columns in the same oven. Inj = injection, Det 1 and 2 = detector 1 and 2, respectively, ^{1}D = first dimension column, ^{2}D = second dimension column, M = modulator and TL = transfer line [12].

Comprehensive two-dimensional gas chromatography (GC×GC) is a new generation of chromatographic technique which is extended and modified from the general MDGC technique for the beneficial analysis of complex samples. In this approach not only specific peaks or regions are transferred to ^{2}D for further separation, but the entire samples can undergo analysis in a fast separation, in the ^{2}D column. Introduced in 1991 by Phillips and Liu [13] for petrochemical analysis, nowadays, GC×GC has been acknowledged as a new and probably one of the most exciting techniques in the chromatographic area. The technique provides a significantly greater peak capacity; it enhances the separation power (resolution), it improves detectability (signal-to-noise ratio), and provides group type separation of the compounds. In over a decade, GC×GC has proved to be a powerful and useful technique for complex sample analysis. A number of principles and basic concepts in GC×GC have been published as new knowledge and greater perception is realised [12,14] including implementation and applications [15-20]. Up till now, approximately 550 papers on the GC×GC topic have been published. The superior efficiency and easy implementation are attracting chromatographers to employ the technique for the analysis of complex samples, which can not be separated effectively with conventional GC prior to this.

1.2 Principles and basic concepts of GC×GC

According to the classification of fast GC based on peak width consideration reported in the analysis by van Deursen et al. [21], it can be assessed that:

1. **Fast GC separation:** is a separation in a range of minutes; peak widths (2.354σ), 1-3 s.
2. **Very fast GC separation:** is a separation in a range of seconds; peak widths of the analyte approximately 30-200 ms.
3. **Ultra-fast GC separation:** is a separation in a range of sub-second and the range of peak widths approximately 5-30 ms.

The GC×GC technique may be classified as very fast GC, due to the separation in ^{2}D basically taking approximately 10 s or less to minimise the broadening of the narrow band, and to obtain resolution of the compound from ^{1}D. Additionally, it was reviewed and proposed by Phillips and Beens as being classified as a hyphenated techniques [22], with the review highlighting that a major difference of GC×GC from GC-MS is the use of a second analytical column, rather than the mass analyser in the second dimension as shown in **Figure 1.2**. Interestingly, Phillips and Beens predicted the future of GC×GC as being "BRIGHT×BRIGHT" in this review.

Nowadays, GC×GC is a well established technique which still depends on the same well known principles that pertain to conventional GC and MDGC. The 1D-GC chromatographic peak will be continuously sampled into small fractions and then compressed using the modulator, before being rapidly re-injected into ^{2}D for further separation. The high degree of orthogonality of two separation dimensions is critical for GC×GC analysis. Orthogonality in GC×GC analysis will be discussed later. An interface which is normally called the modulator is an important element that is added to the conventional GC or MDGC system. The modulator is responsible for collecting, then focusing the fraction of the effluent coming from ^{1}D in a narrow band, before rapidly re-injecting it into ^{2}D for further separation. In GC×GC analysis every single compound in the sample will be subjected to two independent dimensions which comprise a different separation mechanism. **Figure 1.3** shows the general

'focus' and 're-mobilise' process of the modulator when the effluent from ^{1}D is compressed in the modulator before release to ^{2}D as a narrow band. In this implementation a moveable part (trap) of the modulator is cooled by the coolant such as CO_2 or N_2. The effluent from ^{1}D is accumulated in the trap and then remobilised to ^{2}D when the trap moves away from the solute (compressed) band. As a consequence the band of solute from ^{1}D may be sliced into smaller peaks and compressed. Results obtained from GC×GC analysis appear as a series of very narrow peaks, with enhanced peak amplitude. Basically, peak width at base of narrow peaks generated from GC×GC range from 30 to 200 ms width at base and peak amplitude increases by about 10 to 20 times. Detectors required for GC×GC have to respond fast enough to detect very narrow peaks and to be able to reconstruct their shape. All GC detectors with data acquisition rate at least 50 Hz can usually be used as GC×GC detectors. As a rule of thumb, total peak area of the analyte will be preserved, therefore the summation of peak areas of the pulsed peaks produce the same area as obtained for the equivalent 1D-GC peak.

The GC×GC result is normally visualised as a bird's eye view, as a contour plot or colour plot; X axis represents the first dimension retention time in minute ($^{1}t_R$) and Y axis represents the second dimension retention time in second ($^{2}t_R$). Further details of GC×GC data presentation will be explained later. The success of separation of compounds in the second dimension, peak intensity enhancement, and group type separation in the chromatogram is highlighted as general benefits of this technique over 1D-GC and MDGC.

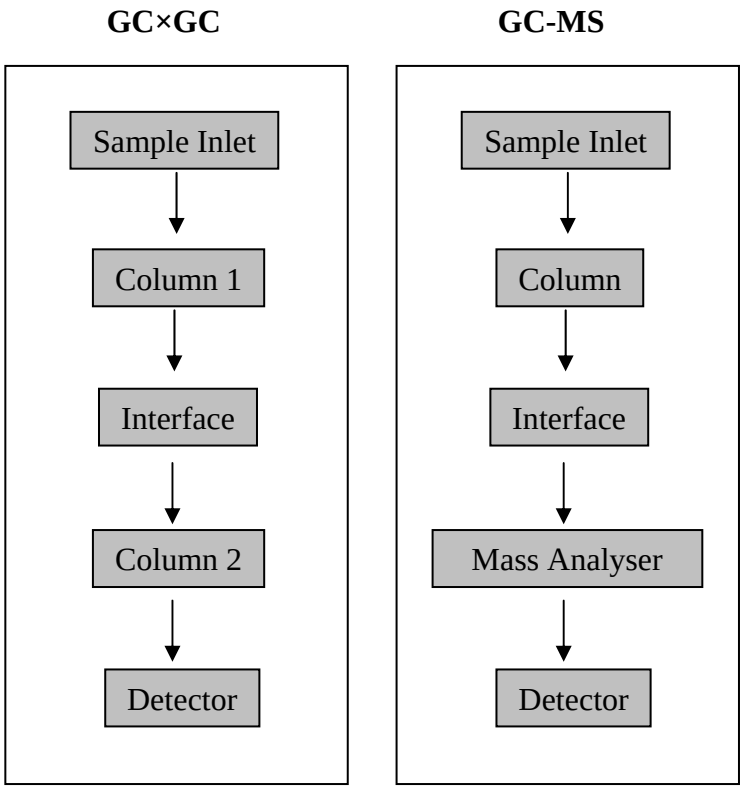

Figure 1.2: Schematic diagram of GC×GC and GC-MS instrumentation [23].

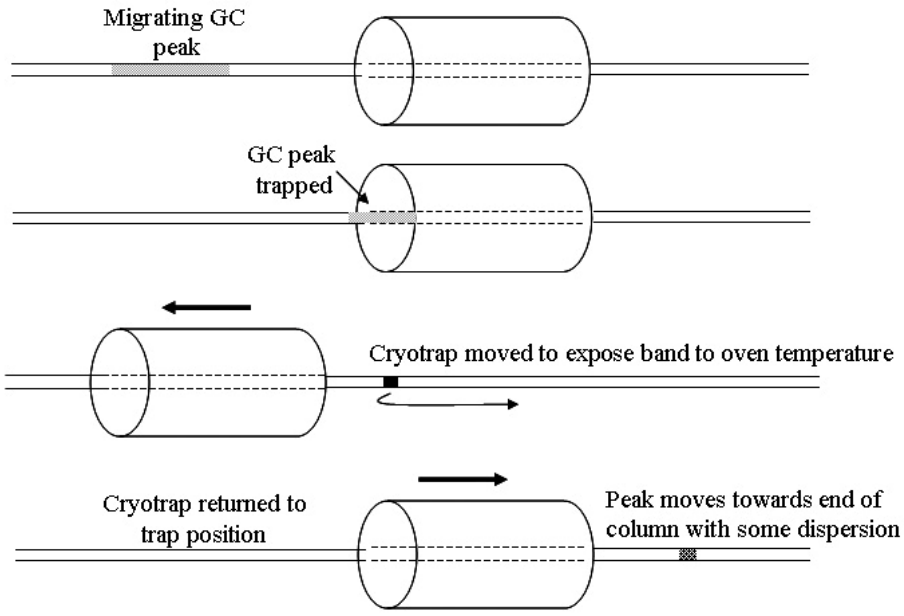

Figure 1.3: The general focus and re-mobilise process of the modulator used in a GC×GC system [24], based upon the longitudinal modulation process.

1.3 Peak capacity in GC×GC

The utilization of two different mechanisms in the column set creates an enormous peak capacity in GC×GC compared to the single column approaches. In 1D-GC, the limitation of peak capacity to resolve compounds in a complex sample is the major drawback. Peak capacity (n_c) in 1D-GC may be defined as the number of peaks that can be separated with a specific resolution in a given time (t_1-t_n) and it can be expressed as follows [25,26];

$$n_c = 1 + \int_{t1}^{tn} \frac{\sqrt{N}}{4} \frac{dt}{t} \qquad (1)$$

where N is the theoretical plate number. For conventional GC analysis with a single column, peak capacity obtained from the system can be represented as shown in **Figure 1.4A**. In this case peak capacity is the number of peaks that can be placed side-by-side in the available separation space in the analytical column. Thus, 1D-GC obtains the smallest peak capacity compared to the other approaches, since necessarily all other approaches are based on a single column, then expanded by use of a second column. Strategies to improve the separation power of 1D-GC are to couple the other independent column(s) to the existing system. MDGC provides more benefit in terms of separation power over 1D-GC due to two (or more) dimensional separations performed by connecting the two analytical columns using an interface or modulator. In this case, peak capacity of the MDGC system is increased by simply the sum of peak capacity obtained in the individual column. Therefore, in the MDGC technique peak capacity is gained by the number of discrete dimensions used in the system. Peak capacity in MDGC can be expressed as follows [27];

$$n_c \cong \sum n_i = m \cdot \bar{n} \qquad (2)$$

where m = the number of second dimension separations performed and $\bar{n}$ is the average peak capacity of the columns. In two-dimensional case with only a single heart-cut, peak capacity of MDGC can be estimated as follows;

$$n_c = n_1 + n_2 \quad (3)$$

where n_1 and n_2 are peak capacity of ^{1}D and ^{2}D column, respectively. **Figure 1.4B** shows a diagram of peak capacity gained in the MDGC system when two heart cut events were performed [28-30]. However, in complex sample analysis, chromatographers have to deal with numerous co-eluting unknown compounds in the sample, such as petroleum samples, thus the entire sample needs to be analysed since selecting just a few regions of the chromatogram provides insufficient information. Because of this reason, MDGC is normally replaced by GC×GC, which now permits the whole sample to be separated following two different decoupled separation mechanisms. Peak capacity gain is now expressed in term of product of peak capacity ($n_1 \times n_2$), which is much more benefit for complex sample analysis. Total peak capacity which is the product of the peak capacities of two individual columns, can be expressed as in **Eq 4**;

$$n_c = n_1 \times n_2 \quad (4)$$

where n_1 and n_2 are peak capacity of the ^{1}D and ^{2}D column, respectively. **Figure 1.4C** shows a diagram of peak capacity gained in GC×GC system. In this case, the ^{1}D column produces a peak capacity the same as it would be in 1D-GC and the ^{2}D peak capacity is usually less than obtained in ^{1}D. For example, $n_1 = 500$ and $n_2 = 20$, thus total peak capacity = 10,000 can be provided by this GC×GC system. The fundamental and theoretical aspects of GC×GC, including the explanation of peak capacity gained in GC×GC, have been reported elsewhere [31-34]

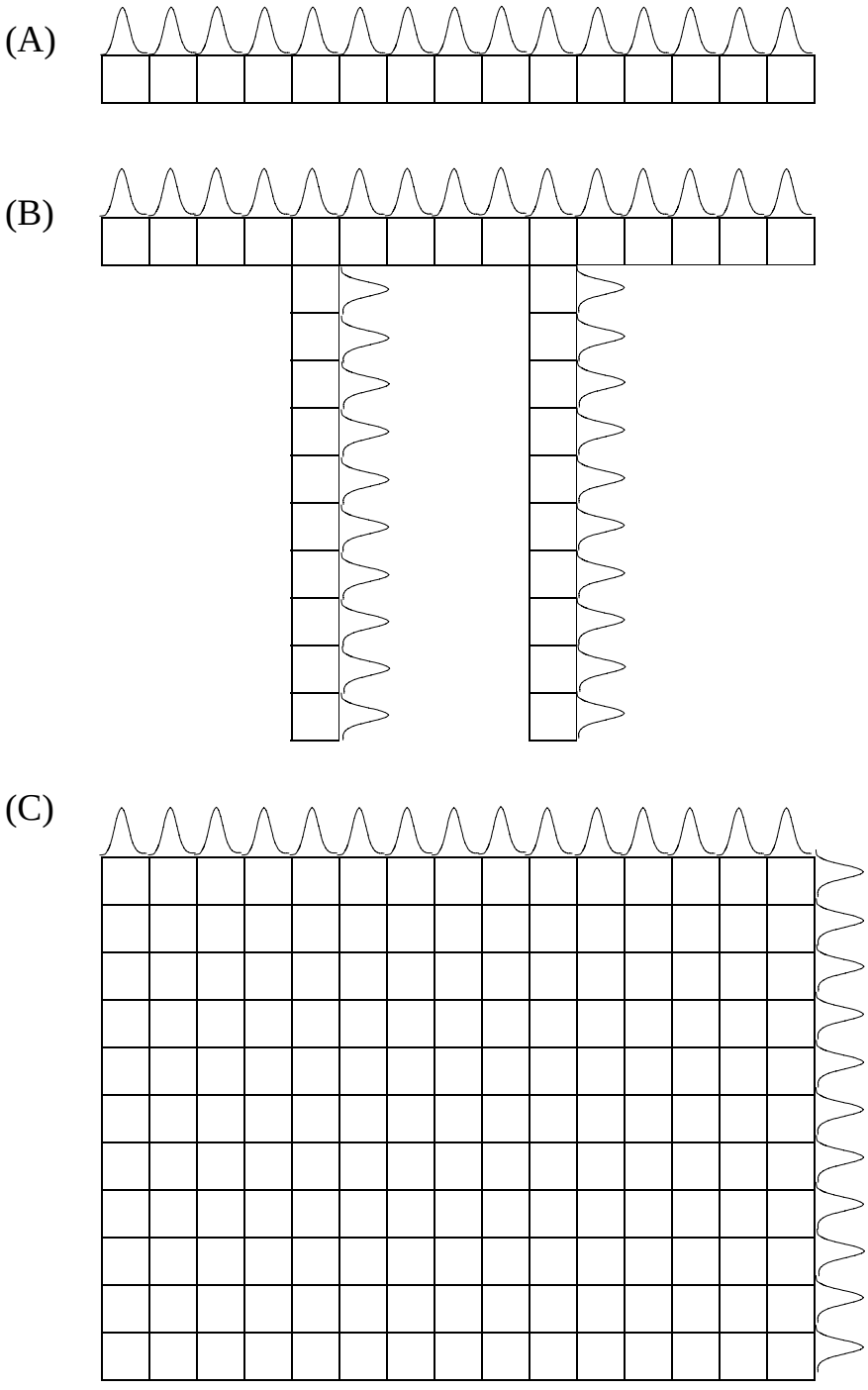

Figure 1.4: Diagram of peak capacity in **(A)** 1D-GC, **(B)** MDGC with two heart cutting events and **(C)** GC×GC, respectively [27].

1.4 GC×GC nomenclatures

Although, GC×GC is a relatively new technique, the increasing use of this technique is indicated by the number of publications. Like other new techniques, the definitions and symbols used in GC×GC must be clarified to ensure their meaning is universally accepted. In 2003, Schoenmakers and colleagues [35] reported nomenclatures and symbols in comprehensive two-dimensional gas chromatography. von Mühlen [36] updated this in the Portuguese language in 2007. GC×GC nomenclatures are explained as shown below;

1. **Apex plot** is a two-dimensional plot representing a comprehensive two-dimensional separation, in which peak apexes of second-dimension peaks are displayed by a symbol on the coordinates at the maxima of the second dimension signal intensity.

2. **Chromatographic structure** is the observed ordering of chemically related compounds in the plane of a comprehensive two-dimensional separation.

3. **Chromatographic structure or group type separation or roof tile effect** is a pattern of compounds normally of a homologues series such that isomers within a homologue display a certain retention relationship, and this relationship is predictable based on the subsequent homologues, and their pattern. This has been observed specially for PCBs and PAHs in previous research.

4. **Colour plot** is a two-dimensional plot representing a comprehensive two-dimensional separation, in which the colour represents the signal intensity of the separation system.

5. **Contour plot** is a two-dimensional plot representing a comprehensive two-dimensional separation, in which similar signal intensities are connected by means of a contour line. The plot is a two-dimensional array where $^{2}t_{R}$ (s) is plotted against $^{1}t_{R}$ (min).

6. **Column set** is the combination of columns used in a given GC×GC experiment.

7. Dual-stage modulation is when the accumulation and focusing process occurs at two locations in the modulator, usually upstream/ down stream processes.

8. Focusing effect is the reduction of the band width (in time, distance and/or volume units = band width without modulation/band width with modulation).

9. In-phase modulation is the modulation phase that produces a symmetrical sequence of peaks with a single maximum pulse peak (see **Figure 1.5**)

10. Modulator is an interface device between two columns in a comprehensive two-dimensional separation system that accumulates or samples narrow bands from the eluate of the first column for fast re-injection into the second column.

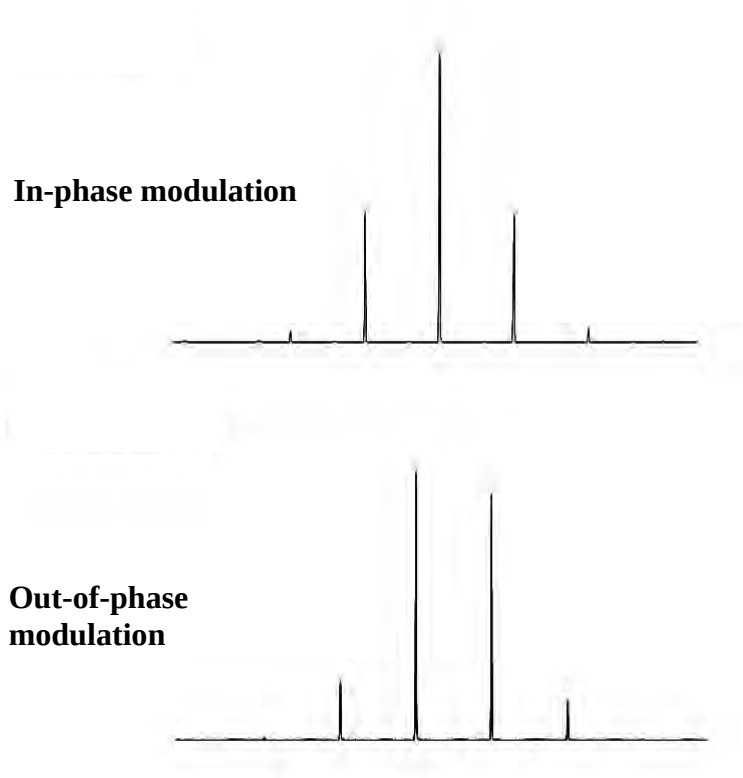

Figure 1.5: Chromatogram of in-phase and out-of-phase (here almost 180° out of phase) modulation.

11. Modulation cycle is the time duration when the modulator repeats the modulation process; focusing and re-injection the target analyte into ^{2}D (sometime the same as P_M).

12. Modulation frequency is a number of modulations per unit of time.

13. Modulation number (n_M) is a number of modulations for a given first-dimension peak. Note that the present research questions the suitability of this definition.

14. Modulation Ratio (M_R) is the ratio of 4 times the first column peak standard deviation (4σ) divided by the modulation period (P_M), or 1.6985 times the half-height width of the peak (w_h): (see more detail in **Chapter 4**).

$$M_R = \frac{4\sigma}{P_M} = \frac{w_b}{P_M} = \frac{w_h \times 1.6985}{P_M}$$

15. Modulated peak is the single narrow peak which is generated from GC×GC system; it's the effluent from the outlet of ^{2}D after being refocused and re-injected into ^{2}D by the modulator. Thus a ^{1}D peak may be modulated into a series of modulated peaks.

16. Modulation phase (F_M) is the pattern of modulated peaks caused by the time relationship between peak distribution and the pulsing process of the modulator in a comprehensive two-dimensional separation system.

17. Modulation time or Modulation period (P_M) is the duration of a complete cycle of modulation in a comprehensive two-dimensional separation system.

18. Orthogonality is the degree of the difference of separation mechanism on ^{1}D and ^{2}D in GC×GC or MDGC which is generally defined as a difference of the polarity of stationary phase of the column set used in the system. The degree of orthogonality can be indicated by using an available separation space definition [37]. The available separation space is the space between the void time (^2t_M) and the most retained of the analytes, when the analytes are measured under the same chromatographic condition within one modulation cycle (no wrap around).

19. Out-of-phase modulation is any phase that produces a non-symmetrical peak pulse distribution, (see **Figure 1.5**) as represented by the in-phase modulation result.

20. Re-injection is an injection of the compressed band or a narrow band of the compounds onto ^{2}D. The process is located at the head of ^{2}D.

21. Roof-tile effect is the observation of a band of compounds, with similar chemical structures, that produce well defined behaviour (structure/ retention) in the separation space.

22. Separation space is the region within the two-dimensional GC×GC plot in which compounds are or may be, distributed; usually defined by the total ^{1}D time and the P_M value (^{2}D time).

23. Single-stage modulation is when the accumulation and focusing process occurs at one location in the modulator.

24. Wrap around is a phenomenon when the analyte retained in ^{2}D longer than P_M.

25. Zone compression is the effect of reducing a chromatographic peak (width) in space or time to give a higher concentration within a chromatographic column.

1.5 GC×GC implementation

The major components in GC×GC implementation which differentiate it, and are added into the existing conventional 1D-GC, are (i) a second-dimension column, which can be in the range of 0.5 to 2 m, (ii) an interface for connecting two columns together, called the “Modulator”, (iii) a fast data acquisition detector of at least 50 Hz for narrow peaks generated from the system, (iv) a high speed computer for large data files from the operation of GC×GC (especially when GC×GC is coupled with TOFMS). **Figure 1.6** shows generic system describing the GC×GC instrument, with four main components in the system, comprising ^{1}D, ^{2}D, modulator and the detector.

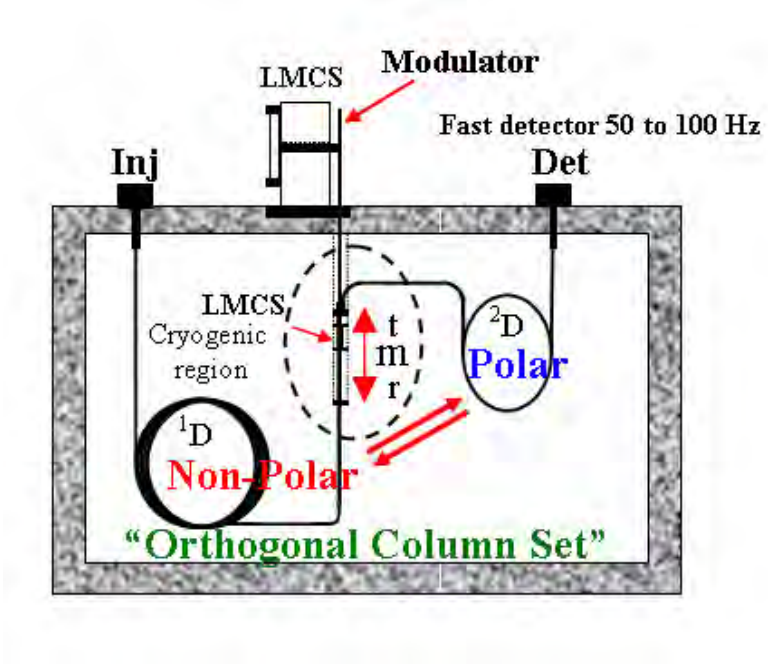

Figure 1.6: General schematic of GC×GC implementation.

Basically, the GC×GC system comprises two analytical columns with different separation mechanism, connected serially through the modulator, where often the first column (^{1}D) a non-polar column and the second column (^{2}D) is a more polar column. An orthogonal column combination in this case provides a separation mechanism based on the difference of compound boiling points through ^{1}D and then by the difference of their polarity through the ^{2}D column; an inverse-type column set performs in the opposite way. The difference between the two columns used in GC×GC indicates the degree of "Orthogonality" of the column set, more discussion of orthogonality will be provided. The modulator is the heart of the GC×GC system, located at the head of ^{2}D, where the comprehensive character of peak pulsing is generated.

Up till now, a number of modulators have been reported and applied for GC×GC. However, the main functions of all modulators are fundamentally the same. Fast data acquisition rate detectors are required to adequately generate sufficient data points from GC×GC analysis. In this chapter each component of GC×GC system will be described and discussed further;

1.5.1 Sample introduction in GC×GC

In GC×GC, most attention has been given to establishing of modulator techniques and their operation for comprehensive purposes. Column combinations seem to be the next most popular element of a GC×GC system, and so have received much attention from researchers. Recently, several research groups have been interested in coupling element selective detectors with the GC×GC system. However, not much attention has been paid to sample introduction techniques. Up till now, most fundamental and application studies in GC×GC analysis involve split and splitless injection as the most frequent injection techniques for sample introduction. The utilisation of sample introduction in GC×GC technique depends on the analyte of interest, sample matrix, and aims of the analysis. The most often used sample introduction techniques for GC×GC will be stated below;

1.5.1.1 Solid Phase Micro Extraction (SPME)

SPME is a sample preparation technique which is fast, simple and solventless. It is widely used in both 1D-GC and GC×GC for volatile compound analysis. SPME methods are based on the adsorption of analytes directly from an aqueous or gaseous sample onto a fiber [38]. Then, the SPME fiber is inserted directly into the GC×GC injector to desorb the analyte, for further chromatographic analysis. The fiber is usually fused silica coated with different materials such as liquid (polymer), solid (sorbent) or a combination of both such as divinylbenzene, carboxen and polydimethylsiloxane (DVB/CAR/PDMS), respectively [39,40]. The technique has gained wide spread acceptance as a technique of choice for many GC×GC applications such as flavour and fragrances, forensic and toxicology, food, biological and environmental samples which have been reported elsewhere [41-44]. The combination of SPME or Head Space-SPME (HS-SPME) sample preparation in GC×GC demonstrated rapid sampling and high sensitivity for trace level analysis of volatile compounds.

1.5.1.2 Thermal desorption in GC×GC analysis

Thermal desorption (TD) is a desorption technique for isolating semi-volatile and volatile compounds from various matrices such as natural products, polymers, food flavours and cosmetics, etc. In environmental analysis, TD is a technique of choice of air analysis including indoor, outdoor, workplace and breath air. Sorbents used for TD technique, for analyte accumulations, are usually porous polymers. Accumulated volatile compounds on the sorbent are transferred to a desorption unit interface to the GC×GC injector for further separation. Advantages of this technique include a reduced time and solvent consumption in sample preparation steps, which also benefits sensitivity. Schnelle-Kreis et al. [45] applied direct thermal desorption (DTD) sample introduction technique with GC×GC-TOFMS for the analysis of organic compounds in ambient aerosol particles. They found that the DTD method is a well-suited technique for the routine analysis of organic compounds associated with ambient particular matter (PM). The combination of this sample introduction with a GC×GC-TOFMS system [46] allows improvement in the identification of compounds which are unidentifiable in 1D-GC-MS analysis.

1.5.1.3 Cold on-column injection in GC×GC analysis

Cold on-column (COC) injection employs a direct introduction of the sample as a liquid into the oven-thermostatted column inlet or a precolumn, without prior vaporization in a heated external chamber [47-49]. In this technique, the composition of the sample introduced into the system is identical to the original sample composition. The technique can be adapted to automated injection by using a wide bore precolumn connected to the analytical column. In GC×GC analysis, Harynuk and colleagues [50] used cold on-column injection to perform fast GC×GC with short primary columns to demonstrate the potential of the method, using pyrethrins analysis as an example. In this research work, a short column set, COC injection technique, and a higher carrier gas flow was explored to demonstrate the fast GC×GC concept and reduced elution temperature to prevent on-column degradation.

The use of cold on-column injection, a short primary column and a high carrier gas flow rate allows pyrethrins to be eluted below 200 °C, with an analysis time of 17 minutes and complete separation from sample matrix. Also in this work, they proposed a new interpretation of the model of "GC×GC optimization pyramid" which was previous proposed by Dimandja [51].

1.5.1.4 Large sample volume injection (LVI)

To meet the requirement of trace analysis for all toxicants in environmental samples and other complex samples, injecting larger volume of sample into the system seems to be an alternative way. The technique for injection of large volumes into the GC column was developed in the 1970s. Two methods are used for large volume injection; solvent vapour exit (SVE) and programmed temperature vaporization (PTV), which were built into a split/splitless inlet [38]. For GC×GC, large sample volume injection has been used for the analysis of pesticides in food extracts [52] and for the determination of polynuclear aromatic hydrocarbons (PAHs) in complex matrices in order to achieve better analyte detectability. The work of Cavagnino et al. [53] combined large volume injection (LVI) with the GC×GC technique using a new automatic LVI based on concurrent solvent recondensation (CRS-LV) [54]. From this research, results show that combining the new splitless large volume injection technique with GC×GC offered a very powerful tool for trace analysis in complex mixtures. The separation of target compounds from the background matrices and detection at low level in the ppb range were achieved.

1.5.2 GC×GC column combinations

Column combinations used in a GC×GC system depend on the analysis goal and the composition of the samples. There are two common types of column sets which have been widely used; (i) the non-polar-polar column set (orthogonal column set) and (ii) the polar-non-polar (inverse) column set. To combine

two columns for GC×GC analysis, with different separation mechanisms between the columns, the term “Orthogonality” has been coined.

1.5.2.1 Orthogonality in GC×GC analysis

Orthogonality is a term that indicates a different characteristic of measured parameters in one dimension, compared to the other dimension in a multidimensional or hyphenated technique. Ryan et al. reported [37] a study of orthogonality in GC×GC analysis. The study was performed by altering the degree of orthogonality through the series of experiments. They concluded that an orthogonal column set is not necessary to obtain the best separation or analyte resolution. But, the orthogonal column set tends to provide the maximum use of the available separation space. Generally, orthogonality in GC×GC is achieved using different polarity stationary phase columns in each dimension. A high degree of column orthogonality (the most disparate of separation mechanisms) does not guarantee optimum resolution obtained from the analysis. The higher degree of orthogonality of the column set achieves more distribution of the analysts of interest into the useable separation space. **Figure 1.7** shows a representation of useable and unusable of space in the GC×GC contour plot. Thus, in GC×GC analysis two columns have to ensure a high degree of orthogonality, though precise measures of this parameter are not apparent in the literature. A numbers of orthogonality studies in GC×GC have been reported in the literature [33,55,56].

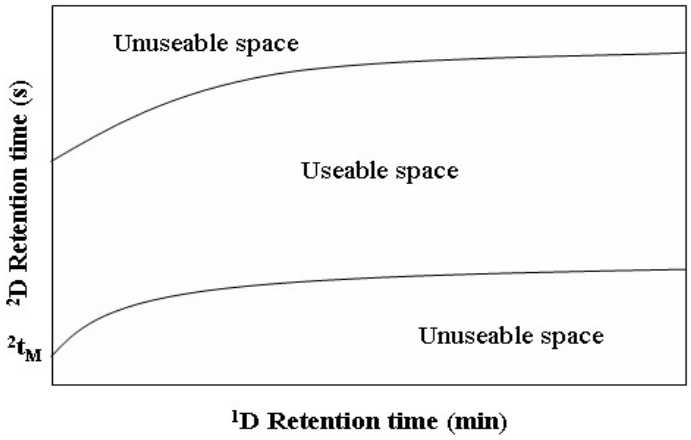

Figure 1.7: Diagram illustrating the general use of the two-dimensional separation space [37].

1.5.2.2 Non-polar–polar (orthogonal) column set

The non-polar–polar column set is a typical column set that is widely used for GC×GC analysis. In this column set, the first-dimension column (^{1}D) is a non-polar column with a longer length (15 to 50 m). The separation mechanism in ^{1}D relies on the analytes' boiling point; the analyte with the lower boiling point will elute earlier than that of higher boiling point. The second dimension column (^{2}D) usually has a higher polarity compared to ^{1}D, hence, the target analytes with the lower polarity will elute from ^{2}D before the higher one. The typical length of ^{2}D ranges from 0.5 to 2.0 m with a thinner film phase and narrower i.d., making separation in ^{2}D fast due to the high carrier flow velocity. Column selection in GC×GC analysis is critical. Basically in an optimization step, different column sets will be trialed to achieve the best separation of the target analytes from each other and from the sample matrix. Nowadays, more than ten commercial GC capillary column types have been combined and used as non-polar–polar column set for the analysis of complex samples, for example BPX5 and BP20 [57] was reported for the analysis of petroleum samples and essential oils, BPX5 and BPX50 [58] was used as a column combination for PCB congener analysis. The orthogonal column set is normally employed for most fundamental and applications studies in GC×GC analysis. **Figure 1.8** shows a

diagram of an elution order of analytes in 2D space when a non-polar–polar column set is employed.

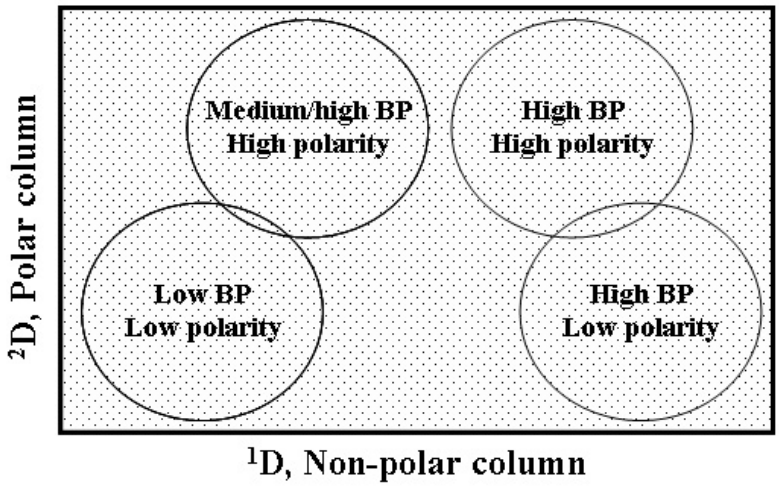

Figure 1.8: Diagram of a contour plot map when a non-polar–polar column set was employed [59].

1.5.2.3 Polar–non-polar (inverse) column set

This column set is normally used when a high polarity column is required to separate medium to high polarity analytes in the first dimension. The analyte with the lower polarity will be eluted from ^{1}D at low elution temperature and then transferred to ^{2}D for further separation. Basically, the first dimension retention in "inverse column sets" is greatly influenced by the analyte vapor pressure. In 2004, Adahchour and colleagues [60] employed the inverse-type column set for the analysis of food samples; they named this type of column set as "non-orthogonal" although there is no agreement that this is an appropriate term. The results show that the 'non-orthogonal' approach provides a complete inversion of the 2D structure order in the food sample. With the inverse column set, peak shape of the polar compounds such as aliphatic acids and alcohols were improved and the inverse type of the ordered structure of the chromatogram in a complex flavor mixture in food was also accomplished. A number of GC×GC applications using inverse column set have been

reported, for example, BPX80 and BPX35 [61] have been reported as a column set for fatty acids analysis, BP20-BPX5 for essential oils and BPX50-BPX5 for petroleum samples. **Figure 1.9** shows a diagram of the elution order of the analytes when the polar–non-polar column set was employed in GC×GC analysis. Once again, **Figure 1.10** shows colour plots of a diesel oil sample analysed when the orthogonal and inverse column set were employed. **Figure 1.10 (A)** is the result obtained from a DB1-BP20 column set and **Figure 1.10 (B)** is the result obtained from BP21-BPX35 column set [60].The completely inverse analyte structure order was observed.

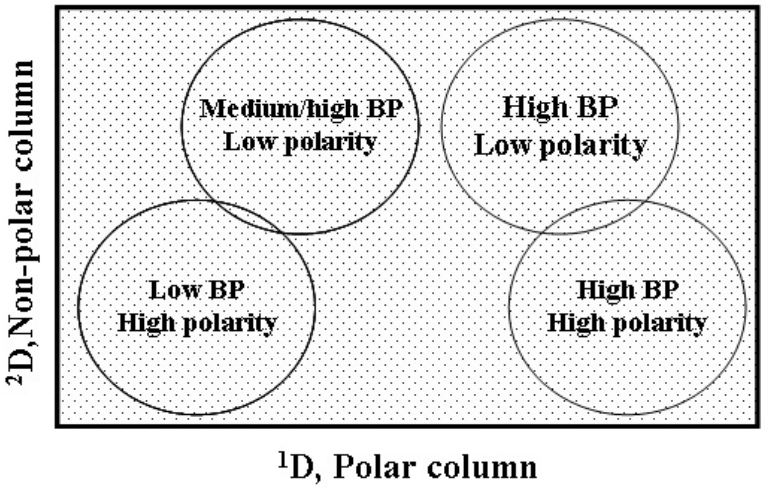

Figure 1.9: Diagram of a contour plot map when the polar–non-polar column set was used [59].

This result is a fascinating demonstration of the structure-retention behavior of different compound types in GC×GC, and the way different columns offer quite different capability for certain chemical classes.

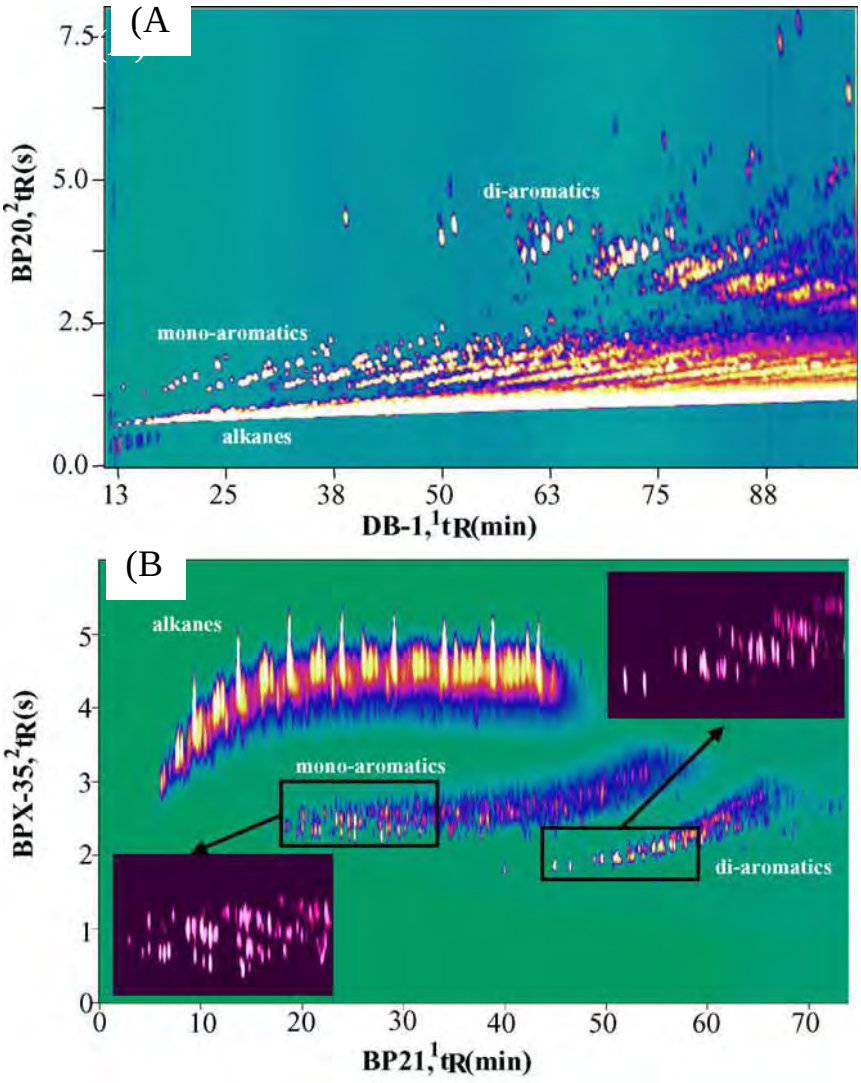

Figure 1.10: Colour plot obtained from GC×GC-FID used for diesel oil sample analysed on **(A)** DB1-BP20 and **(B)** BP21-BPX35 [60].

1.5.3 Modulators in GC×GC analysis

In GC×GC analysis, the modulator must be considered to be the most important element of the system. Up till now, a number of modulators have been reported and used for GC×GC analysis. Lee, et al. [62] reviewed and compared a number of modulators used for the modulation process in GC×GC up to 2000. In 2003, Kristenson and co-workers [63] describe characteristics of six different modulators for the evaluation of the analysis of halogenated organic compounds by using GC×GC coupled with the micro-ECD detector. Basically, the modulator was used as an interface device which is connected between two different analytical columns. It is normally located at the head of the ^{2}D column of the column set. Most modulators use liquid N_2 and CO_2 as a coolant to trap the solute from ^{1}D. The modulator generally serves two functions; (i) collecting and focusing the fraction of peak eluted from ^{1}D and (ii) rapidly re-injecting the collected fraction as a compressed band into ^{2}D for further separation. The development of the modulator and the detector in GC×GC have been reported by several researchers [16]. Principally, modulators can be classified into three different groups based on their modulation process;

(i) Heater based modulator is a modulator that can be heated to different elevated temperature in the modulation process. The trapping process in this modulator is achieved in a tube or in a thicker film of the stationary phase at the oven temperature, whereas desorption occurs when the trapping zone was heated to a higher temperature compared with the GC oven temperature. The heater based modulator used in GC×GC, such as the dual-stage thermal desorption, was one of the first modulators in GC×GC and the sweeper modulator is an example of this. However, the limit of operational temperature is reported to be a disadvantage of this modulator type.

(ii) Cryogenic modulator is a modulator that operates by using CO_2 as a coolant at the trapping zone. In the cryogenic modulator the solute is trapped at the lower temperature and may be released to ^{2}D at the ambient temperature of the oven, thus, no additional heat source is required in this modulator type, or added heating may be employed. Today, it has been accepted that the cryogenic modulator is

a useful and user friendly modulator due to the simplicity of the installation and operation. The cryogenic based modulators used in GC×GC are exemplified as the LMCS modulator and jet based modulator. The LMCS system was the forerunner of the other cryobased system.

(iii) Valve based modulation in GC×GC is based on several valve based interfaces such as a fast switching diaphragm valve [64-68] and the valve based interface using a six port valve [69,70]. The diaphragm valve modulator achieves the modulation process by injecting a small fraction of solute from ^{1}D to ^{2}D. Because of the transfer yield being only 2% of the solute may be this modulator unsuited for trace analysis. In the valve based modulator using a six port valve, a differential flow mode can be used to transfer the solute and there is much greater transfer (80%+) of the solute from ^{1}D to ^{2}D. However, a high gas flow rate in ^{2}D, to achieve band compression in time, is required in this modulator. Therefore, band broadening often accompanies this system. High ^{2}D flows, which requires wide bore, longer columns than for other GC×GC systems, makes their use with MS more difficult. Fundamentals and applications of this modulator have been described elsewhere [22,71-74].

More details of the design and the operation of five modulators used in GC×GC will be described below;

1.5.3.1 The Sweeper-modulator

The sweeper modulator is the first commercial modulator to be developed by Phillips and co-workers [75]. The sweeper modulator has two main components; a modulator capillary (modulator tube) which is a small section of capillary column with a thicker film phase, and a rotating slotted heater. In this modulator, the analyte will be trapped at the ambient temperature of the GC oven, and released when heat is applied to the trapped region by the slotted heater as it passes over the phase. The rotating slotted heater will be moved along the modulator tube to desorb the trapped solute from the modulator tube into ^{2}D. The main disadvantages of the sweeper modulator are its inherent complicated design and installation, and the difficulty of the precise movement of the slotted heater [72]. The use of the sweeper modulator for GC×GC analysis is obsolete due to the drawbacks stated above. However, the analysis of complex sample by using the sweeper modulator in early years of GC×GC has been reported [76]. **Figure 1.11** shows a schematic diagram of a GC×GC system using the sweeper modulator.

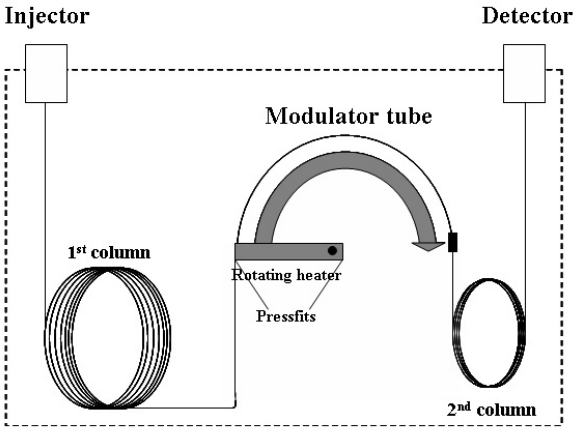

Figure 1.11: Schematic diagram of GC×GC system with sweeper modulator [63]. Nowadays, GC×GC interface with no moving part has been developed by Górecki and co-workers. The approach is now having a high performance compared to the other non-moving modulator, with the new mode called “stop flow GC×GC”.

1.5.3.2 The KT 2001

The KT2001 was invented by Ledford and his colleagues in 2000 [77]. The KT 2001 consists of two hot jets and two cold jets. Nitrogen gas was used as a cool gas in this modulator and hot air was applied in the remobilisation step. The modulator can be cooled down by heat exchange through copper tubing immersed in liquid nitrogen outside the GC and delivered through vacuum-insulated tubing to the cold jets. Two cold jets provided the continuous delivery of cold nitrogen gas at 10 $L.min^{-1}$ while two hot jets (from hot air) provided a short pulse to remobilise the analytes [63]. **Figure 1.12** shows a schematic diagram of a GC×GC system with KT 2001 modulator.

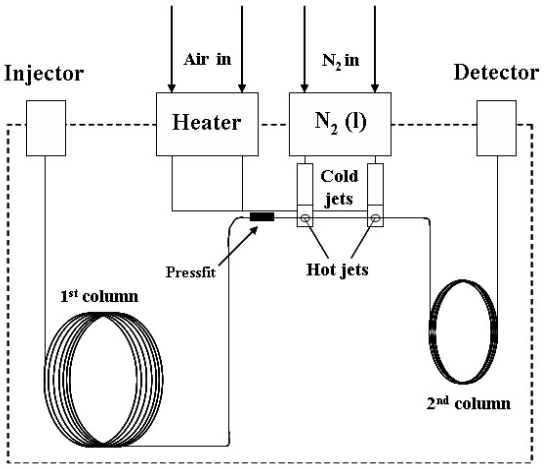

Figure 1.12: Schematic GC×GC system with the KT 2001 modulator [63].

.

1.5.3.3 The dual-jet CO_2 modulator

This modulator consists of two jets and two electrically driven two-way valves. Beens and co-workers followed Ledford's idea and invented the two jets capable of pulsing cooled gas (CO_2) to the modulator [78]. In the dual-jet modulator, the modulation process involves the operation of two jets with the CO_2 cooling system. The process starts when the down stream jet traps the analytes eluting from ^{1}D at the predefined time and then the down stream jet switches off, resulting in the cold spot heating up rapidly by the oven temperature to permit transfer to ^{2}D. The up stream jet is basically switched on to prevent the next fraction from ^{1}D interfering while the previous fraction was in the modulation process. Once the first fraction was sent to ^{2}D then the up stream jet switches off to allow the analytes to move to the down stream jet and the next cycle of the modulation is started. The dual-jet cryogenic modulator has been used for a variety of samples. The narrow peak width at half height and the ability for low boiling point compound analysis is the main advantage of this modulator [53,79,80]. **Figure 1.13** and **1.14** show GC×GC schematics when the dual jet cryogenic modulator was employed, and the modulation process, respectively.

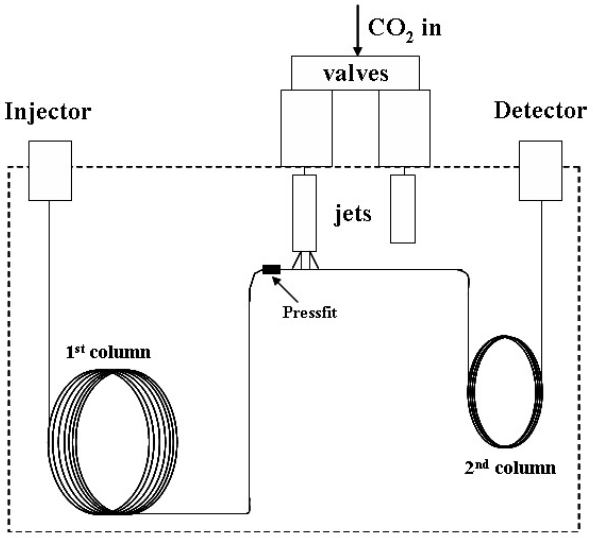

Figure 1.13: Schematic of GC×GC system with the dual-jets CO_2 modulator [63].

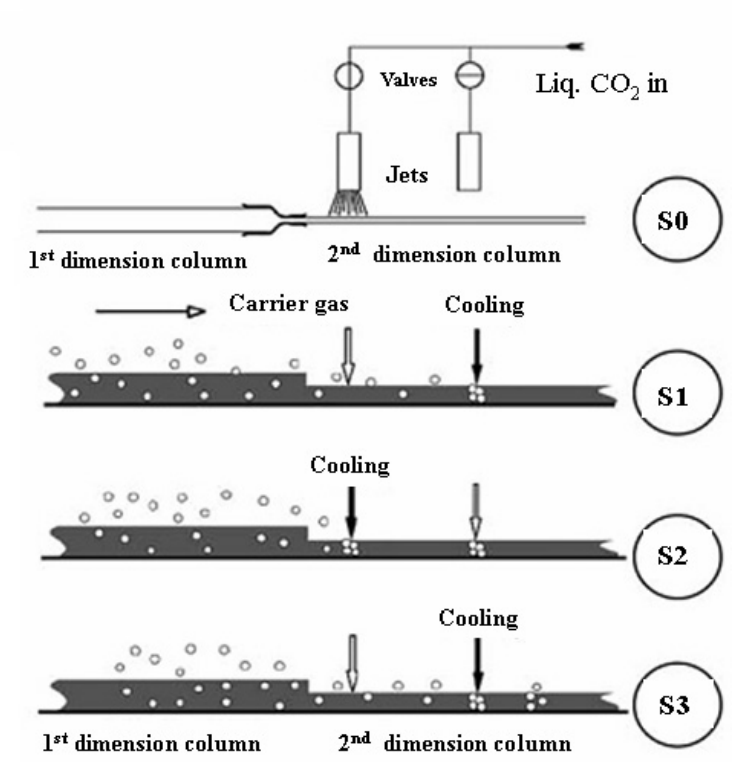

Figure 1.14: Cryogenic modulation of dual jets CO_2 modulator, **(S0)** General set-up of dual-jet cryogenic modulator. **(S1)** down stream jet traps analytes eluting from ^{1}D. **(S2)** down stream jet switched off, cold spot heats up and rapidly released into ^{2}D, simultaneously, up stream jet switched on to prevent leakage of ^{1}D material, **(S3)** next modulation cycle is started [15].

1.5.3.4 The semi-rotating cryogenic modulator

The semi-rotating cryogenic modulator has been developed and evaluated for GC×GC analysis by Hyoetylaeinen et al [81]. The modulator is based on two-step cryogenic trapping of analytes using continuously flowing CO_2. The outer body of this modulator is made of stainless steel and constructed to fit the empty injector port of an Agilent gas chromatograph model 6890. The CO_2 line is installed inside the body of the modulator and the revolving metal is attached at the end of the CO_2 line to prevent ice formation and to ensure the precise spray of CO_2. The ^{2}D was kept in place by a holder to avoid vibration and contact of the metal part of the modulator. The single 180° revolving CO_2 jets with a constant CO_2 spray move in the

up and down stream position for 1.8 and 1.2 s, respectively with the turning time of the jet taking about 1 ms. The system showed success for an application for the analysis of aerosol sample. The latest version of the semi-rotating modulator was reported in 2003. Principally, this modulator is similar to the dual-stage CO_2 jet modulator which was reported by Beens and co-workers. However, in the new version of this modulator just only one nozzle is used to spray the CO_2 to the column. This nozzle can rotate through 180° angle back and forth when the modulation was performed. Improved utility and robustness, and all performance data of this modulator was reported [82]. **Figure 1.15** shows a schematic diagram of a GC×GC system retrofitted with a semi-rotating cryogenic modulator.

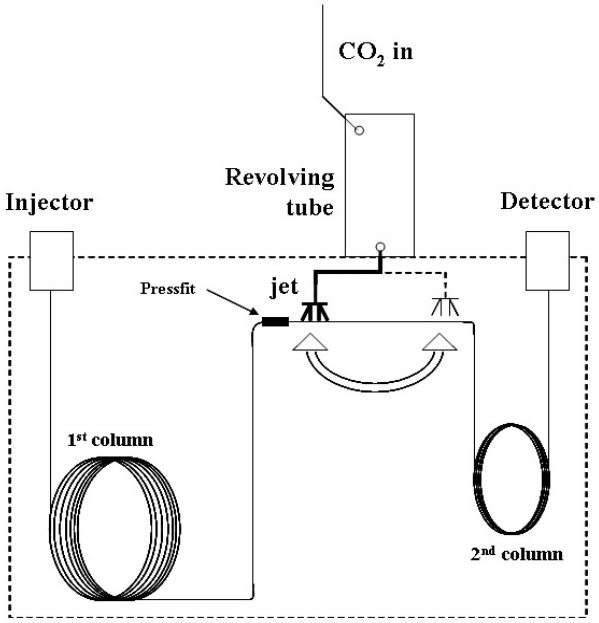

Figure 1.15: Schematic of a GC×GC system with the semi-rotating cryogenic modulator [63].

1.5.3.5 The KT 2003, CO_2 loop modulator

This modulator consists of one cold jet, one hot jet and the modulation loop, which consists of a 1.2m x 0.1 mm i.d. uncoated capillary. This modulator is modified from the KT 2001 design [83]. The cold jet consists of stainless

steel tubing squeezed at the end to create a nozzle. The tubing is placed inside a vacuumed double-wall jacketed tube to isolate it from the GC oven temperature and located to focus the cold jet stream onto the modulator loop. The CO_2 expansion and the temperature of the cold jet can be controlled by coupling the stainless steel tubing to the CO_2 tank via a needle valve. On the other hand, the hot jet which uses air as the heating medium consists of an aluminium tube incorporating a heater controlled by the AUX output of the GC. The hot air stream is switched by an electronic valve controlled by an external electronic box by which modulation time, opening time of the valve, GC run time and modulation delay can be programmed. The modulator loop is housed inside an aluminium holder which is mounted on the cold jet. The key to this design is that two spots, on the two column segments, (about 0.6 mm apart) are cooled and heated simultaneously by operation of the jet where the capillary loop crosses. When the hot jet is closed, a flow of expanding CO_2 traps the analytes in both the up and down stream spots. After a very short hot-jet pulse (ca. 200 ms), the analytes trapped in the downstream spot are injected onto the second dimension column, and simultaneously the analytes from the upstream spot are released to the modulator loop, which is of sufficient length to liberate these analytes during the hot-jet pulse but ensure the down stream segment is cool enough for them to trap again in the downstream spot. **Figure 1.16** shows a schematic diagram of the GC×GC system with the KT 2003, CO_2 loop modulator. The KT 2003 is commercialised by Zoex corperation, and the applications of this system have been demonstrated in a wide range of samples such as petroleum liquids, environmental, PCB/dioxins/pesticides, flavours & fragrances, industrial process diagnosis, catalysis, soils and sediments.

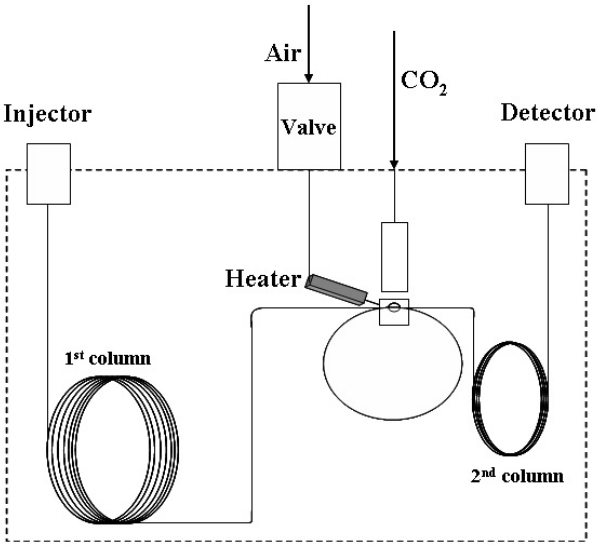

Figure 1.16: Schematic of a GC×GC system with the KT 2003, CO_2 loop modulator [63] .

1.6 Longitudinal Modulated Cryogenic System (LMCS)

Longitudinal Modulated Cryogenic System (LMCS) is the first modulator which employed the cryogenic modulation approach in GC×GC, hence it preceded the system reported above and should be seen as the revealing technology for these other systems. Marriott and colleagues pioneered this modulator, proposed in 1995 [84]. The LMCS provides advantages over the previous heat based modulators such as there being no additional heating system required (heat is provided by the GC oven) and the better resolution obtained from the analysis. It has been successfully applied for a wide range of samples such as petrochemical products, drugs, food, perfumes and fragrances, essential oils, FAME, novel molecular processes and, environmental samples.

The LMCS modulator consists of a 3 cm long cryogenic region with operation achieved by linear motion (back and forth) in a longitudinal direction along the column in the GC oven. Liquid CO_2 is applied to a small capillary, and then expands to cool down the cryogenic region of the LMCS modulator. The modulator temperature can be adjusted as desired by using a solenoid switch, controlled by a thermocouple. The cool trap comprises two concentric stainless-steel tubes connected

and sealed at the end to form a chamber between the two tubes. The trap is cryogenically cooled with liquid CO_2 and can be moved back and forward in a number of different motions (usually based on the time duration of movement) according to the particular requirement of the study. Three operational modes of the LMCS modulator will be explained later in **Section 1.6.1**.

The modulation process is achieved by moving the cryo-region from the trap position, to the release position, and then the trapped fraction from ^{1}D will be reheated and remobilised by the oven temperature. The incoming peaks from ^{1}D will be trapped in the trap-position at the head of ^{2}D and then rapidly re-injected as a compressed band for further separation in ^{2}D when the cold cryogenic region moves down to the release position [85,86]. In the release step, the cryogenic trap is moved away from the focused region, thus the capillary column is exposed to the ambient oven temperature and delivers trapped compounds to ^{2}D. **Figure 1.17** is a schematic diagram of GC×GC system based on the LMCS modulator. A numbers of fundamental studies and applications of GC×GC analysis using the LMCS modulator have been published [87].

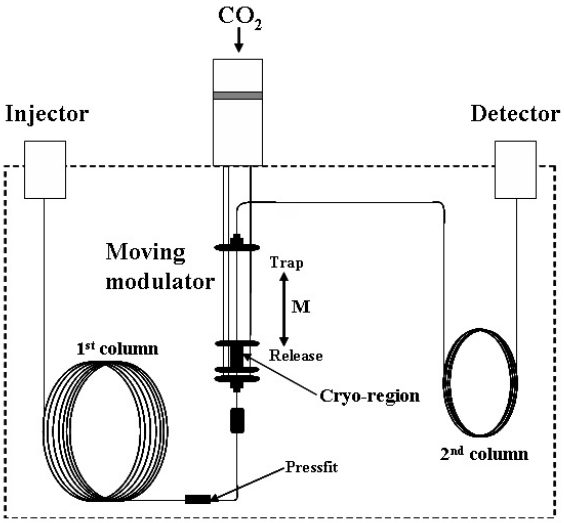

Figure 1.17: Schematic diagram of a GC×GC system with the LMCS modulator, where **M** is a movement of the cryo-region between trap and release position [63].

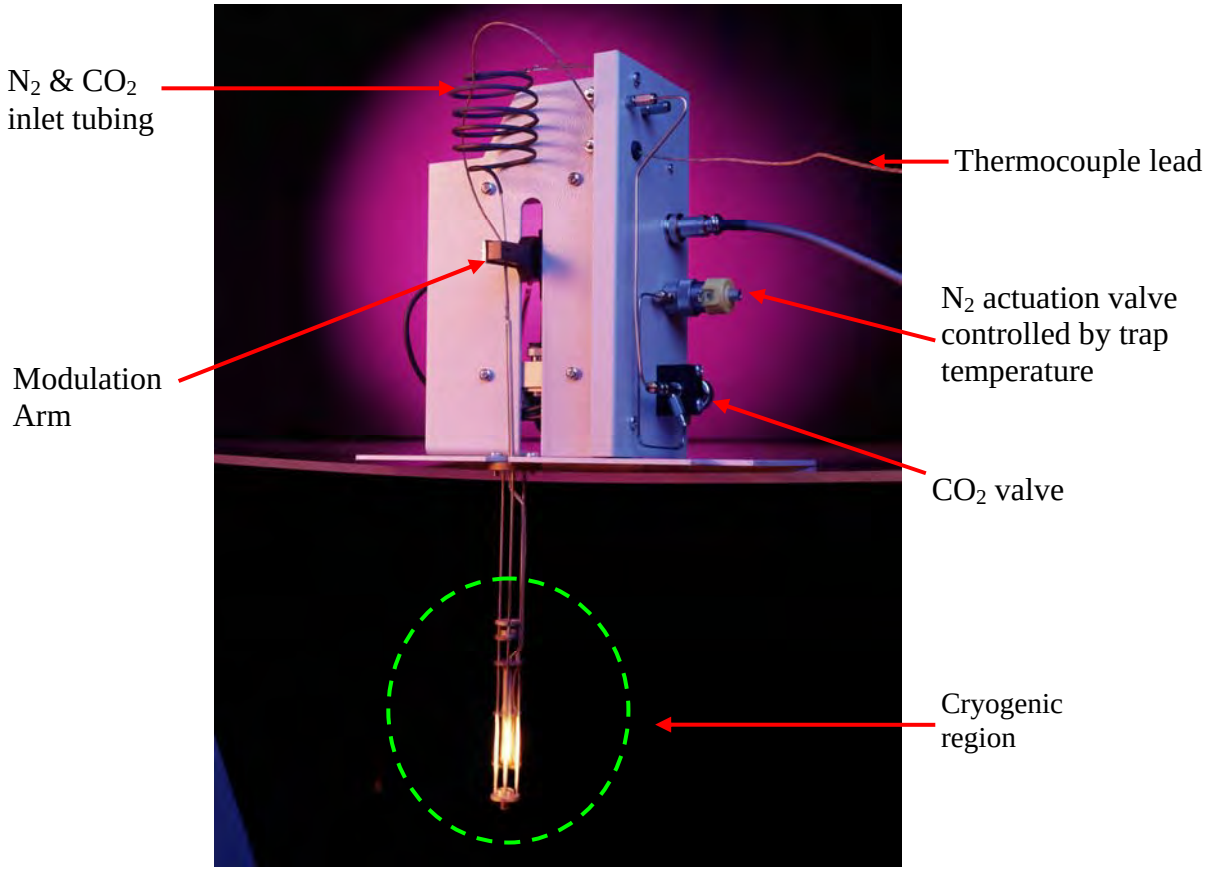

Figure 1.18: The LMCS modulator showing the essential part of this modulator.

Figure 1.18 shows an LMCS system photograph. The modulator has been developed and utilised as a modulator in a wide range of GC×GC applications at the Australian Centre for Research on Separation Sciences, (ACROSS), School of Applied Sciences, RMIT University since it was invented.

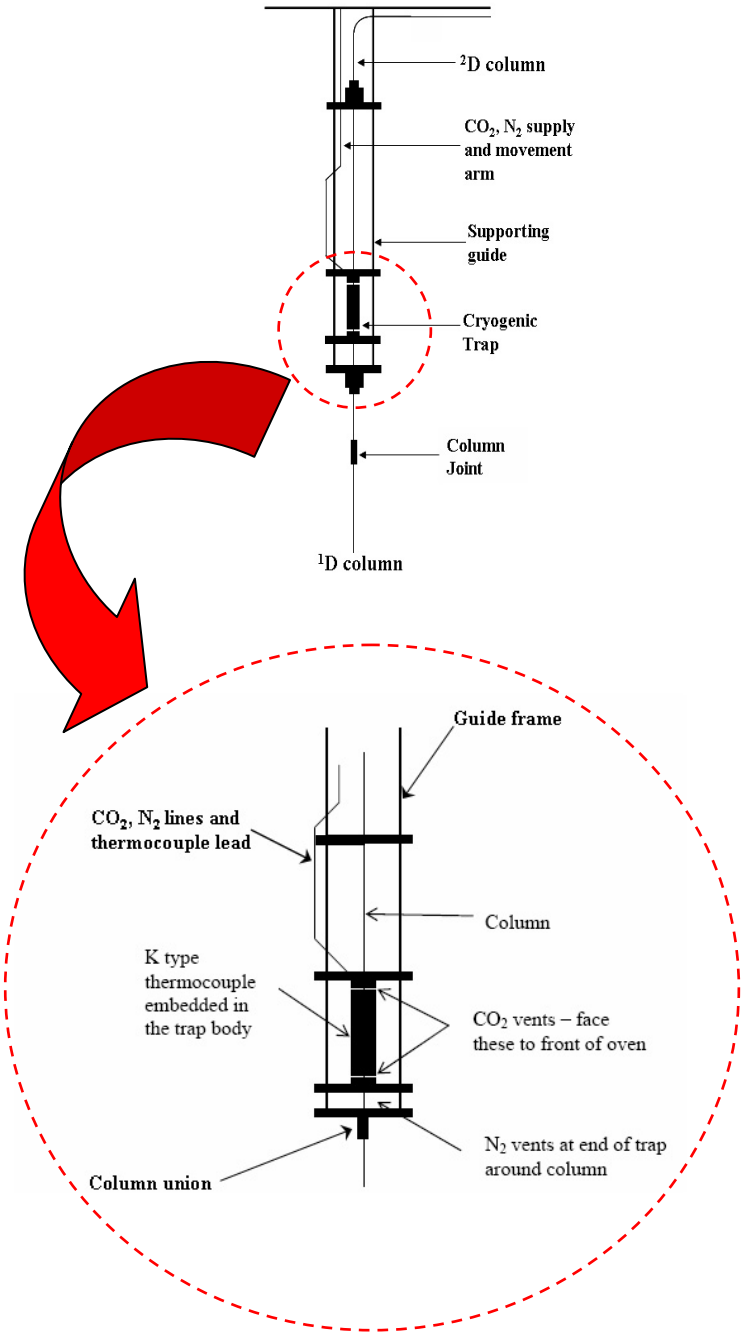

Figure 1.19: Schematic of LMCS modulator [88].

In **Figure 1.19** the expanded view of the LMCS device and the trap assembly are shown. The LMCS comprises electronic control module, a modulator drive unit, and a cryotrap. The cryogenic trap is located inside the GC oven and can move back

and forth at the predetermined time by a moveable arm of the modulator. In the latest version, the cryogenic trap region is approximately 3-4 cm long and consists of two stainless steel tubes. The smaller inner tube has an inner diameter slightly greater than the capillary column which is passed through the cryotrap. The bigger outer tube contains two ports through which the flow of the expanded CO_2 gas can be passed and vented out. The two tubes are connected at the end to form the chamber for the cryogenic gas. The capillary column is feed through the narrow inner tube and held in position by retaining nuts. The trap region slides up and down along the guide frame of the trap to perform the modulation process. The trap has one inlet supply of cryogenic fluid (liquid CO_2) to provide coolant to the trap and two CO_2 outlet holes to vent the CO_2 gas to the GC oven. A small flow of N_2 is also applied to prevent ice formation. The cryogenic fluid used can be turned on and off any time during the analysis. Cryogenic cooling will be applied to the tube when the system is turned on, thus compounds eluting from ^{1}D can be trapped. The LMCS is controlled through a control module with a digital timer accurate to 1/1000s, and is moved with a stepper motor. It also provides a minimum continuous modulation frequency of 1 Hz with a release position dwell time of 100 ms.

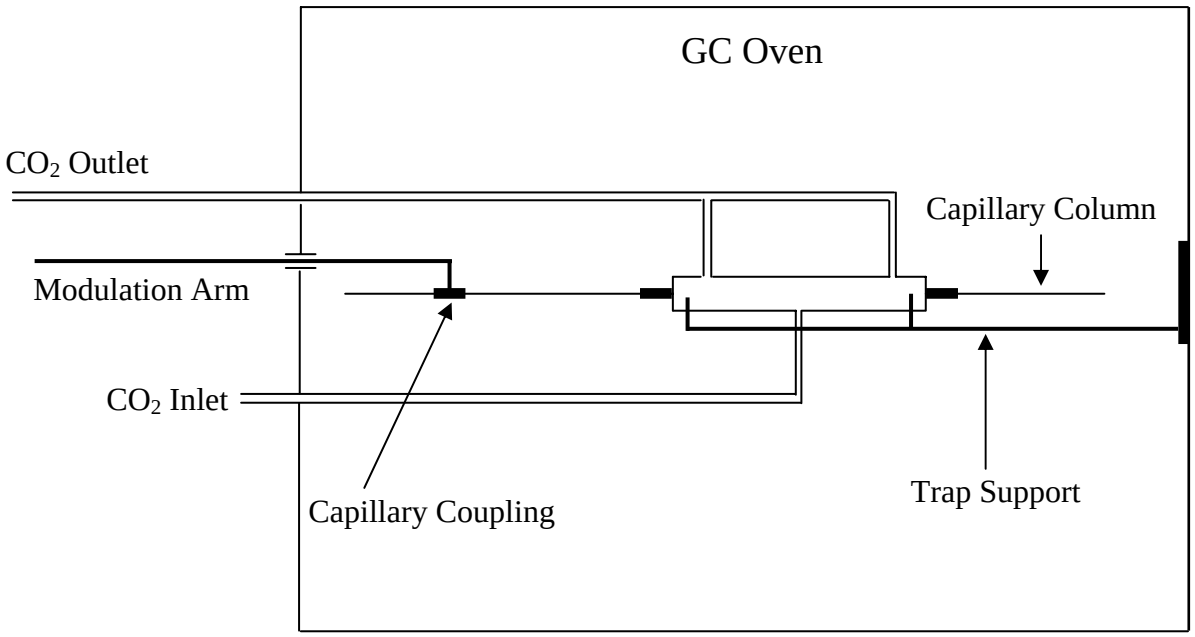

Figure 1.20: Schematic of the cryogenic region of LMCS modulator [24].

Figure 1.20 presents details of the trap construction and the cryogenic gas flow in the trap assembly of the LMCS modulator in the first version developed at RMIT University. The trap support guide was fixed inside the GC oven wall. The capillary column was inserted through the cryogenic region and held in the position by the nuts. One CO_2 inlet and two CO_2 outlet holes was constructed in the outer tubing. The cavity inside the cryogenic region is the place where the ice was formed by the cryogenic fluid supplied. The difficulty of the movement due to the ice formation was removed by a small N_2 flow.

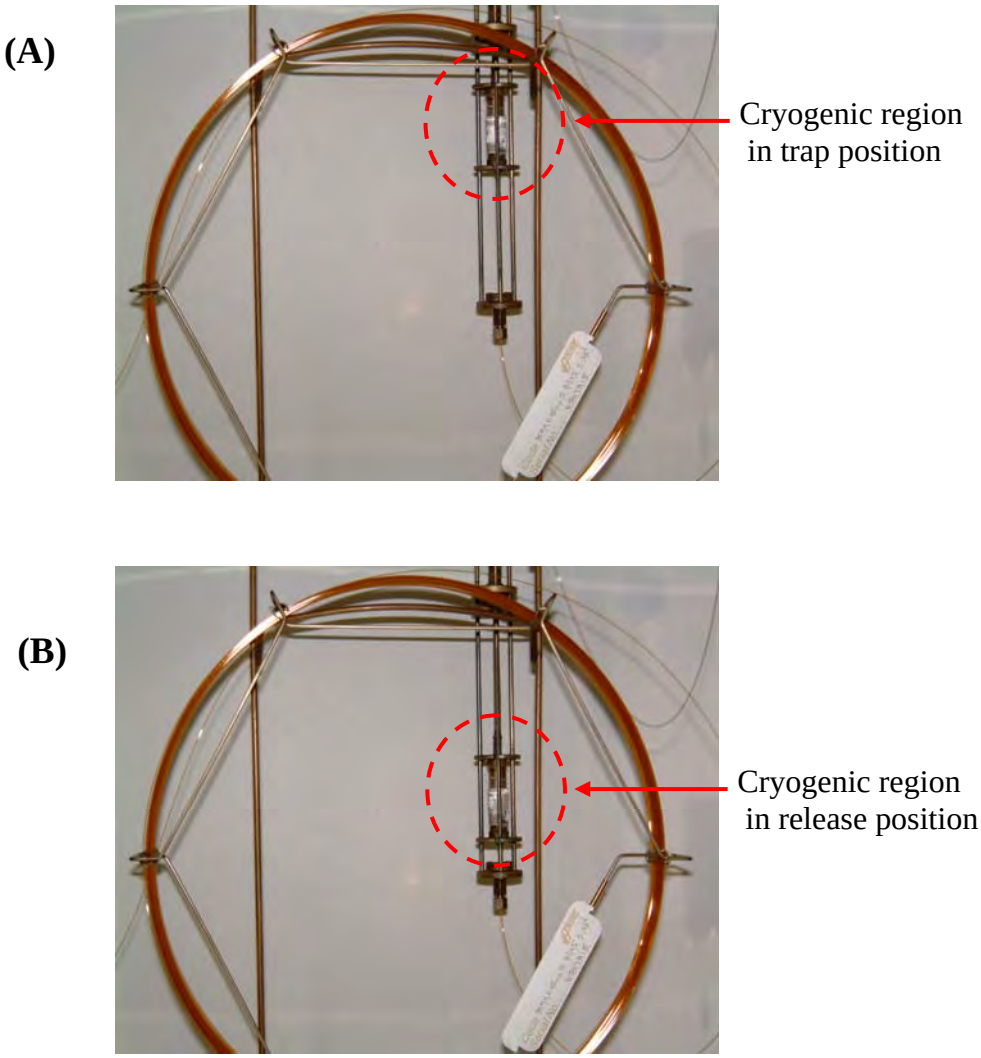

Figure 1.21: Photograph of cryogenic trap movement in vertical direction of LMCS modulator **(A)** when cryogenic region is in the trap position **(B)** when cryogenic trap is in the release position.

Figure 1.21 shows a photo of the movement of the cryogenic region in the LMCS modulator. Basically, the cryogenic region is able to moved back and forward from the trap and release position. When CO_2 is applied to the cryogenic region the temperature of the region was cooled down to the set-up temperature. The temperature range is important, with a minimum temperature of operation down to CO_2 (l) temperature and the upper temperature can be up to the oven temperature. In the release step, the cold region is moved away from the trapped zone to allow the solute to heat to the oven temperature and then be transferred to ^{2}D.

1.6.1 LMCS modes of separation

There are several ways to operate the cryotrap system depending on the modulator types, the nature of samples and research goals. Three operational modes of LMCS modulator in experiments can be identified; targeted multidimensional mode (TMDGC), comprehensive mode and targeted mode using micro-switching valves mode. All operational modes using the LMCS modulator have been reported by Marriott and colleagues [89] who invented the LMCS modulator. In two targeted modes, a normal GC run is performed in order to determine the modulation event timetable to effectively trap the entire peak and release it into ^{2}D at an exact time. In comprehensive mode, the cold region is moved in a small period of time called modulation period (P_M) resulting in the peak from ^{1}D being sliced into narrow sampled pulsed peaks. Truong et al [90] reported the comparison of chromatographic results such as peak areas, peak height and reproducibility obtained from normal GC, targeted mode and comprehensive mode in GC×GC analysis when the LMCS modulator was employed .

Nowadays, a retrofitted LMCS modulator and a short capillary column fitted into an existing GC system can make the GC system operational for advanced GC analysis. For example, 1D-GC can be performed when the modulator coolant is turned off; MDGC can be performed in targeted modes for specific regions in the chromatogram and for quantitative proposes; and finally, comprehensive mode is normally applied for the separation and characterization of very complex samples.

1.6.1.1 Targeted mode using LMCS modulator

Targeted operational mode in GC×GC using the LMCS modulator can be considered as a simplified version of heart-cutting in conventional MDGC. There is no switching valve nor any supplemental heating system involved. This operational mode of LMCS modulator have been reported and applied for the analysis of PAHs and drugs analysis [91,92]. To perform this mode, careful timed events selection for specific peaks or regions is required. Generally, normal 1D-GC

has to be performed to determine the required modulation event timetable in order to obtain an effective trapping of the entire peak and subsequent release into ^{2}D. The cryogenic region of the LMCS modulator is set to move at these predetermined times, so the entire peaks or regions will be trapped and then fully remobilised for further separation when the cryogenic region moves away from the compressed zone. Basically, while targeted peaks or regions are selected and transferred to the ^{2}D column, the rest of the chromatogram is restrained by the cryotrap from passing into the ^{2}D column. A longer ^{2}D column is possible to use in this operational mode when the separation of the selected peaks is not sufficient. Since data obtained from this operation are presented in time-response format, thus $^{2}t_{R}$ for a giving peak obtained is the time that analytes are retained in ^{2}D. The $^{2}t_{R}$ can be calculated by recording the retention time obtained from the experiment, minus the analyte release time to ^{2}D. In this mode, the selected peaks or region separation is enhanced as well as the intensity gained by the primary peaks. Peak intensity improves approximately 10 to 20 times, peak area is preserved, and this makes targeted operation perfect for trace and quantitative analysis. **Figure 1.22** shows an example obtained from targeted operational mode of LMCS modulation. A whole ‘single’ peak from ^{1}D was collected and re-injected into ^{2}D (1 to 5m) for further separation. In this case, three individual compounds were observed in the raw 2D-GC chromatogram obtained from one single peak at the outlet of ^{1}D. The difference in height h1 to h2 is the sensitivity increase; the resolution increases it also apparent.

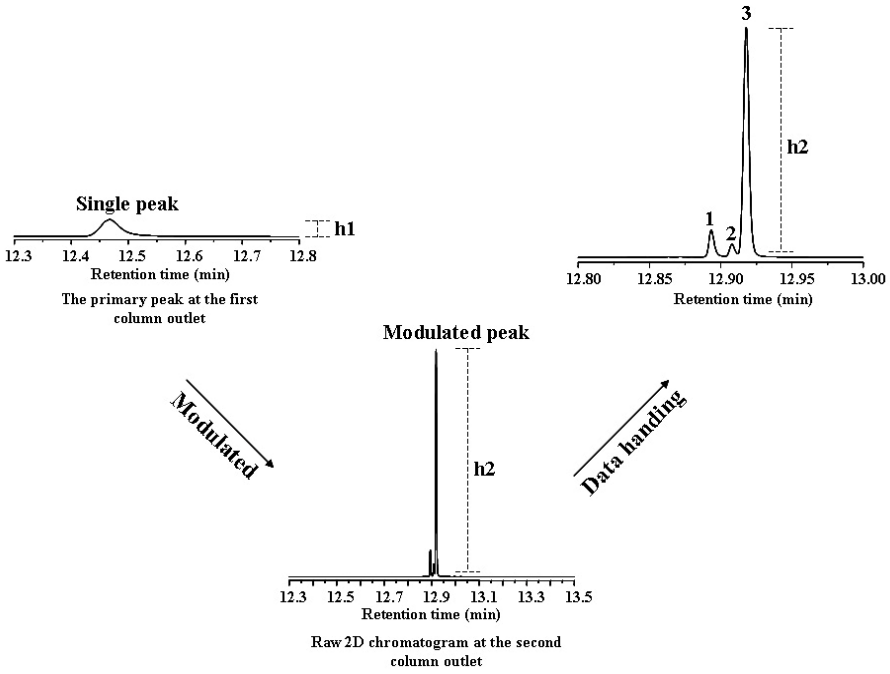

Figure 1.22: Example of the raw 1D-GC and 2D-GC chromatograms obtained from targeted operational mode, where a broad single peak is collected, focused, then released into a very high efficiency ^{2}D column.

1.6.1.2 Comprehensive mode using LMCS modulator

Comprehensive operational mode is the mode that is normally used for fundamental and application studies in GC×GC analysis since the LMCS modulator was introduced. It is an operational mode of choice for the analysis and characterisation of complex samples such as petroleum products, food, fragrance and perfume etc. Instead of a specific peak or region being cut and transfered to ^{2}D, in this mode the entire sample undergoes both dimension separations for further analysis. Therefore, every single compound contained in the sample will be sampled in small fractions, focused and then rapidly re-injected into ^{2}D. In comprehensive mode, a cold cryogenic region is moved in a small period of time (modulation period, P_M) to sample and compress a portion of first dimension peak. The modulation process (trap and release) will be performed simultaneously during the analysis time. Results obtained from this operational mode are a series of narrow pulsed peaks. Data generated in this mode are normally visualised in a two-dimensional arrangement

image where the first dimension retention time (^1t_R) is plotted against the second dimension retention time (^2t_R). GC×GC data interpretation and manipulation will be discussed later. **Figure 1.23** shows a 1D-GC chromatogram, the modulated peak distribution, and a colour plot obtained from GC×GC comprehensive mode. The small and broad primary peak is sliced into narrow peaks according to the modulation period. Peak height is increased while the summation of peak area of all the tall pulsed peaks will be equal to the primary peak area. The raw chromatogram is normally visualised as the contour or colour plot as shown. Each spot in the GC×GC result is a discrete peak. Peak intensity increase, the separation of co-eluted 1D compounds, and group type separation are advantages of this operational mode. The fundamentals and applications of this mode have been described elsewhere [93-96]

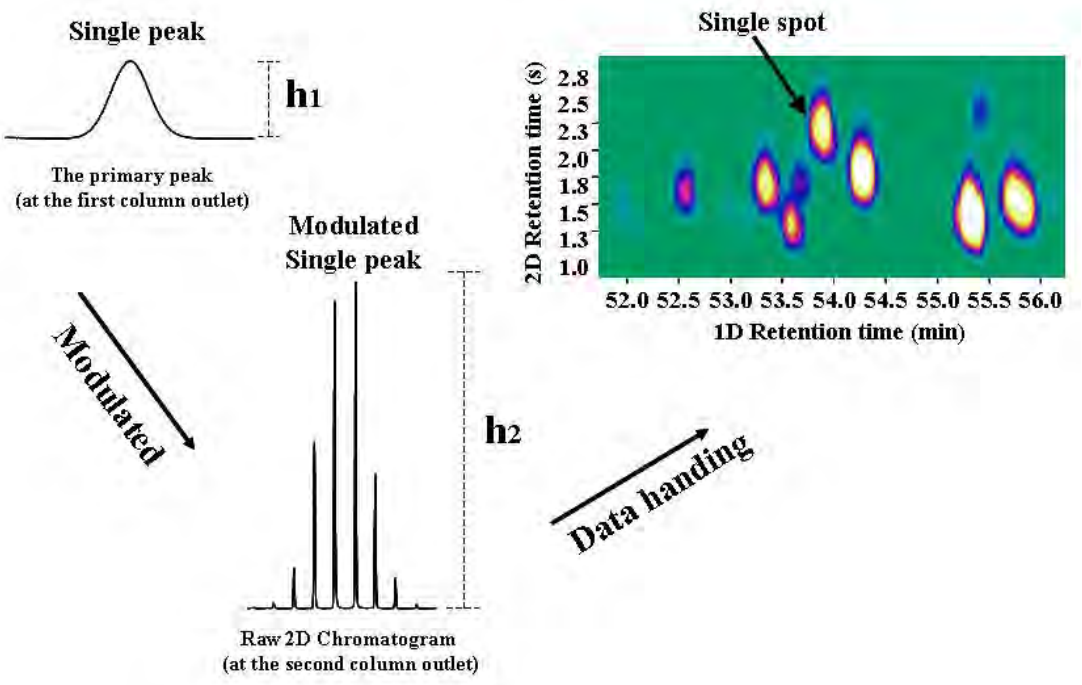

Figure 1. 23: Results obtained from GC×GC comprehensive mode.

1.6.1.3 Micro-switching valve mode using LMCS modulator

In this mode, LMCS was used as a modulator in MDGC to compress the region from the heart cutting process and send to the detector as a narrow band for detection. The essential device used in this mode is a valve called; "micro-switching valve". The heart cut process was performed by switching the valve at the target region of the chromatogram obtained from ^{1}D. The cut region then is sent to the LMCS modulator to re-focuses as a narrow band. Again, in this mode 1D-GC analysis has to be performed and used for timing events for the heart-cut process. Basically, the co-eluted peaks or complex region normally are cut and sent to ^{2}D for further separation. Advantages of this operational mode are similar to the targeted mode as stated above. However, band broadening, any leakage of the targeted region and any cold spots in the system from the valve body have to be considered. More detail of this operational mode was reported by Marriott and co-workers in 2003 [97] and applied for the quantitative analysis of suspected allergens in fragrance products [98,99]. **Figure 1.24** shows chromatograms obtained from the LMCS micro-switching valve mode. **A** and **B** were selected regions, both regions were cut and transferred to the LMCS modulator. The regions were compressed and re-injected into ^{2}D. Generally, peak width resulting from this operation is in the range of 50 to 200 ms at base and sensitivity is increased by approximately 20 to 30 times.

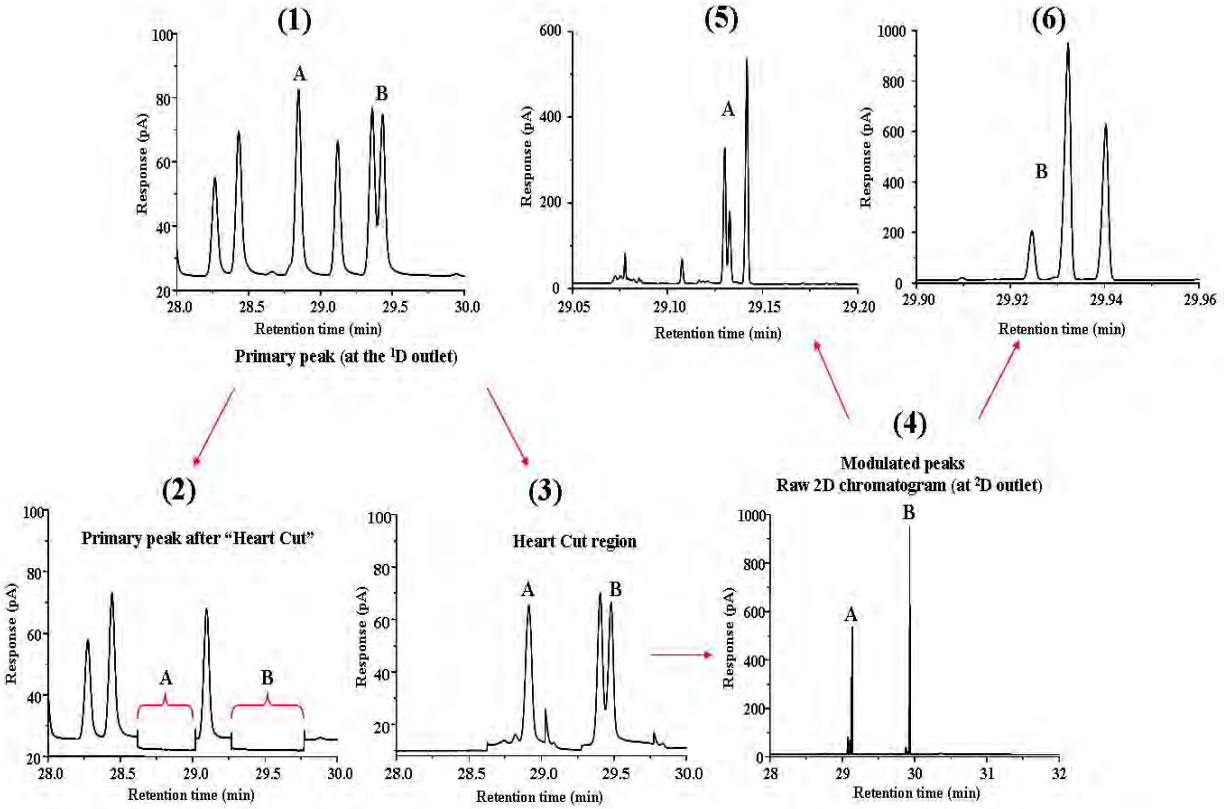

Figure 1.24: Results obtained from switching valve operational mode using LMCS modulator. Peak **A** and **B** are selected for cryotrapping, with all other peaks passed to a monitor detector. Cryotrapped peaks **(4)** are separately expanded **(5)** and **(6)**. Note, peaks at **(3)** are shown without cryotrap being initiated.

1.7 Detector technologies for GC×GC analysis

Flame ionisation detector (FID) was the first detector used in GC×GC systems due to a fast data acquisition rate up to 400 Hz. Nowadays, several detectors have been used as a detector for GC×GC systems, depending on the analytes of interest and the analysis aims, such as ECD, NPD, AED, SCD, NCD and Olfactory (GC×GC-O). They demonstrate variable levels of compatibility and potentiality to be used as a detector for a GC×GC system. Generally, widths of the pulsed peaks at the end of ^{2}D are approximately 60 ms. Therefore, the rise time of the detectors for GC×GC analysis have to be short. The detection systems have to be fast enough to detect very

fast peaks eluting from ^{2}D, hence the sampling rates have to be at least 50 to 100 Hz to ensure the proper reconstruction of the second dimension chromatogram.

It is important to note that all detectors mentioned above allow peak recognition but no corroborative identification or structure information. Therefore, the use of spectrometric detection especially quadrupole and time-of-flight mass spectrometry, qMS [100-103] and TOFMS [79,104,105] is rapidly growing in GC×GC. Detector technologies for GC×GC analysis have been reported [106] and more information will be discussed in the next Chapter.

1.8 GC×GC data handing and visualisation

Up till now, data presentation and software for the interpretation and handing of GC×GC data are still in a development stage. Basically, the large amount of data obtained from GC×GC may be handed by using in-house data conversion programs or some commercial packages. However, at this stage, it is enough to ensure that all small pulsed peaks of compounds of interest are correctly detected and assigned. In this study, raw data obtained from GC×GC analysis were exported in .csv format by using Chemstation software from Agilent Technologies. Then the .csv file was converted to ASCII matrices using an in-house conversion program (Marriott, RMIT, Melbourne, Australia). Then, the contour plot or colour plot was generated by the Transform Program (version 3.4, Fortner Research LLC, Sterling, VA, USA). **Figure 1.25** shows the raw-2D chromatogram obtained from GC×GC analysis and a contour plot which is generated by stacking of the raw-2D chromatograms side by side. The different intensity of each pulsed peak will be presented in different colour shade in the colour plot, depending on the contour level or the colour/intensity scale chosen.

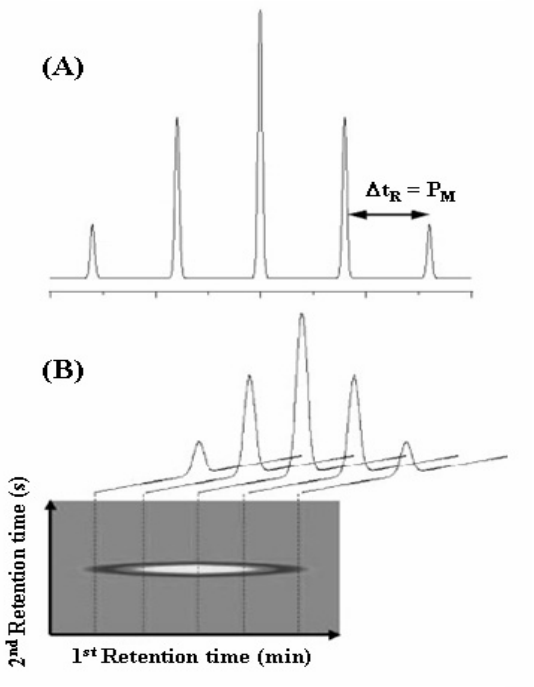

Figure 1.25: Raw 2D chromatogram and contour plot generation of a compound obtained from GC×GC analysis [27]

Different forms of data presentation can be used for different purposes; raw-2D chromatogram data may be used for the measurement of basic parameters of chromatographic analysis; summed data may be used in quantitative analysis; the 2D plot can be used for validation purposes. The contour plot or 3D plots are normally used to visualize separation of the compounds of interest within the separation space. In some cases, the 3D plot can be generated, containing two retention times (^1t_R (min) and ^2t_R (s)) of compounds obtained from GC×GC analysis, plotted against a signal intensity as a third axis. **Figure 1.26** shows the visualisation format of the data obtained from GC×GC analysis.

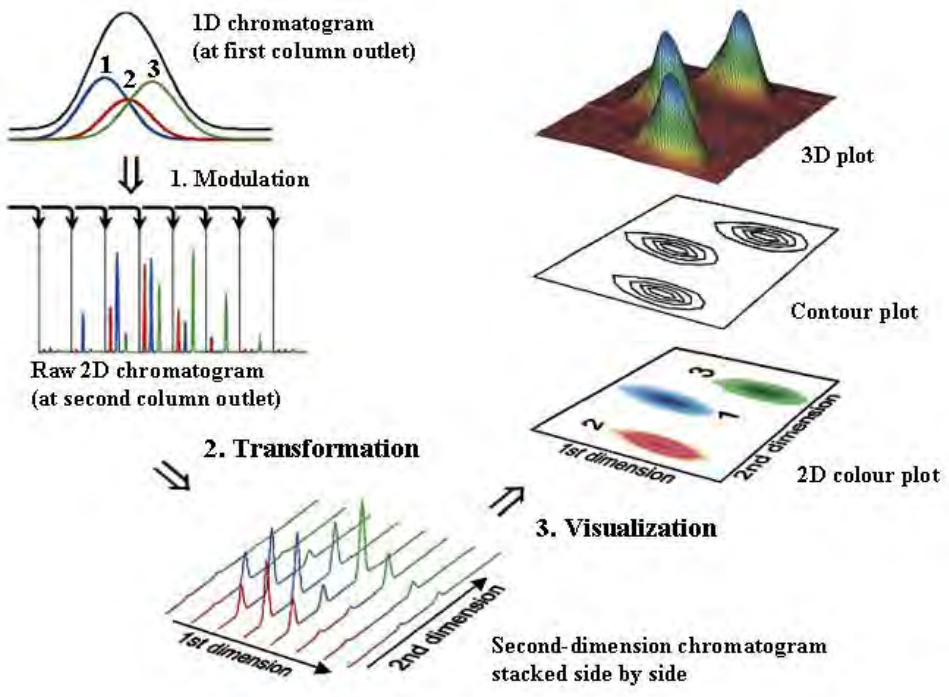

Figure 1.26: Presents visualization of data obtained from GC×GC analysis [72].

1.9 GC×GC optimisation parameters

In GC×GC analysis, several parameters have to be considered in the optimisation step, such as oven temperature program, column combination, detector type and modulation period (P_M) of modulator, in order to achieve the best separation. The temperature program used in GC×GC for the first and the second dimension separation is critical. Basically, the oven temperature program used in GC×GC will be relatively slow with a low temperature ramp rate in order to separate target analytes from each other and from the sample matrix on classical type columns. The column combination is normally tested before the analysis will be performed. Detector conditions, especially when a selective detector is used, have to be optimised. von Mühlen and colleagues reported the modification of a NPD detector and the optimisation of NPD detector gas flows for petroleum sample analysis.[107,108]. However, the optimum chromatographic condition used in GC×GC is aimed not just only for the best separation but also to avoid wrap around occurrence during the

analysis. Therefore, the P_M has to be optimized for the ^2D separation. Principally, an acceptable value of P_M used should be approximately the same as the ^1D peak standard deviation (σ) in order to get about three to four pulsed peaks, or to obtain M_R value of about 3 to 4 to preserve the resolution obtained from ^1D. If P_M is too small, some peaks may not elute within one modulation cycle, and can cause peak wrap around. More details of wrap around phenomena will be discussed in the next section. **Figure 1.27** shows the strategies to reduce wrap around in GC×GC analysis based on optimisation of parameters in the second dimension. The strategies to reduce wrap around are listed below;

1.) A longer ^2D can cause wrap around, therefore ^2D column lengths of about 0.5 to 1 m are widely used in all analyses. The reduction of ^2D column length provides faster solute elution and a smaller analyte retained time in ^2D.

2.) Increased carrier gas velocity will reduce the residence time in ^2D of the target analytes, but causes peaks to elute earlier in ^1D which increase ^2t_R.

3.) Higher temperature programme and ramp rate will reduce the ^2t_R elution time of the target analysis, and increase T_e.

4.) P_M used in TMDGC analysis has to be longer than the time that analytes spend in ^2D to allow the target analyte to move from ^2D to the detector within a single P_M.

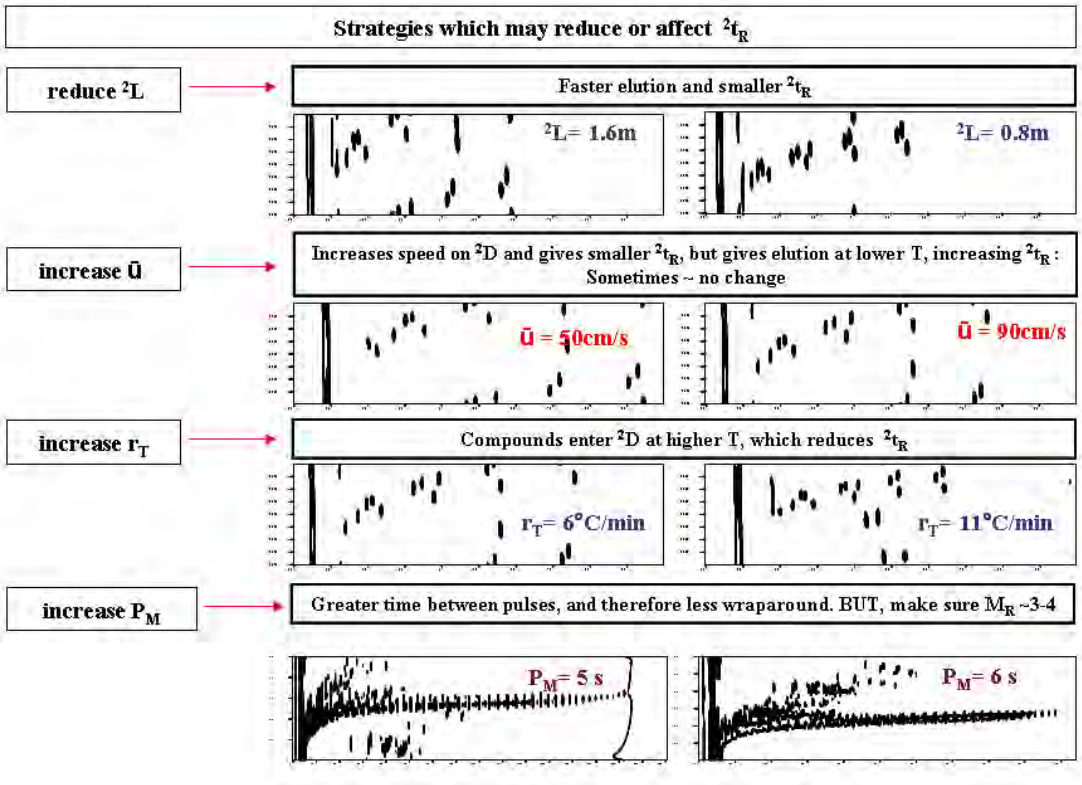

Figure 1.27: Optimisation steps to reduce wrap around phenomena in GC×GC. This optimise strategy is normally used in Australian Centre for Research on Separation Sciences, (ACROSS), school of Applied Sciences, RMIT University.

Several researchers have studied parameters and the effect of both columns to achieve the separation goals. For example; Ong et al. [109] studied the influence of chromatographic conditions for GC×GC analysis as well as the optimisation of chromatographic condition for the analysis of polychlorinated dibenzo-p-dioxins (PCDDs) and dibenzofurans (PCDFs), and GC×GC-TOFMS was reported by Hoh and colleagues in 2007 [110].

Banerjee and co-workers [111] reported the optimization of separation and detection condition for the multiresidue analysis of pesticides in grapes by GC×GC-TOFMS. The developed method can resolve the co-elution problem of 51 pesticides within a 24 min run time with library-searchable mass spectrometric confirmation. In this study, a similar approach to Hoh and co-workers was attempted to optimize separation such as the temperature program for 1D-GC separation, before optimisation of oven temperature of GC×GC. The optimum separation of 51 analytes

was evaluated in terms of resolution ($Rs = 2\Delta t_R / (w_1+w_2)$), where Δt_R represents the difference in t_R of two adjacent peaks and w_1 and w_2 are their width at base. Then the optimum chromatographic condition was applied in the GC×GC optimisation strategies. The study demonstrated that GC×GC parameters, and P_M have to be adjusted depending on the oven temperature program used to minimise wrap around occurrence.

1.10 Wrap around phenomena in GC×GC

In GC×GC analysis, it is often stated that the minimum number of modulation per ^1D peak should be at least three to four modulations, to preserve the first dimension resolution. In terms of the modulation ratio concept (M_R) the P_M should be equal to about one standard deviation (σ) of the ^1D peak width to maintain the M_R value of about 3 to 4 [112]. This indicates that P_M is a critical parameter in the GC×GC experiment. The P_M can be estimated by using the M_R concept, and then used as the selected P_M for GC×GC experiment. However, there is no guarantee that analytes will elute from ^2D within the chosen P_M. The analyte ^2t_R may exceed P_M such that it elutes during subsequent modulation cycles, which can cause co-elution with compounds in that modulation cycle.

Thus, wrap around in GC×GC is a phenomenon where the analytes are retained in the ^2D column longer than modulation period used in the particular experiment. However, there are no problems from this phenomenon unless they interfere or co-elute with analytes of interest. Generally, the wrap around peak appears as a broader peak shape due to the longer time spent in the ^2D column.

References

[1] M. Harju, C. Danielsson, P. Haglund, J. Chromatogr. A 1019 (2003) 111.

[2] M. Zakaria, M.-F. Gonnord, G. Guiochon, J. Chromatogr. 271 (1983) 127.

[3] J.C. Giddings, Anal. Chem. 56 (1984) 1259A.

[4] J.C. Giddings, " Use of Multiple Dimensions in Analytical Separations" In Multidimensional Chromatography Cortes, H.J. Ed. (1990) New York.

[5] J.M. Davis, J.C. Giddings, Anal. Chem. 55 (1983) 418.

[6] J.M. Davis, J.C. Giddings, Anal. Chem. 57 (1985) 2178.

[7] J.C. Giddings, J. Chromatogr. A 703 (1995) 3.

[8] D.R. Deans, Chromatographia 1 (1968) 18.

[9] G. Schomburg, H. Husmann, F. Weeke, J. Chromatogr. 112 (1975) 205.

[10] W. Bertsch, J. High Resol. Chromatogr. 85 (1978) 289.

[11] F. Begnaud, A. Chaintreau, J. Chromatogr. A 1071 (2005) 13.

[12] P. Marriott, R. Shellie, Trends Anal. Chem. 21 (2002) 573.

[13] Z. Liu, J.B. Phillips, J. Chromatogr. Sci. 29 (1991) 227.

[14] R.C.Y. Ong, P.J. Marriott, J. Chromatogr. Sci. 40 (2002) 276.

[15] M. Adahchour, J. Beens, R.J.J. Vreuls, U.A.T. Brinkman, Trends Anal. Chem. 25 (2006) 438.

[16] M. Adahchour, J. Beens, R.J.J. Vreuls, U.A.T. Brinkman, Trends Anal. Chem. 25 (2006) 540.

[17] M. Adahchour, J. Beens, R.J.J. Vreuls, U.A.T. Brinkman, Trends Anal. Chem. 25 (2006) 726.

[18] M. Adahchour, J. Beens, R.J.J. Vreuls, U.A.T. Brinkman, Trends Anal. Chem. 25 (2006) 821.

[19] T. Gorecki, J. Harynuk, O. Panic, J. Sep.Sci. 27 (2004) 359.

[20] T. Gorecki, O. Panic, N. Oldridge, J. Liq. Chromatogr. Relat. Technol. 29 (2006) 1077.

[21] M.M. van Deursen, J. Beens, H.G. Janssen, P.A. Leclercq, C.A. Cramers, J. Chromatogr. A 878 (2000) 205.

[22] J.B. Phillips, J. Beens, J. Chromatogr. A 856 (1999) 331.

[23] J.B. Phillips, J. Xu, J. Chromatogr. A 703 (1995) 327.

[24] P.J. Marriott, R.M. Kinghorn, Anal. Chem. 69 (1997) 2582.

[25] Y. Shen, M.L. Lee, Anal. Chem. 70 (1998) 3853.

[26] Y. Shen, M.L. Lee, Chromatographia 49 (1999) 333.

[27] R. Shellie, P. Marriott, Flavour Frag. J. 18 (2003) 179.

[28] G. Schomburg, J. Chromatogr. A 703 (1995) 309.

[29] W. Bertsch, J. High Resol. Chromatogr. 22 (1999) 647.

[30] W. Bertsch, J. High Resol. Chromatogr. 23 (2000) 167.

[31] L.M. Blumberg, J. Chromatogr. A 985 (2003) 29.

[32] J. Harynuk, T. Gorecki, J. de Zeeuw, J. Chromatogr. A 1071 (2005) 21.

[33] C.J. Venkatramani, J. Xu, J.B. Phillips, Anal. Chem. 68 (1996) 1486.

[34] L.M. Blumberg, F. David, M.S. Klee, P. Sandra, J. Chromatogr. A 1188 (2008) 2.

[35] P.J. Schoenmaker, P.J. Marriott, J. Beens, LC-GC Europe (2003) 1.

[36] C. von Muhlen, C.A. Zini, E.B. Caramao, P. Marriott, Quimica Nova 30 (2007) 682.

[37] D. Ryan, P. Morrison, P. Marriott, J. Chromatogr. A 1071 (2005) 47.

[38] M.J.D. Somenath, John Wiley & Sons 0471328456 (2003) 488.

[39] Supelco, Supelco Bulletin 923 (1998) 1.

[40] T. Gorecki, J. Pawliszyn, Anal. Chem. 67 (1995) 3265.

[41] M. Adahchour, J. Beens, R.J.J. Vreuls, A.M. Batenburg, E.A.E. Rosing, U.A.T. Brinkman, Chromatographia 55 (2002) 361.

[42] M. Adahchour, J. Wiewel, R. Verdel, R.J.J. Vreuls, U.A.T. Brinkman, J. Chromatogr. A 1086 (2005) 99.

[43] A. Williams, D. Ryan, A. Olarte Guasca, P. Marriott, E. Pang, J. Chromatogr. B: Biomed. Appl. 817 (2005) 97.

[44] D. Ryan, P. Watkins, J. Smith, M. Allen, P. Marriott, J. Sep. Sci. 28 (2005) 1075.

[45] J. Schnelle-Kreis, W. Welthagen, M. Sklorz, R. Zimmerman, J. Sep. Sci. 28 (2005) 1648.

[46] Z. Ozel Mustafa, F. Gogus, C. Lewis Alastair, J. Chromatogr. A 1114 (2006) 164.

[47] D.E. Clay, R. Wenske, R. Anderson, Thermo Electron Corporation Application note.

[48] W. Engewald, J. Teske, J. Efer, J. Chromatogr. A 842 (1999) 143.

[49] J.-F. Focant, A. Sjödin, D.G. Patterson, J. Chromatogr. A 1019 (2003) 143.

[50] J. Harynuk, P.J. Marriott, Anal. Chem. 78 (2006) 2028.

[51] J.-M. Dimandja, Mediterranean Separation Science Symposium University of Messina (July, 2005).

[52] J. Dallüge, M. van Rijn, J. Beens, R.J.J. Vreuls, U.A.T. Brinkman, J. Chromatogr. A 965 (2002) 207.

[53] D. Cavagnino, P. Magni, G. Zilioli, S. Trestianu, J. Chromatogr. A 1019 (2003) 211.

[54] P. Magni, T. Porzano, J. Sep. Sci. 26 (2003) 1491.

[55] J.V. Seeley, J. Chromatogr. A 962 (2002) 21.

[56] N.E. Watson, J.M. Davis, R.E. Synovec, Anal. Chem. 79 (2007) 7924.

[57] R. Shellie, L. Mondello, P. Marriott, G. Dugo, J. Chromatogr. A 970 (2002) 225.

[58] C. von Muhlen, C.A. Zini, E.B. Caramao, P.J. Marriott, Quimica Nova 29 (2006) 765.

[59] P.J. Marriott, P. Haglund, R.C.Y. Ong, Clin. Chim. Acta 328 (2003) 1.

[60] M. Adahchour, J. Beens, R.J.J. Vreuls, A.M. Batenburg, U.A.T. Brinkman, J. Chromatogr. A 1054 (2004) 47.

[61] B. Vlaeminck, J. Harynuk, V. Fievez, P. Marriott, European Journal of Lipid Science and Technology 109 (2007) 757.

[62] A.L. Lee, A.C. Lewis, K.D. Bartle, J.B. McQuaid, P.J. Marriott, J. Microcolumn Sep. 12 (2000) 187.

[63] E.M. Kristenson, P. Korytár, C. Danielsson, M. Kallio, M. Brandt, J. Mäkelä, R.J.J. Vreuls, J. Beens, U.A.T. Brinkman, J. Chromatogr. A 1019 (2003) 65.

[64] C.A. Bruckner, B.J. Prazen, R.E. Synovec, Anal. Chem. 70 (1998) 2796.

[65] B.J. Prazen, R.E. Synovec, B.R. Kowalski, Anal. Chem. 70 (1998) 218.

[66] C.G. Fraga, B.J. Prazen, R.E. Synovec, Anal. Chem. 72 (2000) 4154.

[67] C.G. Fraga, B.J. Prazen, R.E. Synovec, J. High Resol. Chromatogr. 23 (2000) 215.

[68] B.J. Prazen, K.J. Johnson, A. Weber, R.E. Synovec, Anal. Chem. 73 (2001) 5677.

[69] J.V. Seeley, F. Kramp, C.J. Hicks, Anal. Chem. 72 (2000) 4346.

[70] J.V. Seeley, F.J. Kramp, K.S. Sharpe, J. Sep. Sci. 24 (2001) 444.

[71] T. Gorecki, J. Harynuk, O. Panic, J. Sep. Sci. 27 (2004) 359.

[72] J. Dalluge, J. Beens, U.A.T. Brinkman, J. Chromatogr. A 1000 (2003) 69.

[73] C. Vendeuvre, R. Ruiz-Guerrero, F. Bertoncini, L. Duval, D. Thiebaut, Oil & Gas Science and Technology 62 (2007) 43.

[74] M. Pursch, K. Sun, B. Winniford, H. Cortes, A. Weber, T. McCabe, J. Luong, Anal. Bioanal. Chem. 373 (2002) 356.

[75] J.B. Phillips, R.B. Gaines, J. Blomberg, F.W.M. Van Der Wielen, J.-M. Dimandja, V. Green, J. Granger, D. Patterson, L. Racovalis, H.-J. De Geus, J. De Boer, P. Haglund, J. Lipsky, V. Sinha, E.B. Ledford, Jr., J. High Resol. Chromatogr. 22 (1999) 3.

[76] J. Beens, J. Dalluge, M. Adahchour, R.J.J. Vreuls, U.A.T. Brinkman, J. Microcolumn Sep. 13 (2001) 134.

[77] E.B. Ledford, Jr., C. Billesbach, J. High Resol. Chromatogr. 23 (2000) 202.

[78] J. Beens, M. Adahchour, R.J.J. Vreuls, K. van Altena, U.A.T. Brinkman, J. Chromatogr. A 919 (2001) 127.

[79] J.-F. Focant, E.J. Reiner, K. MacPherson, T. Kolic, A. Sjodin, D.G. Patterson, S.L. Reese, F.L. Dorman, J. Cochran, Talanta 63 (2004) 1231.

[80] C. Vendeuvre, F. Bertoncini, L. Duval, J.-L. Duplan, D. Thiebaut, M.-C. Hennion, J. Chromatogr. A 1056 (2004) 155.

[81] T. Hyoetylaeinen, M. Kallio, K. Hartonen, M. Jussila, S. Palonen, M.-L. Riekkola, Anal. Chem. 74 (2002) 4441.

[82] M. Kallio, T. Hyoetylaeinen, M. Jussila, K. Hartonen, S. Palonen, M. Shimmo, M.-L. Riekkola, Anal. Bioanal. Chem. 375 (2003) 725.

[83] E.B.J. Ledford, C. Billesbach, J. TerMaat, Pittcon March Contribution#2262P (2002) 17.

[84] P.J. Marriott, R.M. Kinghorn, J. High Resol. Chromatogr. 19 (1996) 403.

[85] R.M. Kinghorn, P.J. Marriott, J. High Resol. Chromatogr. 21 (1998) 620.

[86] R.M. Kinghorn, P.J. Marriott, J. High Resol. Chromatogr. 23 (2000) 245.

[87] R.M. Kinghorn, P.J. Marriott, J. High Resol. Chromatogr. 22 (1999) 235.

[88] P.J. Marriott, R.M. Kinghorn, Anal. Sci. 14 (1998) 651.

[89] P.J. Marriott, R.C.Y. Ong, R.A. Shellie, Environmental Application Note 33 (2001) 44.

[90] T.T. Truong, P.J. Marriott, N.A. Porter, R. Leeming, J. Chromatogr. A 1019 (2003) 197.

[91] P.J. Marriott, R.C.Y. Ong, R.M. Kinghorn, P. Morrison, J. Chromatogr. A 892 (2000) 15.

[92] A.J. Kueh, P.J. Marriott, P.M. Wynne, J.H. Vine, J. Chromatogr. A 1000 (2003) 109.

[93] P. Marriott, K. Aryusuk, R. Shellie, D. Ryan, K. Krisnangkura, V. Schurig, O. Trapp, J. Chromatogr. A 1033 (2004) 135.

[94] M. Junge, S. Bieri, H. Huegel, P.J. Marriott, Anal. Chem. 79 (2007) 4448.

[95] W. Khummueng, C. Trenerry, G. Rose, P.J. Marriott, J. Chromatogr. A 1131 (2006) 203.

[96] G. Purcaro, P. Morrison, S. Moret, L.S. Conte, P.J. Marriott, J. Chromatogr. A 1161 (2007) 284.

[97] P. Marriott, M. Dunn, R. Shellie, P. Morrison, Anal. Chem. 75 (2003) 5532.

[98] M. Dunn, R. Shellie, P. Morrison, P. Marriott, J. Chromatogr. A 1056 (2004) 163.

[99] M.S. Dunn, N. Vulic, R.A. Shellie, S. Whitehead, P. Morrison, P.J. Marriott, J. Chromatogr. A 1130 (2006) 122.

[100] M. Adahchour, M. Brandt, H.-U. Baier, R.J.J. Vreuls, A.M. Batenburg, U.A.T. Brinkman, J. Chromatogr. A 1067 (2005) 245.

[101] S.M. Song, P. Marriott, P. Wynne, J. Chromatogr. A 1058 (2004) 223.

[102] P. Korytar, J. Parera, P.E.G. Leonards, J. de Boer, U.A.T. Brinkman, J. Chromatogr. A 1067 (2005) 255.

[103] L. Mondello, A. Casilli, P.Q. Tranchida, G. Dugo, P. Dugo, J. Chromatogr. A 1067 (2005) 235.

[104] D. Ryan, R. Shellie, P. Tranchida, A. Casilli, L. Mondello, P. Marriott, J. Chromatogr. A 1054 (2004) 57.

[105] T. Cajka, J. Hajslova, J. Cochran, K. Holadova, E. Klimankova, J. Sep.Sci. 30 (2007) 534.

[106] C. von Muhlen, W. Khummueng, C.A. Zini, E.B. Caramao, P.J. Marriott, J. Sep. Sci. 29 (2006) 1909.

[107] C. von Muhlen, C.A. Zini, E.B. Caramao, P.J. Marriott, J. Chromatogr. A 1105 (2006) 39.

[108] C. von Muhlen, E.C. de Oliveira, P.D. Morrison, C.A. Zini, E.B. Caramao, P.J. Marriott, J. Sep. Sci. 30 (2007) 3223.

[109] R. Ong, P. Marriott, P. Morrison, P. Haglund, J. Chromatogr. A 962 (2002) 135.

[110] E. Hoh, K. Mastovska, S.J. Lehotay, J. Chromatogr. A 1145 (2007) 210.

[111] K. Banerjee, S.H. Patil, S. Dasgupta, D.P. Oulkar, S.B. Patil, R. Savant, P.G. Adsule, J. Chromatogr. A 1190 (2008) 350.

[112] W. Khummueng, J. Harynuk, P.J. Marriott, Anal. Chem. 78 (2006) 4578.

Chapter

2

OVERVIEW OF DETECTOR TECHNOLOGIES FOR COMPREHENSIVE TWO-DIMENSIONAL GAS CHROMATOGRAPHY

This chapter has been published as "Overviews of Detector Technologies for Comprehensive Two-Dimensional Gas Chromatography", by von Mühlen C., Khummueng W., Zini C.A., Caramão E. B., Marriott P. J., J. Sep. Sci., 29, 1909-1921 (2006)

Abstract

The detector is an integral and important part of any chromatographic system. The chromatographic results should, ideally, be unaffected by the detector – it should only provide the sensing capacity required at the end of a column separation process. The relatively new technique of comprehensive two-dimensional gas chromatography (GC×GC) extends the performance of GC many folds, but comes at a price – existing GC systems may not be adequately designed with the requirements of GC×GC in mind. This is primarily the need for precise measurement of very fast peak fluxes entering the detector (e.g. as fast as 50 ms width in some instances). The capacity for the detector to closely track a rapidly changing chromatographic peak profile depends on a number of factors, from design of flow paths and make-up gas introduction, type of detector response mechanism, and the chemistry of the response. These factors are discussed here as a means to appreciating the technical demands of detection in GC×GC.

2.1 Introduction

Comprehensive two-dimensional gas chromatography (GC×GC) is now firmly established on the gas chromatography scene. By any measure, GC×GC has significantly altered the way in which the GC experiment is conducted, **Figure 2.1**. From modulation of the migrating chromatographic band, to data presentation, experimental set-up, and even terminology, the analyst who performs GC×GC is faced with negotiating their way through coupled column systems, routinely performing very fast (ultra-fast in some instances) separations, interpreting their results from a new viewpoint, and optimising the experiment in ways that are, whilst ultimately logical, a significant departure from the classical single column experiment. One of the less-considered aspects of the GC×GC experiment is the detector. It is due to the extra separation performance that reduces the need for a selective detector, or the reliance on the FID workhorse, or the belief that there will be operational difficulties with most selective detectors in GC×GC, there is a lack of information in the literature on alternative detectors for use with GC×GC. The applications of element selective detectors with GC×GC presented in the literature are summarized on **Table 2.1**.

The first question likely to be asked when adapting a different detector for use with GC×GC will be acquisition speed. Since the normal GC×GC experiment produces peaks at the end of the second dimension column on the order of 100 ms (or less), which pass into the detector, the chromatographer is dealing with peaks that are perhaps 10-50 times narrower than any they have previously had to contemplate. Detector speed has two connotations. The first is the electronic processing of the output of the transducer (A-D conversion) to input the signal into a computerised data system. The second is a chemical-physical consideration. How fast does the detector respond to the input chemical signal, and produce an electronic measure of the instantaneous amount of the chemical? This is the effectiveness of the detector as a chemical transducer, and ultimately must take into consideration the detector geometry, the detector and make-up gas flow rates, any unswept volumes, chemical reactions in flames, plasmas, or at surfaces, and the sensing elements recording the

signal changes. Whilst the community recognises the revolution that took place when packed columns gave way to the general acceptance of capillary GC, and that the manufacturing industry had to redesign their equipment to cater for the demands of injection and detection systems that had to operate with carrier flows maybe 10-50 times smaller in the capillary system, it is probably just as much of a technical challenge to take the step to GC×GC technology. Will current detectors adequately cope with this new requirement? Will there need to be a 'third generation' of detector developments to provide performance commensurate with the GC×GC peak flux.

This chapter seeks to provide an insight into the applications of GC×GC that have employed different detectors, to give an example of the information the authors sought, and indicate whether the detector succeeded in providing an acceptable level of performance in maintaining the quality of the GC separation, or whether the analyst has to accept a performance compromise at the end of the column. The chapter concludes by proposing the suitability of different detectors, which have been used for GC×GC, to this purpose.

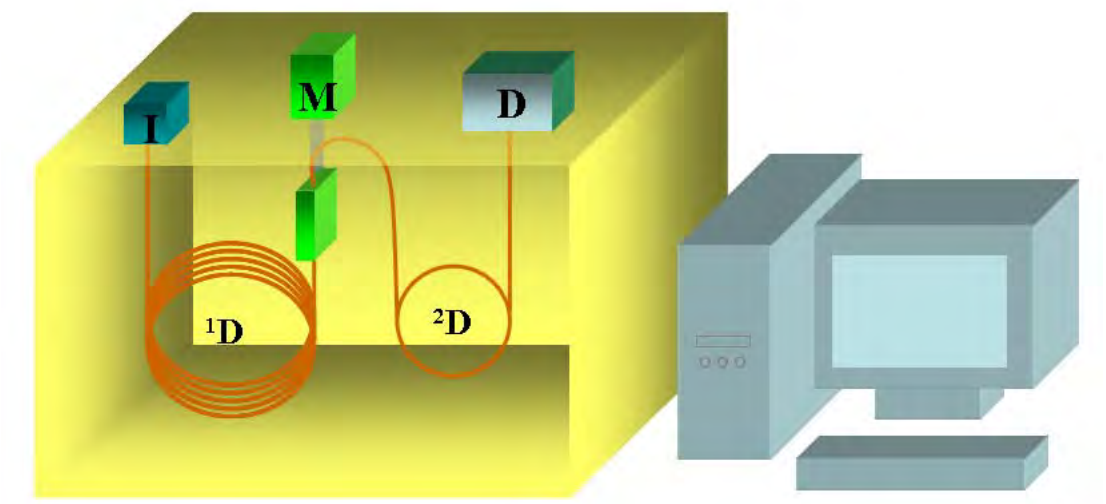

Figure 2.1: Schematic diagram of the GC×GC instrument, showing use of a short, fast elution second dimension column which produces very narrow peaks at the detector. Where: I – Injector; ^{1}D – First column; ^{2}D – Second column; M – Modulator; D – Detector.

Table 2.1: Applications of comprehensive two-dimensional gas chromatography with element-selective detectors.

Detector	Analyte	Column sets	Det. temp. (°C)	Acquisition rate (Hz)	Reference
NPD	methoxypyrazines in wine	BPX5 (30 m x 0.25 mm x 0.25 μm) BP20 (1 m x 0.1 mm x 0.1 μm)	300	100	[1]
NPD	N-containing compounds in heavy gas oil	BPX5 (30 m x 0.25 mm x 0.50 μm) BPX-50 (1 m x 0.15 mm x 0.15 μm)	325	50	[2]
NPD/qMS	Nanoparticles in roadside atmosphere	BPX5 (30 m x 0.25 mm x 0.25 μm) BPX-50 (1 m x 0.10 mm x 0.10 μm)	-	100	[3]
μECD	CBs, PCDDs, PCDFs	1. HP-1 (30 m x 0.25 mm x 0.25 μm) HT-8 (1 m x 0.1 mm x 0.1 μm) 2. HP-1 (30 m x 0.25 mm x 0.25 μm) SupelcoWax-10 (1 m x 0.1 mm x 0.1 μm)	300	50	[4]
μECD	toxaphene	HP-1 (30 m x 0.25 mm x 0.25 μm) HT-8 (1 m x 0.1 mm x 0.1 μm)	300	50	[5]
μECD	2,3,7,8,-substituted PCDDs, PCDFs and PCBs	DB-XLB (30 m x 0.25 mm x 0.25 μm) LC-50 (0.9 m x 0.18 mm x 0.1 μm)	300	50	[6]
μECD	Chiral PCBs	BGB-176SE (30 m x 0.25 mm x 0.25 μm) SupelcoWax-10 (2 m x 0.18 mm x 0.1 μm)	300	50	[7]
μECD	2,3,7,8,-substituted PCDDs, PCDFs and PCBs	DB-XLB (30m x 0.25 mm x 0.25μm) LC-50 (0.9 m x 0.18 mm x 0.15 μm)	300	50	[8]
μECD	Atropisomeric PCBs	Chirasil-Dex CB (10 m x 0.1 mm x 0.1 μm) LC-50 (1.0 m x 0.1 mm x 0.15 μm)	260	50	[9]
SCD	sulphur containing compounds	Vary five column sets	800	100	[10]
SCD	sulphur containing compounds in light catalytically cracked cycle oil (LCCCO)-heavy gas oil (HGO) mixture	DB-1 (10 m x 0.25 mm x 0.25 μm) BPX-50 (17.5 m x 0.1 mm x 0.05 μm)	800	50	[11]
SCD	Sulphur containing compounds in crude oils	VB-5 (6 m x 0.18 mm x 3.5 μm) 007-17 (2 m x 0.1 mm x 0.1 μm)	800	50	[12]
NCD	Nitrogen-containing compounds in diesel fuel	SPB-5 (30 m x 0.25 mm x 0.1 μm) BPX-50 (3 m x 0.25 mm x 0.25 μm)	-	100	[13]
AED	sulfur-containing compounds in crude oil	DB1 (15 m x 0.25 mm x 0.25 μm) BPX50 (0.6 m x 0.1 mm x 0.1 μm)	cavity 300	10	[14]

2.2 GC×GC detectors

2.2.1 Flame Ionization Detector (FID)

Flame ionization detection (FID) is more used in gas chromatography than any other method for signal detection [15,16]. FID was also the first detector applied to GC×GC [17], specifically because it was the only universal detector that presents an acquisition rate up to 200 Hz, fast enough to measure properly the fast GC×GC peak at the end of the ^{2}D column [18,19]. As implied by its name, the FID works because burning of carbon compounds produces ions in the flame. A schematic diagram of a FID detector is presented in **Figure 2.2**. The FID system is a "carbon counting" device because hydrocarbons give ionization responses in proportion of the number of carbon atoms [15].

$$C-compound \xrightarrow{FID\ flame} CHO^{+} \xrightarrow{H_2O} \left[H_3O\left(H_2O\right)_n\right]^{+} + CO \qquad (1)$$

Thus the ion current generated will be proportional to the amount of C-compound present, and the ion-generation reaction is fast (**shown in Equation 1**). However, the chemical nature of the sample molecule influences the effectiveness of the carbon atom in producing a flame ionization response [20]. This is reflected in the varying response factors found for different compounds; however there is an equal response factor for a given class of compounds, in many cases. The development of FID took place on an empirical basis, with little understanding of the basic principles involved. The study of flames by mass spectrometry showed that an important intermediate ion was the formylium ion, CHO^{+} [15]. The latest study on the mechanism was done by Holm [21], using a fused silica capillary probe to take samples from the flame, with analysis by GC/MS. This experiment showed that degradation of all hydrocarbons to methane takes place at low temperatures by the reaction of hydrogen atoms which are generated in the burning air-hydrogen flame. Compounds containing a single halogen atom may undergo elimination or hydrogenation in the flame. The detector response obtained from fully halogenated

compounds is still not fully understood. Other heteroatom and isotope effects were also presented in that report. The use of FID as a universal GC×GC detector has produced impressive results in terms of sensitivity, resolution, and quantitation capabilities, in comparison to the system for one dimensional (1D) GC. It is apparent for analyses the traditionally required MS detection (ie. where unresolved peaks are to be quantified), it is now possible that a non-spectroscopic detector can be employed – if the peaks are fully resolved, then ideally they can be quantified. The fast ionization and acquisition process, and negligible internal volume [22] minimizes the contribution of the detector to peak broadening. As a result, the FID produces narrower peaks than other detectors, a very important characteristic for GC×GC where the short ^{2}D column and its limited peak capacity demands maximum or high efficiency on that column. Other positive aspects of the FID include a very large linear range – 10^{6} or 10^{7} – depending on the system [23-27] – due to the fast ionization and acquisition process, and detection limits ranging from 2 to 5 pg carbon.s^{-1}, depending on the detected compound. FID is also an extremely robust detector, requiring little experience to operate, and produces reliable operation and stability. Because of this characteristic, limited information is generally available about the detection conditions in the GC×GC-FID literature, other than simple mention that the FID was used. Generally, this information is sufficient to get reproducible results, as the other analytical parameters are given. Despite the obvious performance comparison of conventional GC and GC×GC detectors, the higher information obtained via the separation space in the GC×GC plots in ways hitherto impossible in GC analysis, along with the sensitivity and resolution enhancement afforded by GC×GC operation, gives the FID a special position. With GC×GC, the FID is not only used as a quantitation tool [28] associated with or without GC×GC-MS data [29] or GC×GC-TOFMS [30], but may be used for peak identification, due to the structure of chemical classes shown on the 2D plot (roof-tile effect). The identification and diagnosis capabilities of the FID were employed for environmental problems [31-33], industrial process evaluation [34,35], and other analytical problems impossible to be solved before GC×GC implementation, even with a GC/MS system [36]. Exemplifying a GC×GC-FID application, Beens and collaborators [37] have characterized non-

aromatic solvents using GC×GC-FID. Several compounds were separated and grouped in different bands, where it was possible to see that not only the alkenes were separated from the naphthenes, but also that the mono- and di-naphthenes were grouped in different bands. However, within the alkane band, there is still overlap between alkanes with different carbon numbers.

The PIONA (Paraffins, Iso-paraffins, Olefins, Naphthenes, Aromatics) analyzer, usually employed for this kind of analysis, fails to completely separate naphthenes and alkanes with carbon numbers exceeding eleven (and it is a time-consuming analytical process). Since the carbon number distribution of hydrocarbon solvents ranges from seven to twenty, the GC×GC system was able to separate a larger range of compounds than the time consuming and complex PIONA analysis. The same group [38] also presented a comparison of group-type quantitation of heavy gas oils, contrasting the hyphenation of LC and GC (LC-GC) and GC×GC-FID. The results clearly showed that with GC×GC-FID excellent quantitative analyses can be performed, increasing reliability of compound identifications and improving the detection limit, making GC×GC the technique of choice for this type of analyses. Since the FID response of hydrocarbons depends on the mass of carbon in a molecule, as presented previously, quantification of (groups of) analytes can be performed even if no individual standards are available.

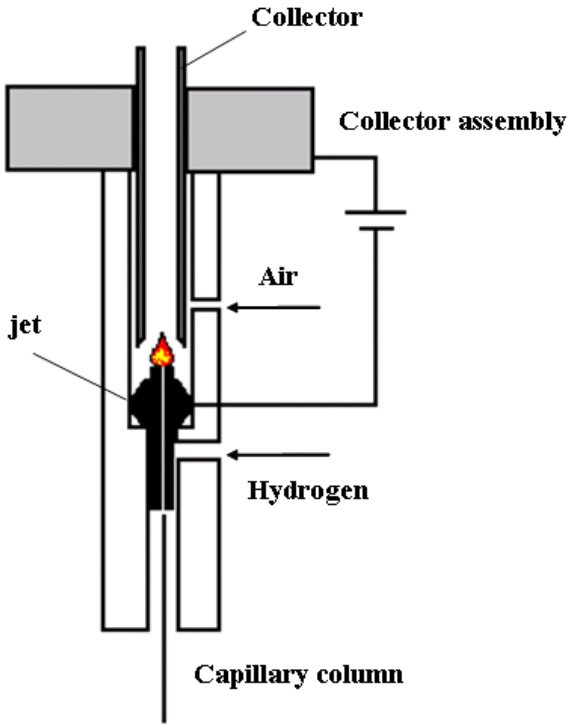

Figure 2.2: Schematic diagram of a Flame Ionization Detector.

2.2.2 Thermionic Detector (TID)

The term Thermionic Detector (TID) principally refers to the nature of the ionization process, because the sample molecules are converted to negative ions in the detector by extracting electrons emitted from a hot solid surface [39]. The often interchangeably used term Nitrogen Phosphorus Detector (NPD) should be used only when the TID is used in specific mode for nitrogen- and phosphorus-containing compounds [40]. As shown in **Figure 2.3**, the basic difference between a FID and a TID is the bead – an electrically heated thermionic source, consisting of an alkali salt in an inorganic ceramic cement matrix [39]. The operating principles of the NPD have not yet been completely established, and the detailed mechanism of the specific ionization process is apparently not fully understood [39-41]. The most acceptable mechanism is the surface catalytic ionization theory [42,43]. According to this theory

the alkali atoms do not leave the bead surface (which cannot be named a “source” in this case), but catalyze the electron transfer taking place on the bead surface [39,42]. Since the ceramic beads were developed, Patterson and Howe [44] studied the effects of bead composition, surface temperature, voltage, and the composition of the gaseous environment surrounding the bead’s surface, on the response of the detector. Patterson [42] found that the bead surface temperature and the composition of the gaseous environment determine the gaseous products formed from the decomposition of sample compounds, affecting the selectivity of the detector. In his studies with thermionic detectors operating in different environments [40], Patterson discussed both sensitivity and specificity for several compounds, but his results also show that the gas environment affects the peak shape, although this observation was not discussed. The detection process was considered to be too slow to achieve the high acquisition frequencies necessary for GC×GC, since this technique produces much narrower peaks (100 ms) than those obtained with conventional fast and regular gas chromatography (<1s) [41].

Specially related to GC×GC, the effect of detector response time and any lack of symmetry arising from the detection step are important. Although recognizing this possible limitation, Ryan and coworkers [1] presented the first application of NPD detection to GC×GC analysis, studying methoxypyrazines in wine, using an acquisition frequency of 100 Hz. Analysis by GC×GC-NPD enabled detection limits of 0.5 $ng.L^{-1}$ for the quantitation of 2-methoxy-3-(2-methylpropyl) pyrazine, which was superior to that obtained using GC×GC coupled with time-of-flight mass spectrometry (TOFMS) (1.95 $ng.L^{-1}$). Optimum performance was achieved by optimizing hydrogen, air, and nitrogen detector flows, in order to establish the best detector flow conditions with respect to peak magnitude and peak asymmetry (A_s). As a result of selective detection using GC×GC-NPD, the complexity of the real wine headspace was simplified. In a separate study, the NPD performance was correlated with peak response [41]. Peak asymmetry was seen to vary from a high of 8.0 to an acceptable 1.6 over a range of detection gas flow settings. A flow setting that gives best peak symmetry does not necessarily deliver best response magnitude. The Agilent NPD is capable of up to 200 Hz data acquisition, and so should be suited to analysing

peaks of width down to 50 ms basewidth (this gives 10 points per peak on 2-5 data points per peak standard deviation). Whilst fast electronics may support the notion of fast peak analysis, if the mechanism of the detector does not preserve the peak profile as it elutes from the column, then the detection of the peaks will deteriorate. As related above the chemistry of the detection process may be the limiting factor in preventing narrow peak shape being preserved, and imposing an exponential-type delay process on the peak flux as it enters and is then exhausted, from the detector.

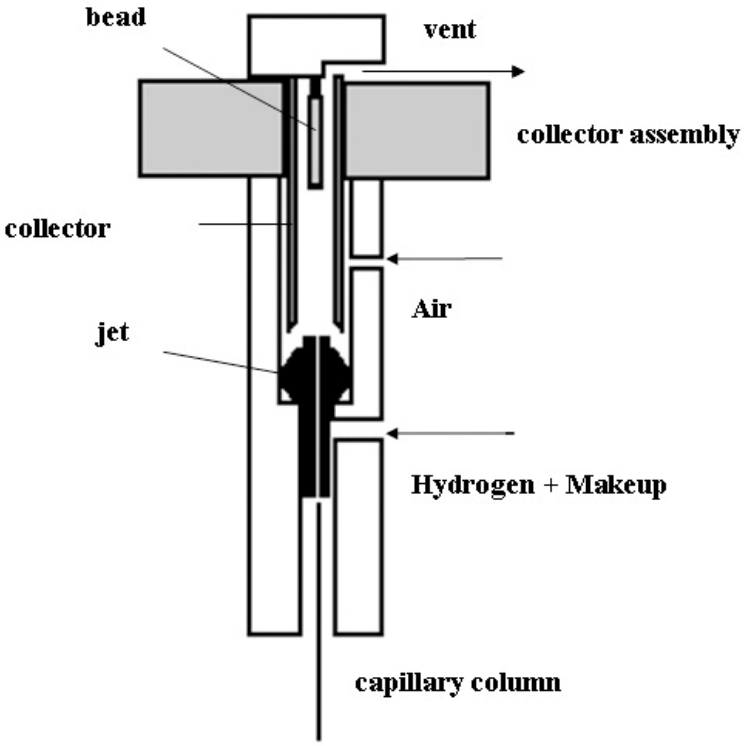

Figure 2.3: Schematic Diagram of Nitrogen-Phosphorus Detector; Thermionic Detector.

Recently, von Mühlen and colleagues [2] reported the developed method for separation and quantitated N-containing compounds in Brazilian heavy gas oil (HGO) using GC×GC-NPD system. The geometry of NPD detector was modified in order to achieve the best GC×GC performance, where the extended jet and the standard collector were used for a new geometry, and detector gas flow (H_2, N_2 and Air) was optimised for a good peak shape and separation. In addition, the

thicker film phase column set was employed to reduce the tailing effect of the analytes. The separation and quantitation of N-containing compounds in HGO demonstrated a good potential of this developed method in oil analysis.

In 2007, Ochiai et al [3] characterized nanoparticles in roadside atmosphere using GC×GC-HRTOF-MS, GC×GC-NPD/qMS and GC×GC-qMS. They found that by increasing the selectivity of the system with the use GC×GC-HRTOF-MS, a group type separation of selected chemicals such as oxygenated polycyclic aromatic hydrocarbon (oxy-PAHs) was achieved. The simultaneous detection of NPD and qMS in GC×GC system of 15 N-containing compounds was achieved and the elution time of compounds from NPD detection were used for a NIST library search for compound identification. In addition, selected PAHs were quantitated; the results showed that good linearity and high sensitivity was achieved for all target PAHs.

2.2.3 Electron Capture Detector (ECD)

James E. Lovelock [45,46] first reported an improved selectivity and sensitivity for the electron capture detector (ECD) from the argon ionisation detector in the late 1960s. Electron capture detectors use a radioactive beta (electron) emitter to ionize some of the carrier gas and produce a standing current between a biased pair of electrodes. When organic molecules, containing electronegative functional groups, such as halogens, phosphorous, and nitro groups enter the detector, they capture some of the electrons and reduce the current measured between the electrodes. The ECD detector is probably the most sensitive and selective of the traditional gas chromatography detectors available and is widely used in the detection and analysis of high electron affinity compounds [47]. Therefore, the ECD detector has long been recognised as the detector of choice for trace analysis of halogenated organic compounds such as organochlorine pesticide, herbicides and halogenated hydrocarbon in a range of samples. Consequently for multiresidue analysis of such compounds by using GC×GC-ECD is a natural choice of detection system.

The ECD detector contains a low energy β-ionisation source, which is used to produce electrons for subsequent capturing by appropriate atoms. A flux of beta particles generated by a radioactive source, eg ^{63}Ni, collides with the carrier gas

molecules causing them to ionize by ejecting thermal electrons (low energy electrons). The thermal electrons migrate to an anode thereby generating a current signal. If a sample containing compounds with high electron affinity substituents enters the detection region, capture and removal of thermal electrons results. This results in a reduction in the baseline current, and provides the signal response related to the thermal electrons captured by the compound [48]. The ECD detector can be used in two modes, either with a constant potential applied across the cell – the so-called "DC mode" or with a pulsed potential across the cell – the "pulsed mode". The process in ECD detector can be summarised as follows:

$$Ni_{63} \rightarrow \beta \ particles \quad \rightarrow N_2 \ (carrier \ gas) + \beta \rightarrow N_2^+ + 2e^-$$

$$X^- (F, Cl \ and \ Br \ or \ another \ high \ electron \ affinity \ atom) \ containing \ samples$$

$$Ion \ re-combination: X^- + N_2^+ \rightarrow X + N_2$$

In the DC mode, hydrogen or nitrogen can be used as the carrier gas and a small potential is applied across the cell that is just sufficient to collect all the electrons available, and provide a small standing current. If an electron-capturing molecule enters the cell, the electrons are captured by the molecule, which becomes charged. The mobility of the captured electrons is much smaller than the free electrons and the electrode current falls dramatically. Operating in the pulsed mode, a mixture of 10% methane in argon may be employed, which changes the nature of the electron-capturing environment. The electrons generated by the radioactive source rapidly assume only thermal energy and in the absence of a collecting potential, exist at the source surface in an annular region about 2 mm deep at room temperature, and about 4 mm deep at 400 ^{o}C. A short period square wave pulse is applied to the electrode collecting the electrons, producing a base current. The standing current, using 10% methane in argon is about 10^{-8} amp with a noise level of about 5×10^{-12} amp [49]. Due to the large internal volume of a normal ECD detector (about 1.5 mL) which can cause peak broadening (less resolution) and insufficient data points to reconstruct the peak

generated from the GC×GC system, therefore a normal ECD detector is inappropriate for coupling to as GC×GC system. To date, the most appropriate technology for ECD application in GC×GC is that of the micro-Electron Capture Detector (μECD). Thus, this is separately mentioned in **Section 2.2.4** below.

2.2.4 Micro-Electron Capture Detector (μECD)

Recent developments in ECD design have seen miniaturisation of the detector, to make it more compatible with lower column flows and more rapidly changing peak fluxes entering the detector. One example of this is the Agilent Technologies micro-ECD (μECD), **Figure 2.4**. It is instructive to consider the design elements of this ECD to interpret the key features driving the detection to faster and more sensitive applications. The μECD design features a smaller detection zone volume than the previous design discussed in **Section 2.2.3** above. Since the present interpretation is directed towards greater sensitivity and acquisition speed, listed here will be simply the stated performance attributes of the detector [50], according to the manufacturer:

a.) Improved sensitivity compared with conventional ECDs.

b.) An internal volume of 150 μL, which is 10 times smaller than other ECDs with detection sensitivity of less than 8 femtograms.s^{-1} of lindane.

c.) A broad dynamic linear range from femtograms to nanograms per microliter, for example, 5 x 10^5 for lindane.

d.) Higher linear velocities through the detection zone to reduce analyte residence time, decreasing cell contamination and improve uptime.

e.) Isolated anode, which minimizes the chance for contamination of the anode.

f.) An optimized electric field that minimizes contamination effects on cell performance.

g.) A replaceable liner that serves as a physical stop for the column, ensuring reproducible column installation and decreasing column contamination of the cell.

h.) A variable sampling rate from 5 to 50 Hz, suitable for fast chromatography.

These attributes suggest a much more suitable detection transducer for GC×GC analysis, and appear to be reasonable outcomes of the miniaturisation of the detector. However, the limits imposed on the signal sampling rate (< 50 Hz) may be inadequate for very fast GC×GC peak quantification.

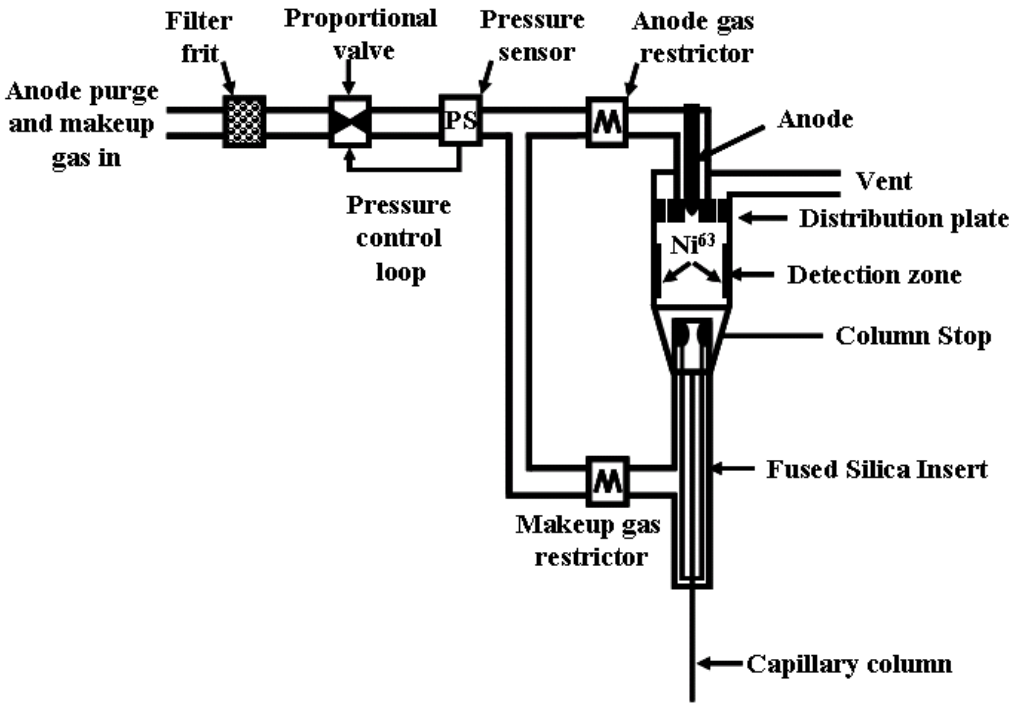

Figure 2.4: Schematic diagram of the Agilent 6890 Series micro-Electron Capture Detector (μECD), designed for fast capillary gas chromatography.

One dimensional GC-μECD was applied to trace level analysis of residue pesticides such as organochlorine, organophosphorus and PCBs (polychlorinated biphenyls) in various samples [51-55]. The μECD normally used is a modification of the classical ECD. This kind of detector is highly sensitive and normally trouble free if very simple recommendations are followed. The validation of μECD performance was reported by Klee and coworkers [50]. A small internal volume and maximum acquisition rate of 50 Hz provides more compatible μECD performance with fast gas chromatography. In order to couple the μECD to GC×GC, it has been reported that it is necessary to operate with a sufficiently high make up gas

flow [56]. The data acquisition rate (50 Hz) should be adequate for fast GC peaks, but possibly not sufficiently fast for those which result from comprehensive two-dimensional gas chromatography (GC×GC) operation. Korytar et al [57] optimised the temperature program and column sets (^{1}D and ^{2}D) for GC×GC with μECD for the analysis of 90 polychlorinated biphenyl congeners. In this study, the μECD detector was operated at 300 ^{o}C with 99.999% pure nitrogen as a make up gas at a flow-rate of 60 mL.min^{-1}, and data acquisition of 50 Hz. They reported that limits of detection for the HP-1/ HT-8 column set of 10 fg can generally be expected for tetra- or higher substituted PCBs in GC×GC with μECD. In 2003, Kristensson et al. [58] studied six different modulators and three ECDs for the analysis of high boiling halogenated organic compounds. A mixture of PCBs, fluorinated polycyclic aromatic hydrocarbons (F-PAHs) and two chlorinated alkanes were used as a test mixture. The ECDs were tested with respect to band broadening in the detector, and for use in fast GC and/or GC×GC analysis. The μECD (Agilent Technologies), with an internal volume of 150 μL was operated at 320 ^{o}C and make up flow of 60-450 mL.min^{-1} (for 450 mL.min^{-1} flow, the make up gas was added via a T-piece at the detector base entrance). Data were collected at 50 or 100 Hz. The Shimadzu GC-2010 ECD, which has an internal volume of approximately 1.5 mL, was operated at detector temperature of 100-340 ^{o}C and make-up gas flow of 15-200 mL.min^{-1}. Data were collected at 250 Hz. The third ECD detector used in this study was from Thermo Finnigan, tested by means of fast GC operation on a Trace GC. The ECD had an internal volume of 480 μL. The conditions were set to create narrow peaks. The detector temperature was 300 ^{o}C, and make-up flows up to 2050 mL.min^{-1} were used. The original Trace GC pressure regulator could achieve make-up flows of up to 375 mL.min^{-1}; higher make-up flows could be obtained when this pressure regulator was bypassed and replaced by wider tubing and a needle valve. The study concluded that the internal volume of the detector is not the only factor which is important when selecting an ECD for use in GC×GC. The smallest internal detector volume (μ-ECD from Agilent Technologies) still had additional band broadening compared with FID, (up to 3-fold greater) and exhibited some second dimension tailing. Moreover, the optimisation of the make-up flow in order to reduce peak widths can have a dilution effect on the solute flux and so

reduce signal response. These make-up flows can be far greater than those recommended for routine operation. However, the introduction of a μECD detector should still be a valuable step forward in the selective and sensitive analysis of organohalogens in GC×GC.

2.2.5 Sulfur Chemiluminescence Detector (SCD)

Sulfur is an important element, responsible for many of the exciting (and not so exciting) flavours and tastes in food and drink. Moreover, sulfur is a major heteroelement in coal and petroleum components, diesel fuel and gasoline. Often, sulfur compounds are present at trace levels, with detection and quantitation being complicated by high levels of interfering components. The adsorptivity of sulfur-containing compounds can make their analysis by using GC problematic. Several analytical techniques can be used to detect organic sulfur compounds, and so GC with a variety of detectors such as Flame Ionization Detection, Flame Photometric Detector, Atomic Emission Detection, Sulfur Chemiluminescence and Mass Spectrometry has been used. However, GC with sulfur chemiluminescence detection (SCD) is an outstanding combination for selective detection for trace concentration of sulfur-containing compounds in different kinds of samples. The SCD possesses advantages over other sulfur selective detectors and it is finding wide spread application in the analysis of petrochemical products [59-61], natural gases [62], foods and beverages [63,64], environmental samples [65], perfume and fragrances, etc. The SCD was first developed as an analyser for the determination of sulfur compounds in air [66], and later it was commercialised as a GC detector utilizing an FID-style arrangement operated under hydrogen-rich conditions to generate sulfur monoxide (SO) as the basis of chemiluminescence [67]. A modification of the detector provided enhanced sensitivity and other benefits, using a heated furnace design. Characteristics of the SCD that have led to its successful application include a linear and equimolar response to sulfur compounds, an absence of quenching, excellent sensitivity (<0.5 pg S/s) and high selectivity (S: C $>10^8$) [68]. In 2002, Yan [69] reported an overview of sulfur and nitrogen chemiluminescence detection when interfaced with GC including their mechanism, operating principles, characteristics in term of selectivity, sensitivity,

linearity and applications. Both sulfur and nitrogen chemiluminescence detectors have a common two-step detection scheme as follows:

Step 1:

Universal conversion of nitrogen/sulfur analytes to their respective ion chemiluminescent species.

Step 2:

Detection of chemiluminescence from the reaction between ozone and the nitrogen/sulfur chemiluminescence species.

For SCD, simple oxidative combustion does not generate a sulfur chemiluminescent species. High temperature reduction by hydrogen is required after the oxidation step in order to produce the chemiluminescent species. Sulfur monoxide (SO) is believed to be the common intermediate species that reacts with ozone in a final elementary reaction to form sulphur dioxide (SO_2*), which generates light when it returns back to ground state. The complex combustion reaction is still not thoroughly understood, however in general terms the sulfur gases are combusted in a hydrogen rich chamber yielding SO, which is then reacted with ozone, producing sulfur dioxide, oxygen and light. The light produced is detected by a photomultiplier tube; the response is proportional to the amount of compound in the sample. The process can be summarised as follows:

1. **Universal conversion to chemiluminescent – generating sulfur species:**

$$Oxidation: R-S + O_2 \rightarrow CO_2 + H_2O + SO_2$$

$$Combustion: SO_2 + H_2 \rightarrow Sulfur\ monoxide\ (SO)$$

2. **Detection of sulfur chemiluminescence**

$$SO + O_3 \rightarrow SO_2^* \rightarrow SO_2 + h\nu\ (UV\ blue)$$

Where hν is light energy in the blue region of the spectrum.

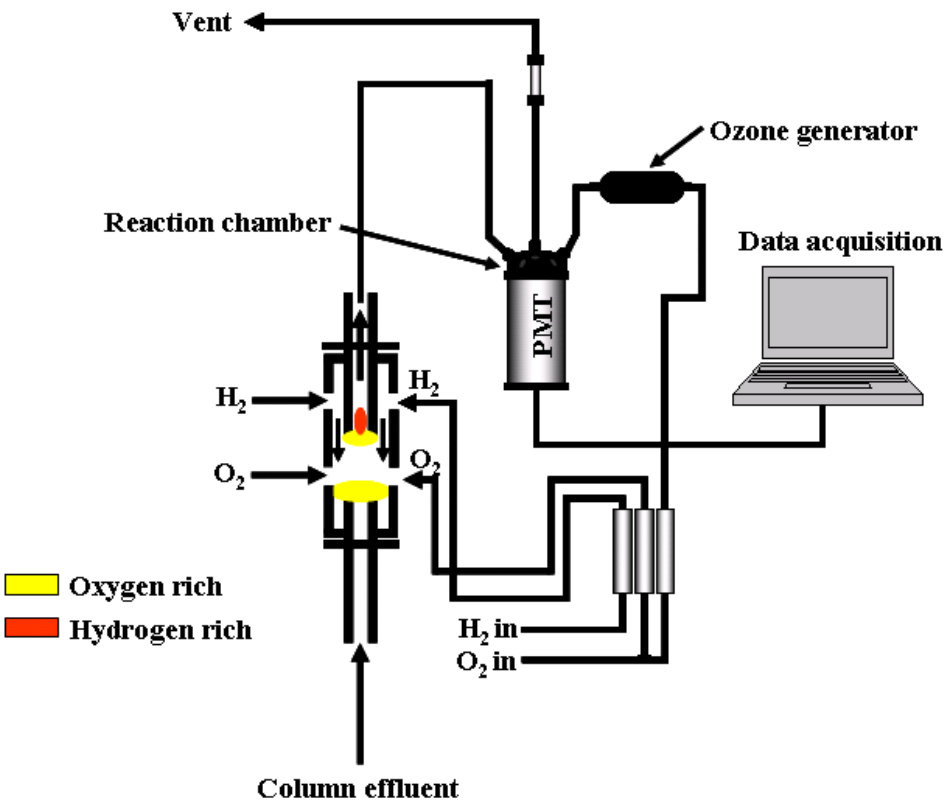

Figure 2.5: Schematic diagram of dual plasma SCD detector.

In **Figure 2.5**, the dual plasma burner of the Sievers 355 Sulfur Chemiluminescence Detector (SCD) is shown. It is a GC detector of choice available for the analysis of sulfur compounds. The complete SCD system includes the dual plasma burner and controller, vacuum pump and detector. The detector can allow for the acquisition of both FID and SCD signals. The SCD utilizes a dual plasma burner to achieve high temperature combustion of sulfur-containing compounds to form sulfur monoxide (SO). A photomultiplier tube (PMT) detects the light produced by the chemiluminescent reaction of SO with ozone. This results in a linear and equimolar response to the sulfur compounds without interference from most sample matrices. The SCD dual plasma burner is designed to enhance production of the sulfur monoxide (SO) intermediate. In the design, the lower flame is oxygen-rich and the upper is hydrogen-rich. The conversion of sulfur-containing compounds to sulfur monoxide (SO) occurs within the ceramic reaction chamber housed in the burner

assembly. Of primary interest to users of GC×GC will be the response speed of the detector reaction processes and the associated electronics, and any unswept or excessive volume that may serve to broaden peaks or dilute the solute.

In 2003, Hua et al [70,71] coupled the SCD detector with GC×GC for determination of sulfur-containing compounds in diesel oils. The study included the optimization of the detector and column set. The SCD detector used in this study was operated at 800 ^{o}C and detected at wavelengths between 260 and 480 nm. The data acquisition rate of the SCD was 100 Hz. The results showed that peak widths generated by the GC×GC-SCD system was 0.8-1.2 s, which is much wider than that generated by an equivalent GC×GC-FID system (0.2-0.3 s), primarily because of a bigger cell volume (480 µL) of the SCD detector. Clearly the 100 Hz data rate was of no consequence in determining suitability for GC×GC operation here. Based on this study, GC×GC–SCD gave relative standard deviations (RSD) of $^{1}t_{R}$ and $^{2}t_{R}$ of 0.93 and 4.25%, respectively. The separation required 135 min to speciate the different sulfur compound groups and important target sulfur compounds in the diesel oil fractions. The results showed various compound classes such as thiols and sulfides, disulfides and thiophenes (TPs), benzothiophenes (BTs), dibenzothiophenes (DBTs) and benzonaphthothiophenes (BNTs), which formed contour horizons in the two dimensional (2D) plot almost parallel to one another. Clearly, coupling of GC×GC with SCD detector will have advantages such as ease of operation, and reliable performance when applied to group separation, identification and quantification of sulfur-containing compounds in diesel oil fractions. The selectivity towards S allows the complex hydrocarbon matrix to be transparent in this analysis. The GC×GC-SCD approach has significant identification advantages over conventional GC-FID and GC-SCD, supporting technologies for diesel oil processes such as desulfurization, and downstream production optimization.

In 2004, Blomberg et al. [72] demonstrated that the lack of speed of the SCD does not originate from its physical dimensions, nor the inherent chemical reactions within the plasma or at the chemiluminescent step, but is largely determined by the speed of the electronics used. In their experiment, the SCD initially gave rise to additional band broadening, but this slow response was caused by system

electronics, rather than dead volumes in the chemiluminescence chamber and/or transfer line between burner and reaction chamber. Improved electronics could overcome the limitations of the commercial system, allowing the successful coupling of GC×GC with the SCD detector.

2.2.6 Nitrogen Chemiluminescence Detector (NCD)

The nitrogen chemiluminescence detector (NCD) has been demonstrated to be useful for the analysis of nitrogen-containing compounds in different kinds of samples. Advantages of the NCD over other nitrogen detectors include equimolar response, higher selectivity and lack of quenching due to matrix effects. The NCD has applications in the petrochemicals [73,74], foods and beverage flavour, and environmental [75] area. In addition, the NCD can be used as a single detector or coupled in series with a Flame Ionization Detector (FID), allowing simultaneous acquisition of selective and universal detection chromatographic traces from both detectors.

The NCD operation is similar to the sulfur chemiluminescence detector. The effluent from a GC column enters the ceramic combustion tube in the stainless steel burner. The hydrogen and oxygen plasma in the combustion tube converts nitrogen compounds to nitric oxide (NO) at temperatures greater than 1800^{o}C. Nitric oxide reacts with ozone to form electronically excited nitrogen dioxide (NO_2*). The excited nitrogen dioxide emits light in the red and infrared region of the spectrum when it relaxes to its ground state. The light emitted is directly proportional to the amount of nitrogen in the sample. A chemiluminescence signal emitted upon decay back to the ground state is directly related to nitrogen concentration. A typical detection limit of the NCD detector is 1 mg.L^{-1}. While diatomic nitrogen (N_2) is not generally detected, there is a slight response to N_2 so air leaks can be a problem. Like the SCD, the detector requires precise control of the hydrogen and air flow rates, and a vacuum system. It has been established that the chemiluminescence is the result of the following reaction.

$$N - compounds + O_2 \rightarrow NO + other\ products + 47.8\ kcal/mole$$

$$NO + O_3 \rightarrow NO_2^* \rightarrow NO_2 + h\nu\ (NIR)$$

The Sievers 255 NCD may employ a dual plasma burner to achieve high temperature combustion of nitrogen-containing compounds to form NO. A photomultiplier tube detects the light produced by the subsequent chemiluminescent reaction of NO with ozone. Because of the specificity of the reaction, complex sample matrices can be analyzed with little or no interference. The dual plasma burner of this detector results in complete conversion of the matrix to products, such as carbon dioxide and water, which do not chemiluminesce with ozone. Burner gas flow dynamics of this detector are shown in **Figure 2.6**.

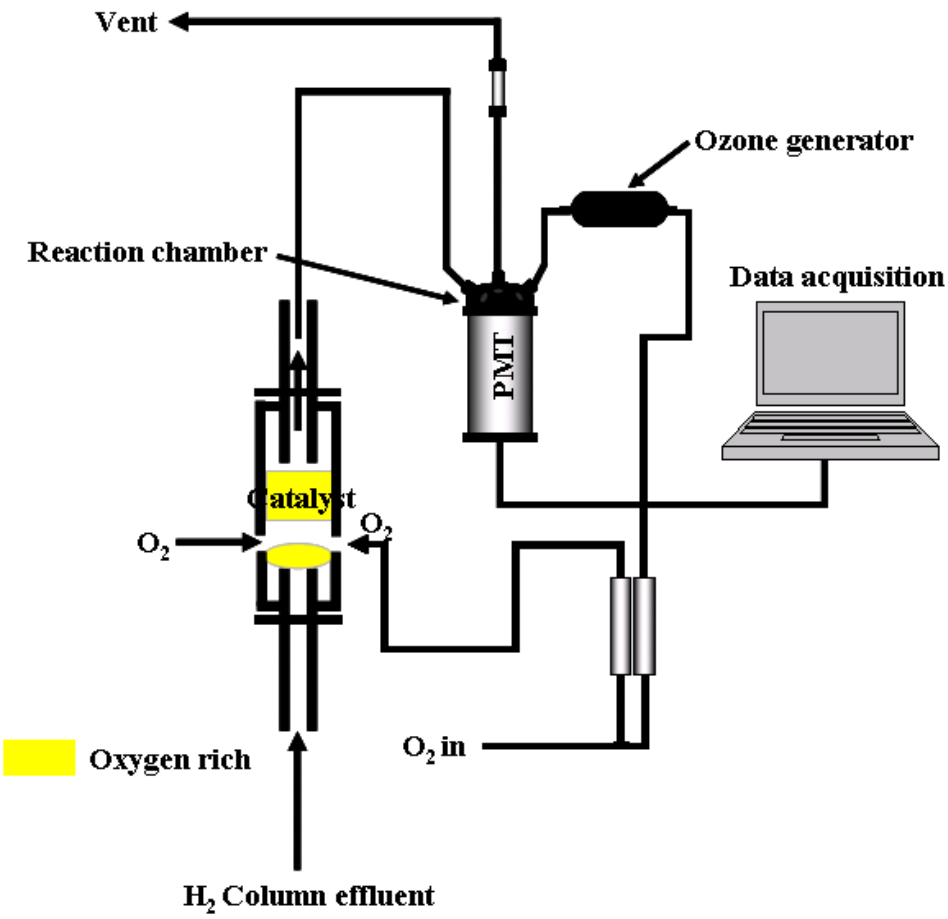

Figure 2.6: Schematic diagram of dual plasma burner in NCD detector.

Wang and co-workers [13] coupled the NCD detector to GC×GC for speciation of nitrogen-containing compounds in diesel fuel, which in typical refinery streams is the fraction boiling between 150 °C and 430 °C, with carbon number from approximately C_8 to C_{28} . This study demonstrated the capability of GC×GC-NCD for separation of individual compounds and classes of nitrogen-containing compounds such as indoles and carbazoles with an appropriate separation column combination. In this research, the NCD was from Ionics Inc., [Boulder, CO], and was operated at a data acquisition rate of 100 Hz. The results of this study showed that GC×GC-NCD can characterize a typical diesel sample. The major peaks of nitrogen-containing compounds were identified by matching retention times with pure compounds or peaks were identified by alternative techniques. The results of this study show the two well separated bands of nitrogen-containing compounds. One of them is carbazoles and the other is indoles. The details of a fingerprint of nitrogen-containing compounds in the sample were described, which provided an opportunity to monitor complex reactions and processes in production of diesel, and this was previously unachievable in the absence of GC×GC technology.

2.2.7 Atomic Emission Detector (AED)

The AED is a multi-element detector that can be used to measure up to 23 different elements. In addition to sulfur and nitrogen, elements such as carbon (universal), hydrogen (universal), oxygen, lead, manganese, fluorine, and silicon, can all be detected [76]. As eluates elute from the capillary column they are introduced into a microwave-energized helium plasma that is coupled to a diode array optical emission spectrometer [77]. The plasma is sufficiently energetic to atomize all of the elements in a sample and to excite these atoms to generate their characteristic atomic emission spectra, as presented in **Figure 2.7**. The light that is emitted by the excited particles is separated into individual lines via a diffraction grating. Computer data acquisition of individual signal channels records emission intensity vs. time and can produce chromatograms made up of peaks from compounds that contain specific elements. The components of the AED include an interface for the incoming capillary GC column into the microwave induced plasma chamber, the microwave chamber

itself, a cooling system for the chamber, a suitable optical system (mirror, diffraction grating and associated optics) to focus then disperse the spectral atomic lines, and a position adjustable photodiode array interfaced to a computer. Microwave cavity cooling is required because much of the energy focused into the cavity is converted to heat [78].

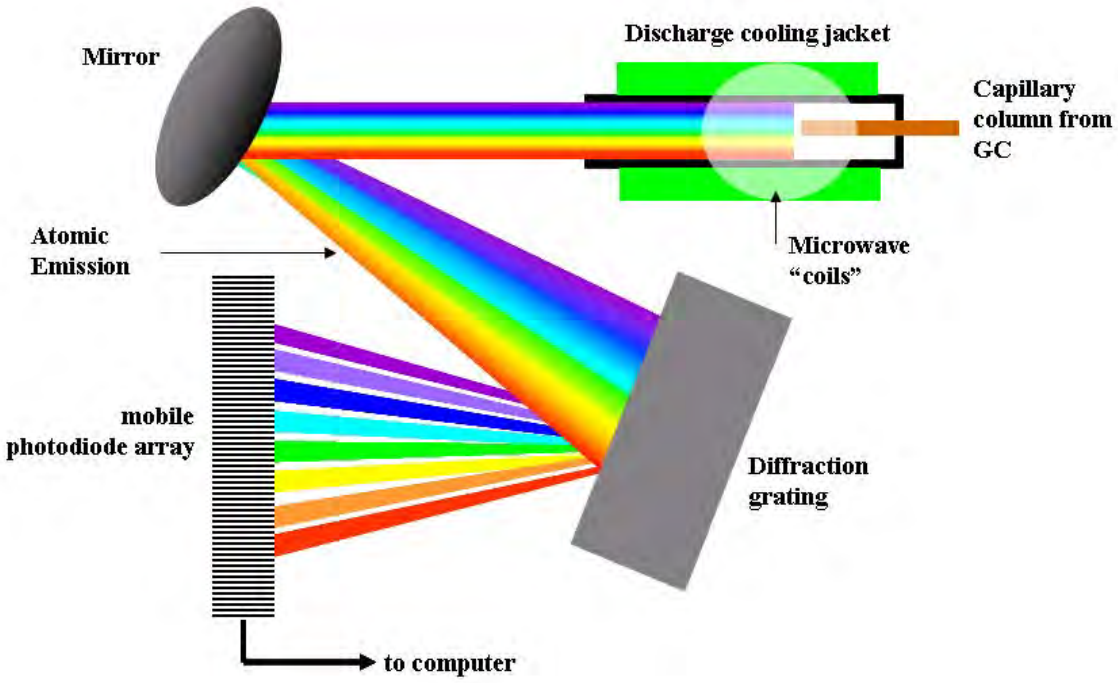

Figure 2.7: Schematic diagram of an Atomic Emission Detection system (AED). From [67] with permission.

GC-AED provides simultaneous multi-channel detection (for up to four elements) with reliable limits of detection (LODs) for most of the important elements (LODs: 1-3 $pg.s^{-1}$), response linearity often over 3-5 orders of magnitude, and an element vs. carbon selectivity of, typically, 4-5 orders of magnitude, for 1D-GC applications [79]. The maximum acquisition rate of the AED, which is 10 $scans.s^{-1}$, is too slow for adequate sampling of the GC×GC peaks for quantitation purposes. Van Stee et al [14] improved the number of samplings per peak (but not the acquisition rate) by using a transfer line between the GC second dimension column and the AED, causing some peak broadening. With this strategy, the peaks had a baseline width of

approximately 500 ms, with some tailing, but the six data points sampled per peak, makes this system suitable for GC×GC qualitative purposes.

The research work used GC×GC-AED to analyze sulfur-containing compounds in crude oil and fluid catalytic cracking (FCC) products. Data obtained were correlated with GC×GC-TOFMS analysis results. FCC is used to convert long (>C12) into shorter alkyl chains to produce lighter fuels; comparison of GC×GC-AED plots prior to and after FCC allowed facile observation of the shortening of sulfur compound carbon chains following FCC treatment. Compounds present in crude oil samples were mainly alkylated benzothiophenes (BT), dibenzothiophenes (DBT), and benzonaphthothiophenes (BNT). In the FCC product, however, the high-boiling sulfur compounds are absent and moderately alkylated (C1-C6) aromatic sulfur compounds dominate. Further study of a class of unknown sulfur compounds required the combined and correlated use of AED and TOFMS detection. Direct matching of GC×GC-AED and GC×GC-TOFMS could not be done, because retention times in both dimensions are different.

2.2.8 Olfactometry detection in GC×GC

Olfactometry is a technique that uses the human sense of smell to detect and evaluate odour active compounds within a volatile sample. It can be considered as a biological sensor technique since a human nose plays the role as a conventional detector in a GC system similar to FID or mass spectrometry detector. Gas chromatography coupled with an olfactometor (GC-O) was first initially proposed as a technique for separation and selection of volatile compounds in 1964 by Fuller and co-workers [80]. The system comprises a standard GC system equipped with a special port called ‘sniffer port’ which allows the operator to sniff the hot dry gases elute from the GC system. The sniff port contains a glass nose cone, detector transfer tube, humidifier, gas control module and splitter kit; the design provides the transfer of the effluent from the gas chromatograph to a nose cone allowing the operator to use their nose to identify individual components. Early in the development of this technique, the discomfort from the sniffing of hot gas is the limitation of an olfactometry detection system. Therefore, the combination of humidified air with the

hot effluent from the GC system to reduce nasal dehydration was published in 1971 by Dravnieks and O'Donnell [81]. The humidified unit was located in between the transfer line and the nose cone to modify the hot air from the GC before it reaches the sniff port. The transfer line needs to be heated up to ensure that the target compounds do not condense during the analysis. **Figure 2.8** shows the internal design of the sniffer port from SGE International, Ringwood, Australia. Further details of GC-O fundamentals and implementation have been reported elsewhere [82-84].

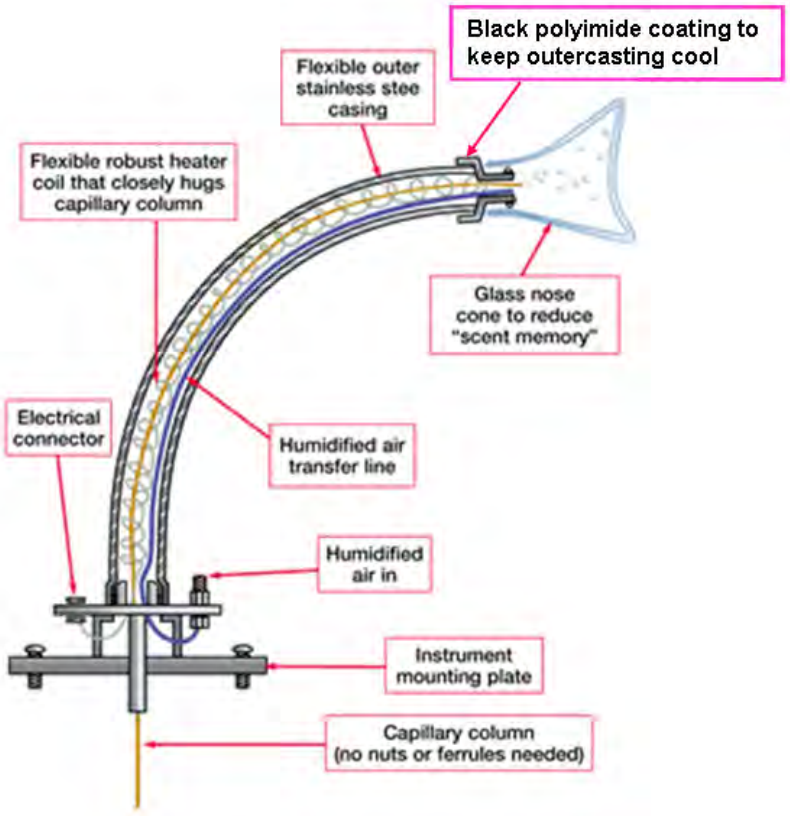

Figure 2.8: Internal design of the sniffer port of GC-O system [Product Data, SGE International, Ringwood, Australia].

Basically, at the end of a chromatographic column a splitter was installed to allow an equal portion of the effluent from the GC system to be split to the sniffer port (human nose) and the other detector (mostly FID or MS). Utilising a FID detector or mass selective detector as a simultaneous detector in a GC-O system makes GC-O become a powerful technique due to the compounds being smelled at the

exact time they enter to the MS. This benefits the identification of the individual compounds in complex sample like essential oils. **Figure 2.9** shows a GC system coupled to an olfactory detector (ODO II) and MS detector, from SGE International, Ringwood, Australia.

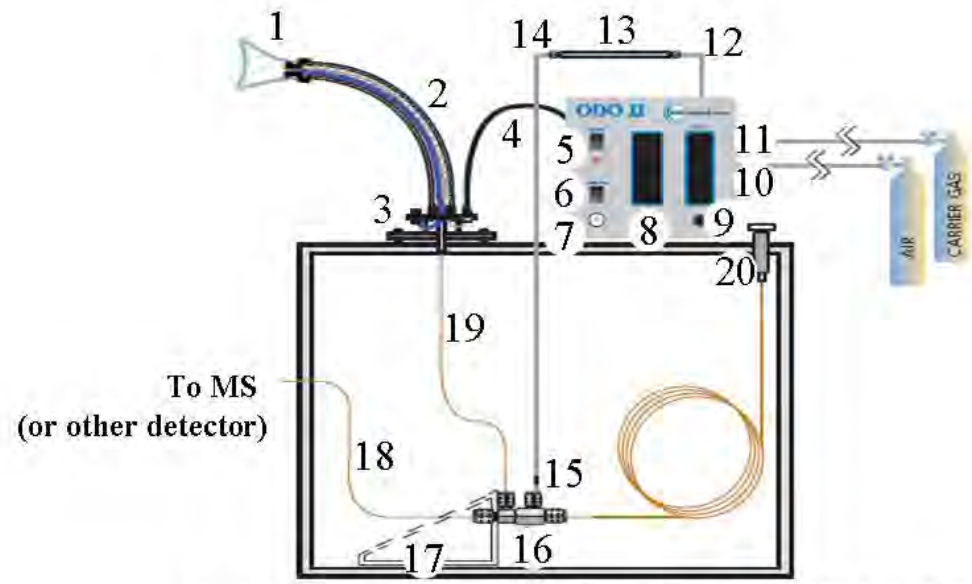

1. Glass Nose Cone
2. ODO II heated transfer line
3. Mounting Plate, 6890
4. Cable link
5. Transfer line heater switch
6. Humidifier switch
7. Humidifier fill port
8. Humidifier
9. Auxiliary gas flow meter
10. 1/16" ss tube with 1/8" sleeve (to "HUMIDIFIER IN")
11. 1/16" ss tube with 1/8" sleeve (to "AUX GAS IN")
12. Tube, ss, 1/16" ×0.8m (200mm long, from "AUX GAS OUT"
13. Adsorption tube (chemical trap, AT-PCS)
14. 1/16" ss Tube, non marked end
15. 1/16" ss Tube, red marked end
16. Column Flow Splitter
17. Splitter support bracket
18. ODO II- ms Restrictor
19. ODO II- Transfer line tubing
20. Injection Port

Figure 2.9: GC system coupled with olfactory detector (ODO II) and MS detector, ODO II, Installation and Operating Instruction, SGE International, Ringwood, Australia.

In a GC-O system, the separation of the compound mixture was performed in one column, before the hot gas transfer to the sniff port, mixing with humid air and detection by the human nose. The analytical signal measured is the time recorded for the appearance of smell, which corresponds to retention time. The operator needs to describe the smell of the odour active compounds when it reaches

the nose, such as woody, fresh grass, and vanilla etc. A number of methods have been developed to collect and process the data obtained from a GC-O system. van Ruth reported the state of art of GC-O methods and classified them into four categories as shown below [84];

1.) Dilution analysis methods for producing potency values based on stepwise dilution to threshold.
2.) Detection frequency methods for recording detected odours over a group of assessors.
3.) Posterior intensity methods for producing estimates of perceived intensity, which are recorded after a peak has eluted.
4.) Time-intensity methods for producing estimates of perceived intensity recorded simultaneously with the elution of the chromatographic peaks.

The dilution analysis is the most applied method which is based on the successive dilutions of an aroma extract until no odour is perceived by the panellists [83]. Basically, GC-O is suitable for determining a range of volatile samples, especially in food, perfumes and fragrances, and essential oils analysis [85-88]. However, insufficient separation power and sensitivity of the odour active compounds in the complex mixture is a disadvantage in GC-O systems. The co-elution of odour active compound peaks may result in the perception of “odour clusters” during the analysis. To overcome this problem, the GC×GC technique appears to be the most appropriate solution in order to enhance the separation power and sensitivity. **Figure 2.10** shows a schematic diagram of GC×GC coupled with an olfactometer (GC×GC–O) [89]. The system comprises an additional column with different phases to the conventional column and both were connected via the modulator. The effluent eluted from two columns was split to the sniffer port and the other detector for characterisation and identification.

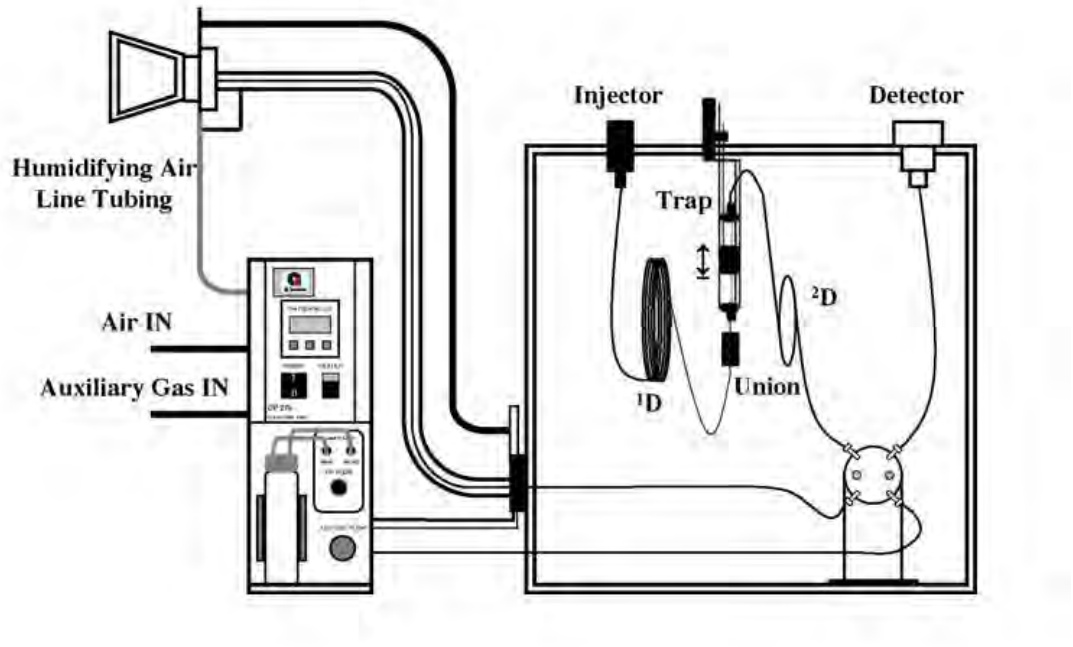

Figure 2.10: Schematic diagram of an olfactometry detection for GC×GC system (GC×GC-O) [89].

In 2005, Eyres et al. [90] stated that GC×GC is one possible solution to identify character-impact odorants where co-elution occurs. The study identified the character-impact odorants in *C. sativam* and *E. foetidum* essential oils using GC-O and identified the compounds responsible using GC×GC-TOFMS.

In 2007, d'Acampora Zellner et al [89] investigated and developed the method for perfume analysis by using a GC×GC-O technique. The results show that the number of odor active compounds found in perfume sample increased when GC×GC-O was employed compared to GC-O analysis. The odor fingerprint obtained from the analysis demonstrated the complexity of the commercial perfume where conventional GC-O would fail to adequately record the presence of all constituents. The research work showed that GC×GC-O can be considered to be a useful technique for perfume and fragrance quality control in these industries.

In 2007, Eyres et al. [91] developed the method to identify the compounds responsible for character-impact odorants in essential oil (hops) samples using GC-O, MDGC-O and GC×GC-TOFMS. The GC-O technique was used to locate the odour active regions in the chromatogram and the profile of the whole

analysis. GC×GC-TOFMS was carried out to resolve and identify compounds eluting in the odor active regions. The conventional heart-cutting MDGC-O method was used to transfer selected co-eluting odor regions for further separation in the second dimension. The co-eluting odor regions were heart-cut from the first column and cryotrapped before subsequent release and separation on the ^{2}D column in the MDGC-O system.

2.3 Case studies of GC×GC-selective detection

By way of demonstration of the performance comparison of selective detection vs. the flame ionisation detector in GC×GC, **Figure 2.11A** illustrates the tailing effect commonly seen with the NPD in single column GC analysis for a selection of N- and P-containing compounds, with GC-FID giving symmetric peak shape on the same column under the same conditions. The result when using cryogenic modulation to generate fast ^{2}D peaks in GC×GC is illustrated in panel **2.11B**, especially, for the ethion component. In this case, if tailing arises from detector-based effects, one might suspect tailing to be worse due to the fast peak flux. Expanded GC peaks are shown in panel **2.11A1 and B1** for both FID and NPD detection. The same considerations can be drawn for any other detector where performance attributes do not meet the needs of the fast response of GC×GC. Thus the ECD would be expected to give broad peaks, and the slow data acquisition of the AED would be expected to give truncated or a non-smooth peak profile. Rather than provide examples of each of these, only the NPD GC×GC chromatogram will be included here. Thus **Figure 2.12** is a 2D GC×GC presentation of the modulated data shown in **Figure 2.11B**. The advantages of selective detection are evident from the GC×GC-NPD (**Figure 2.12B**) plot which now does not respond to the many impurities which occur in the GC×GC-FID result (**Figure 2.12A**). The tailing behaviour of the NPD response are seen as elongated tails and expanded peak zones of each compound spot, compared to the GC×GC-FID. Peak position reliability is good for the two experiments.

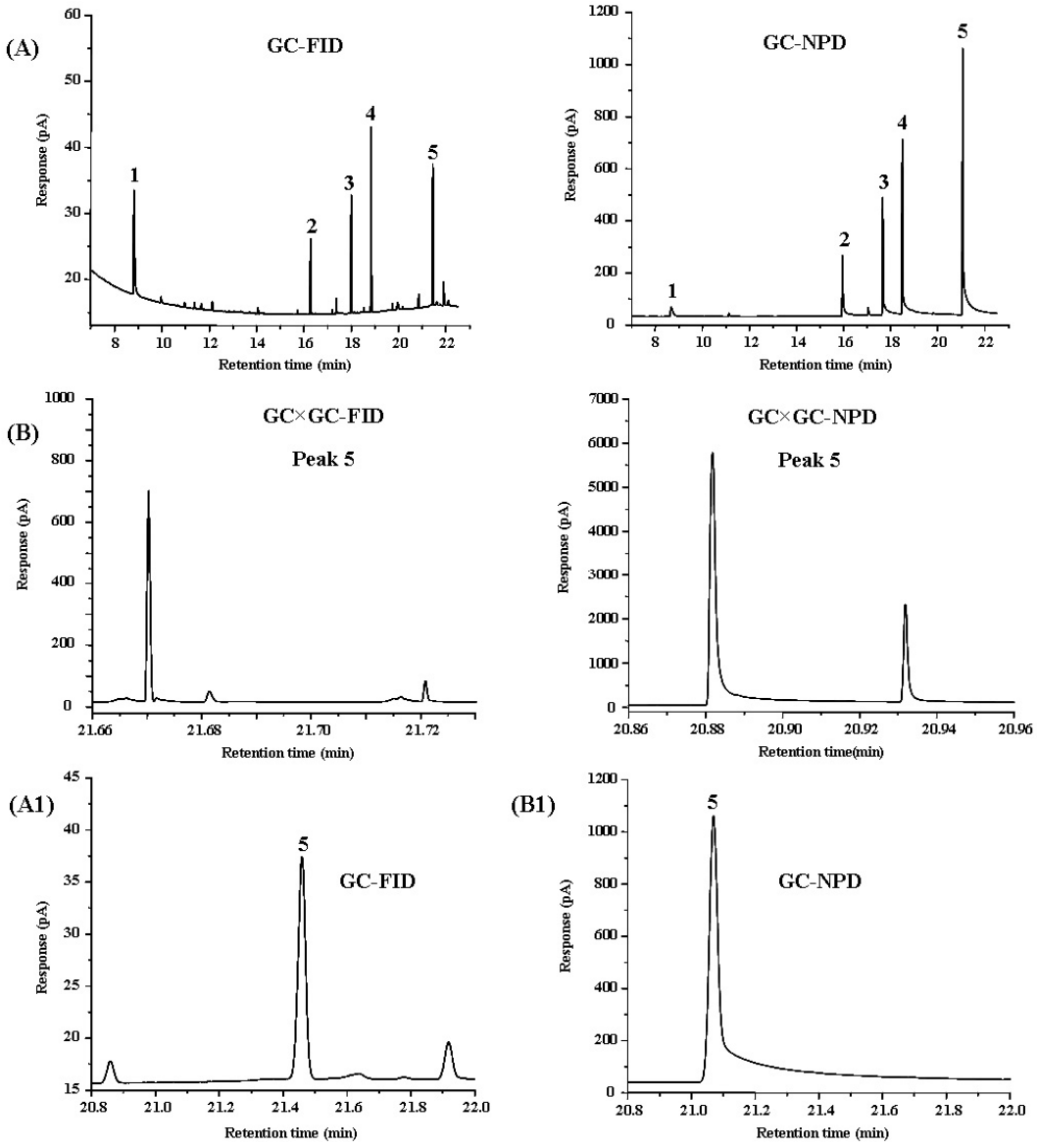

Figure 2.11: (A) GC-FID and GC-NPD chromatograms for a N- and P- containing compound mixture, **(B)** GC×GC-FID and GC×GC-NPD modulated peaks for ethion, under similar conditions. **(A1 and B1)** expanded traces showing peak shape differences for GC-FID and GC-NPD respectively for ethion from part **(A and B)**. Compounds **1**. iso-butyl methoxy pyrazine, **2**. dimethoate, **3**. methyl parathion, **4**. fenthion, **5**. ethion.

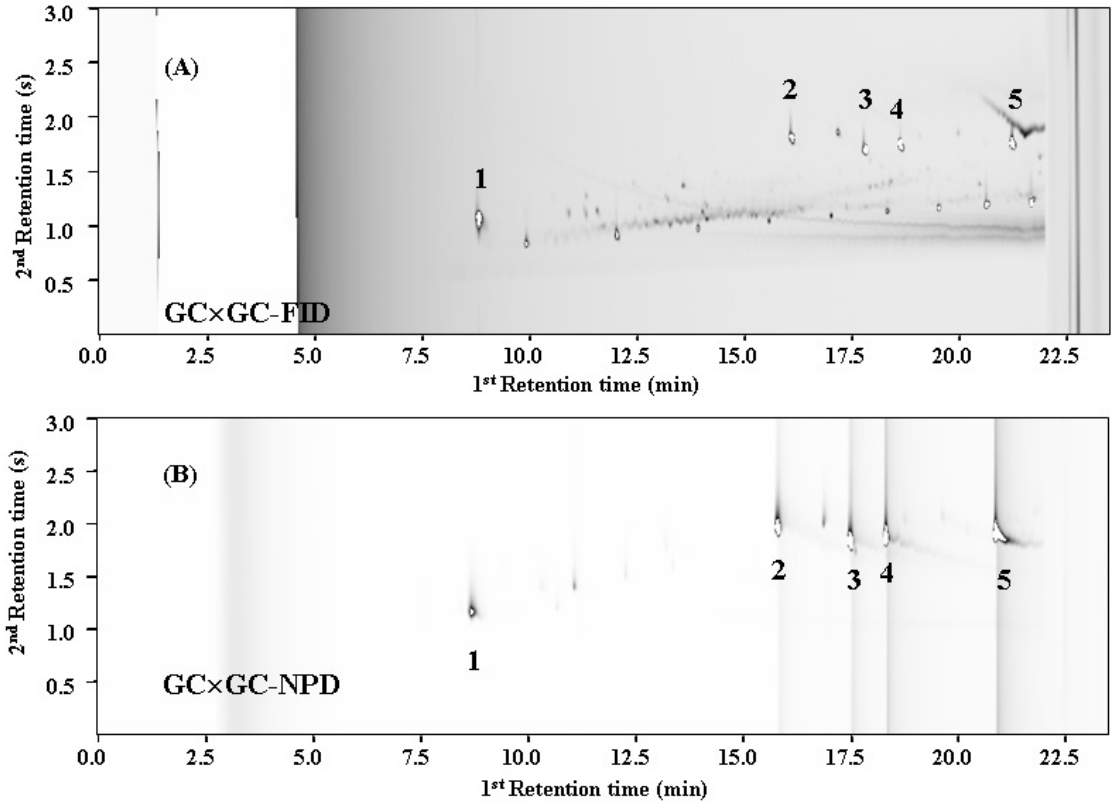

Figure 2.12: (A) - GC×GC-FID and **(B)** - GC×GC-NPD chromatograms for a N- and P containing compound mixture, under similar chromatographic conditions. Same compounds as in **Figure 2.11**.

2.4 Conclusion

There is understandably an increasing interest in selective / alternative detection systems for GC×GC. The classical need for a selective detector is to reduce the interferences from co-eluting compounds in 1D-GC, as dictated by the selectively of the detector towards the active element over the interfering element. A second benefit can be an improved detectability. The GC×GC experiment reduces this problem through improved separation performance; however the other advantage of selective detection – detection sensitivity – is also a benefit. The studies of GC×GC detectors reveals that simple use of the detector in the GC×GC experiment may not be adequate for obtaining maximum performance from the detector, nor for preserving the peak shape and response fidelity of the chromatographic peak, since either the detector construction is not optimised, for the very narrow peaks, or there are chemical-physical reasons (eg. slow kinetics) associated with the response mechanism which limits the speed of the detector and in turn imposed broadening phenomena on the chromatographic peak. Clearly, some of these factors must be addressed in a suitable range of new generation of detectors, adequate for GC×GC analysis, as this technology becomes more accepted in the future.

References

[1] D. Ryan, P. Watkins, J. Smith, M. Allen, P. Marriott, J. Sep. Sci. 28 (2005) 1075.

[2] C. von Muhlen, E.C. de Oliveira, P.D. Morrison, C.A. Zini, E.B. Caramao, P.J. Marriott, J. Sep. Sci. 30 (2007) 3223.

[3] N. Ochiai, T. Ieda, K. Sasamoto, A. Fushimi, S. Hasegawa, K. Tanabe, S. Kobayashi, J. Chromatogr. A 1150 (2007) 13.

[4] P. Korytar, P.E.G. Leonards, J. de Boer, U.A.T. Brinkman, J. Chromatogr. A 958 (2002) 203.

[5] P. Korytar, L.L.P. van Stee, P.E.G. Leonards, J. de Boer, U.A.T. Brinkman, J. Chromatogr. A 994 (2003) 179.

[6] P. Korytar, C. Danielsson, P.E.G. Leonards, P. Haglund, J. De Boer, U.A.T. Brinkman, J. Chromatogr. A 1038 (2004) 189.

[7] L.R. Bordajandi, L. Ramos, M. Gonzalez, J., J. Chromatogr. A 1078 (2005) 128.

[8] C. Danielsson, K. Wiberg, P. Korytar, S. Bergek, U.A.T. Brinkman, P. Haglund, J. Chromatogr. A 1086 (2005) 61.

[9] M. Harju, P. Haglund, J. Microcolumn Sep. 13 (2001) 300.

[10] R. Hua, Y. Li, W. Liu, J. Zheng, H. Wei, J. Wang, X. Lu, H. Kong, G. Xu, J. Chromatogr. A 1019 (2003) 101.

[11] J. Blomberg, T. Riemersma, M. van Zuijlen, H. Chaabani, J. Chromatogr. A 1050 (2004) 77.

[12] R. Hua, J. Wang, H. Kong, J. Liu, X. Lu, G. Xu, J. Sep. Sci. 27 (2004) 691.

[13] F.C.-Y. Wang, W.K. Robbins, M.A. Greaney, J. Sep. Sci. 27 (2004) 468.

[14] L.L.P. van Stee, J. Beens, R.J.J. Vreuls, U.A.T. Brinkman, J. Chromatogr. A 1019 (2003) 89.

[15] T. Holm, J. Chromatogr. A 842 (1999) 221.

[16] A. Amirav, Am. Lab. 33 (2001) 28.

[17] Z. Liu, J.B. Phillips, J. Chromatogr. Sci. 29 (1991) 227.

[18] R. Shellie, P. Marriott, Flavour Frag. J. 18 (2003) 179.

[19] P. Marriott, R. Shellie, Trends Anal. Chem. 21 (2002) 573.

[20] D.J. David, Gas Chromatographic Detectors, John Wiley & Sons, New York (1974).

[21] T. Holm, J. Chromatogr. A 782 (1997) 81.

[22] J. Dalluge, J. Beens, U.A.T. Brinkman, J. Chromatogr. A 1000 (2003) 69.

[23] PerkinElmer, Inc. Specifications - Clarus 500 Gas Chromatograph, www.perkinelmer.com, accessed in 14/08/2005.

[24] Thermo Electron Corporation, Trace GC Ultra Gas Chromatograph Operationg Manual, www.thermo.com/com/cda/product/detail/1,1055,10121492,00.html, accessed in 28/07/2005.

[25] Shimadzu Corporation,GC-2010 Specifications, www.ssi.shimadzu.com, accessed in 28/07/2005.

[26] Varian, Inc. Flame Ionization Detector and Thermoionic Specific Detector, www.varianinc.com, accessed in 28/07/2005.

[27] Agilent Technologies, Agilent 6890N Network Gas Chromatograph Specifications, www.agilent.com, accessed in 28/07/2005.

[28] C.G. Fraga, B.J. Prazen, R.E. Synovec, J. High Resol. Chromatogr. 23 (2000) 215.

[29] M. Kallio, T. Hyoetylainen, M. Lehtonen, M. Jussila, K. Hartonen, M. Shimmo, M.-L. Riekkola, J. Chromatogr. A 1019 (2003) 251.

[30] S. Zhu, X. Lu, L. Dong, J. Xing, X. Su, H. Kong, G. Xu, C. Wu, J. Chromatogr. A 1086 (2005) 107.

[31] C. Reddy, M., T.I. Eglinton, A. Hounshell, H.K. White, L. Xu, R.B. Gaines, G.S. Frysinger, Environ. Sci. Technol. 36 (2002) 4754.

[32] G.S. Frysinger, R.B. Gaines, L. Xu, C.M. Reddy, Environ. Sci. Technol. 37 (2003) 1653.

[33] G.F. Slater, H.K. White, T.I. Eglinton, C.M. Reddy, Environ. Sci. Technol. 39 (2005) 2552.

[34] C. Vendeuvre, F. Bertoncini, L. Duval, J.-L. Duplan, D. Thiebaut, M.-C. Hennion, J. Chromatogr. A 1056 (2004) 155.

[35] C. Vendeuvre, R. Ruiz-Guerrero, F. Bertoncini, L. Duval, D. Thiebaut, M.-C. Hennion, J. Chromatogr. A 1086 (2005) 21.

[36] A. Williams, D. Ryan, G.A. Olarte, P. Marriott, E. Pang, J. Chromatogr. B: Biomed. Appl. 817 (2005) 97.

[37] J. Beens, J. Blomberg, P.J. Schoenmakers, J. High Resol. Chromatogr. 23 (2000) 182.

[38] J. Beens, H. Boelens, R. Tijssen, J. Blomberg, J. High Resol. Chromatogr. 21 (1998) 47.

[39] H. Carlsson, G. Robertsson, A. Colmsjo, Anal. Chem. 73 (2001) 5698.

[40] P.L. Patterson, J. Chromatogr. Sci. 24 (1986) 41.

[41] D. Ryan, P. Marriott, J. Sep. Sci. 29 (2006) 2375.

[42] P.L. Patterson, J. Chromatogr. 167 (1978) 381.

[43] K. Olah, A. Szoke, Z. Vajta, J. Chromatogr. Sci. 17 (1979) 497.

[44] P.L. Patterson, R.L. Howe, J. Chromatogr. Sci. 16 (1978) 275.

[45] J.E. Lovelock, J. Chromatogr. 99 (1974) 3.

[46] J.E. Lovelock, J. Chromatogr. A 112 (1975) 29.

[47] E.C.M. Chen, E.S. Chen, J. Chromatogr. A 1037 (2004) 83.

[48] http://www.uga.edu/srel/AACES/GCtutorial/page18.html, accessed in 12/09/2005.

[49] http://www.chromatography-online.org/topics/electron/capture/detector.html, accessed in 12/09/2005.

[50] M.S. Klee, M.D. Williams, I. Chang, J. Murphy, J. High Resol. Chromatogr. 22 (1999) 24.

[51] J. Zrostlikova, S.J. Lehotay, J. Hajslova, J. Sep. Sci. 25 (2002) 527.

[52] X. Quan, S. Chen, B. Platzer, J. Chen, M. Gfrerer, Spectrochim. Acta, Part B 57B (2002) 189.

[53] K. Conka, B. Drobna, A. Kocan, J. Petrik, J. Chromatogr. A 1084 (2005) 33.

[54] J. Aybar-Munoz, E. Fernandez-Gonzalez, L.E. Garcia-Ayuso, A. Gonzalez-Casado, L. Cuadros-Rodriguez, Chromatographia 61 (2005) 505.

[55] B. Gomara, L. Ramos, M.J. Gonzalez, J. Chromatogr., B: Anal. Technol. Biomed. Life Sci. 766 (2002) 279.

[56] P. Korytar, H.-G. Janssen, E. Matisova, U.A.T. Brinkman, Trends Anal. Chem. 21 (2002) 558.

[57] P. Korytar, P.E.G. Leonards, J. de Boer, U.A.T. Brinkman, J. Chromatogr. A 958 (2002) 203.

[58] E.M. Kristenson, P. Korytar, C. Danielsson, M. Kallio, M. Brandt, J. Makela, R.J.J. Vreuls, J. Beens, U.A.T. Brinkman, J. Chromatogr. A 1019 (2003) 65.

[59] T.H. Pham, H.-G.M. Janssen, C.A. Cramers, J. High Resol. Chromatogr. 18 (1995) 333.

[60] S. Ng, Y. Briker, Y. Zhu, T. Gentzis, Z. Ring, C. Fairbridge, F. Ding, S. Yui, Energy Fuels 14 (2000) 945.

[61] B.L. Jaycox, D.L. Olsen, Applied Occupational and Environmental Hygiene 15 (2000) 695.

[62] B. Chawla, F. Di Sanzo, J. Chromatogr. A 589 (1992) 271.

[63] D. Rauhut, H. Kurbel, K. MacNamara, M. Grossmann, Analusis 26 (1998) 142.

[64] M. Mestres, O. Busto, J. Guasch, J. Chromatogr. A 881 (2000) 569.

[65] K.K. Gaines, W.H. Chatham, S.O. Farwell, J. High Resol. Chromatogr. 13 (1990) 489.

[66] L.R. Benner, H.D. Stedman, Anal. Chem. 61 (1989) 1268.

[67] R.S. Hutte, N.G. Johansen, M.F. Legier, J. High Resol. Chromatogr. 13 (1990) 421.

[68] R.L. Shearer, L.M. Meyer, J. High Resol. Chromatogr. 22 (1999) 386.

[69] X. Yan, J. Chromatogr. A 976 (2002) 3.

[70] R. Hua, Y. Li, W. Liu, J. Zheng, H. Wei, J. Wang, X. Lu, H. Kong, G. Xu, J. Chromatogr. A 1019 (2003) 101.

[71] R. Hua, J. Wang, H. Kong, J. Liu, X. Lu, G. Xu, J. Sep. Sci. 27 (2004) 691.

[72] J. Blomberg, T. Riemersma, M.v. Zuijlen, H. Chaabani, J. Chromatogr. A 1050 (2004) 77.

[73] B. Chawla, J. Sep. Sci. 35 (1997) 97.

[74] C.Y. Wing, D.H. Fine, K.S. Chiu, K. Biemann, Anal. Chem. 56 (1984) 1158.

[75] N. Kashihira, K. Makino, K. Kirita, Y. Watanabe, J. Chromatogr. 239 (1982) 617.

[76] B.D. Quimby, V. Giarrocco, Hewlett Packard 1997, Application Note Gas Chromatography, 1-11.

[77] D.A. Skoog, F.J. Holler, T.A. Nieman, Principles of Instrumental Analysis, Saunders College Pub. and Harcourt Brace College Publishers, Philadelphia, 1998, p. 709.

[78] T.G. Chasteen, Atomic Emission Detector, www.chemistry.adelaide.edu.au 12.09.2005.

[79] L.L.P. van Stee, U.A.T. Brinkman, H. Bagheri, Trends Anal. Chem. 21 (2002) 618.

[80] G.H. Fuller, R. Steltenkamp, G.A. Tisserand, Ann. N.Y. Acad. Sci. 116 (1964) 711.

[81] A. Dravnieks, O' Donnell, J. Agric. Food Chem. 19 (1971) 1049.

[82] C.M. Delahunty, G. Eyres, J.-P. Dufour, J. Sep. Sci. 29 (2006) 2107.

[83] B.d.A. Zellner, P. Dugo, G. Dugo, L. Mondello, J. Chromatogr. A 1186 (2008) 123.

[84] S.M. van Ruth, Biomolecular Engineering 17 (2001) 121.

[85] G.T. Eyres, P.J. Marriott, J.-P. Dufour, J. Agric. Food Chem. 55 (2007) 6252.

[86] L.D. Falcao, G. de Revel, J.-P. Rosier, M.T. Bordignon-Luiz, Food Chem. 107 (2007) 497.

[87] D. Machiels, S.M. van Ruth, M.A. Posthumus, L. Istasse, Talanta 60 (2003) 755.

[88] R.F.A. Moreira, C.A.B. de Maria, Flavour Frag. J. 20 (2005) 13.

[89] B.d.A. Zellner, A. Casilli, P. Dugo, G. Dugo, L. Mondello, J. Chromatogr. A 1141 (2007) 279.

[90] G. Eyres, J.-P. Dufour, G. Hallifax, S. Sotheeswaran, P.J. Marriott, J. Sep. Sci. 28 (2005) 1061.

[91] G. Eyres, P.J. Marriott, J.-P. Dufour, J. Chromatogr. A 1150 (2007) 70.

Chapter

3

MODULATION RATIO (M_R) IN COMPREHENSIVE TWO-DIMENSIONAL GAS CHROMATOGRAPHY

This chapter has been published as "Modulation Ratio in Comprehensive Two-Dimensional Gas Chromatography", Khummueng W., Harynuk J., Marriott P.J., Anal.Chem., 78, 4578-87 (2006).

Abstract

Comprehensive two-dimensional chromatography employs a serially-coupled two-column arrangement where effluent from the first column is collected or sampled and then introduced to the second column according to a chosen modulation period (P_M). This is affected by use of a modulator at or near the column junction. One of the considerations in applying the technique is the period of the modulator which determines the sampling duration of the first column effluent. Here, we propose that the sampling rate can be most effectively described by a new term, called modulation ratio (M_R). This is defined as the ratio of 4 times the first column peak standard deviation (4σ) divided by P_M, or peak width at base (w_b) divided by P_M, or 1.6985 times the half-height width of the peak (w_h):

$$M_R = \frac{4\sigma}{P_M} = \frac{w_b}{P_M} = \frac{w_h \times 1.6985}{P_M} \quad (1)$$

The 4σ value is more commonly recognised as the peak base width (w_b). The use of 4σ as the numerator is preferred to simply σ because when the P_M value used for an experiment is equal to σ then the M_R value is calculated to be 4; implying that the primary peak will be modulated about 4 times as is normally recommended for a comprehensive multidimensional separation. The less well-defined term of modulation number (n_M) has been previously used and proposed as the number of modulations per peak, and therefore is intended to convey the manner in which the primary column peak is sampled; this is a subjective and not well-characterised value. The use of M_R should provide users with a meaningful and strictly defined value when reporting experimental conditions. The utility of M_R is demonstrated through a mathematical model of the modulation process for both Gaussian and tailing peaks, supported by an experimental study of the modulation ratio. It is shown that for the analysis of trace compounds where precise quantitative measurements are being made, the experiment should be conducted with an M_R of at least 3. Conversely, for semi-quantitative methods or the analysis of major components, an M_R of about 1.5 should suffice.

3.1 Introduction

Whilst, the application of comprehensive two-dimensional chromatography (GC×GC) in different complex samples is increasing, fundamental studies are still being conducted for the further understanding of basic GC×GC principles. Murphy, Shure and Foley found that the number of modulations required of the first dimension peaks, in order to produce the best two-dimensional resolution in a GC×GC experiment, should be at least 3 for peaks that are in-phase and at least 4 if the peak phase is not considered [1]. This publication has now entered the lore of GC×GC, having been cited over 40 times in GC×GC publications, where analysts set up their method with an aim to achieve about this number of modulations. However, an immediate problem can be recognised; that of defining the number of modulations for a peak. Depending on how far from the peak maximum a measurement is taken, and how low a signal response is to be (or can be) measured, the modulation number (n_M) that is quoted for a single peak can vary substantially, as will be shown below. In a paper on nomenclature on comprehensive chromatography, Schoenmakers et al defined a variety of different terms such as modulation phase, frequency, and modulation number [2]. It is proposed that the latter is not an appropriately rigorous term to be used for accurately describing the nature of the modulation in an experiment. One of the reasons for this was highlighted by Ong and Marriott in an original study on modulation phase and frequency, where they showed how the peak pattern can vary if the modulation timing varies slightly [3], equivalent to altering the phase of modulation. Interestingly in the context of the present study, they showed how the relative significance (i.e. relative response heights or areas) of different peaks changed for different phase and frequency settings. A second difficulty in using modulation number (n_M) is due to the presence of overloaded or tailing peaks which arise frequently in GC×GC and have received the attention of a number of researchers [3-5]. These non-linear peaks (in the sense that they arise from non-linear chromatographic conditions) are almost invariably broadened, and consequently the modulation number – and modulation ratio – will increase for these peaks compared to the linear chromatography case. The definition of modulation ratio should be able

to take these peaks into account, using an easily measured feature of the peak. In an earlier work investigating the efficiency of sampling and the potential undersampling of the first dimension in GC×GC separations using valve-based modulators, Seeley defined a parameter termed the ***dimensionless sampling period*** as the ratio of the modulation period to the standard deviation of the primary peak ($\tau_z = P_M/^1\sigma$) [6]. This definition succeeds in relating the primary peak width to the modulation period and providing a single number to describe the sampling. However, it has a name which could be easily confused with the modulation period, and it has the disadvantage that as τ_z increases, the number of observed modulations actually decreases. Thus, the term Modulation Ratio (M_R) is proposed to be defined as in **Equation (1)**,

$$M_R = \frac{4\sigma}{P_M} = \frac{w_b}{P_M} = \frac{w_h \times 1.6985}{P_M} \quad (1)$$

where the factor of 1.6985 is the ratio of the half height width (w_h) to the base width (w_b) of a symmetrical Gaussian peak in terms of σ. The reason for the factor of 1.6985 is that it should cause the value of M_R to be approximately equal to the number of modulated pulses that will be generated for a given peak. Basically, the 4σ value is more commonly recognised as the peak base width (w_b). The use of 4σ as the numerator is preferred over σ, because if the P_M value is used for an experiment, and it happens to be equal to σ, then the M_R value is calculated to be 4. This is equivalent to having 'about 4 modulations' in the experiment. Clearly, M_R is a meaningful and strictly defined value when reporting experimental conditions in GC×GC analysis instead of the less well defined term of modulation number (n_M). The importance of the modulation ratio, while demonstrated using GC×GC separations, is not limited to this field. As with previous studies into comprehensive two-dimensional chromatography [1,6], the modulation ratio can be extended to other comprehensive multidimensional chromatographic separations. Through the use of mathematical models of the modulation process, the concept of the modulation ratio will be explored; the results of a series of experiments to show practical implications of the modulation ratio will be presented. Recently, M_R has been used by researchers for interpretation of the results and reporting the experimental parameters. For instance,

Seeley and co-workers [7] used the M_R concept for the determination of the correct choice of P_M to minimize the inconsistent transfer of the fraction of the peaks from the first column to the second column in the Deans' Switch modulator. They used the M_R term to indicate the precision of the fraction transfer. The results showed that the RSD of peak area of the modulated peak decreased less than 0.5% when the modulation ratio is greater that 2.5 or when a smaller P_M was performed. Clearly, M_R has been used as a parameter to decide P_M in GC×GC and quantitative aspects of GC×GC data will be simplified when the M_R concept is utilised, as will be discussed in detail below.

The M_R concept was proposed to be relevant to the P_M value chosen in GC×GC analysis. The M_R value may imply the number of modulated peaks that need to be summed-up to obtain an acceptable peak area and peak height measure of compounds compared to peak area and height obtained from 1D-GC results. For example, Amador-Munoz et al [8], reported a model of quantitative analysis based on the M_R concept using the GC×GC technique. The summation of the modulated peaks was investigated. The results show that either 2 or 3 major peaks of compounds can be chosen for quantitative analysis. The developed model was applied to the analysis of PAH in air particulates. The approach offers a simplified and relative robust quantitative analysis method for GC×GC techniques.

3.2 Experimental

3.2.1 Chromatographic conditions

The split/splitless GC injector was operated at 250 ^{o}C; an injection volume of 1.0 μL was employed in split mode at split ratio 15:1. The FID detector was operated at 280 ^{o}C with data collection frequency of 100 Hz, for both non-modulated and modulated gas chromatography analysis. The GC oven was isothermal at 95 ^{o}C, held for 30 min. Carrier gas was operated in the constant flow mode, with a column flow rate of 1.0 mL.min^{-1} (average velocity ($\bar{u}$) = 40 cm.s^{-1}).

3.2.2 Column sets

The first dimension (^{1}D) column was a 30 m x 0.25 mm i.d. capillary column, with 0.25 μm d_f comprising a 5% phenyl polysilphenylene-siloxane (BPX5) phase. The second dimension (^{2}D) column consisted of 1 m x 0.1 mm i.d., 0.1 μm d_f BP20 polyethylene glycol. All columns were from SGE International, Ringwood, Australia.

3.2.3 Standards

A 17 compound standard mixture was prepared consisting of the following components; hexan-1-ol, nonane, α-pinene, propylbenzene, heptan-1-ol, decane, γ-terpinene, octan-1-ol, undecane, linalool, nonan-1-ol, terpinene-4-ol, naphthalene, dodecane, decan-1-ol, bornyl acetate and tridecane were prepared in pesticide grade hexane at an appropriate concentration. The choice of mixture was to allow selection of compounds, which varied in asymmetry (i.e. alcohols will tend to exhibit tailing; alkanes will be more symmetric) and the isothermal analysis allows peaks of varying width to be easily generated over the analysis time, thus allowing for testing of peaks with different modulation ratio (M_R) values.

3.2.4 Data analysis

For data analysis, peak height and total peak area data was generated using Chemstation software program from (Agilent Technology). All graphs were re-plotted use the Origin 6.0 program. Peak asymmetry was measured according to the calculation (distance of peak maximum to peak tailing edge) / (distance of peak leading edge to peak maximum) at a height of 10% peak height.

3.2.5 Modulation period study

Modulation periods (P_M) of 2, 3, 4, 5, 6, 7 and 9 s were used for the 17 compound standard mixtures. The modulation start time was kept constant at 3.00 min, (except for **Section 3.2.6** below) and stopped at 28 min for the analysis, while the modulation period was varied over a series of analyses.

3.2.6 Modulation phase study

In this study, the start time was sequentially incremented by 0.02 min in order to alter the modulation phase of the cryotrap with respect to the peak elution [3]. Modulation period was kept constant at 6 s while modulation start time was varied from 3.00, 3.02, 3.04, 3.06, 3.08 and 3.10, respectively. The start time of 3.10 min corresponds to a modulation phase equivalent to that for a start time of 3.00 min (i.e. 6 s = 0.10 min), provided the component retention time does not vary from run-to-run (or at least only varies negligibly compared with the selected modulation period).

3.3 Results and Discussion

To consider a GC×GC separation with a given P_M, and with 1st dimension peaks having a given σ, the modulation ratio (M_R) as defined by **Equation (1)** will generate a given number of modulations of the primary peak in a specific ratio of areas and heights, depending on the phase of the modulation. However, this does not answer the question of how many modulations will be observed, and the fraction of the peak area that will be accounted for by the modulations. For instance, an abundant analyte may give rise to 3 large modulated peaks and 2 or more small peaks, and maybe some very small peaks. Under identical conditions, a trace analyte having the same σ may only exhibit 1 large peak and 2 or more small peaks. This implies that the modulation number (n_M; how many modulated peaks are obtained) will be poorly defined. When tailing peaks are analysed, there is the issue of how many of the small tailing peaks must be included in order to accurately determine the total area of the peak. To answer these questions from a sound theoretical background, a mathematical model of the modulation process was constructed in Mathcad (Mathsoft, Cambridge, MA) for both symmetrical and tailing first dimension peaks. Following the development of the model, experiments were conducted to determine if the effects shown by the model were reflected in an actual GC×GC operation.

3.3.1 Theoretical study of the modulation ratio

In order to mathematically model the concentration profile of a symmetrical primary dimension peak, the normal distribution **Equation (2)** was used.

$$C(t) = \frac{A}{\sqrt{2\pi\sigma^2}} e^{\left(-\frac{(t-t_R)^2}{2\sigma^2}\right)} \qquad (2)$$

In this equation, C(t) is the concentration of the analyte as a function of time t, A is the amplitude of the peak, t_R is the retention time of the peak, and σ is the

standard deviation of the peak in the first dimension. For the purposes of demonstration and to facilitate the calculation of suitable modulation periods to obtain the desired modulation ratios, A was set to 1, t_R was set to 16 s, and σ was set to 2 s (w_h = 4.71 s) **Figure 3.1(A)**.

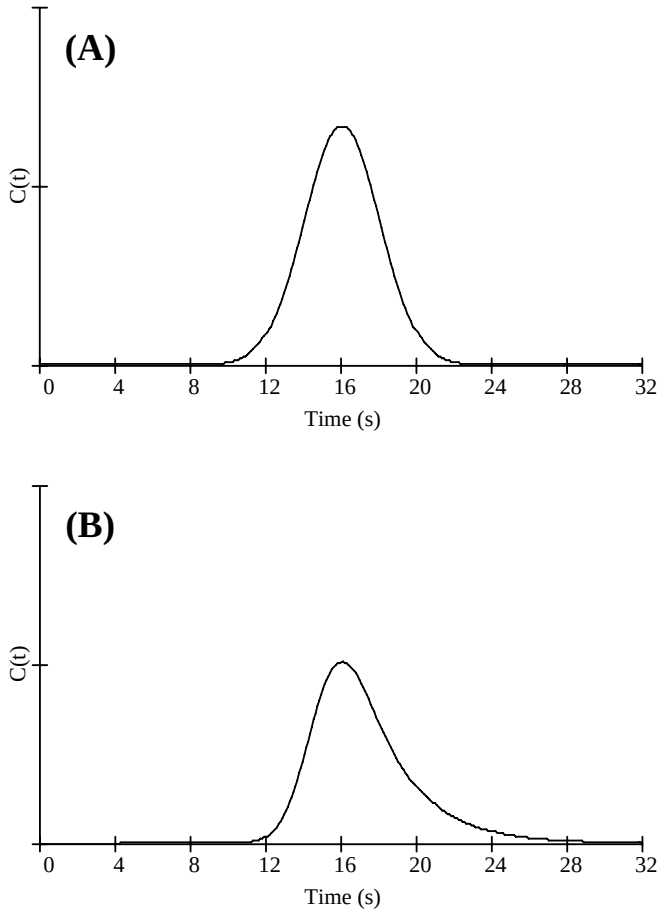

Figure 3.1: Models of primary dimension peaks having half-height widths of 4.7 s and retention times of 16s. **(A)** Gaussian peak **(B)** Tailing peak modelled using the exponentially modified Gaussian and having an asymmetry value of 2.00.

To model a tailing primary peak, the exponentially modified Gaussian (EMG) equation was used, as this has been shown to be applicable to tailing GC peaks **Equation (3)** [9].

$$C(t) = \frac{A\sigma_G}{\tau\sqrt{2}} e^{\left[\left(\frac{\sigma_G}{\tau}\right)^2 \frac{1}{2} - \frac{(t-t_G)}{\tau}\right]} \int_{-\infty}^{Z} e^{-x^2} dx \qquad (3)$$

The EMG equation uses a parent Gaussian curve with amplitude A, standard deviation σ_G, and retention time t_G and then applies a decay time constant τ which also appears in the equation for *Z*, the upper bound of the integration **Equation (4)**.

$$Z = \frac{\frac{t-t_G}{\sigma_G} - \frac{\sigma_G}{\tau}}{\sqrt{2}} \qquad (4)$$

For the modelling of tailing peaks, the values of A, t_G, σ_G, and τ that were used were 1, 14.668 s, 1.333 s, and 2.565 s, respectively. This yielded a peak with an asymmetry of 2.00 having a retention time of 16 s and a w_h of 4.71 s **Figure 3.1(B)**, which were the same as those for the symmetrical peak that was being modelled. The modulation process was simulated by calculating a series of integration times (x_n) based on P_M such that $x_n = (n \times P_M) + x_0$, where x_0 was the initial start time and was used to adjust the phase of modulation. P_M values that were used were 2.0 s, 2.66 s, 4.0 s, 5.33 s, and 8.0 s to yield modulation ratios of 4, 3, 2, 1.5, and 1, respectively for both the symmetrical and the tailing peaks. Values of x_0 were set to be equal to $j \times P_M / 4$ where j had values of 0, 1, 2, 3 with 0 being 180° out-of-phase and 2 being perfectly in-phase. The series of integrals for each slice as given by **Equation (5)** was then calculated for each simulation to obtain the area of the original peak that was contained in each slice (Ar_n).

$$Ar_n = \int_{x_n}^{x_{n+1}} C(t)dt \tag{5}$$

These areas were then used to calculate a series of Gaussian peaks p_n with $^2\sigma$ = 0.05 s (200 ms base width) each having height H_n, and retention time in the primary dimension of x_{n+1}. Summing the series of peaks p_n yields the equation for the modulated primary peak, P, plotted in **Figure 3.2 (A) and 3.2 (B)**.

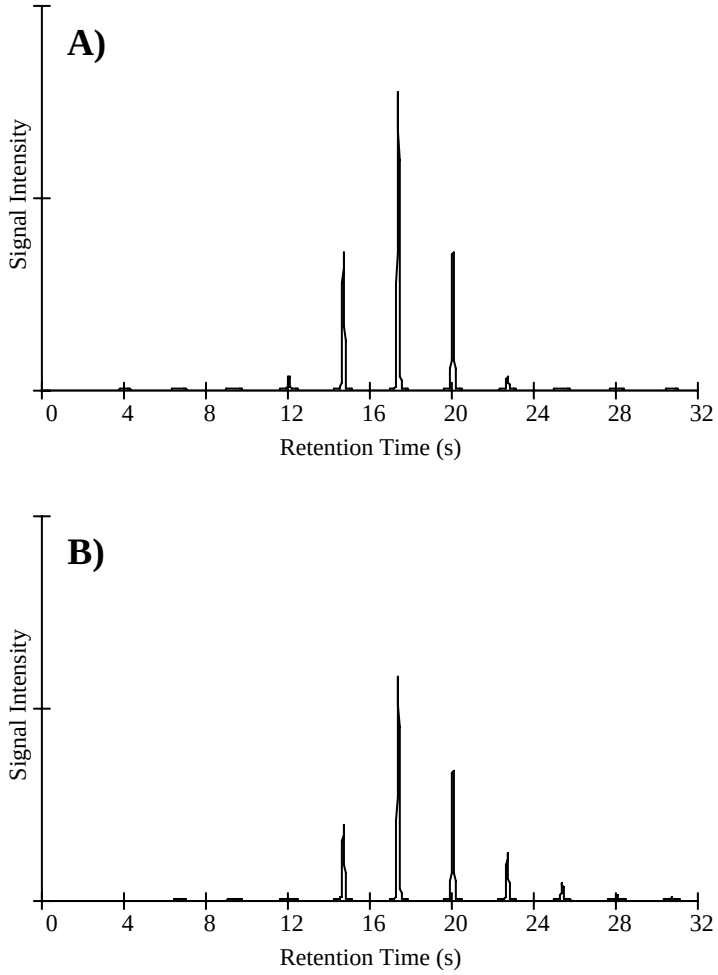

Figure 3.2: Models of the modulated peaks from **Figure 3.1** using a modulation period of 2.6667 s, (M_R of 3.0). **(A)** Modulated peak from **Figure 3.1 (A)**, **(B)** modulated peak from **Figure 3.1(B)**. Modulated peaks are modulated with a period of 2.6667s (M_R = 3.0).

To determine the effect of the intensity of the primary peak on the detectability of the modulated peaks, a series of normally distributed random numbers with σ_N = 0.0378 pA and μ_N = 8.0 pA was added to P at a rate of 100 Hz to simulate detector noise. These parameters were determined by measuring the baseline of an isothermal GC×GC column blank with P_M of 5.0 s in the region free from the primary column bleed blank. The blank was performed isothermally at 200 °C with an Agilent 6890GC with an FID operating at 100 Hz. With different detectors, instrument configurations, or operating conditions the actual noise values will vary; however, these parameters were seen as adequate for demonstration purposes. To scale the peaks, the base peak height (BPH) (highest value of H in P) was set to values of 100, 10, and 1 pA above baseline, and all of the other peaks in the simulation were scaled according to their relative heights.

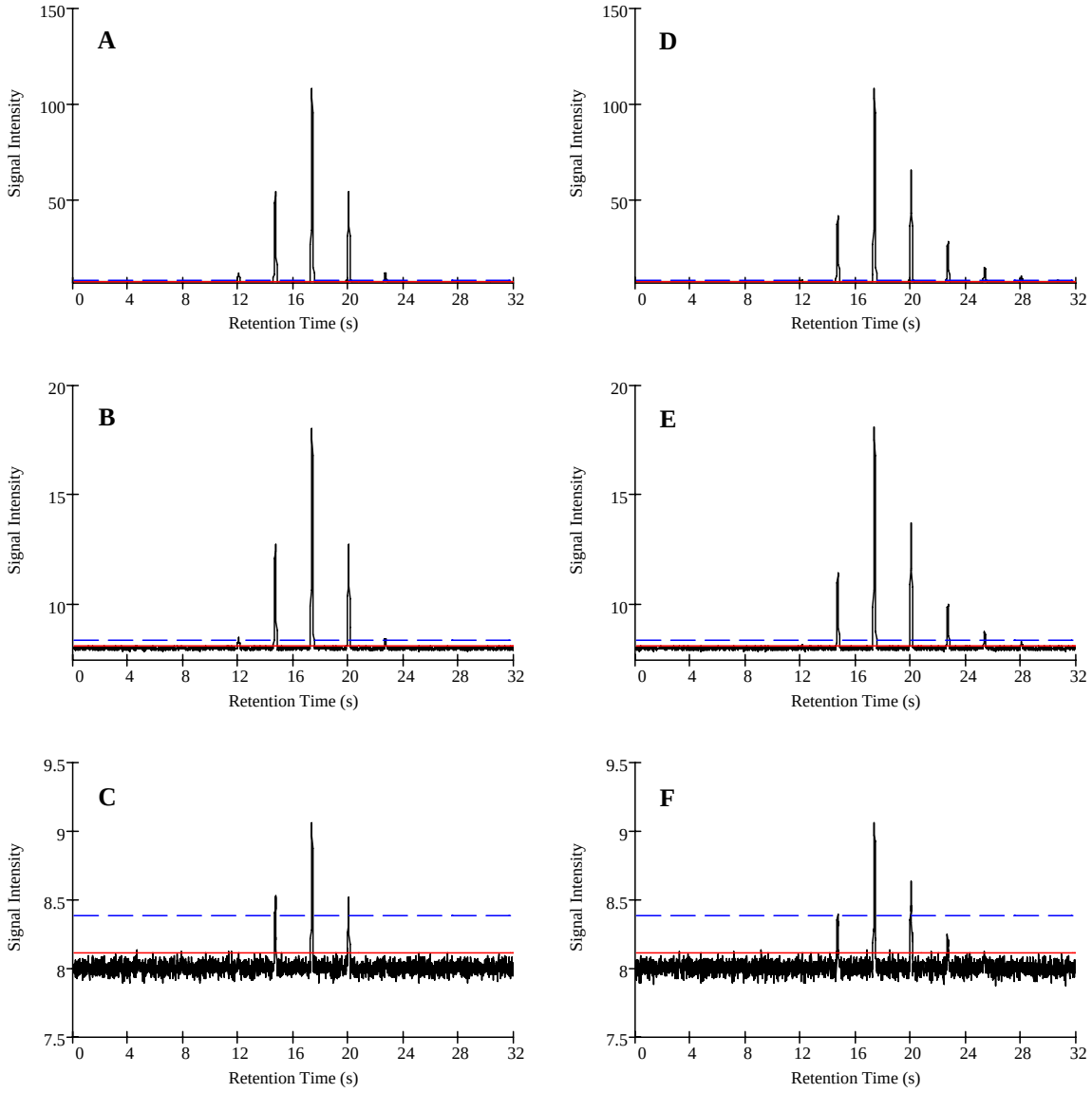

Figure 3.3: Effect of peak intensity on the number of observed modulation pulses. Peaks are scaled for the base peak intensities of 100, 10, and 1 pA above the baseline (**A, B, C,** respectively for symmetrical peaks, and **D, E, F,** respectively for tailing peaks). The solid horizontal line represents the LOD (3σ) and the dashed line represents the LOQ (10σ).

Added to **Figure 3.3** are horizontal lines to represent the limit of detection (LOD; defined as $3\sigma_N$) and limit of quantitation (LOQ; $10\sigma_N$) above the baseline. Inspection of the figure shows the potential for a philosophical debate. In most 1DGC measurements, there is a single response for a single component and

determining whether the response is above or below certain thresholds of measurement certainty is a simple matter. However, in GC×GC there are multiple responses for a single component, and some may fall below $10\sigma_N$ but above $3\sigma_N$. It is the authors' assumption that most chromatographers will include the reported areas for these small peaks in the total area for the compound. However, this will increase the uncertainty in the measurement of trace compounds. Thus, in **Tables 3.1 and 3.2**, which summarise the results of the modelling study for all values of M_R, phase, and the three base peak intensities that were studied, two cumulative areas were calculated. For the values of n(LOQ) and Area %(LOQ), only those peaks p_n with heights H_n greater than $10\sigma_N$ above the baseline were added as contributors to the total Area %. Likewise, for the n (LOD) and Area %(LOD) values, all peaks with H_n greater than $3\sigma_N$ above the baseline were included. It should be noted that for symmetrical peaks, there is no difference between a phase of 90° and 270° other than a reflection of the modulated peak pattern about the ^{1}D retention time. Thus, **Table 3.1** only has calculations for three modulation phases.

Table 3.1: Results of modelling study of symmetrical peak for different M_R and phase. BPH – Base Peak Height above baseline. n(LOQ): number of observable modulated pulses with S/N > 10. Area % (LOQ): fraction of total peak area represented by the peaks with S/N > 10. n(LOD): number of observable modulated pulses with S/N > 3. Area % (LOD): fraction of total peak area represented by the peaks with S/N > 3.

M_R	**4**			**3**			**2**			**1.5**			**1**		
Phase	**0**	**90**	**180**	**0**	**90**	**180**	**0**	**90**	**180**	**0**	**90**	**180**	**0**	**90**	**180**
BPH = 100															
n (LOQ)	7	7	8	5	5	6	3	4	4	3	3	4	3	2	2
Area % (LOQ)	99.95	99.93	99.99	99.91	99.85	99.99	99.73	99.98	99.99	99.99	99.96	100	100	99.86	99.99
n (LOD)	7	8	8	5	6	6	5	4	4	3	3	4	3	3	2
Area % (LOD)	99.95	99.93	99.99	99.91	99.99	99.99	100	9.98	99.99	99.99	99.96	100	100	100	99.99
BPH = 10															
n (LOQ)	5	5	6	5	4	4	3	3	4	3	2	2	1	2	2
Area % (LOQ)	98.76	98.48	99.73	99.91	98.83	99.23	99.73	99.36	99.99	99.99	97.68	99.23	95.45	99.86	99.99
n (LOD)	7	6	6	5	5	4	3	3	4	3	3	2	3	2	2
Area % (LOD)	99.95	99.64	99.73	99.91	99.85	99.23	99.73	99.36	99.99	99.99	99.96	99.23	100	99.86	99.99
BPH = 1															
n (LOQ)	3	3	4	3	2	2	1	2	2	1	1	2	1	1	2
Area % (LOQ)	86.64	85.43	95.45	95.45	79.36	81.75	68.27	92.7	95.45	81.76	72.47	99.23	95.45	84	99.99
n (LOD)	5	4	4	3	3	4	3	2	2	1	2	2	1	2	2
Area % (LOD)	98.76	94.77	95.45	95.45	94.239	99.23	99.73	92.7	95.45	81.76	97.68	99.23	95.45	99.86	99.99

Table 3.2: Results of modelling study of asymmetrical peak for different M_R and phase. BPH – Base Peak Height above baseline. n(LOQ): number of observable modulated pulses with S/N > 10. Area % (LOQ): fraction of total peak area represented by the peaks with S/N > 10. n(LOD): number of observable modulated pulses with S/N > 3. Area % (LOD): fraction of total peak area represented by the peaks with S/N > 3.

M_R	**4**				**3**			
Phase	**0**	**90**	**180**	**270**	**0**	**90**	**180**	**270**
BPH = 100								
n (LOQ)	10	11	11	11	8	8	8	8
Area % (LOQ)	99.76	99.84	99.86	99.88	99.78	99.82	99.85	99.81
n (LOD)	13	13	12	12	10	9	9	10
Area % (LOD)	99.96	99.96	99.94	99.94	99.97	99.94	99.94	99.96
BPH = 10								
n (LOQ)	7	7	7	7	5	5	6	5
Area % (LOQ)	97.92	98.19	98.25	97.917	97.84	97.36	98.92	97.59
n (LOD)	9	9	9	9	6	7	7	7
Area % (LOD)	99.53	99.52	99.36	99.47	98.99	99.51	99.61	99.62
BPH = 1								
n (LOQ)	3	3	3	3	2	3	3	2
Area % (LOQ)	76.72	78.24	77.69	74.91	70.23	87.7	88	73.44
n (LOD)	5	6	6	5	4	4	4	4
Area % (LOD)	93.41	96.21	96.61	93.65	94.56	94.84	93.51	93.35

Table 3.2 (Continued)

M_R	2				1.5				1			
Phase	**0**	**90**	**180**	**270**	**0**	**90**	**180**	**270**	**0**	**90**	**180**	**270**
BPH = 100												
n (LOQ)	5	5	6	6	5	4	4	5	4	3	3	3
Area % (LOQ)	99.71	99.76	99.87	99.91	99.95	99.78	99.85	99.92	99.97	99.71	99.87	99.94
n (LOD)	6	6	7	7	5	5	5	6	4	4	4	3
Area % (LOD)	99.94	99.92	99.97	99.98	99.95	99.97	99.97	99.99	99.97	99.99	99.99	99.94
BPH = 10												
n (LOQ)	4	4	4	4	3	3	3	3	2	3	3	2
Area % (LOQ)	98.62	99.02	98.99	97.96	96.99	98.21	98.92	98.99	98.99	99.71	99.87	98.62
n (LOD)	5	5	4	5	4	4	4	3	2	3	3	3
Area % (LOD)	99.71	99.76	98.99	99.57	99.62	99.78	99.85	98.99	98.99	99.71	99.87	99.94
BPH = 1												
n (LOQ)	2	1	2	2	1	1	2	2	1	1	2	2
Area % (LOQ)	85.44	58.59	85.31	88.16	72.46	70.23	91.47	94.56	85.31	85.44	96.99	98.62
n (LOD)	3	3	3	3	2	3	3	2	2	1	2	2
Area % (LOD)	93.43	95.51	96.62	95.82	93.51	98.21	98.92	94.56	98.99	85.44	96.99	98.62

Another way to approach the data is presented in **Figure 3.4** for M_R values from 4.0 to 1.0 for the symmetric peak and in **Figure 3.5** for the tailing peak. Here, the fraction of the primary peak area in each modulation slice was calculated. These values were then sorted in order from the tallest to the shortest ^{2}D peak, and then the cumulative area of the slices was determined and plotted. The horizontal dashed and solid lines indicate levels of 90, 95, and 99 % of the total peak area. The dashed and solid vertical lines indicate the largest number of modulated peaks that can be observed for peaks at a given base peak height (n(LOD)) from **Tables 3.1 and 3.2**). In the cases where the number of peaks above a threshold level changes in **Tables 3.1 and 3.2** depending on the phase of the modulation, the largest of the possible number of observable peaks is chosen as the position of the vertical line. When examining the data in these figures, one must realise that the number of included peaks denoted by these vertical lines is for the highest number of modulations that is observable. Depending on the modulation phasing and whether one is concerned with peaks above the LOD or above the LOQ, the number of observable peaks will decrease. It will also change depending on the noise in the signal, most likely resulting in a decrease in the number of observable peaks because the models here have a modest estimate of signal noise. The figure also shows that as the M_R decreases from 4.0 to 1.0, the effect of subtle changes in the modulation phase on the observed cumulative peak area becomes more significant, as evidenced by the spread in the cumulative peak areas across the different phases. These subtle changes can be brought about by numerous factors that could alter the retention on the primary column including, for example a septum leak, degradation of the primary column, or a minor shift in the modulator timing. This error will of course be more significant for trace analytes which may only have two or three observable modulation pulses, and of less importance for peaks from analytes present in high abundance as it will be possible to observe peaks which account for most of the analyte signal. Some insight into how many peaks must be counted in determining the response from a peak can also be gathered from the figures. Though there may be many observable peaks, especially for compounds that tail on the ^{1}D column, the fraction of area included in these smaller peaks may not be significant within the scope of the method. For

example, with a symmetrical peak and M_R = 4, there could be 7 or 8 observable modulation slices for a peak with BPH = 100. Depending on the abundance of the compound, the noise, and $^2\sigma$ of the modulated pulses, this number could be greater or smaller in a given separation. However, the largest 7 peaks contain 98% of the peak response. By including additional peaks, there may be more error introduced into the measurement than one gains from the additional area (especially as these additional peaks may be below the LOQ). A discussion of the error in GC×GC measurements and an analysis of the error associated with summing peaks in situations such as these is a subject deferred for future study [8]. However, the data presented here give an indication of potential errors involved in failing to include an adequate number of peaks in the total area for a compound.

Examination of **Tables 3.1** and **3.2** and **Figure 3.4 and 3.5** suggest the following guidelines in determining appropriate values for M_R in GC×GC separations. For separations where the utmost accuracy and precision in the measurement of trace analytes is required, a M_R of 3 or more should be used. In this way, the chromatographer will be certain that even trace analytes (here compounds with a BPH = 1 pA above the baseline) will be sampled such that at least three modulations will be detected, and that at least 2 of them should have heights above the LOQ, allowing the areas to be determined with a high degree of confidence. The data also suggest that for analyses that are used for screening or determination of analytes that are present in high abundance, a modulation ratio of 1.5 would be sufficient. A minimum of three pulses per peak would be observed for symmetrical and tailing peaks having a BPH > 10 pA above the noise in most cases, thus satisfying the criteria for preserving the primary separation for all but the trace peaks and some perfectly out-of-phase peaks. However, these few poorly modulated peaks would be detected and likely measured well enough for a semi-quantitative analysis.

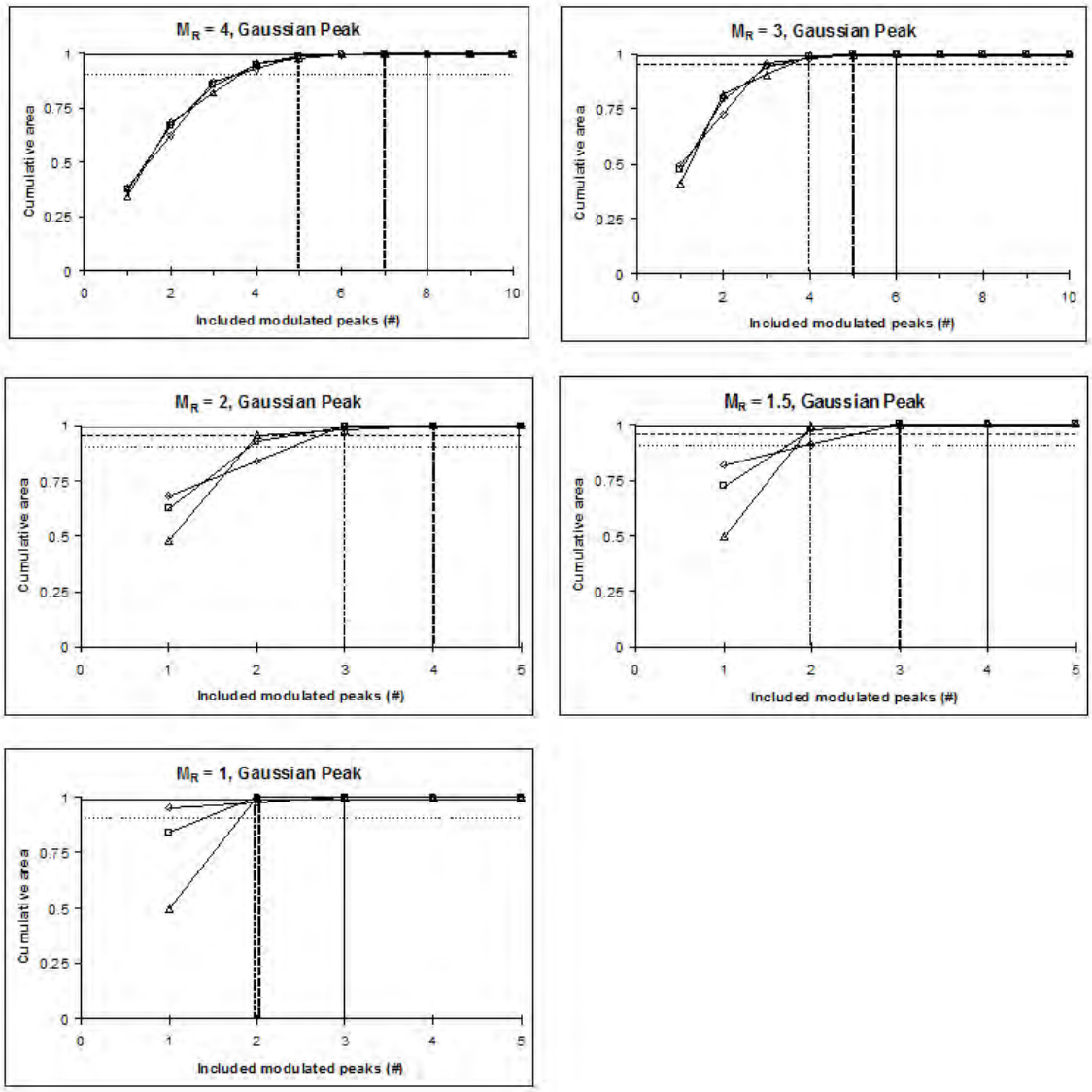

Figure 3.4: Cumulative peak areas for different values of M_R and modulation phase from the models of Gaussian peaks. Phases indicated by: 0° (◊), 90° (□) and 180° (Δ). Horizontal lines indicate 90, 95, and 99% cumulative peak area. Vertical lines indicate the greatest number of visible modulation pulses for peaks having a BPH = 1 (short dash), 10 (long dash), and 100 pA above the baseline (solid).

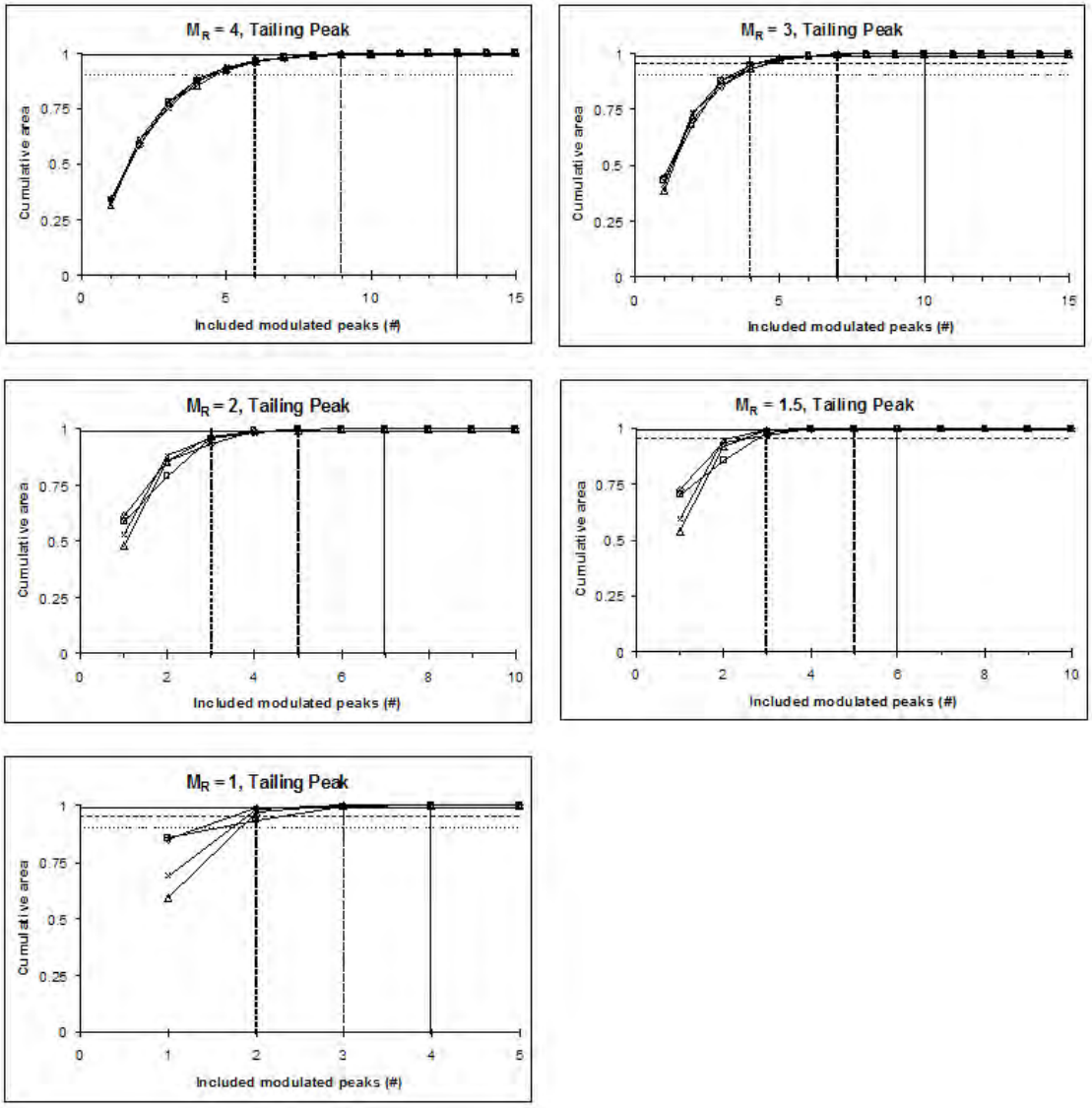

Figure 3.5: Cumulative peak areas for different values of M_R and modulation phase from the models of tailing peaks (As = 2.0). Phases indicated by: 0° (◊), 90° (□), 180° (Δ), and 270° (×). Horizontal lines indicate 90, 95, and 99% cumulative peak area. Vertical lines indicate the greatest number of visible modulation pulses for peaks having a BPH = 1 (short dash), 10 (long dash), and 100 pA above the baseline (solid).

3.3.2 Experimental testing of the modulation ratio

Upon isothermal separation of the sample mixture without modulation, tridecane was identified as a symmetrical peak with an appropriate width for study under the conditions used (As = 1.00, w_h = 5.30 s). Likewise, nonan-1-ol was found to be a suitable tailing peak (As = 5.18, w_h = 2.64 s). A 1D-GC chromatogram of standard mixture is shown in **Figures 3.6.** Peak distributions for tridecane and nonan-1-ol respectively for different modulation periods are shown in **Figure 3.7 and Figure 3.8**.

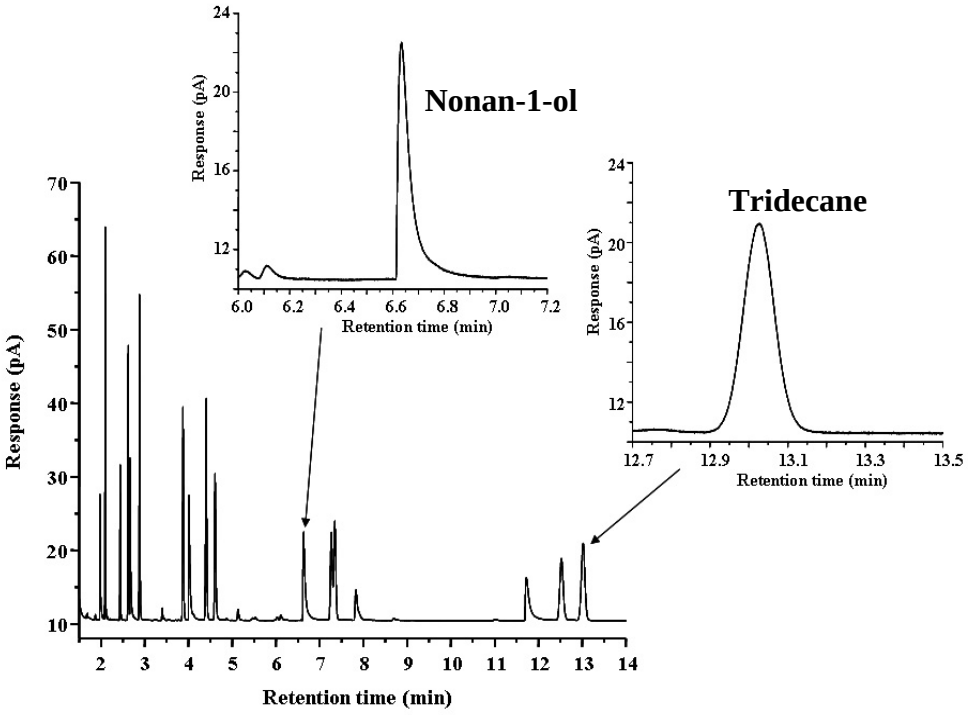

Figure 3.6: 1D-GC chromatogram of the 17 compounds standard mixture.

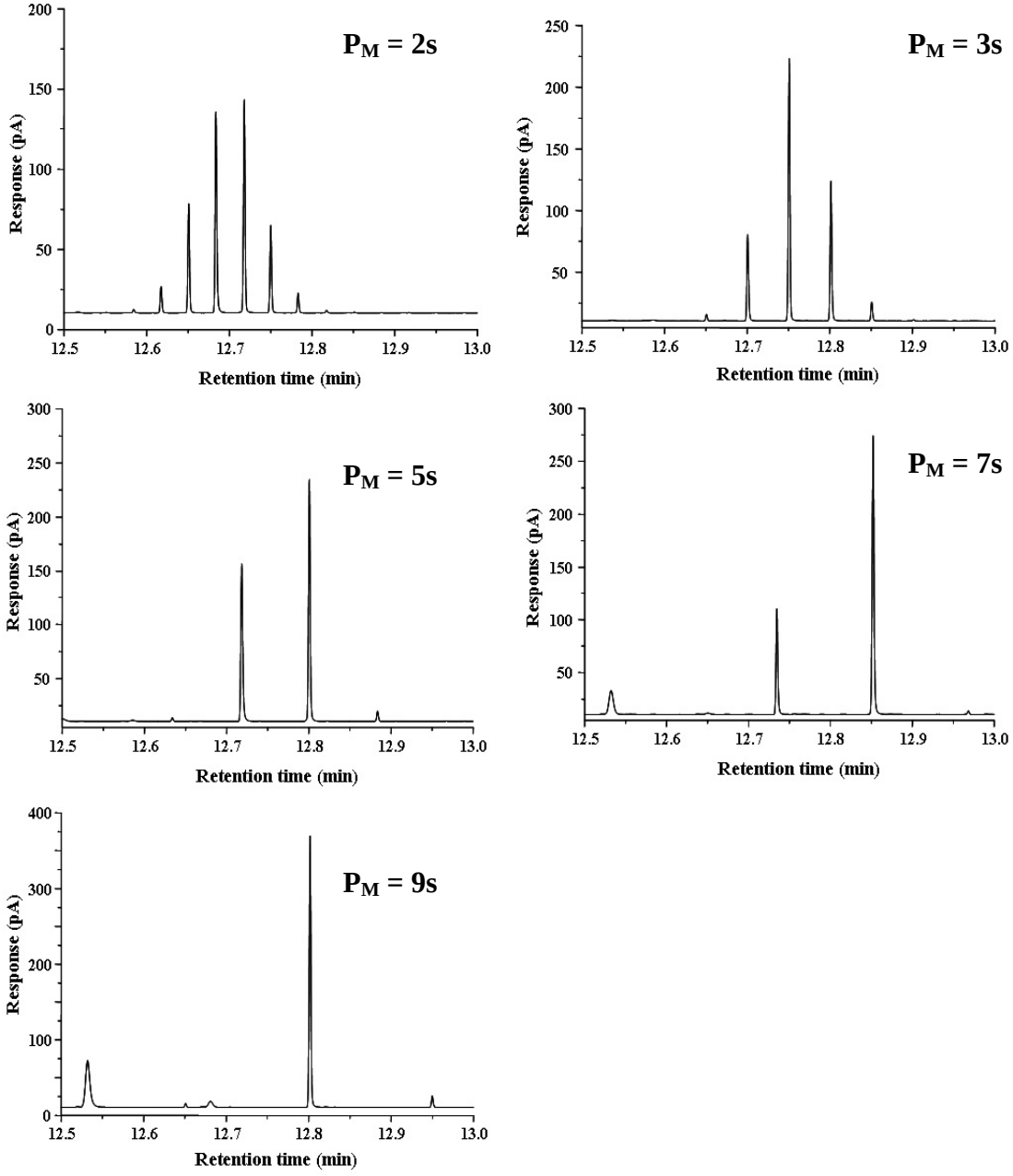

Figure 3.7: Experimental data from the modulation of a symmetric peak (Tridecane) using modulation periods of 2, 3, 5, 7 and 9s.

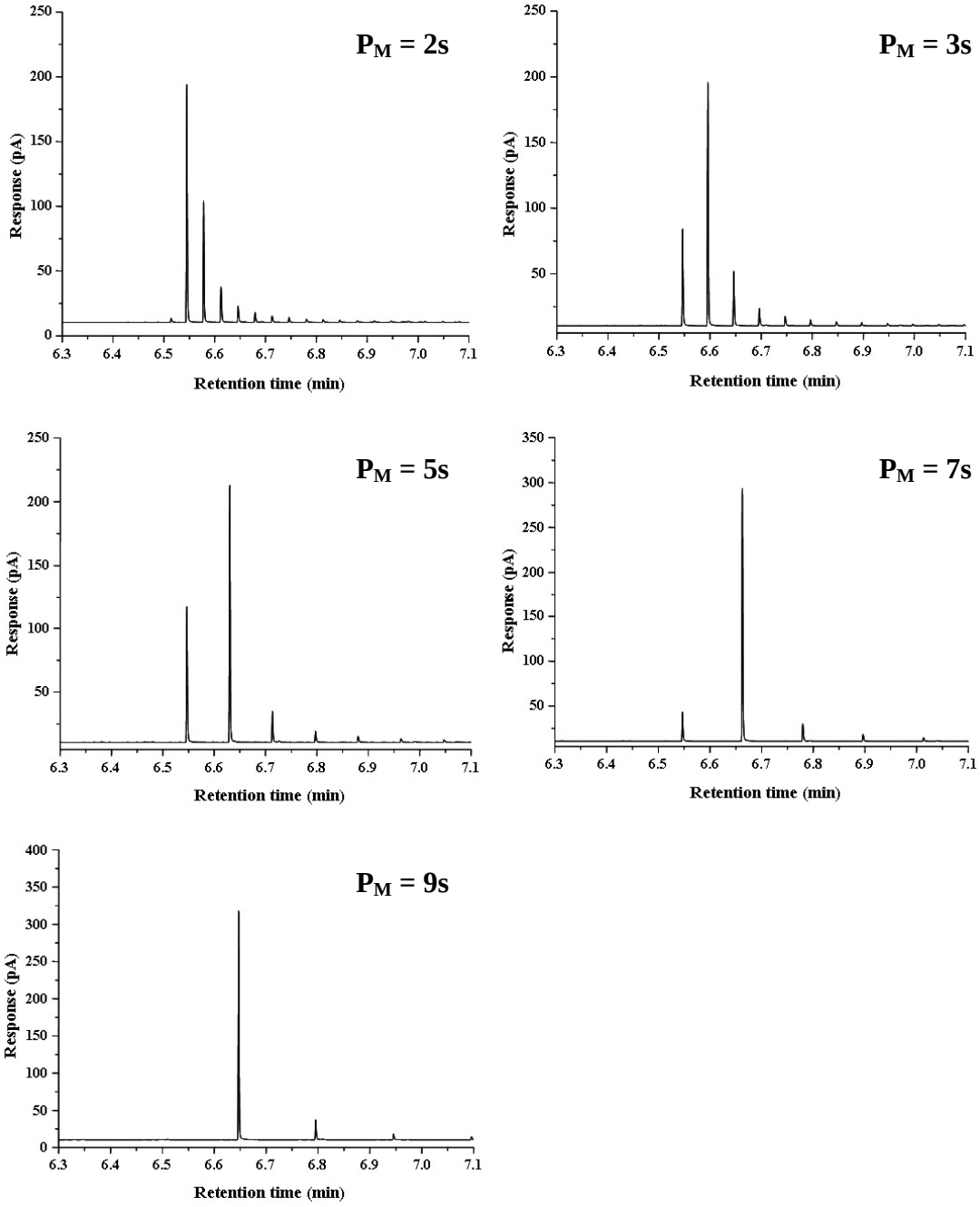

Figure 3.8: Experimental data from the modulation of a tailing peak (Nonan-1-ol) using modulation periods of 2, 3, 5, 7 and 9s.

It has been suggested above that modulation phase also alters the number of modulations found for a given ^{1}D peak. By systematically varying the delay in the modulation start time, it is possible to vary the sampling pattern of the ^{1}D peak by stepping through different modulation phases. The initial experiment is not intended to generate a specific phase, but rather will establish a point of reference to observe the phase changes in the subsequent experiments. This experiment will only be valid if the component's ^{1}D retention time varies negligibly with respect to the time shift of the sampling windows of the modulator that is chosen to increment the phase. The analytical reproducibility for the test mixture was investigated to verify the reproducibility of peak position for replicate analyses, including the reproducibility of peak area, peak height and peak width at half height. It was found that for ^1t_R this was better than 0.05% (a shift of 60 – 300 ms) in these experiments (shown in **Table 3.3**). This is important for studying the modulation process in detail as shifts in ^{1}D retention would have the effect of altering modulation phase even if the start time was controlled precisely, or would cause an uncontrolled adjustment of modulation phase when a systematic study was attempted. To demonstrate the effect of phase on modulation number, the tridecane and nonan-1-ol peaks from a separation with P_M of 6 s (0.1 min) were chosen. Modulation was initially started at 3.00 min and then in subsequent experiments the phase was adjusted by altering the start time by 1.2 s (0.02 min) in equal steps until arriving at 3.10 min which provides the same phase as when the modulator is started at 3.00 min.

Table 3.3: Reproducibility of retention time, peak area, and peak width at half height for the 17 compounds standard mixture using normal GC.

Peak#	^1t_R (min)			Peak Area			Peak Height			Peak width at half height		
	average	SD	%RSD	average	SD	%RSD	average	SD	%RSD	average	SD	%RSD
1	1.9783	0.0006	0.03	17.0667	0.2517	1.47	16.9333	0.2517	1.49	0.8800	0.0173	1.97
2	2.0980	0.0010	0.05	44.4333	1.1504	2.59	53.2333	1.2055	2.26	0.7780	0.0035	0.45
3	2.4410	0.0010	0.04	21.6667	0.5033	2.32	21.0333	0.4509	2.14	0.9600	0.0000	0.00
4	2.6250	0.0010	0.04	41.3000	0.9539	2.31	37.1000	0.8544	2.30	1.0440	0.0000	0.00
5	2.6660	0.0010	0.04	27.8333	0.7638	2.74	21.7000	0.6557	3.02	1.1300	0.0125	1.11
6	2.8837	0.0015	0.05	51.4333	1.5177	2.95	43.8667	1.1676	2.66	1.0840	0.0035	0.32
7	3.8773	0.0021	0.05	47.7667	1.3650	2.86	28.9000	0.7550	2.61	1.5400	0.0035	0.22
8	4.0123	0.0021	0.05	30.7333	1.1240	3.66	16.5667	0.7095	4.28	1.6640	0.0193	1.16
9	4.4050	0.0026	0.06	55.6667	1.8877	3.39	29.8000	1.0149	3.41	1.7400	0.0000	0.00
10	4.6100	0.0026	0.06	39.6333	1.2583	3.17	19.6333	0.6658	3.39	1.8680	0.0271	1.45
11[a]	6.6317	0.0035	0.05	43.2000	0.9000	2.08	11.9000	0.5568	4.68	2.6420	0.0510	1.93
12	7.2640	0.0036	0.05	36.3000	1.3115	3.61	11.8000	0.4583	3.88	2.8100	0.0797	2.84
13	7.3467	0.0042	0.06	43.7667	1.5695	3.59	13.3000	0.4583	3.45	2.9800	0.0408	1.37
14	7.8293	0.0031	0.04	14.3333	0.5508	3.84	3.9000	0.1732	4.44	3.2980	0.0624	1.89
15	11.7247	0.0021	0.02	27.4667	1.5695	5.71	5.5333	0.3055	5.52	4.3700	0.1089	2.49
16	12.5257	0.0045	0.04	45.9000	1.7776	3.87	8.2333	0.3055	3.71	4.9560	0.1717	3.46
17[b]	13.0223	0.0050	0.04	59.4667	2.5325	4.26	10.2667	0.4163	4.06	5.3040	0.0692	1.30

(n = 3)

[a] Tailing peak (nonan-1-ol) chosen in this study

[b] Symmetric peak (tridecane) chosen in this study

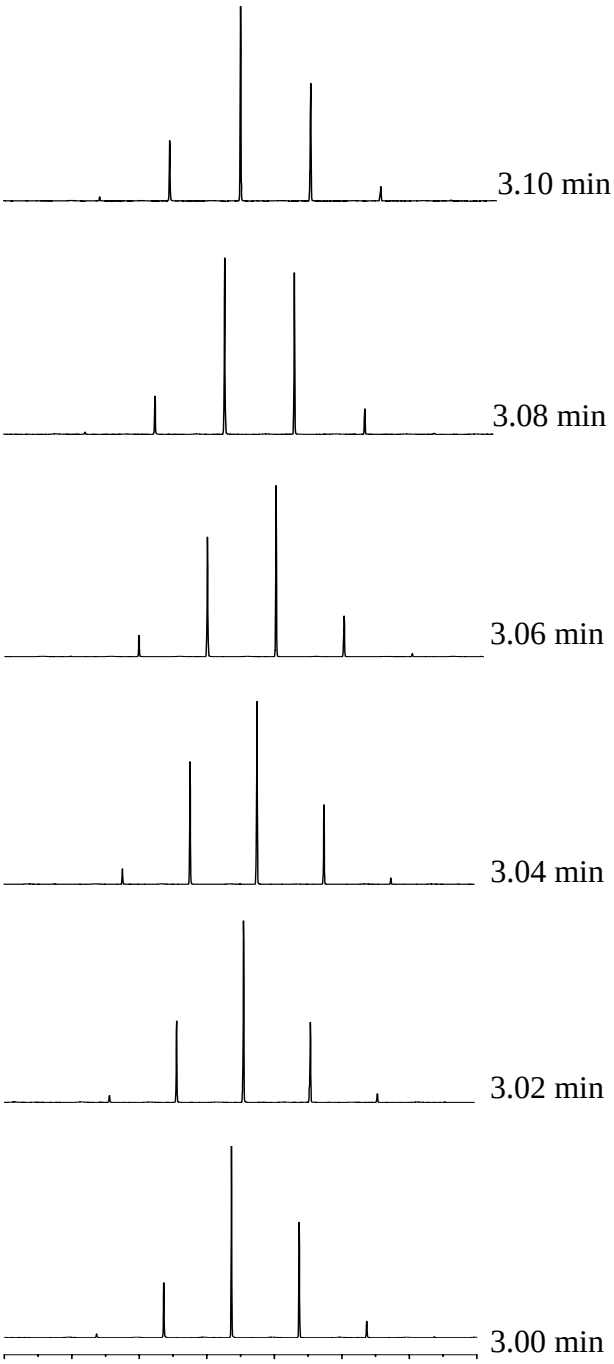

Figure 3.9: GC×GC chromatogram of tridecane using different modulation phase with modulation period of 6 s. Modulation start times are 3.00, 3.02, 3.04, 3.06, 3.08 and 3.10 min, as shown. Note that 3.00 and 3.10 min start time should give the same peaks distribution, since they have the same phase.

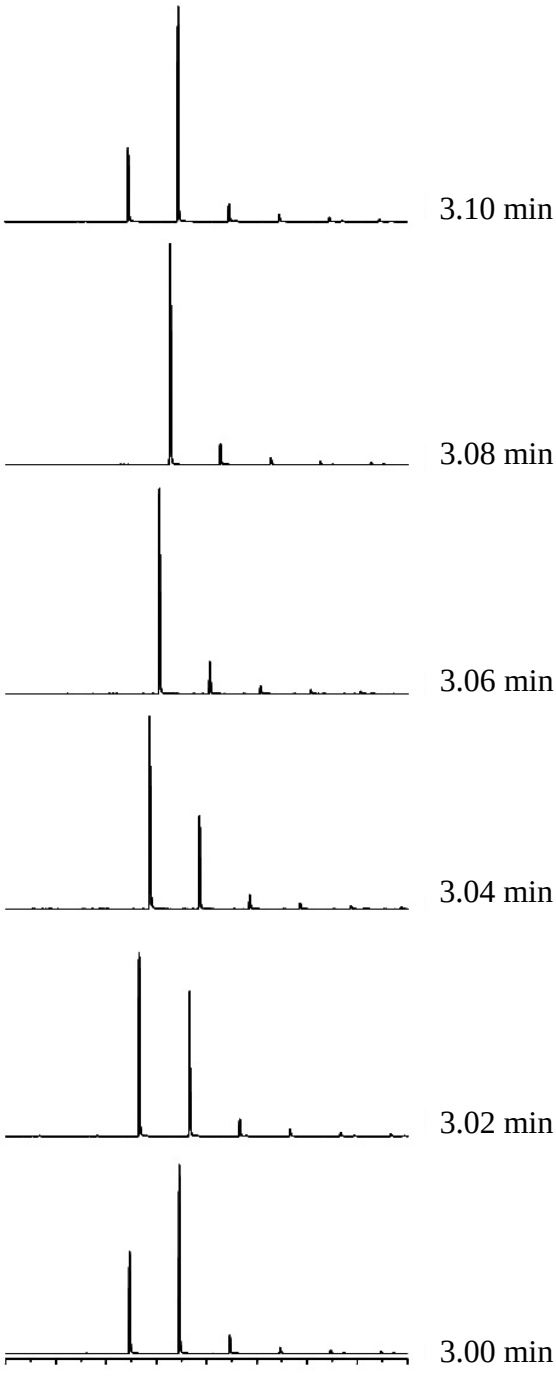

Figure 3.10: GC×GC chromatogram of nonan-1-ol using different modulation phase with modulation period of 6 s. Modulation start times are 3.00, 3.02, 3.04, 3.06, 3.08 and 3.10 min, as shown. Note that 3.00 and 3.10 min start time should give the same peaks distribution, since they have the same phase.

Figure 3.9 shows GC×GC chromatograms of tridecane using different modulation phase with modulation period of 6 s. Modulation start times are 3.00, 3.02, 3.04, 3.06, 3.08 and 3.10 min, respectively. Results of similar experiments were obtained for the nonan-1-ol peak as shown in **Figure 3.10**. Given the scenarios above, with 'n_M' varying depending on peak size and extent of tailing, it seems advisable to quantify the sampling rate of the primary dimension using an easily-measured parameter which is based upon the width of primary peaks, hence the development of the concept of modulation ratio presented above and defined in **Equation (1)**. Accepting that selecting an appropriate modulation period should relate peak width in ^{1}D to the modulation time, it is necessary to only decide what value of M_R is required. If the position of having "about 4 modulations" per peak is accepted, then the magnitude of P_M will be about one standard deviation of a Gaussian peak in the first dimension, $^1\sigma$. This equates as M_R = 4; however this does not mean that fully 4 modulated peak slices are obtained as this depends on the intensity of the ^{1}D peak, the phase of modulation, and how small a modulated peak is to be measured. Since phase is not implicitly included in the M_R value, a given M_R will not guarantee the pattern of observable peak slices, but it will guarantee a minimum number of observable slices, as seen for the model in **Tables 3.1 and 3.2 and in Table 3.4** which compares the results for the studies of tridecane and nonan-1-ol with modelled peaks having the same asymmetry, modulation ratio, and base peak height for different P_M. When the number of observed slices for the peaks under these conditions is compared with the predicted number of slices for a peak with a base peak 100 pA above the baseline, a good agreement with the number of observed modulation slices can be seen. Modulation ratio (M_R) value of all compounds used in this study for P_M = 2, 3, 5, 7 and 9 s are shown in **Table 3.5**. Clearly, M_R values from the calculation using **Equation (1)** shown in the table corresponded with the results obtained from the experiment. For example, M_R of nonan-1-ol (peak 11) and tridecane (peak 17) for P_M = 2 s were 2.24 and 4.50, respectively and they were matched with the experimental results when P_M = 2 s was performed as shown in **Figure 3.7 and 3.8.**

Table 3.4: Number of observed modulation pulses for modulated and tailing peaks in the experimental study compared to the values expected from the model.

Gaussian (tridecane)			**Tailing (nonan-1-ol)**		
Modulation Ratio (M_R)	**Experiment**	**Model**	**Modulation Ratio (M_R)**	**Experiment**	**Model**
4.50	10	9	2.33	18	12
3.00	6	6	1.56	12	9
1.80	5	4	0.93	7	5
1.29	4	4	0.66	6	4
1.00	4	3	0.52	4	3

Table 3.5: Modulation ratios (M_R) of all 17 compounds in the standard mixture for modulation periods of 2, 3, 5, 7 and 9 s.

Peak no.	W_h (s)	SD	%RSD	W_b (W_h*1.6985)	M_R				
					P_M (s)				
					2	3	5	7	9
1	0.8800	0.0173	1.97	1.4947	0.75	0.50	0.30	0.21	0.17
2	0.7780	0.0035	0.45	1.3214	0.66	0.44	0.26	0.19	0.15
3	0.9600	0.0000	0.00	1.6306	0.82	0.54	0.33	0.23	0.18
4	1.0440	0.0000	0.00	1.7732	0.89	0.59	0.35	0.25	0.20
5	1.1300	0.0125	1.11	1.9193	0.96	0.64	0.38	0.27	0.21
6	1.0840	0.0035	0.32	1.8412	0.92	0.61	0.37	0.26	0.20
7	1.5400	0.0035	0.22	2.6157	1.31	0.87	0.52	0.37	0.29
8	1.6640	0.0193	1.16	2.8263	1.41	0.94	0.57	0.40	0.31
9	1.7400	0.0000	0.00	2.9554	1.48	0.99	0.59	0.42	0.33
10	1.8680	0.0271	1.45	3.1728	1.59	1.06	0.63	0.45	0.35
11	***2.6420***	***0.0510***	***1.93***	***4.4874***	***2.24***	***1.50***	***0.90***	***0.64***	***0.50***
12	2.8100	0.0797	2.84	4.7728	2.39	1.59	0.95	0.68	0.53
13	2.9800	0.0408	1.37	5.0615	2.53	1.69	1.01	0.72	0.56
14	3.2980	0.0624	1.89	5.6017	2.80	1.87	1.12	0.80	0.62
15	4.3700	0.1089	2.49	7.4224	3.71	2.47	1.48	1.06	0.82
16	4.9560	0.1717	3.46	8.4178	4.21	2.81	1.68	1.20	0.94
17	***5.3040***	***0.0692***	***1.30***	***9.0088***	***4.50***	***3.00***	***1.80***	***1.29***	***1.00***

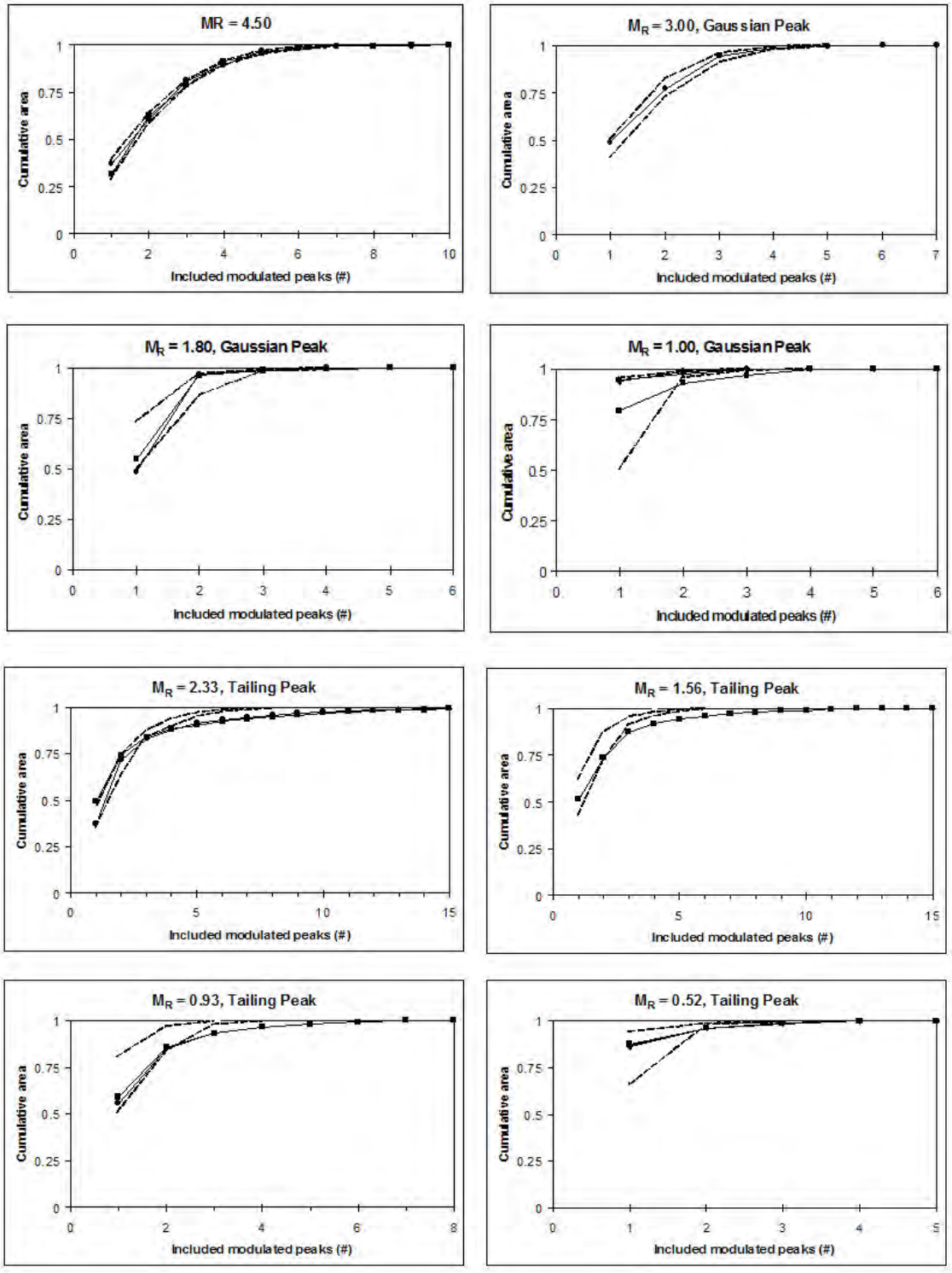

Figure 3.11: Cumulative peak areas plots of symmetric peak and tailing peak from experimental data.

Furthermore, if plots similar to those in **Figure 3.4 and 3.5** are constructed for the experimental data and plotted with results for cumulative area of peaks modelled with the same P_M, w_h, and A_S the result in **Figure 3.11** is obtained. The results show relatively good agreement to the model data. The slight difference in the pattern for the tailing peaks can be attributed to the fact that the tailing of the primary peak is likely not adequately represented by an ideal tailing peak as is assumed in the EMG model. When M_R becomes sufficiently small that a ^1D peak can be fully trapped in the modulation process, the plot of the type shown in **Figure 3.11** will exhibit the trivial case of having a point at 0.5 and one point at 1.0 for the two modulated pulses when the modulation phase is 180° and a single point at 1.0 for the entire peak when the phase of the modulation is 0°. Thus all experiments will give both one or two modulated peaks, and no more.

3.4 Conclusion

The theory of the modulation ratio, M_R, has been presented. This parameter is calculated using **Equation (1)**, and is based on the easily measured ^1w_h and on the choice of P_M, which is set by the experimenter. It was shown that as M_R is increased, the number of observable modulation pulses increases, and the fluctuation in the fraction of the primary peak area that is included in a given modulation pulse due to changes in phasing is lessened. The errors associated with these fluctuations will likely be more important for the analysis of trace analytes where only a few peak pulses will be observed. A detailed study of potential errors associated with summing multiple modulation pulses, especially for tailing peaks, will be the subject of future study and so out of the scope of the present chapter.

The results for the model of both Gaussian peaks, and tailing peaks modelled by the Exponentially Modified Gaussian equation, were supported by an experimental study of real GC×GC peaks. Considering these results and the model, the following recommendations for choosing a M_R value are proposed. For separations where the utmost precision in measuring trace analytes is important, a M_R value of at least 3 should be chosen, as this will ensure that at least 3 modulations are observed, even for trace analytes, and that the error associated with slight changes in phasing will be minimised. However, the model also suggests that if the analyst is performing a separation for rapid, semi-quantitative screening purposes, and is primarily interested in major components, the separation can be operated with a M_R value closer to 1.5 which increases modulated peak signals.

This is significant in that by decreasing the M_R value from 3 to 1.5, the P_M can be doubled (allowing more time for the ^{2}D separation) or the primary peaks may be made narrower (for example by increasing the oven programming rate and decreasing the overall analysis time). However, with a decrease in the M_R value from 3 to 1.5 and the potential gains in analysis time or separation time in the second dimension, the analyst must be aware that the observed resolution in the first dimension will be significantly reduced as well, and this must be taken into consideration. Though the concept of the modulation ratio was developed using GC×GC separations, it should

be equally applicable to other comprehensive multidimensional separation techniques, such as LC×LC, SFC×SFC, LC×CE or LC×GC.

References

[1] R.E. Murphy, M.R. Schure, J.P. Foley, Anal. Chem. 70 (1998) 1585.

[2] P. Schoenmakers, P. Marriott, J. Beens, LC-GC Eur. 16 (2003) 335.

[3] R.C.Y. Ong, P.J. Marriott, J. Chromatogr. Sci. 40 (2002) 276.

[4] J. Harynuk, T. Gorecki, J. de Zeeuw, J. Chromatogr. A 1071 (2005) 21.

[5] Z. Zhu, J. Harynuk, T. Gorecki, J. Chromatogr. A 1105 (2006) 17.

[6] J.V. Seeley, J. Chromatogr. A 962 (2002) 21.

[7] J.V. Seeley, N.J. Micyus, S.V. Bandurski, S.K. Seeley, J.D. McCurry, Anal. Chem. 79 (2007) 1840.

[8] O. Amador-Munoz, P.J. Marriott, J. Chromatogr. A 1184 (2008) 323.

[9] J.P. Foley, J.G. Dorsey, Anal. Chem. 55 (1983) 730.

Chapter

4

TARGETED AND COMPREHENSIVE
TWO-DIMENSIONAL GAS CHROMATOGRAPHY
WITH MULTI-PASS LOOP CRYOGENIC MODULATION

Abstract

In this chapter new geometries of Longitudinal Modulated Cryogenic System (LMCS) for targeted and comprehensive modes in comprehensive two-dimensional gas chromatography (GC×GC) will be presented. In this study, a thin wall column of 0.1 mm. i.d. allowed multi-insertion of the capillary through the cryogenic trap in various arrangements. Thus, the column was inserted through a single ferrule and held in place to allow both regular single column and looping of the column arrangements at the LMCS modulator so called “Multi-pass Loop” cryogenic modulation process. Two new approaches of multi-pass loop cryogenic modulation were developed in this study. The operation of each multi-pass loop type in targeted and comprehensive modes was demonstrated. Results obtained are discussed and compared to the regular straight through type. It is demonstrated that the multi-pass loop type 2 gives similar results as the straight through type. The mechanism of cryogenic trap movement; slow upward travel of the trap position followed by a rapid down stroke in the release step was invoked to explain peak broadening problems in multi-pass loop type 1. However, the advantages of the newly proposed geometries is the capacity to hold the second and the third fractions separately from the first fraction in the cryogenic region, while the first fraction of the target analyte was introduced and separated on the second column. This multi-pass loop cryogenic modulation will be of benefit for the investigation of the targeted compounds in a complex mixture such as multi-residues in environmental samples. Therefore, standard mixtures of organochlorine pesticides (OCs) were utilised to demonstrate this approach. The results from both target and comprehensive modes will be discussed.

4.1 Introduction

Multidimensional gas chromatography (MDGC) is a well-known separation technique for complex samples, which was established early after the invention of conventional gas chromatography (1D-GC) [1]. The technique involves the combination of two or more different chromatographic columns to separate components in samples. Flexibility of the technique, separation power increase and the peak capacity gained are attractive aspects of this technique. The state of art of this technique, principle, implementations, mode of operations, advantages and applications of complex samples analysis have been discussed elsewhere [2-4]. In addition, two reviews of this subject by Bertsch [5,6] provide an excellent relevant summary of the history and development of this technique to date. To be classified as a multidimensional separation technique, a second analytical column needs to be added to the basic single column GC system, directly coupled or via an interface to an original/primary column (^{1}D) in which the first separation step was performed. As a rule of thumb, two columns must be different with respect of their separation mechanisms in a MDGC system to guarantee that the "orthogonal" concept, or at least a measure of orthogonality, was achieved. Both columns can be located within separate GC ovens depending on the condition or requirement of the method. Two detectors are usually used, one as a monitor detector to pre-determine the time of heart cutting events, and the other as an analytical detector to detect the analytes eluted from ^{2}D. Additionally, principles and implementations of MDGC are also reported elsewhere [7]. Basically, MDGC can be performed without peak or zone compressing using two conventional 1D-GC systems. However, to increase sensitivity which would be of benefit for trace analysis, a modulator which involves cryogenic and thermal trapping and desorption processes is generally installed into the system. The selected peak/fraction of solute from ^{1}D will be trapped by a modulator which is located at the end of ^{1}D, or more logically at the beginning of ^{2}D. Nevertheless, the most important part of the system is the switching device, which will transfer the solute from ^{1}D to ^{2}D. The transfer process of selected fractions from ^{1}D to ^{2}D is critical for this technique and is termed "heart-cutting" [5,7,8]. In heart-cutting, the

unresolved fraction from ^{1}D is transferred to ^{2}D where the fractions will be separated faster and/or better. Mostly, MDGC operation is achieved by on-line heart-cutting using either mechanical moving valves or pneumatic pressure controlled switches (such as Deans'switch) [9-11]. The use of a micro-switching valve is the simplest way to implement a MDGC system due to absence of pressure or flow control requirement, with two columns of similar diameters used [12]. However, a number of serious drawbacks can occur when micro-switching valves are employed in the heart-cutting process, for instance;

1.) Degradation of the labile compounds when they contact a hot surface such as that in a stainless steel valve.

2.) Memory effects by the adsorption or accumulation of compounds or interferences on the surface of the valve.

3.) The valve introduces a "cold spot" in the GC oven when a temperature program was used [7].

4.) The dispersion of selected fraction in the internal dead volume of the valve can cause peak broadening when narrow bore capillary columns are employed.

5.) The following fraction from ^{1}D can be combined with the target fraction in the switching valve.

To overcome many of these limitations caused by the use of a switching valve, a pneumatic pressure controlled switch such as "Deans' Switch" performed by means of pressure balancing, has been used in the heart-cutting process. This pressure balance device provides precise heart-cutting and relatively good results for MDGC analysis without the problems stated above [13]. A number of residual disadvantages of MDGC have been reported for this technique in a number of laboratories, including (i) careful time events for heart-cuts have to be performed; (ii) the total number of selected fractions from ^{1}D transferred to ^{2}D is limited, (iii) it is expensive compared to 1D-GC. Additionally, the perceived complication of the system has led to the

development of new operation modes of the MDGC technique without using any transfer devices.

Comprehensive two-dimensional gas chromatography (GC×GC) is a relatively new technique, introduced about a decade ago. The ^{2}D column and the modulator were added to the basic GC system to perform the comprehensive separation experiment. Peaks eluted from the ^{1}D column were re-focused and re-injected at the head of ^{2}D where the modulator was located. Several modes of operation of GC×GC can be performed depended on the analysis goal. The operational modes of GC×GC using LMCS modulator have been reported elsewhere [14].

In GC×GC not only is the entire sample simultaneously sampled, but also the specific regions of the chromatogram can be transferred to ^{2}D for further separation as in the MDGC technique [15-17]. In 2000, Marriott and co-workers [18] proposed a new operational mode for MDGC by using the Longitudinal Modulated Cryogenic System (LMCS), the mode called “whole trapping” GC×GC mode which is also referred to as targeted MDGC (TMDGC) in later work. The heart cutting process in this mode was performed without any transfer devices, thus, no void volume, no inadvertent cold spots and no ancillary instruments need to be added into the system. Moreover, the study shows the possibility to combine three operational modes including; normal GC, whole peak trapping, and comprehensive mode together during the single analysis, which is referred as “multi-modal chromatography”. To implement this mode, the cryogenic region of the LMCS can be moved at pre-determined times to trap a selected peak or peaks and then be fully remobilised to ^{2}D. This operational mode has the same concept as MDGC but the additional transfer devices are not necessary. The same research group also demonstrated time resolved cryogenic modulation method for targeted MDGC analysis [19]. The operation can be controlled using timed events by means of Chemstation Software from Agilent Technologies. The simplicity and significant sensitivity and separation enhancement of this new operational mode were achieved compared to conventional GC and MDGC. In 2003, Kueh et al. [20] compared results obtained from targeted MDGC (TMDGC) and comprehensive modes for illicit drugs and their metabolites. In this study, quantitative results of normal GC, TMDGC and comprehensive GC×GC

modes such as second dimension retention of compounds (^2t_R), R^2 of calibration curves of compounds (using the summation of peak area) and limit of detection (LOD) were compared. The results show that the most linear calibration curves and the lowest LOD were obtained from TMDGC operational mode. Clearly, TMDGC is a suitable mode for quantitative and trace residue analysis. To date, MDGC is an appropriate technique for the analysis of target compounds in a range of complex samples such as petroleum [12,21] and environmental samples [7].

Recently, Begnaud et al. [22] presented a new approach of multidimensional gas chromatography using a double cool-strand interface (DCSI). This new technique demonstrated the simplicity of implementation of DCSI without the requirement of special column connections. The design was based on the cryo-control (using the LMCS modulator) to transfer the analytes from ^{1}D to ^{2}D through use of looped double cooled strands of a single capillary column. In operation, each cool strand is a segment of capillary column which is passed through the cryogenic trap of the LMCS modulator but Begnaud and co-workers passed the column through the LMCS twice to give two discrete trapping segments (i.e. in a loop arrangement). The looped capillary column is a unique feature of this technique were subsequent incoming fractions were able to be held while the first fraction was re-injected into ^{2}D. The technique has been patented in 2004 [23].

The present study of multi-pass loop had been started in 2004 and it appears to be a parallel work as a double cool-strand interface (DCSI) which was reported by Begnaud et al in 2005 [22]. Thus, the contribution of this study to original publication rests with the use of the multi-pass loop modulation in the GC×GC mode, to evaluate if it has advantages to collect and modulate peaks better than a single modulation column

In this Chapter, three configurations of the LMCS modulator for the MDGC and GC×GC techniques will be presented. Two new geometries termed the multi-pass loop cryogenic modulation types 1 and 2 were reported and the type 3 configuration was suggested for further study. However, separation of several compounds obtained from some multi-pass loop arrangements were not achieved compared to the straight through type due to the slow downwards movement of the LMCS modulator, and the

limitation of time events of “Chem. Station” software. The new version of software offers considerably more control events, to this latter problem can now be overcome. More consideration of this limitation will be explained herein, and results obtained from both targeted and comprehensive modes of two multi-pass loop types and the normal operation, are compared and discussed.

4.2 Experimental

4.2.1 Gas Chromatographic system

An Agilent 6890 gas chromatograph equipped with two FID detectors and retrofitted with a longitudinal modulated cryogenic system (LMCS) (Chromatography Concepts, Doncaster, Australia) was used throughout this study. The split/splitless GC injector was operated at 250 ^{o}C; an injection volume of 1.0 μL was employed in split mode at split ratio 20:1. The flame ionisation detector (FID) was operated at 300°C with data collection rate of 100 Hz. The GC oven was programmed from 60 ^{o}C to 160 ^{o}C at 20 ^{o}C.min^{-1} and to 240 ^{o}C at 5 ^{o}C.min^{-1} then held for 6 min; giving a total run time of 22 min. Carrier gas was operated in constant flow mode, which gave a column flow rate of 2.0 mL.min^{-1} (average velocity ($\bar{u}$) = 66 cm.s^{-1}).

4.2.2 Column sets

The first dimension (^{1}D) column was a 30 m x 0.25 mm i.d. capillary column, with 0.25 μm d_f – 5% phenyl polysilphenylene-siloxane (BPX5) phase and was operated at an initial head pressure of 20.10 p.s.i. The second dimension (^{2}D) consisted of 2 m x 0.1 mm i.d. narrow bore capillary, with 0.1 μm d_f 50% phenyl-dimethyl polysilphenylene (BPX50) phase. All columns were from SGE International, Ringwood, Australia. The ^{2}D column was a thin wall capillary with o.d. of 0.27 mm, which permitted two columns to be simultaneously passed through the cryogenic region.

4.2.3 Standards

A standard organochlorine pesticides mixture was obtained from Ultra Scientific (Kingston, RI, USA; part number M8080). This standard contains the following pesticide components: 1. α-Hexachlorocyclohexane; 2. γ-Hexachlorocyclohexane; 3. β- Hexachlorocyclohexane; 4. δ- Hexachlorocyclohexane;

5. Heptachlor; 6. Aldrin; 7. Heptachlor Epoxide; 8. Endosulfan; 9. Diedrin; 10. p,p'-DDE; 11. Endrin;12. p,p'-DDD; 13. Endosulfan II;14. Endrin aldehyde;15. p,p'-DDT; 16. Endosulfan sulfate;17. Methoxychlor. The initial standard concentration was 20 mg/L. This standard was diluted as required in pesticide grade hexane for further analysis.

4.2.4 Multi- pass loop geometries

A regular cryogenic modulator with construction described elsewhere [24], with an inner channel of 0.9 mm i.d. was used in this study. This i.d. will not permit two capillary columns of regular o.d. to be passed through the cryogenic region. In this study, a length of thin wall column of 0.1 mm i.d. and 0.27 mm o.d. was supplied by SGE International, Ringwood, Australia. This allowed two columns to be inserted through the cryogenic region in various arrangements described. To facilitate timing control for operation of the cryogenic region events, the ^{1}D column was interfaced to two downstream columns, one being an uncoated deactivated capillary (1.0 m x 0.10 mm. i.d.) connected to FID1 as a monitor detector. The other was the ^{2}D separation column, which was passed through the cryogenic region and then connected to FID2 as an analytical detector. The LMCS was located at the head of the ^{2}D separation column. In addition, the thin wall ^{2}D was formed in a loop shape for the multi-pass cryogenic loop operation propose.

4.3 Results and Discussion

4.3.1 General concept and multi-pass loop arrangements

The cryogenic region and hence the cryotrap is a moveable part of the LMCS modulator which can be moved longitudinally along the column and is generally operated in a regular modulation period manner. The regular operational mode of the cryotrap of the LMCS traps the incoming solute from ^{1}D in the trapping position **(t)** and remobilises the compressed band into ^{2}D for further separation when the cryotrap moved down to the release position **(r)** (see **Figure 4.1**), then the cryotrap returns to the trap position for a new cryotrap cycle; and then the process repeats. This regular operation has been known and used as a routine mode in MDGC and GC×GC laboratories. Unlike the regular mode, the multi-pass loop modulation mode proposed here allowed the analytes to be trapped and retained in the cryotrap for one and a half, and two cycles, in multi-pass loop type 1 and 2, respectively, before the compressed band was re-injected into ^{2}D. Therefore, a narrower solute band compare to regular operation was achieved. However, due to the limitation of movement of the cryotrap, the multi-pass loop type 1 performance can not perform as expected since the down-stroke of the cryotrap is fast, and the up stroke is slow for the arrangement shown in **Figure 4.1 (B)**. A more appropriate operation would be for the loop in **Figure 4.1 (B)** to be inverted (see later). Further details of the multi-pass loop will be discussed later. Loop arrangements developed here would benefit by isolating the second and third fractions eluting from ^{1}D, away from the first fraction which will be sent to ^{2}D. Thus, re-combination of the fractions eluted after the targeted fraction can be avoided. The comparison of results obtained from the loop types and regular mode will be discussed later in the chapter.

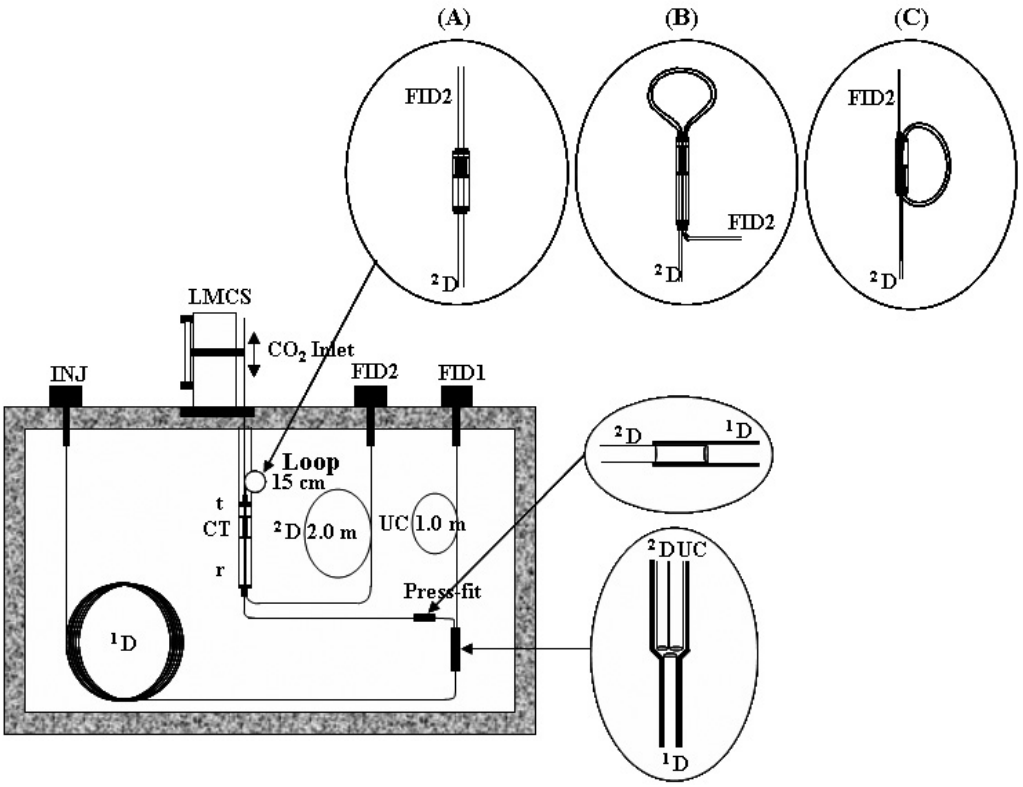

Figure 4.1: The multi-pass loop cryogenic modulation gas chromatography system. **(A)** Regular operation of LMCS modulator. **(B)** Multi-pass loop type 1 of LMCS operation. **(C)** Multi-pass loop type 2 of LMCS modulation. UC = uncoated capillary transfer line, CT = cryogenic region, t = trap position, r = release position, ^{1}D and ^{2}D are first and second columns, respectively. The column arrangement shows the option **(B)** above.

The conceptual development of multi-pass loop modulation implementation is shown in **Figure 4.1.** The expanded insets show the regular cryogenic region and type 1 and type 2 multi-pass loop modulators. **Figure 4.1A** shows a regular LMCS geometry normally used in this laboratory **Figure 4.1B** shows multi-pass loop type 1 which, constructed from thin wall capillary column (^{2}D) of dimension 15 cm long, was shaped as a loop at the top of the LMCS, then re-inserted from the top through to the bottom part of the LMCS modulator. The looped columns are inserted through a single ferrule and held in place by using a regular coupling. **Figure 4.1C** shows multi-pass loop type 2, in which the thin wall column is passed through the LMCS from bottom to the top, and then re-inserted in the same orientation, passing to FID2 from the top of the LMCS. It is important to recognise

that the LMCS moves in a fast manner in its down-stroke, and only slowly moves back to the trap position. A recent version moves fast in both directions.

4.3.2 The multi-pass loop operation

Figure 4.2 illustrates a diagram describing the operation processes of each multi-pass loop arrangement using LMCS modulators including the regular straight through type mode. The difference between the regular straight through type and the loop types is that the latter permits temporal isolation of a selected zone of effluent from both incoming and outgoing solute, whereas the regular straight-through modulator has continual introduction of solute into the trapping stage. The looped systems described here act rather like a series of spatially discrete cryogenic regions. The cryogenic trap is moved back-and-forth by an actuator unit. The system was developed for single column modulation with slow upward movement of the trap, and rapid downstroke. The fast movement is intended to encourage fast heating of the cryogenic regions of solute. This function is operative for the loop type 2, but for loop type 1, when solute is trapped in the exit strand, the trap moves up rather slowly, and this may not allow quite as fast remobilisation. Ideally, the loop in type 2 should have been inverted to allow rapid movement for the solute exiting to the ^{2}D column to test this theory. The drive of the actuator will require modification to permit fast movement in each direction.

Figure 4.2A illustrates the regular mode of LMCS in MDGC analysis. The operation is performed recognising the trap and release positions. For instance, solute labelled **a,** was completely trapped in the cryotrap, and then fully remobilised by the ambient temperature of the GC oven when the cryotrap moved down to the release position. The trap and release process is a sequential process, the solutes continue to be sent from ^{1}D to ^{2}D for further separation. Basically, liquid CO_2 can be switched off to allow the non targeted analytes to pass through the cryotrap in a usual way and can be turned on when the target region is about to enter to the cryotrap. This operation is acknowledged to improve response sensitivity approximately 10 to 20 times.

In **Figure 4.2B** is shown the arrangement of multi-pass loop type 1. In this operation mode, the selected peak or fractions will remain in the cryogenic region one and a half cycles compared to the regular cycle. Solute labelled **a,** was trapped in the cryotrap in the first step and then migrated along the loop when the cryotrap is moved to the release position. The solute is trapped again at the release position of the cryotrap, while solute **b** was also trapped in the incoming strand of ^{2}D column. In the next step, solute **a** was released from the trapping zone to the detector while solute **b** is still retained in the cryotrap waiting for the process to be repeated. Interestingly, in this mode the target peak was released to ^{2}D when the cryotrap returned slowly back to the trap position. The slow release in this step apparently caused some solute band broadening. More details of this effect will be discussed below.

Multi-pass loop type 2 operation is shown in **Figure 4.2C** Solute **a** was trapped when the process starts at the trap position. After, the cryotrap moves down, solute **a** is mobilised to travel along in the loop and then is focussed again at the release position, while solute **b** also traps at the incoming strand of ^{2}D. Solute **a** is retained in the cryotrap when the cryotrap returns to the trap position. In the next step, solute **a** was released to ^{2}D while solute **b** is remobilised into the loop and traps a second time. It is important to note that in this operation solute **b** and **c** can be held in the cryotrap regions while solute **a** has been expelled for further separation in ^{2}D, thus mixing of neighbouring solutes can be prevented. Unlike loop type 1, solute was released from multi-pass loop type 2 when the cryotrap moved down to the release position in a fast stroke operation, thus results obtained from this operation are similar to the regular mode i.e. it seems desirable to have the solute released to the 2D column when rapid movement of the cryotrap is performed.

(A) Normal

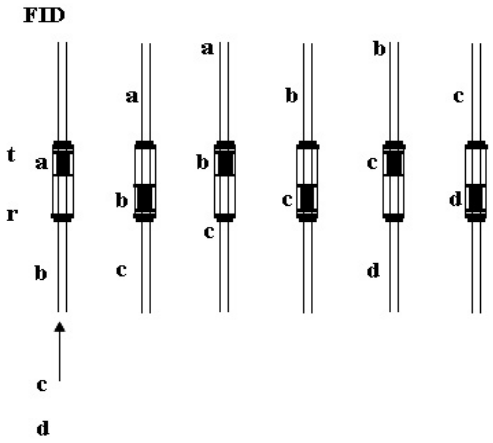

(B) Loop type 1

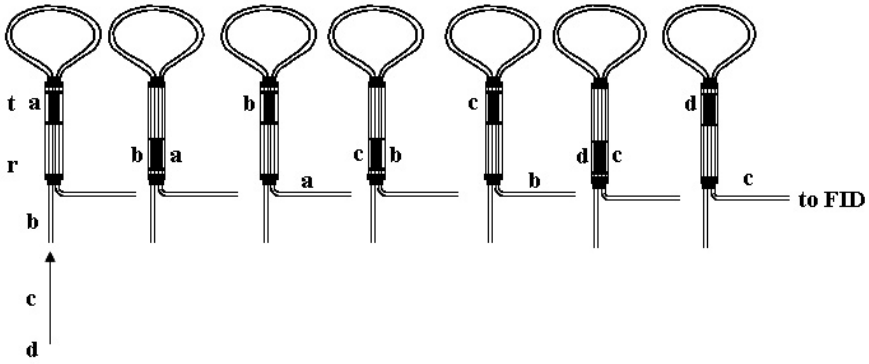

(C) Loop type 2

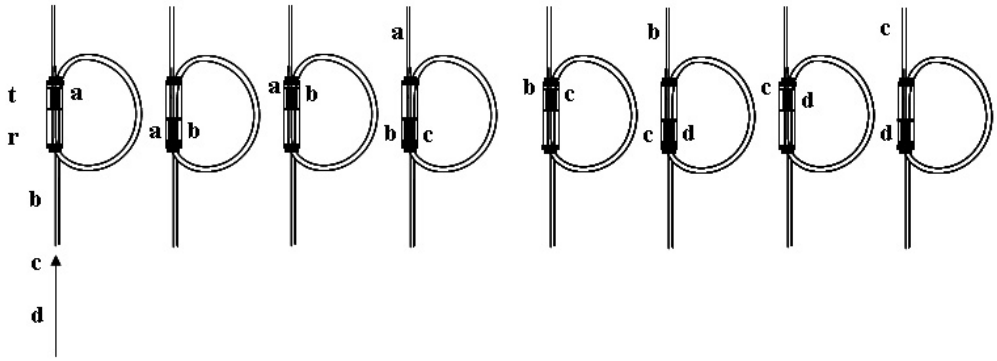

Figure 4.2: Illustration of the operational modes of the cryogenic trap when solute from ^{1}D was introduced into the regular and multi-pass loop modulator and was remobilised to ^{2}D. **(A)** Regular operation **(B)** Loop type 1 operation **(C)** Loop type 2 operation. T_1 and T_2 are the first and second cryogenic trapping position; R_1 and R_2 are first and second remobilisation position of cryogenic region, respectively.

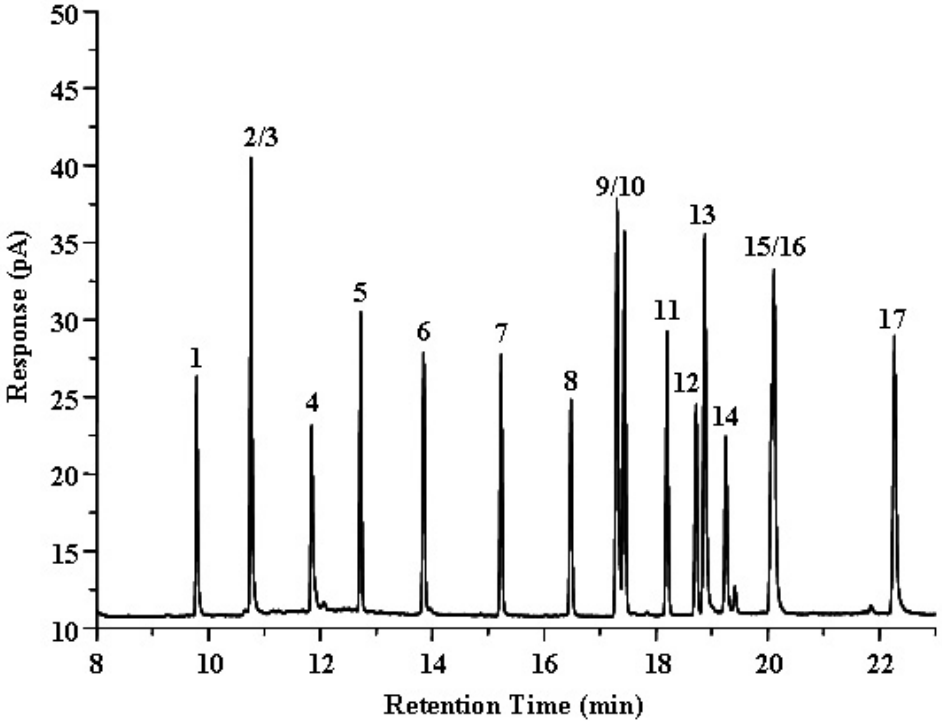

Figure 4.3: 1D-GC chromatogram of 17 organochlorine pesticide standards. The cryofluid (liquid CO_2) was not applied during the analysis. The compounds are **1**. α-Hexachlorocyclohexane (HCH), **2**. γ-HCH, **3**. β-HCH, **4**. δ- HCH, **5**. Heptachlor, **6**. Aldrin, **7**. Heptachlor epoxide, **8**. Endosulfan, **9**. Diedrin, **10**. p,p'-DDE, **11**. Endrin, **12**. p,p'-DDD, **13**. Endosulfan II, **14**. Endrin aldehyde, **15**. p,p'-DDT, **16**. Endosulfan sulphate, **17**. Methoxychlor.

Figure 4.3 illustrates the normal GC analysis of 17 organochlorine pesticide (OCs) standards, all compounds passed through ^{1}D and the uncoated capillary column (**see section 4.2.4**), to the monitor detector (FID1) with CO_2 not applied. This chromatogram was used for predetermined timing of heart cutting events for the targeted MDGC analysis. Following this step, the entire chromatogram will then be separated in small regions; focussed and then sent to ^{2}D and FID2 analytical detector. Peak widths of standards are about 6 to 10 s wide and peak response range from 10 to 30 pA above baseline.

4.3.3 Regular targeted mode of LMCS

Figure 4.4A shows the normal GC analysis and selected regions **a** to **h** which will be trapped by using regular straight through type cryogenic operation. All selected regions were subjected to regular TMDGC mode (described above) and the result in **Figure 4.4B** was obtained. One result from individual collection of **a** to **h** and rapid re-injection for fast separation/elution in ^{2}D, is the peak response enhancement produced. Now, responses ranging from 100 to 700 pA can be observed which are about 15 to 20 times higher than those in normal GC. In addition, the contribution of column bleed from ^{2}D was established during the analysis. The magnitude of the bleed peak was dependent on how long the trap has been kept in the trapping position. To solve this problem, a 'cleaning step' was performed in order to release contaminating compounds and column bleed peaks from the trap region before the incoming targeted solute entered into the cryogenic region. In this experiment, peaks labelled * in **Figure 4.4B** and in **Table 4.1** are column bleed peaks when the cryotrap was moved without trapping the targeted solute in the cleaning step. However, there are small bleed peak observed in every individual selected region, and these peaks are little-retained so are eluted before the target peaks as can be seen in **Figure 4.4B** and all expanded regions in **Figure 4.5**. Expansions of selected regions in the chromatogram of **Figure 4.4A** are shown in **Figure 4.5** and an excellent peak shape and peak response was observed for all solutes. For instance, the single peak (peak 6) in region **b** was retained in ^{2}D by 3.72 s with peak attitude gain about 30 times from 8.75 pA to 262.50 pA. Similar results were also observed in region **c** and **d**. By fully collecting peaks and fast analysis in ^{2}D and with good peak symmetry, peak area and peak height, measurement should more precise for small peaks. Interestingly, region **a** which contains 5 peaks, peak number 2 and 3 in this region are completely co-eluted in 1D-GC but now are partially separated as seen in **Figure 4.5A.** Additionally, positions of two peaks (peak 15 and 16) in region **g** were swapped over during the operation. This can be explained by referring to the GC×GC results, where it was shown that $^{2}t_{R}$ of peak 16 is shorter than $^{2}t_{R}$ of peak 15. Region

e, with two peaks that were completely co-eluted in this operation, generated the same $^{2}t_{R}$ of these two peaks in GC×GC contour plot. Details of pesticides retention in the GC×GC contour plot will be discussed in **Section 4.3.4**. The other expanded regions are shown in **Figure 4.5**. Due to many peaks being trapped in the region, for instance, region marked **f** shows that the ^{2}D column used in this study has an insufficient efficiency or separation power to separate all of them, unless a longer ^{2}D column can be employed. However, solute band dispersion will be increased. Results obtained from this regular target operation including heart cutting events, $^{1}t_{R}$, $^{2}t_{R}$, elution temperature (T_e), peak width and peak symmetry are shown in **Table 4.1**

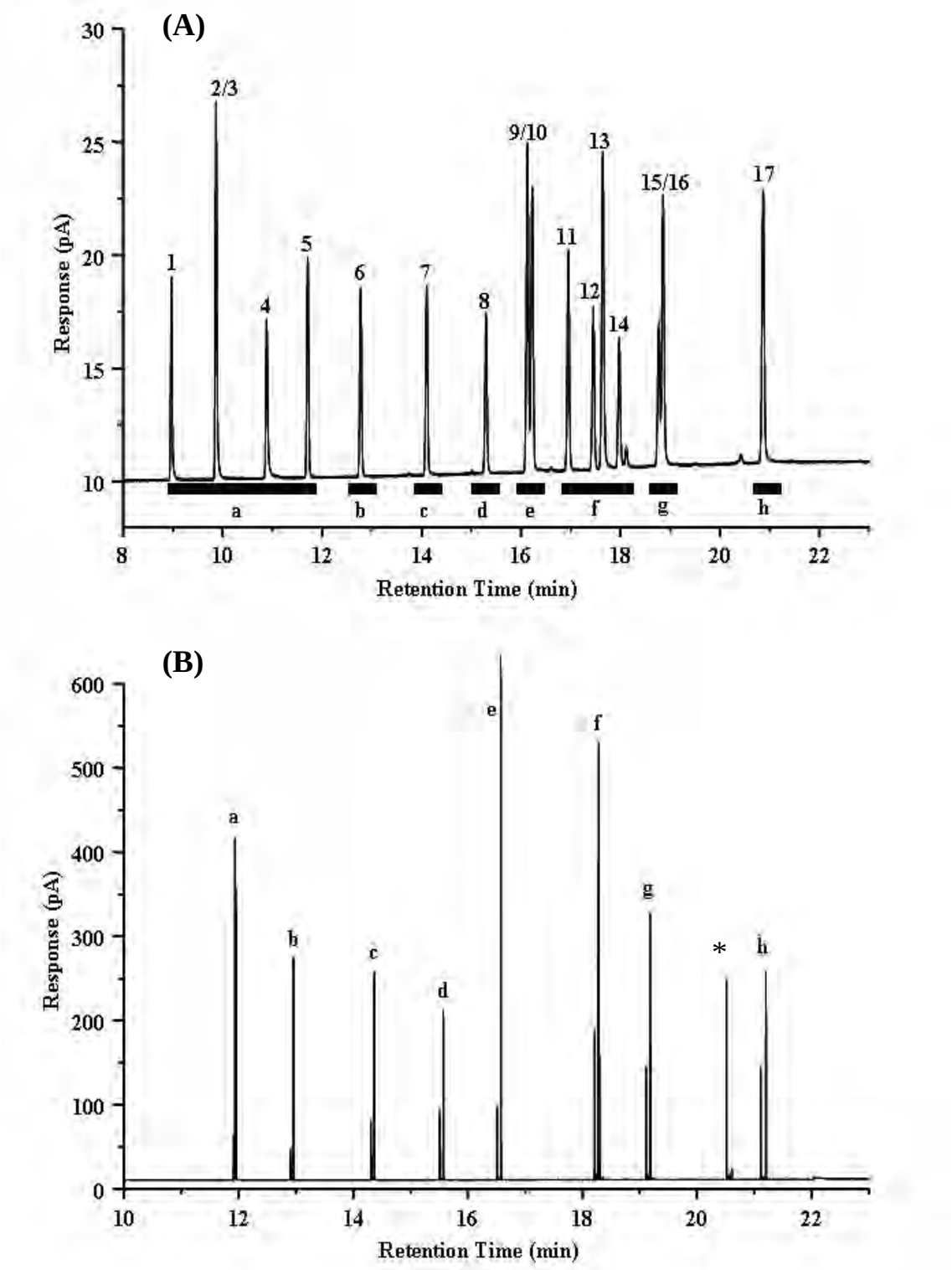

Figure 4.4: (A) 1D-GC chromatogram of 17 OCs pesticides. Solid line show selected regions (labelled in a to h) which will be trapped by the straight through type LMCS. **(B)** Shows raw 2D-GC chromatogram of the selected regions from **a** to **h** when targeted mode was performed.

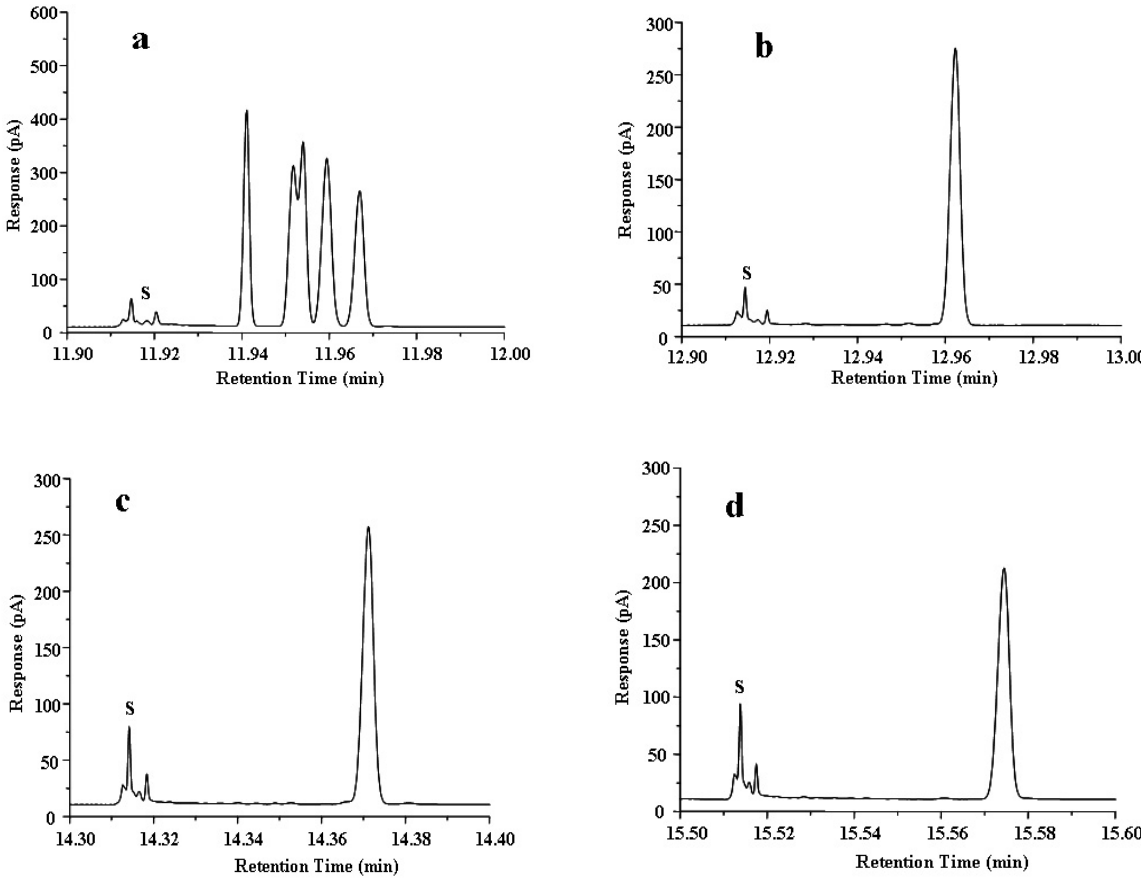

Figure 4.5: Expanded regions of **a** to d as shown in **Fig 4.4 (B)**, when targeted mode of the straight through type cryogenic LMCS was performed. Peaks marked '**s**' are from column bleed.

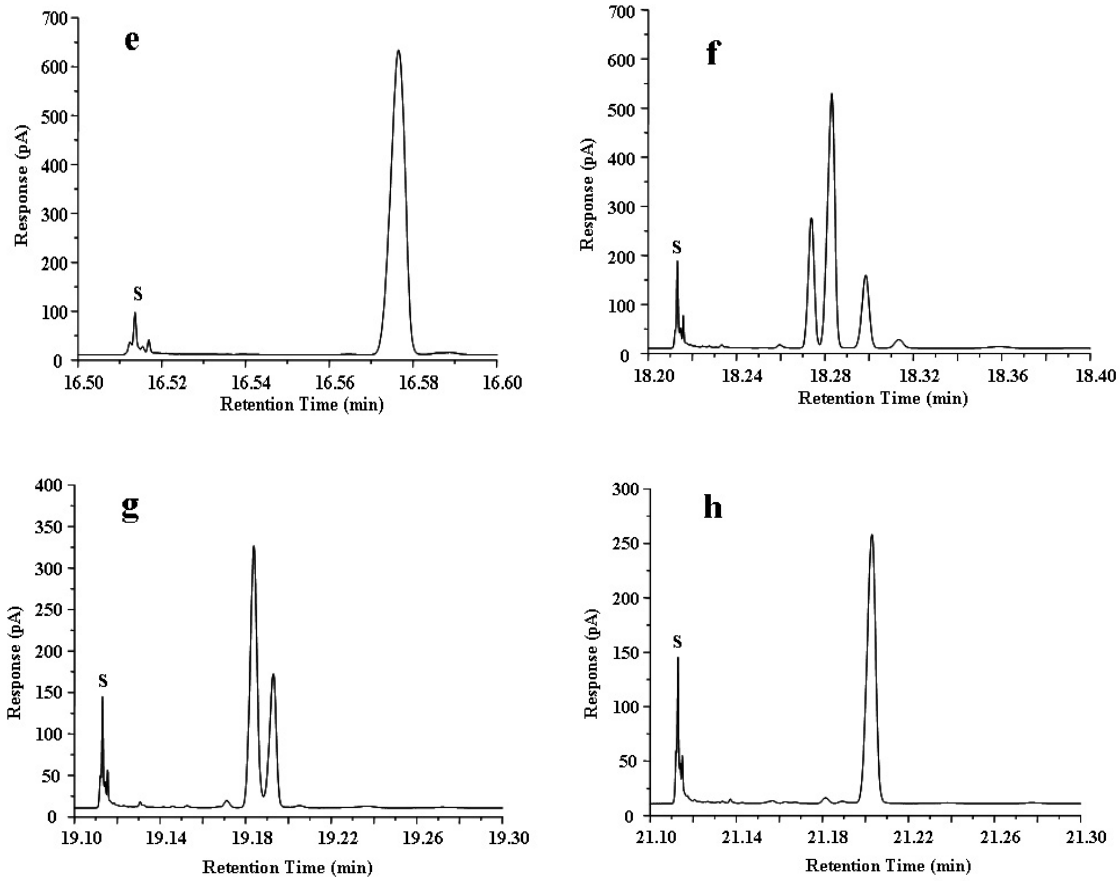

Figure 4.6: Expanded regions of e to **h** as shown in **Fig 4.4 (B)**, when targeted mode of the straight through type cryogenic LMCS was performed. Peaks marked '**s**' are from column bleed.

Table 4.1: Results obtained from targeted mode using regular straight through type operation, including heart cutting events.

Time Events	Cryo-trap position	Peak trapped	T	R	^1t_R(min)	^2t_R(s)	T_e (^oC)	$W_{0.5}$ (ms)	W_b (ms)	A_s
8.50	T	1-4	a							
11.90	R			a	11.9540	3.24	194.6	Peaks are co-eluted		
12.50	T	5	b							
12.90	R			b	12.9620	3.72	199.7	154	324	0.99
13.90	T	6	c							
14.30	R			c	14.3710	4.26	206.7	169	360	1.00
15.10	T	7	d							
15.50	R			d	15.5740	4.44	212.7	176	384	1.00
15.90	T	8-9	e							
16.50	R			e	16.5770	4.62	217.7	Peaks are co-eluted		
16.70	T	10-14	f							
18.20	R			f	18.2830	4.98	226.1	Peaks are co-eluted		
18.60	T	15-16	g							
19.10	R			g	19.1840	5.04	230.6	Two peaks solved to swap position		
20.10	T	Clean trap	*							
20.50	R			*				Column bleed peak		
20.60	T	17	h							
21.10	R			h	21.2030	6.18	240.7	263	564	1.11

4.3.4 Multi-pass loop type 1 operation

Loop type 1 employs one and a half modulation cycles compared with that of the straight through system, to send the incoming solute from ^{1}D to the detector. Firstly, the incoming solute from ^{1}D was trapped at the trap position, and then the analyte band was flushed or released into the loop and trapped again when the trap is in its lower position. The cryotrap was slowly returned to the trap position waiting for the new incoming peak; this allows the selected band to be exposed to the surrounding oven temperature and transfer to the detector as a concentrated band. **Figure 4.6A** shows selected groups **a** to **g** which will be trapped using multi-pass loop type 1; the same condition as used in the regular straight through type was carried out. The raw 2D chromatogram obtained from targeted multi-pass loop type 1 operation is shown in **Figure 4.6B**. Once again, higher peak response from the modulation process can be seen. Three cleaning steps marked * in **Figure 4.6 B** were applied in this operation to remove ^{1}D contaminants and/or column bleed. It is important to note that the amplitude of the cleaning peak can be increased depending on the magnitude of column bleed, column temperature and the duration of the collection. For instance, high column bleed peaks can be observed when a long duration of the cleaning step was performed. However, ^{2}D column bleed peaks were observed in each region to have no significant interference on target peaks since they are not longer retained in ^{2}D. **Figure 4.7** shows expanded regions of selected peaks when the targeted mode multi-pass loop type 1 was employed. Clearly, regions **a** and **f** showed insufficient ^{2}D column efficiency to resolve all peaks in this region. Additionally, the slow upward motion of the trap position and rapid down stroke of the cryogenic trap movement design is important and needs to be noted. The slowly release from the cryo-region when the cryotrap returns to the trap position clearly explains peak broadening problems in this case. Rapid remobilisation of the heart-cut regions at the start of ^{2}D is critical for fast GC analysis in order to maintain narrow bands for all analytes of interest. Therefore, broader peaks and lower peak response compared to the regular mode resulted in this type 1 operation mode. Peaks 6, 7, 8 and 17 in region **b**, **c, d** and **g,** respectively, can be seen as broader peaks compared

to the straight through type. Peak 9 and 10 (region **e**) completely co-elute in this modulation mode. Results obtained from targeted mode using multi-pass loop type 1 are summarised in **Table 4.2.**

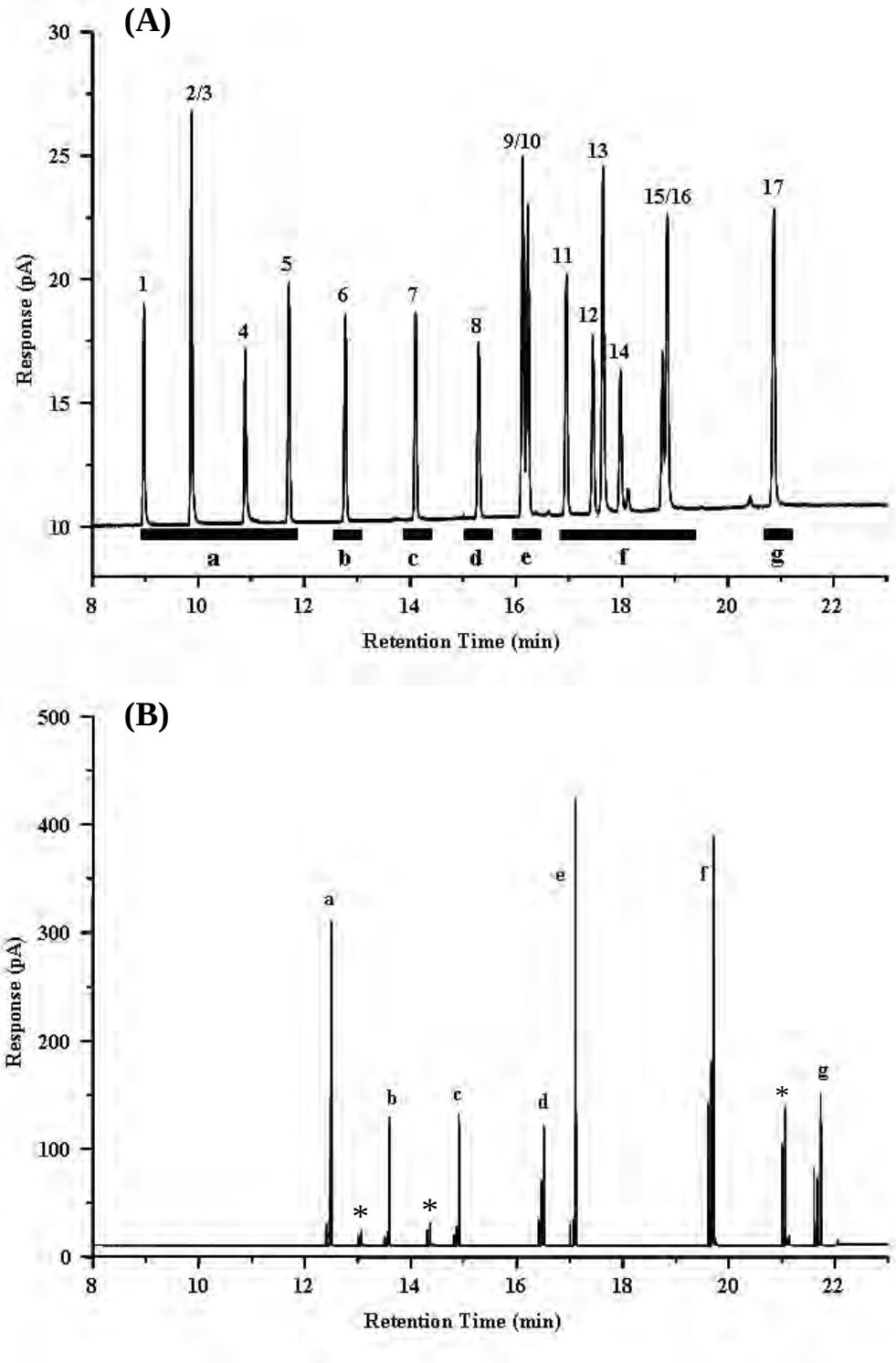

Figure 4.7: Multi-pass loop modulation type 1 results. **(A)** 1D-GC chromatogram of 17 OCs pesticides. Solid line show the region (labelled in **a** to **g**) which will be trapped by the multi-pass cryogenic loop type 1. **(B)** Shows raw 2D-GC chromatogram of the selected region from **a** to **g** when targeted mode using multi-pass loop type 1 was performed.

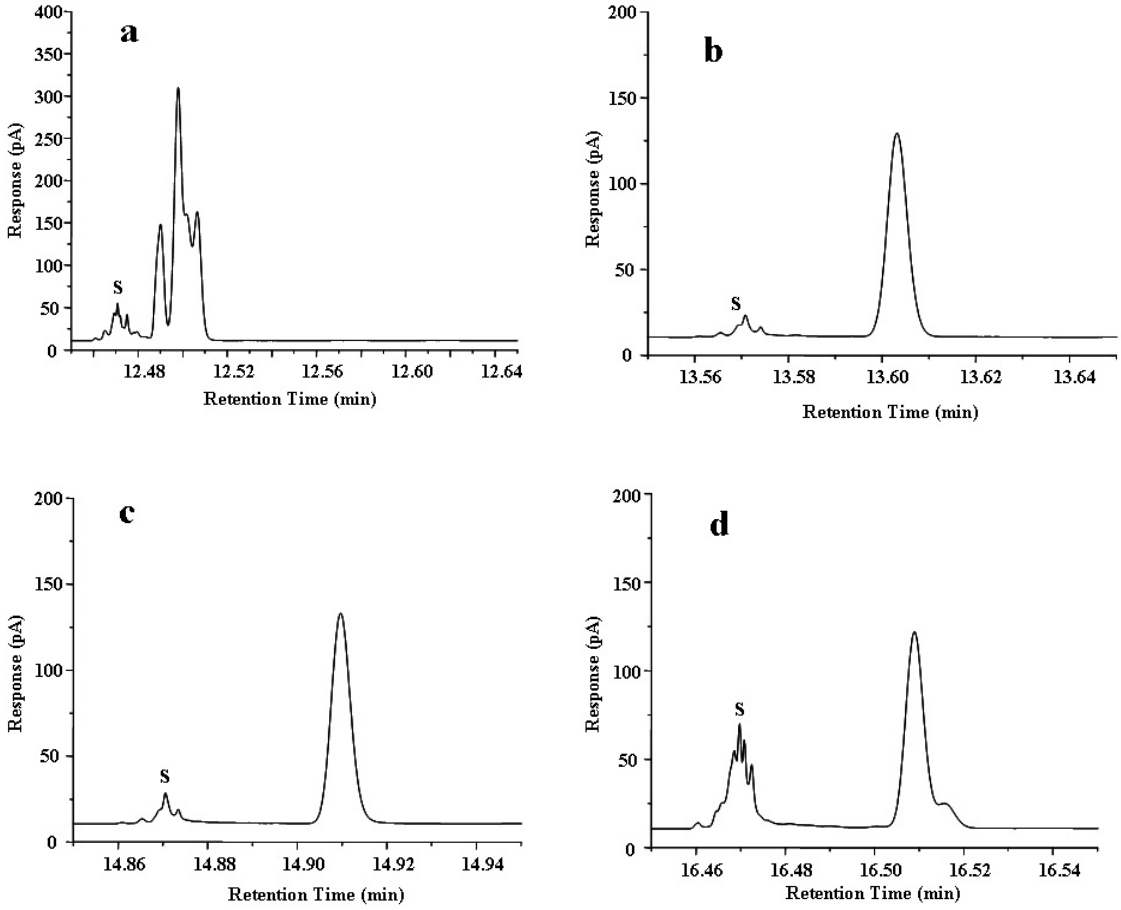

Figure 4.8: Expanded regions of **a** to **d** as shown in **Fig 4.7 (B)**, when the targeted MDGC using multi-pass loop type 1 was performed. Peaks marked '**s**' are from column bleed.

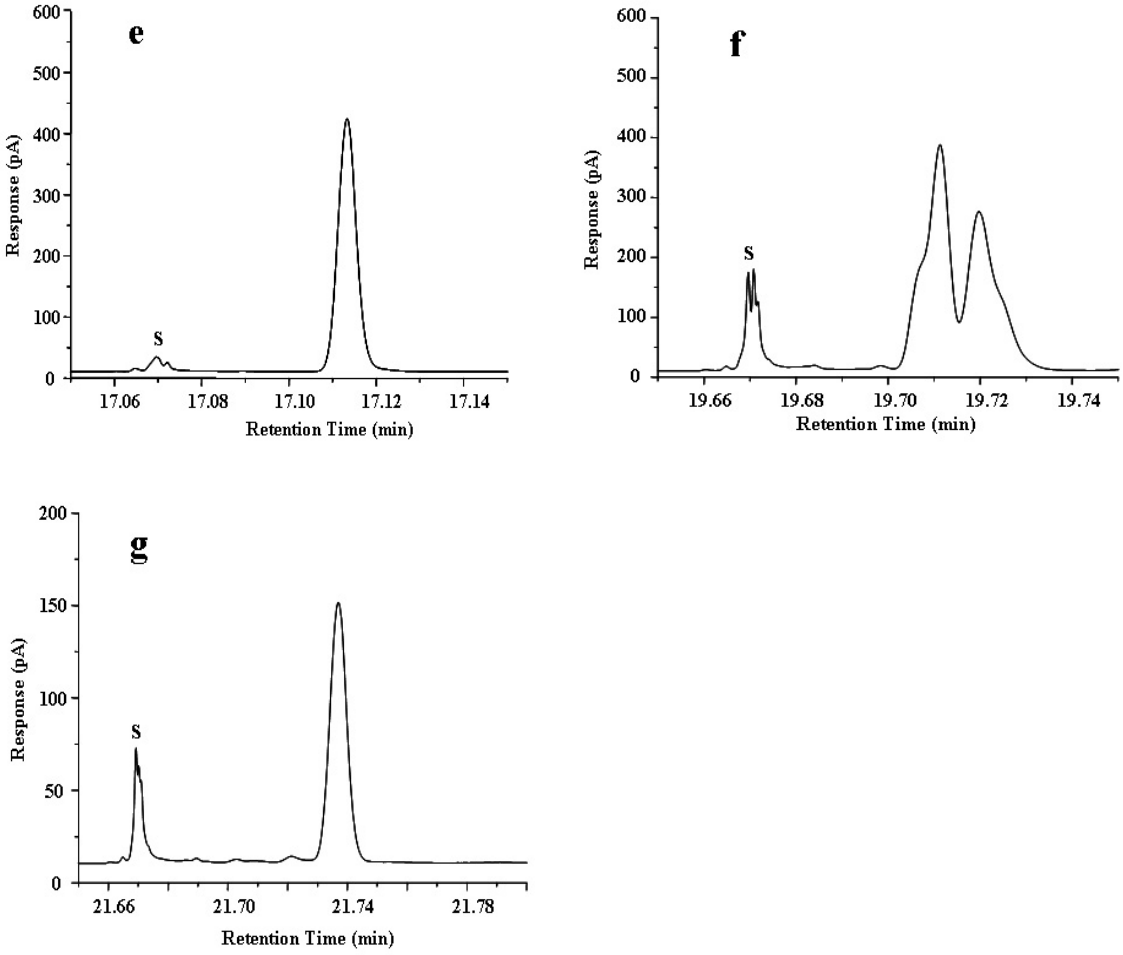

Figure 4. 9: Expanded regions of **e** to **g** as shown in **Fig 4.7 (B)**, when the targeted MDGC using multi-pass loop type 1 was performed. Peaks marked '**s**' are from column bleed.

Table 4.2: Results obtained from targeted mode using multi-pass loop type 1operation including heart cutting events.

Time Events	Cryo-trap position	Peak trapped	T	R	$^{1}t_R$(min)	$^{2}t_R$(s)	T_e (^oC)	$W_{0.5}$ (ms)	W_b (ms)	A_s
8.50	T	1-4	a							
12.40	R									
12.45	T	Clean loop	*	a	12.4980	2.88	197.3	Peaks are co-eluted		
13.00	R									
13.05	T	5	b	*	*			Column bleed peak		
13.50	R									
13.55	T	Clean loop	@	b	13.6030	3.18	202.8	283	570	0.92
14.30	R									
14.35	T	6	c	@	@			Column bleed peak		
14.80	R									
14.85	T	7	d	c	14.9090	3.54	209.3	283	594	0.89
16.40	R									
16.45	T	8-9	e	d	16.5100	3.60	217.3	273		0.64
17.00	R									
17.05	T	10-16	f	e	17.1130	3.78	220.3	Peaks are co-eluted		
19.60	R									
19.65	T	Clean loop	#	f	19.7200	4.20	233.3	Peaks are co-eluted		
21.00	R									
21.05	T	17	g	#	#			Column bleed peak		
21.60	R									
21.65	T			g	21.7370	5.22	243.4	376	744	0.98

4.3.5 Multi-pass loop type 2 operation

Multi-pass loop type 2 requires two regular cycles of the cryotrap movement to send the targeted solute to the detector. This means, the target solute will be trapped three times in this mode (**refer to Figure 4.2**). Again, analyte was trapped at the trap position, when cryotrap moves down to its release position the analyte band flushes out and is trapped again in the cryotrap release position after its travel along the loop. Consequently, when the cryogenic trap returnes back to the original trap position, the first solute still remains within the cryogenic region. The second remobilisation of solute and transfer to ^{2}D arises when the cryotrap moves down to release position; the same process is repeated for new incoming solute. **Figure 4.8A** shows selected regions **a** to **h** which will be trapped using multi-pass loop type 2, at the same condition as in both two types of modulation previously studied. The raw 2D chromatogram of this operation is shown in **Figure 4.8B**. Due to the need for 4 time events for each individual region to pass to the detector, and since Chemstation Software is limited to 25 events, this reduces the total operation of the type 2 modulation. Each region was expanded and these are shown in **Figure 4.9**. Two cycles compared with one for the regular cycle are required, thus the solutes are expelled to ^{2}D during the rapid movement of the cryotrap (compared with loop type 1 which is during a slow cryotrap movement) narrower band and higher response in this mode compared to the previous two types. Similar observations noted in both types stated above, such as insufficient efficiency of ^{2}D to separate all peak in regions **a** and **f** , smaller peak width, higher peak response and better peak shape for all individual peaks (peak 6, 7, 8 and 17) was observed. Again, peak 9 and 10 remained completely co-eluted and peak 15 and 16 swap over. The summary of results of this mode is shown in **Table 4.3**.

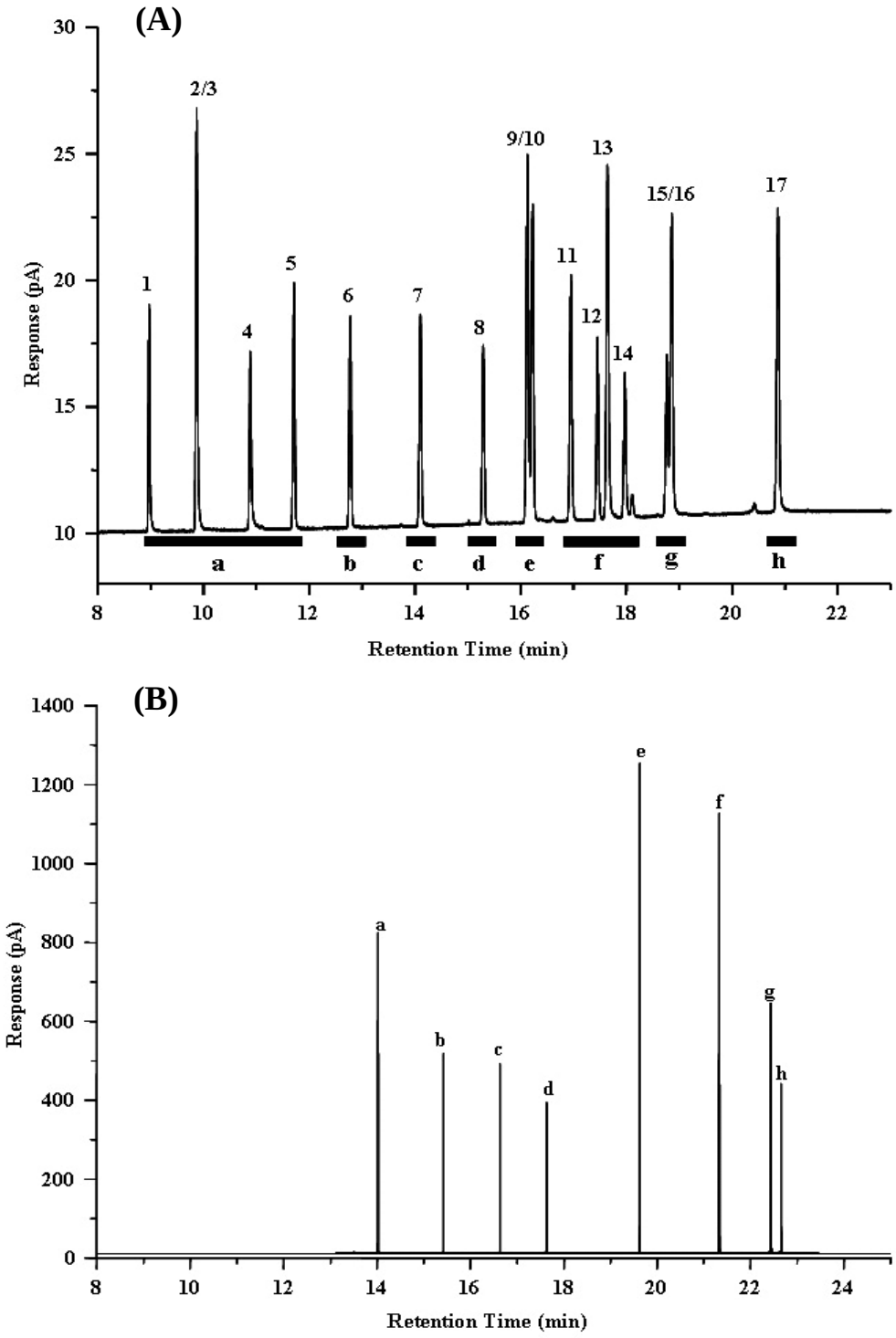

Figure 4. 10: Multi-pass loop modulation type 2 results. **(A)** 1D-GC chromatogram of 17 OCs pesticides. Solid line show the region (labelled in **a** to **h**) which will be trapped by the multi-pass loop type 2. **(B)** Shows raw 2D-GC chromatogram of the selected region from **a** to **h** when targeted mode was performed.

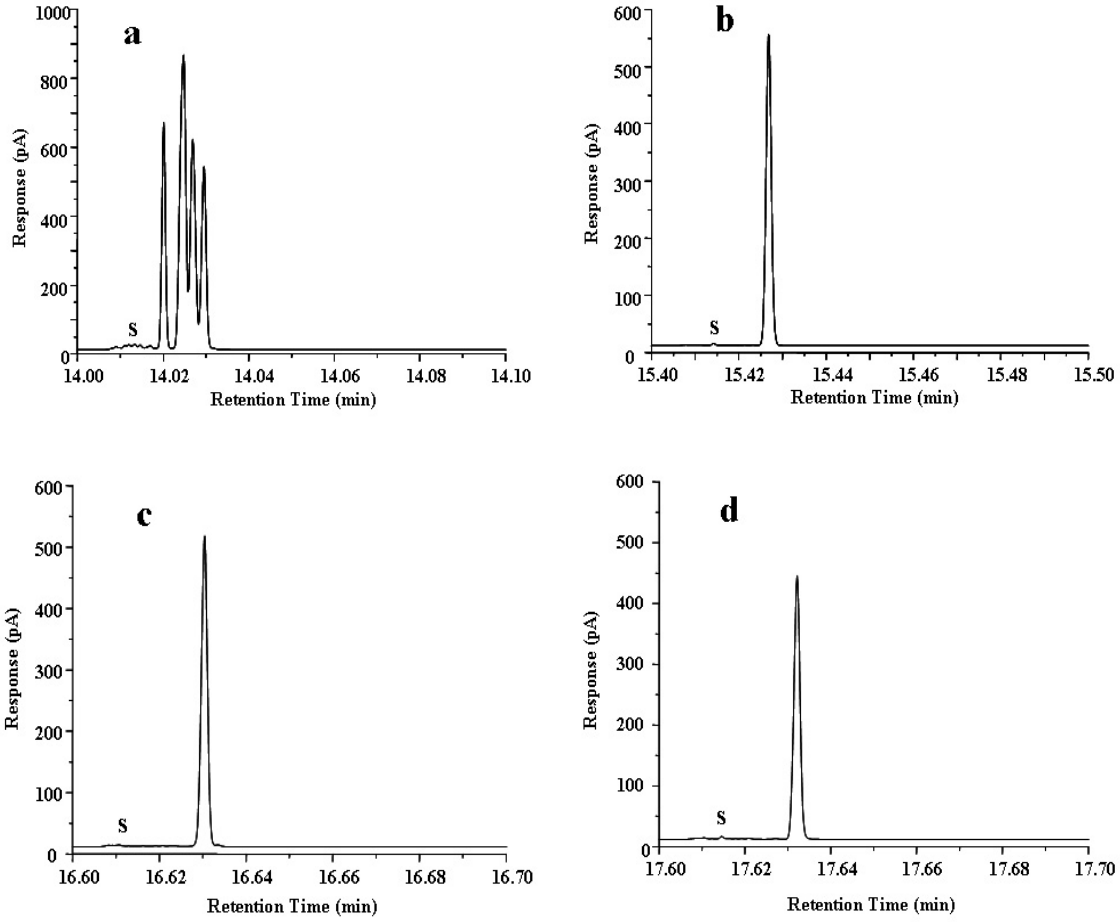

Figure 4.11: Expanded regions of **a** to **d** as shown in **Fig 4.10 (B)**, when targeted mode using multi-pass loop type 2 was performed. Peaks marked '**s**' are from column bleed.

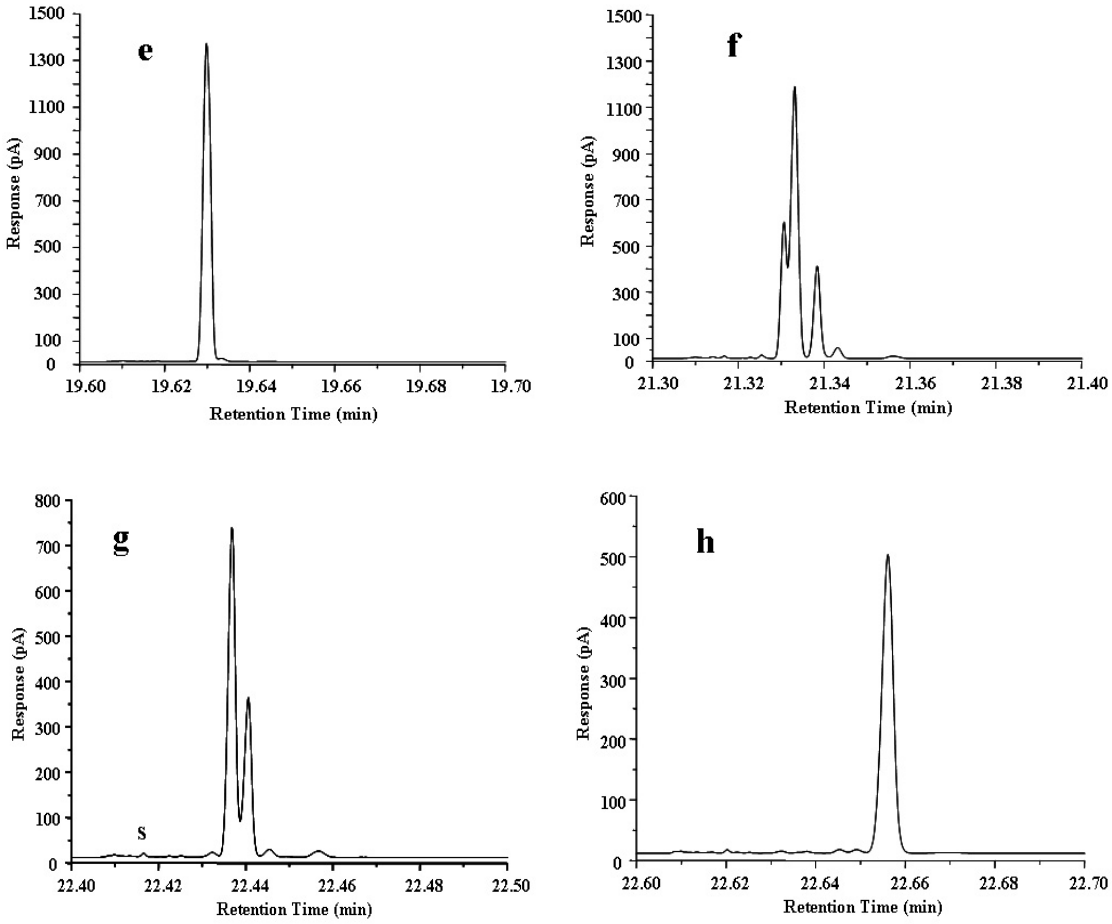

Figure 4.12: Expanded regions of **e** to h as shown in **Fig 4.10 (B)**, when targeted mode using multi-pass loop type 2 was performed.

Table 4.3: Results obtained from targeted operation using multi-pass loop type 2 operation.

Time Events	Cryo-trap position	Peak trapped	T	R	$^{1}t_R$(min)	$^{2}t_R$(s)	T_e (^{o}C)	$W_{0.5}$ (ms)	W_b (ms)	A_s
9.00	T	1-4	a							
13.50	R									
13.60	T	5	b							
14.00	R			a	14.0200	1.20	204.9	Peaks are co-eluted		
14.10	T	6	c							
15.40	R			b	15.4270	1.62	211.9	70	174	0.98
15.50	T	7	d							
16.60	R			c	16.6300	1.80	217.9	90	198	1.05
16.70	T	8-9	e							
17.60	R			d	17.6320	1.92	222.9	79	204	1.05
17.70	T	10-14	f							
19.60	R			e	19.6300	1.80	232.9	Peaks are co-eluted		
19.70	T	15-16	g							
21.30	R			f	21.3330	1.98	241.3	Peaks are co-eluted		
21.40	T	17	h							
22.40	R			g	22.4370	2.22	246.8	Two peaks was swap over		
22.50	T									
22.60	R			h	22.6560	3.36	247.9	160	318	1.09

4.3.6 Comprehensive mode in GC×GC using multi-pass loop modulation

Results obtained from comprehensive mode of GC×GC with all types of the multi-pass loop arrangements are shown in **Figure 4.13**. The results are presented in a contour plot, in which the first column retention time (^1t_R) is given on the horizontal axis, and second column retention (^2t_R) on the vertical. Each approach was carried out for the analysis of 17 organochlorine pesticide standards in comprehensive mode with the same modulation period (P_M = 3s). From the 2D plots it appears that the chemical properties of the OC pesticides with respect to polarity are similar, therefore, the polarity separation in ^{2}D in this study can not spread out OC pesticide standards over the full polarity dimension the 2D space. Thus, ^2t_R of the pesticides are relatively comparable. **Figure 4.13A** shows a contour plot of 17 OC pesticide standards when comprehensive mode in regular straight through type was employed. In this geometry a lower carrier gas flow rate from ^{1}D was split to an uncoated capillary column and ^{2}D column. Therefore, all OCs are retained longer in ^{1}D and ^{2}D column. Better separation of the partially resolved peaks from ^{1}D; peak number 9/10 and 15/16 was achieved. However, peak 2 and 3 can not be separated in this study. **Figure 4.13B** shows the contour plot of OC standards when comprehensive mode using multi-pass loop type 1was employed. In this loop type the first and second column were directly connected without an uncoated capillary column (transfer line). Thus, the total flow of carrier gas was passed though ^{1}D to ^{2}D, therefore all compounds came out faster when compared with the straight through type. Due to the slower remobilisation in the cryotrap modulation process broader peaks can be seen in this case. Once again, unresolved peaks are now separated. **Figure 4.13C** shows the contour plot resulting from comprehensive loop type 2 approach, which is also a set up without the transfer line. This approach gave a relatively good peak shape and smaller peak width compared to the previous two modes due to the solute being trapped twice and faster elution from the cryotrap. Additionally, it is obviously, that there is more wrap around of OC pesticides obtained from the regular straight through type operation (**Figure 4.13A**) compared to the other

two obtained from multi-pass loop type 1 and 2 (**Figure 4.13B and C**), respectively. These results can be explained by the modulation process performed in each mode. In the regular straight through type operation, analytes were transfered to ^{2}D faster than in the multi-pass loop type due to there being no loop configuration which can be hold the analytes in the cryotrap longer. Thus, less wrap around was demonstrated in the contour plot obtained from the loop types.

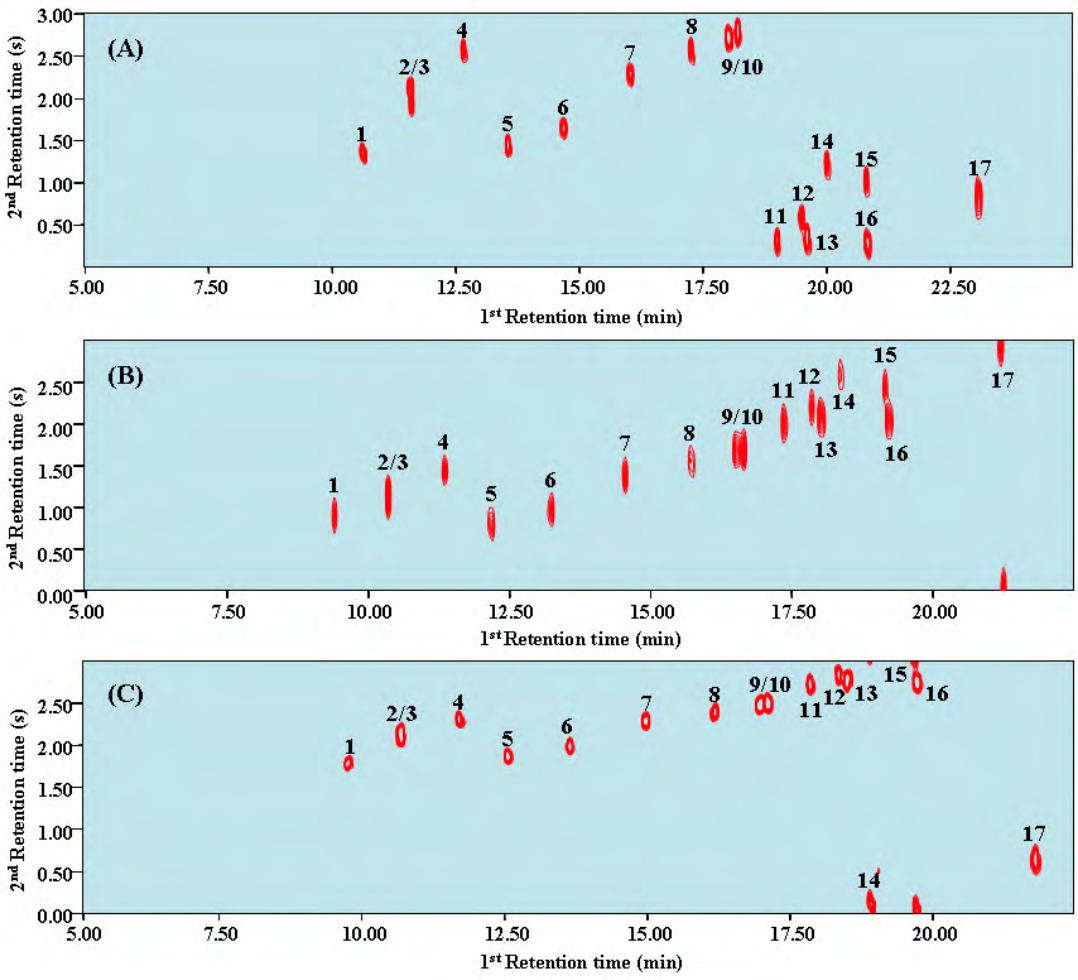

Figure 4.13: Contour plot of the analysis of 17 organochlorine pesticides in comprehensive mode using regular and loop types. **(A), (B) and (C)** are colour plots of the straight through type, multi-pass loop type 1, and type 2, respectively. P_M = 4s was used for all experiments.

4.4 Further study of LMCS multi-pass loop modulation

There are two solutions to solving band broadening problems in multi-pass loop type 1. Firstly, the thin wall capillary column should be set up as shown in **Figure 4.14** when the earlier model of the LMCS was used as a modulator in GC×GC analysis. This geometry of the multi-pass loop modulator will provide rapid movement and so improved performance to reduce band broadening of the analytes used in this study due to the rapid remobilisation when targeted analyte is re-injected to ^{2}D. However, the latest model of the LMCS modulator has both fast up and down strokes. This model might be a solution of band broadening in multi-pass loop modulation especially for multi-pass loop type 1, but generally the use of a second opportunity to trap solute in cryogenic modulation may offer a general improvement in solute focussing when the loop arrangement is employed.

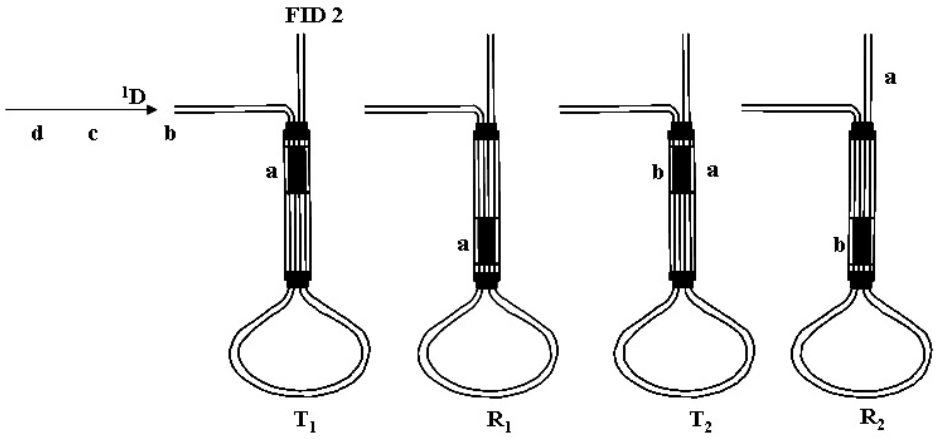

Figure 4.14: Suggested diagrams of the multi-pass loop cryogenic modulation. This proposed geometry might be the solution to band broadening when the operation of the LMCS was performed in the slow upstroke and rapid down stroke.

4.5 Conclusion

In this chapter, LMCS has been applied in a number of new modes. The operational modes presented here described a process for performing heart-cutting in MDGC technique with multi-pass loop modulation using the LMCS thermal modulator. The potential of LMCS to be used as a transfer device in MDGC method was demonstrated. The system is more complex than 1D-GC, but in the respect of MDGC, this approach is simpler than conventional MDGC due to transfer devices being un-necessary. Multi-pass loop approach provides for second and third selected fractions from ^{1}D to be held separately while the first fraction is sent to ^{2}D for further separation. A series of results obtained from these new geometries of LMCS, demonstrate the enhanced sensitivity of detection and relative simplicity of implementation compared to conventional MDGC. The method can be offered as an alternative choice to the chromatographer for the analysis of complex samples. Both continuous and selective sampling processes demonstrate the flexibility of the LMCS modulator to be used in the MDGC technique. Column bleed from ^{2}D found in this study can be separated and remobilised before the elution of the target peak. Superior peak sensitivity was observed in the analysis of individual peaks when multi-pass loop modulation was performed and this would be of benefit in quantitative analysis. The method shows the possibility for accurate quantification. Insufficient column efficiency (separation) was found when many peaks were contained in the selected region. Use of a longer ^{2}D column could solve this problem. However, a thicker film phase might be not possible due to limitation of the LMCS cryotrap inner channel size which means regular capillary columns cannot pass through. Like other conventional MDGC modes, heart cutting events need to be chosen carefully. Note that a wide bore trap is now available, and this will assist in use of conventional o.d. columns for this approach.

References

[1] J.C. Giddings, Anal. Chem. 56 (1984) 1259A.

[2] G. Schomburg, J. Chromatogr. A 703 (1995) 309.

[3] H.-J. de Geus, J. de Boer, U.A.T. Brinkman, Trends Anal. Chem. 15 (1996) 168.

[4] P.J. Marriott, P.D. Morrison, R.A. Shellie, M.S. Dunn, E. Sari, D. Ryan, LC-GC Eur. (2003) 2.

[5] W. Bertsch, J. High Resol. Chromatogr. 22 (1999) 647.

[6] W. Bertsch, J. High Resol. Chromatogr. 23 (2000) 167.

[7] L.F. de Alencastro, D. Grandjean, J. Tarradellas, Environmental Analysis 57 (2003) 499.

[8] D.R. Deans, Chromatographia 1 (1968) 18.

[9] P. Marriott, M. Dunn, R. Shellie, P. Morrison, Anal. Chem. 75 (2003) 5532.

[10] M. Dunn, R. Shellie, P. Morrison, P. Marriott, J Chromatogr. A 1056 (2004) 163.

[11] M.S. Dunn, N. Vulic, R.A. Shellie, S. Whitehead, P. Morrison, P.J. Marriott, J. Chromatogr. A 1130 (2006) 122.

[12] F. Bertoncini, C. Vendeuvre, D. Thiebaut, Oil & Gas Science and Technology 60 (2005) 937.

[13] G.L. Johnson, A. Tipler, D. Crowshaw, J. High Resol. Chromatogr. 13 (1990) 130.

[14] P.J. Marriott, R. Ong, R. Shellie, Environmental Application Note 33 (2001) 44.

[15] P.J. Marriott, R.A. Shellie, Trends Anal. Chem. 21 (2002) 573.

[16] J. Beens, U.A.T. Brinkman, Analyst 130 (2005) 123.

[17] M. Adahchour, J. Beens, R.J.J. Vreuls, U.A.T. Brinkman, Trends Anal. Chem. 25 (2006) 438.

[18] P.J. Marriott, R.M. Kinghorn, J. Chromatogr. A 866 (2000) 203.

[19] P.J. Marriott, R.C. Ong, R.M. Kinghorn, P.D. Morrison, J Chromatogr. A 892 (2000) 15.

[20] A.J. Kueh, P.J. Marriott, P.M. Wynne, J.H. Vine, J. Chromatogr. A 1000 (2003) 109.

[21] C. Vendeuvre, R. Ruiz-Guerrero, F. Bertoncini, L. Duval, D. Thiebaut, Oil & Gas Science and Technology 62 (2007) 43.

[22] F. Begnaud, A. Chaintreau, J. Chromatogr. A 1071 (2005) 13.

[23] F. Begnaud, A. Chaintreau, PCT/IB2004/001589 (2004) 1.

[24] Marriott P. J., K.M. Russell, J. High Resol. Chromatogr. 19 (1996) 403.

Chapter

5

APPLICATION OF COMPREHENSIVE TWO-DIMENSIONAL GAS CHROMATOGRAPHY WITH SELECTIVE DETECTION FOR THE ANALYSIS OF FUNGICIDES RESIDUES IN VEGETABLE SAMPLES

This chapter has been published as, "Application of comprehensive two-dimensional gas chromatography with nitrogen-selective detection for the analysis of fungicide residues in vegetable samples" Khummueng W., Trenerry C., Rose G., Marriott P.J., J. Chromatogr A., 1131(1-2), 203-14 (2006).

Abstract

Comprehensive two-dimensional gas chromatography (GC×GC) with nitrogen phosphorus detection (NPD) has been investigated for the separation and quantitation of fungicides in vegetable samples. The detector gas flows (H_2, N_2 and Air) were adjusted to achieve maximum response of signal whilst minimizing peak width. The comparison of different column sets and selection of the temperature program were carried out with a mixture of nine N-containing standard fungicides, 8 of which were chlorinated. The results from GC×GC-NPD and GC×GC-μECD were compared. External calibrations of fungicides were performed over a concentration range from 1-1000 $\mu g.L^{-1}$. The peak area calibration curves generally had regression coefficients of $R^2 > 0.9980$, however for iprodione which was observed to undergo on-column degradation, an R^2 of 0.990 was found. The limit of detection (LOD) and limit of quantitation (LOQ) were of the order of 28 and 246 $ng.L^{-1}$, respectively. The intra-day and inter-day %RSD values were measured for solutions of concentration 0.100, 0.500 and 1.50 $mg.L^{-1}$. For the 0.500 $mg.L^{-1}$ solution, intra and inter-day precision of peak area and peak height for most of the pesticides were about 2% and 8% respectively. Excellent linearity was observed for these standards, from 0.001 to 25.00 $mg.L^{-1}$. The standard mixture peak positions were identified by using GC×GC/qMS. To illustrate the potential and the versatility of both GC×GC-NPD and GC×GC-μECD, the methods were applied to determination of fungicides in a vegetable extract. Decomposition of one fungicide standard (iprodione) during chromatography elution was readily observed in the 2D GC×GC plot as a diagonal ridge response in the 2D chromatogram between the degrading compound and the decomposition product.

5.1 Introduction

Since its introduction, comprehensive two-dimensional gas chromatography (GC×GC) has been most commonly coupled with the flame ionization detector (FID). This detector has a high data acquisition rate, which is required for the high efficiency (narrow) peaks generated from the GC×GC system. More recently, there has been an increasing interest in coupling several selective detectors with this high resolution technique, including the electron capture detector (ECD) [1-8], thermionic ionization detector (TID) [9,10], atomic emission detector (AED) [11], nitrogen chemiluminescence detector (NCD) [12], sulfur chemiluminescence detector (SCD) [13-15]and both quadrupole and time-of-flight mass spectrometry (qMS and TOFMS) [16-20]. The increased sensitivity of various specific detectors over that of the FID detector is attractive for trace analysis. For example, a micro ECD detector was used for halogenated compounds such as PCBs and pesticides in food and environmental samples.

The thermionic ionization detector (TID) or thermionic specific detector (TSD), specifically in nitrogen phosphorus detection (NPD) mode is a detector of choice commonly used for the analysis of nitrogen and/or phosphorus containing compounds, particularly for trace pesticide and fungicide analysis in various matrices, mainly food products [21-24]. Coupling of GC×GC with the NPD detector offers good sensitivity and selectivity for both N- and P-containing compounds. The overall design of the NPD detector is based on the FID, except the chemical hydrogen/air flame of the FID is operated fuel lean, and a rubidium or cesium chloride ceramic bead is located above the burner jet. Typically, the bead surface is heated to a temperature of 700-900 °C. The flow of gases past this hot bead then can be a described as forming a gaseous boundary layer of high temperature and highly reactive chemical composition. The gas boundary layer contains flame-like radicals such as $H^{\cdot}$, $O^{\cdot}$ and $OH^{\cdot}$, which play an important role in sample decomposition and in the subsequent ionization process. The incoming samples impinge directly onto the gaseous boundary layer and the heated bead surface. Electrically, the bead is biased at

a voltage different from that of the surrounding collector electrode, thereby causing ion current to move from the bead's surface toward the collector. Ion current arriving at the collector is then measured using an electrometer [25,26]. However, the mechanism of the detector is not well understood with respect to the processes that occur at or near the surface of the NPD detector bead and plasma.

The NPD is often believed to cause tailing and asymmetric peaks, and for narrow peaks the effect may be exacerbated. Applications of GC×GC-NPD thus far have been used to analysis of nitrogen-containing compounds in several matrices such as petroleum samples, coffee, and wine components. In 2005, Ryan and coworkers [9] first reported the use of the NPD for GC×GC analysis. The study focused on optimization of all gases used in this detector, with respect to response sensitivity and peak symmetry. For some gases, flow settings were outside those recommended by the manufacturer. Best response and best symmetry were not necessarily achieved for the same gas flow. Recently, von Mühlen and coworkers [10] studied possible geometries of the NPD for characterization of N-containing compounds in petrochemical and related samples. They found that the use of an extended jet with a standard collector (compared with a narrow collector) electrode provided an improved response for the analysis of the N-containing compounds. In order to extend this earlier study, the analysis of N-containing fungicides was conducted here, where most of the compounds of interest also were chlorinated compounds. In this study the performance of the NPD as a specific detector for residue analysis in food samples by using GC×GC, was investigated. Experimental parameters affecting the method of the analysis of fungicides such as the temperature program, column combinations and detector gas flows (H_2, N_2 and air) were optimized. Precision and accuracy of the developed method were investigated. In addition, the comparison of GC×GC-NPD and GC×GC-μECD was also studied in this work for fungicides spiked into a vegetable extract matrix.

Fungicides are substances used to prevent the spread of fungus, which can cause a significant impact on yield and benefit of crops and harvest products. Most fungicides prevent spore germination by metabolic inhibition. The metabolism process of the target fungicides was normally damaged from the fungicides action

such as inactivating critical enzymes, interference with the energy production process and damage to cell membranes. Generally, fungicides can be classified in a number of different ways including;

a) The mobility in the plant

b) Role in protection

c) Breadth of activity

d) Mode of action

e) Chemical group or class

In agriculture, fungicides can be applied pre- or post-harvest to prevent the growth of fungus. Thus fungicides can cause contamination in various compartments of the agriculture field, environment and/or harvest products. Basically, there are three main reasons fungicide are used;

1. To control diseases during the establishment and development of a crop.

2. To increase productivity of a crop and to reduce blemishes.

3. To improve the storage life and quality of harvested plants and produce.

In this study, nine N-containing fungicides were used throughout the study including; chlorothalonil, vinclozolin, metalaxyl, penconazole, procymidone, myclobutanil, propiconazole, tebuconazole and iprodione. Vinclozolin is intensively used in agriculture to control plant diseases. Propiconazole has two isomers which give similar mass spectra for GC-qMS identification. Iprodione has been reported to undergo injection and on-column degradation, thus two peaks from parent and degradation products were observed in chromatograms. Thus, in this section the degradation of iprodione will be described and understood more completely. The study of minimizing degradation of captan and iprodione by using fast Gas Chromatography –Time of Flight Mass Spectrometry (GC-TOFMS) was reported in the separation science application note from LECO [27]. The application stated that, complications in both quantitative and qualitative analysis of these two pesticides was due to their degradation, both in the injector and on the GC column at high temperature. The results show that using a faster analysis and careful selection of the quantification masses (314+316), calibration for iprodione was easily accomplished and gave a low detection level (pg). Meanwhile, iprodione can be hydrolysed and

photodegraded in plant and soil, for example, it will be completely degraded in less than 24 hours at pH 9.0 and also can be photodegraded under UV wavelengths greater than 280 nm; the hydrolysis and photodegradation of iprodione are shown in **Figure 5.1** and **Figure 5.2,** and thermal degradation in **Figure 5.3.**

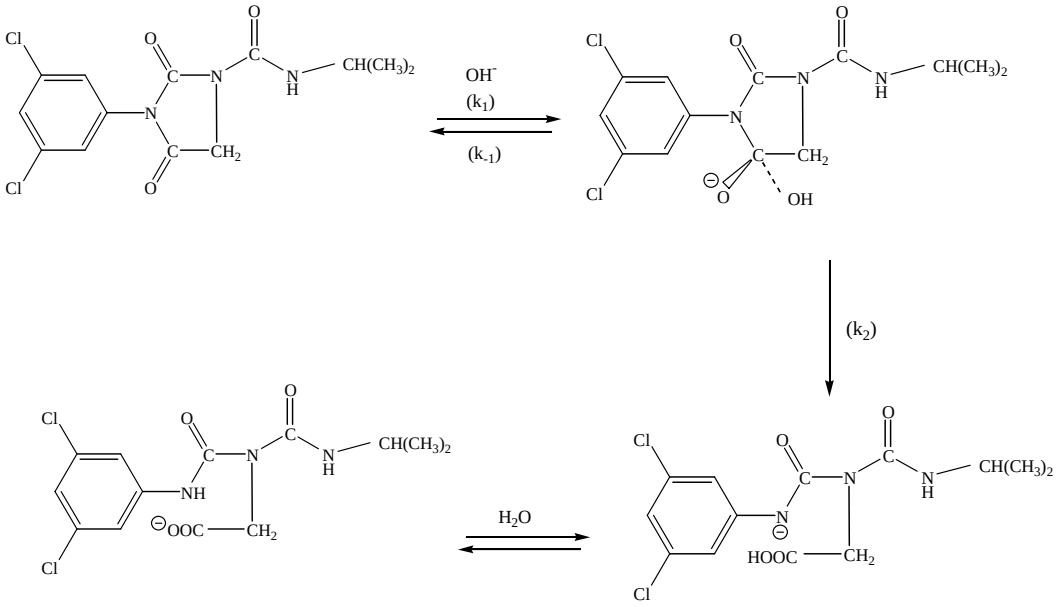

Figure 5.1: Mechanism of hydrolysis of iprodione [28].

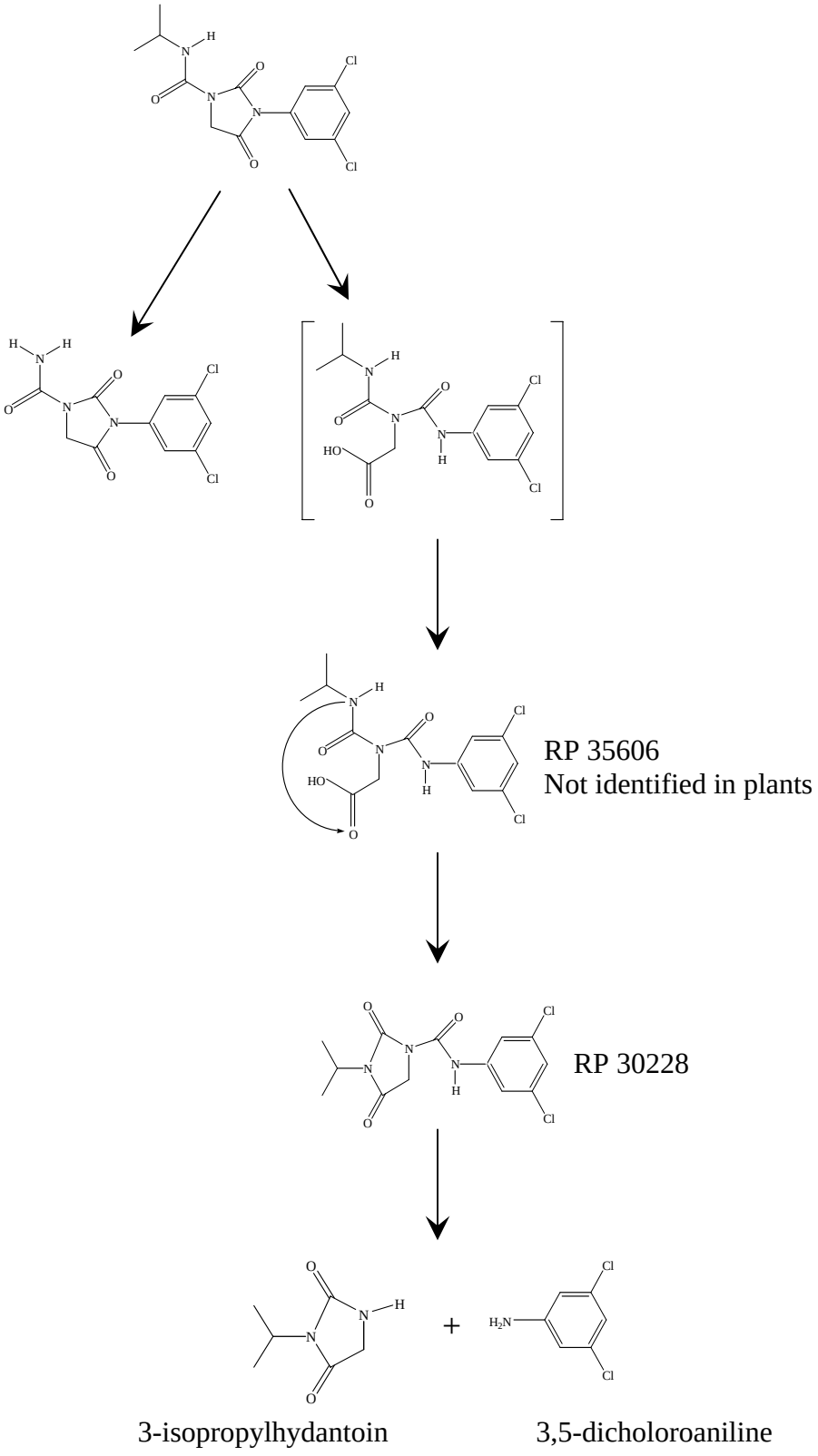

Figure 5.2: Degradation of iprodione under UV wavelength in plants and soil [Rhone-Poulenc, 1973, 1976].

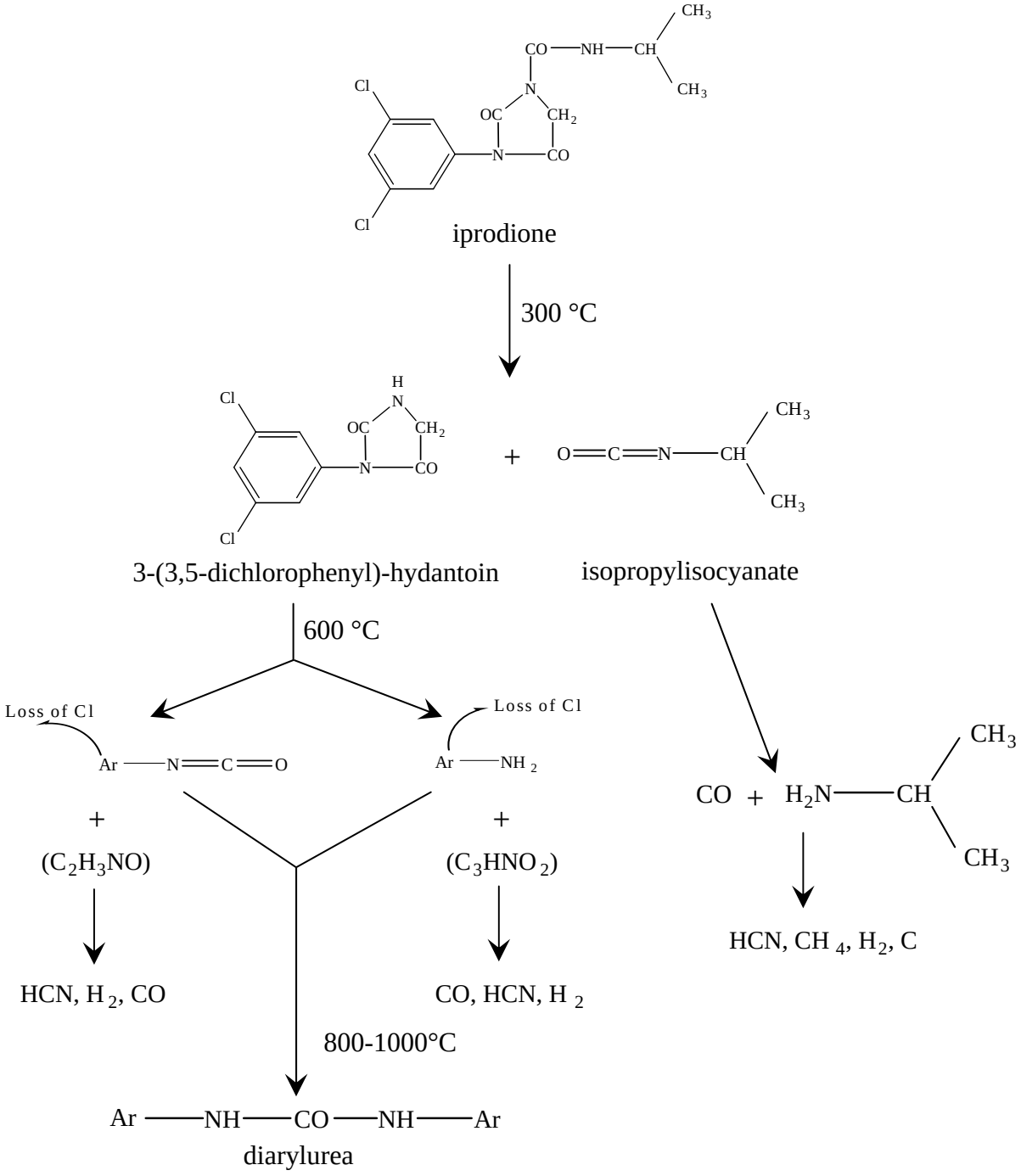

Figure 5.3: Thermal degradation scheme of iprodione [29].

5.2 Experimental

5.2.1 Instrumentation

An Agilent 6890 gas chromatograph was used throughout this study. Injections were facilitated by the CombiPAL Focus system (CTC Analytics AG, Zwingen, Switzerland), which was serially connected to an Optic 3 high performance injector (ATAS GL International, Veldhoven, The Netherlands). In order to conduct GC×GC analysis, the Agilent 6890 GC was retrofitted with a longitudinally modulated cryogenic system (LMCS) from Chromatography Concepts (Doncaster, Australia). Chemstation software was used to instruct the electronic modulator control to commence modulation at a predefined time. The CombiPAL Focus system and Optic 3 injector were controlled using Cycle Composure version 1.5.2 and ATAS Evolution Workstation version 1.2 software, respectively. Various column sets were tested with the fungicide standard mixture (**Table 5.1**). The final selected column set for all subsequent studies comprised a first dimension of 30 m x 0.25 mm I.D., 0.25 μm d_f BPX5 phase (5% phenyl polysilphenylene siloxane) column, coupled to a second dimension of 1.0 m x 0.15 mm i.d., 0.15 μm d_f BPX50 (50% phenyl polysilphenylene siloxane) coated column (all columns were from SGE International, Ringwood, Australia).

Table 5.1: GC×GC-NPD column sets used in preliminary study. The column set in bold was used throughout the remainder of this study.

Column sets	1st Dimension	2nd Dimension
1	Solgel-Wax, 30m, 0.25 mm, 0.25 μm	BP1, 1m, 0.1mm, 0.1μm
2	BPX50, 30 m, 0.25 mm, 0.25 μm	BP1, 1m, 0.1mm, 0.1μm
3*	***BPX5, 30 m, 0.25 mm, 0.25 μm***	***BPX50, 1 m, 0.15 mm, 0.15 μm***

*The final selected column set

5.2.2 Chromatographic conditions

Injections were performed in the splitless mode using the Optic 3 injector where the temperature was ramped from 50 ^{o}C to 280 ^{o}C at 15 ^{o}C.s^{-1}, with transfer time of 1 min. Hydrogen was used as a carrier gas at a flow rate of 1.0 mL.min^{-1}. The GC oven temperature was started at 50 ^{o}C and then ramped at 10 ^{o}C.min^{-1} to 210 ^{o}C and 5 ^{o}C.min^{-1} to 260 ^{o}C (held for 5 min). The NPD detector was operated at 300 ^{o}C, with the final selected conditions for detector gas flows at 1.5, 7 and 100 mL.min^{-1} for H_2, N_2 make-up gas and air, respectively. Prior to deciding these conditions, an optimization study was conducted. An adjust offset of 30 pA was used with the NPD. All data were collected at 50 Hz acquisition rate. The μECD detector was operated at 300 ^{o}C at its maximum data rate of 50 Hz, with make-up flow of 120 mL.min^{-1}.

5.2.3 Mass spectrometric detection

GC-qMS was performed for the identification of all standard fungicides. An acquisition rate of 15.15 Hz and mass range 40-500 u was used for the mixture of standard fungicides. The ion source temperature was 230 ^{o}C, transfer line temperature 280 ^{o}C, and detector voltage 1529 V.

5.2.4 Data analysis

The GC×GC data were transformed using an in-house program and visualized as contour plots using Transform software (Fortner Research, Virginia, USA). For data analysis, total peak height and area data were generated using an in-house Matlab program. Peak widths and second dimension peak symmetry were calculated using a peak profile calculation program.

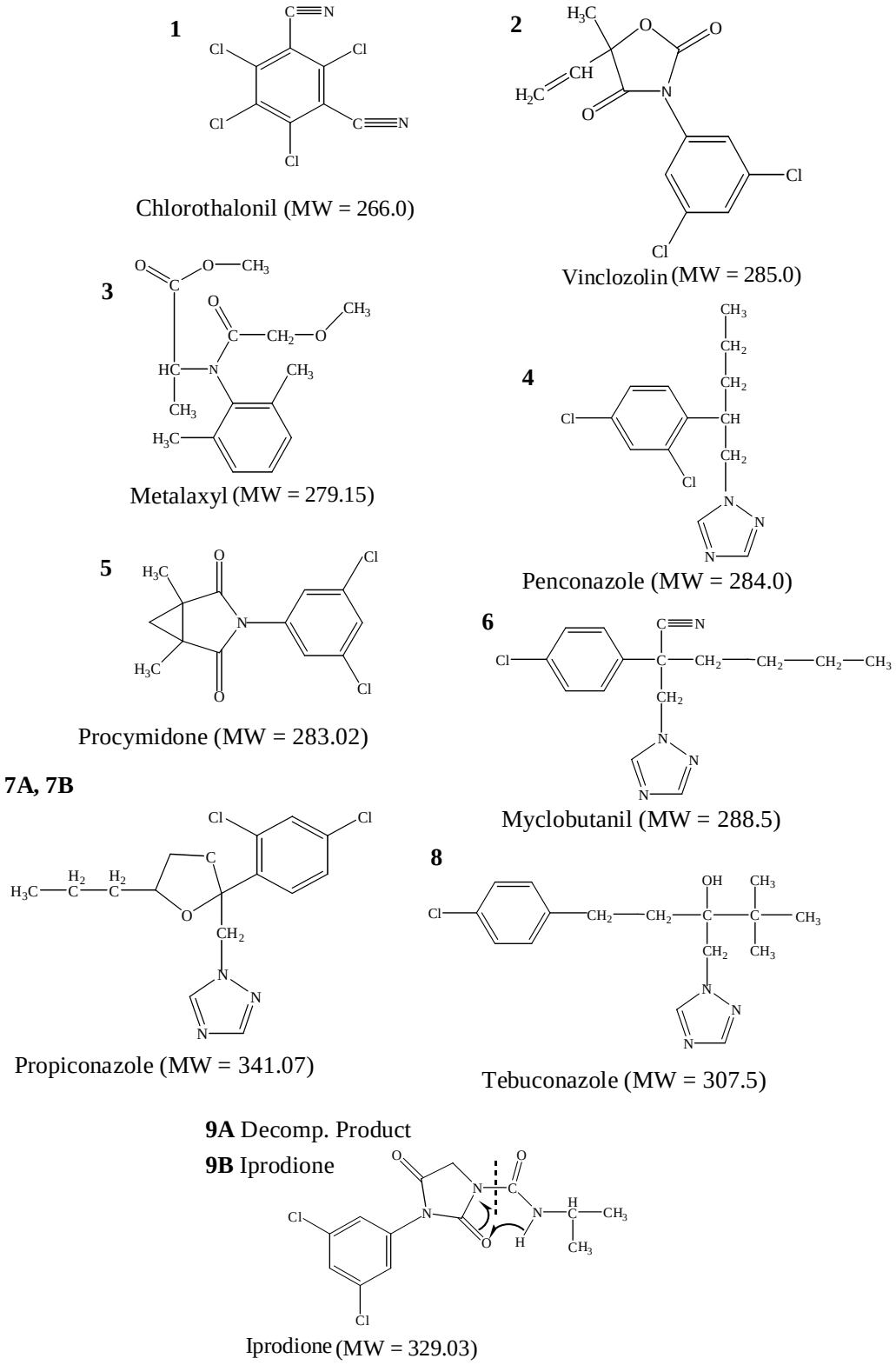

Figure 5.4: Names and structures of the nine standard fungicides. Note propiconazole **(7A, 7B)** has two diastereomers; iprodione **(9B)** has a decomposition product **(9A)** with a proposed structure indicated by the bond break and atom shift as shown.

5.2.5 Standards and calibration solutions

The standard mixture used in this study was a fungicides standard which contained nine standard fungicides: Chlorothalonil (98.5% purity), Procymidone (98.0%), Iprodione (99.0%), and Metalaxyl (99.5%) were purchased from Dr. Ehrenstorfer-Schafers, Augsburg, Germany. Penconazole (99.0%) and Myclobutanil (99.9%) were purchased from Riedel de Haan, Hanover, Germany. Vinclozolin (99.5%) was purchased from the Institute of Organic and Industrial Chemistry, Propiconazole (89.8%) (mixture of two isomers) and Tebuconazole (96.2%) were purchased from the National Measurement Institute, Pymble Australia. Structures of all standard fungicides are shown in **Figure 5.4**. The stock solution had a concentration of 25 $mg.L^{-1}$ in each component, and was diluted with hexane as required. The external calibration standard solutions ranged from 1 to 1000 $\mu g.L^{-1}$. To test linear range, a solution standard up to 25 $mg.L^{-1}$ was used.

5.2.6 Repeatability and reproducibility

The repeatability was calculated at 3 levels of concentration: 0.1, 0.5 and 1.5 $mg.L^{-1}$ (n=5). Data were analysed by using standard deviation of the measurement values. The reproducibility of the method was evaluated for concentrations of 0.1, 0.5 and 1.5 $mg.L^{-1}$ (n=3) by conducting repeat analyses on different days.

5.2.7 Limits of detection (LOD) and quantitation (LOQ)

The limit of detection (LOD) of an analytical procedure is the lowest amount of an analyte that can be detected, but not necessarily quantitated as an exact value. The LOD value is a value of the lowest concentration of the standard, which produces an instrumental response that is 3 times larger than the standard deviation of the instrument (baseline) noise level. Solutions were injected 5 times. The average response (X) and the standard deviation (SD) were calculated. The LOD is 3×SD. The

limit of quantitation (LOQ) is the lowest amount of the analyte that can be quantitatively determined with defined precision under the stated experimental conditions. The accepted LOQ is that concentration of analyte (matrix dependent), which produces an instrumental response that is 2 to 10 times larger than the standard deviation of the instrument (baseline) noise level. Solutions were injected 5 times. The average response and the standard deviation (SD) of the 5 results were calculated. The LOQ is taken as 10×SD.

5.2.8 Sample extraction

A portion (50 g) of homogenized sample (Brussel sprouts) was weighed into a blender jar, with 150 mL of acetone. This was blended for 5 min. The acetone extract was filtered, and transferred to a 1 L separation funnel with 650 mL of 4% Na_2SO_4 solution added. The aqueous solution was extracted by shaking with 1 x 100 mL then 2 x 50 mL portions of dichloromethane. The combined dichloromethane extracts were passed through a Na_2SO_4 drying column into a 500 mL round bottom flask. The extract was then concentrated under vacuum on a boiling water bath, with inversion into hexane, to a final volume of 10 mL. Appropriate dilution was made where necessary. The final extract was spiked with fungicides at a level of 2.50 $mg.L^{-1}$.

5.3 Results and discussion

5.3.1 Optimization of NPD detector gas flow for fungicides analysis

The NPD is a specific detector comprising a rubidium or cesium ceramic bead, burner jet and collector electrode. The geometry of these components affects the operational performance of the NPD. It is commonly observed that the NPD is associated with some tailing of nitrogen and phosphorus containing compounds. The source of tailing could arise from the collector electrode, burner jet, detector gas environment, the plasma formed about the bead, and possibly the distance of the jet to the ceramic bead. In order to achieve maximum response (area and height) and a satisfactory peak shape it is necessary to optimize the performance of the NPD detector by optimizing the flow rate of gases and the detector component geometry. Hydrogen and air function to generate the plasma or the gaseous boundary layer, at high temperature. A higher nitrogen gas flow will provide stability to the bead voltage and results in narrower peaks. In a previous study by von Mühlen et al. [10] the geometry producing best response and most symmetric peak shape for N-containing compounds in petroleum samples was found to be a wide collector electrode, and an extended jet. For the application of the NPD to N-containing fungicides here, optimization was performed to confirm best operational conditions. A white ceramic bead, which is compatible with nitrogen-containing compounds, was also used in this work. **Table 5.2** shows the results of the optimization of NPD detector gas flows. A low hydrogen flow gave a higher bead voltage and temperature at the bead surface. N_2 and air flows of 7 and 100 $mL.min^{-1}$, and H_2 flow of 1.5, gave 3.991 V for bead voltage, and 40.5 pA and 596.6 pA.s for peak area and peak height respectively, for 2.50 $mg.L^{-1}$ procymidone. Higher H_2 flows gave reduced response. The bead voltage increased when N_2 make-up gas and air were increased at H_2 gas flow of 1.5 $mL.min^{-1}$. From **Table 2**, whilst condition 10 gave a higher response compared with condition d, it was accompanied by long equilibrium time and higher

adjust offset. **Figure 5.5** shows peak shape variation with different NPD detector gas flows. Not surprisingly, the results show that the high nitrogen gas flow gave the better peak shape. Condition d) with 1.5, 7 and 100 mL.min^{-1} for H_2, N_2 and air respectively gave good peak shape and highest response for N-containing fungicides, so was used for further experiments in this study. Interestingly, condition a) is the recommended condition suggested by the manufacturer (3, 5 and 60 mL.min^{-1} for H_2, N_2 and air) and gave the lowest response compared with the others tested (**Figure 5.5**).

Table 5.2: The optimization conditions and results for the NPD detector gas flows (H_2, air and N_2), bead voltage of NPD detector, peak response (area and height) of procymidone (2.5 mg.L^{-1}) in each condition. Flows in bold are those used for the remainder of the study.

Conditions	NPD detector gas flow (mL.min^{-1})				Procymidone	
	H_2	Air	N_2	Bead voltage	Peak area (pA*s)	Peak height (pA)
a	3	60	5	3.876	22.92	260.5
b	1.5	70	7	3.963	35.00	452.6
c	1.5	70	10	4.026	35.86	514.0
d	***1.5***	***100***	***7***	***3.991***	***40.53***	***596.6***
e	3	100	7	3.844	29.54	431.5
f	4	100	7	3.835	27.44	411.8
g	2	100	7	3.952	35.30	514.7
h	1.5	120	7	4.017	40.95	623.1
i	1.5	100	10	4.045	40.70	607.2
j	1.5	120	10	4.007	44.20	683.5

* selected condition or optimum condition

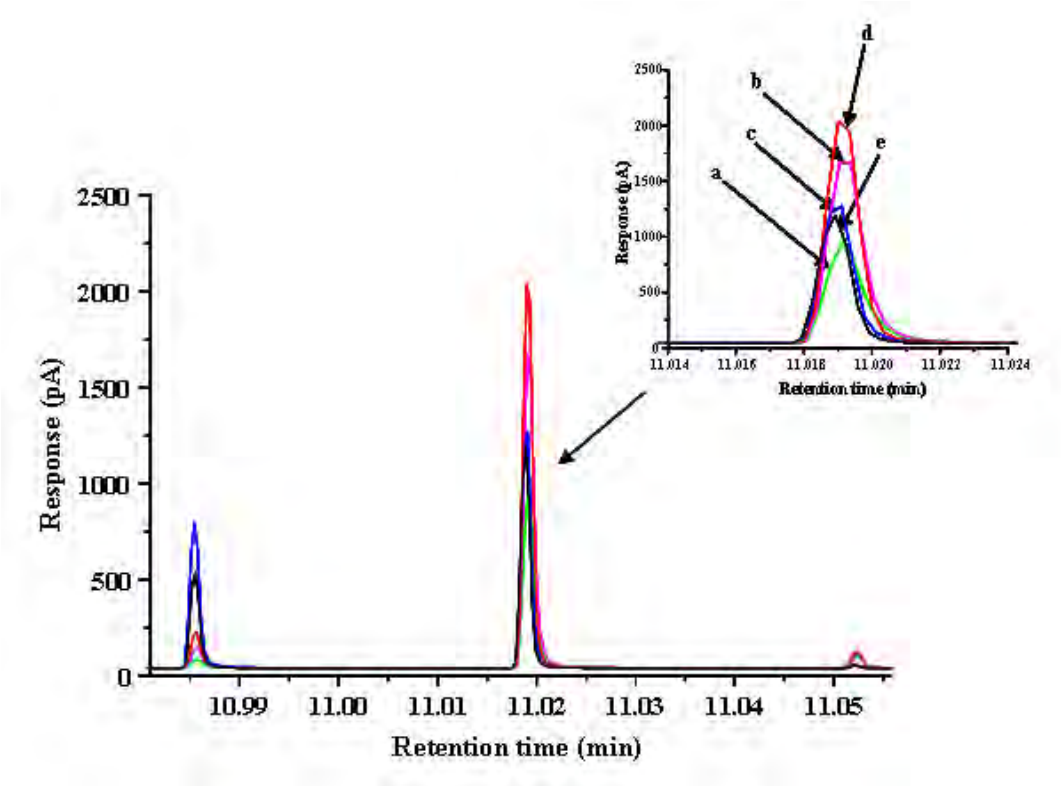

Figure 5.5: Effect of selected conditions of detector gas flows on NPD peak response and peak shape. Conditions of H_2, N_2 and Air: **a)** 3, 5,60; **b)** 1.5, 7, 70; **c)** 1.5, 10, 70; ***d) 1.5, 7, 100***; **e)** 3, 7,100.

5.3.2 GC×GC column sets for fungicide analysis

The temperature program was set such that adequate separation in the first dimension might be achieved with short analysis time. For simplicity, the same program was used for all analyses. Generally, a relatively low elution temperature was desired, so that separation on the ^{2}D column might be maximized. Therefore, the GC oven temperature was started at 50 ^{o}C, ramped at 10 ^{o}C.min^{-1} to 210 ^{o}C, then at 5 ^{o}C.min^{-1} to 260 ^{o}C (held for 5 min), giving a total analysis time of 31.0 minutes. All the compounds eluted during the slow temperature program ramp.

Three column sets with different polarities were tested. **Table 5.1** lists these column sets. Two of the column sets employ more polar phases as ^{1}D and a lower polarity phase as ^{2}D, and the third column set resembles the typical type normally used in GC×GC (lower polarity phase as ^{1}D with higher polarity phase ^{2}D). **Figure 5.6** show results of the analysis of the nine fungicide standard mixture on all column sets. The first column set was not considered efficient for the separation of the fungicides because vinclozolin and metalaxyl peaks co-eluted with most temperature programs tested. The second column set was not considered further for this study because of the lesser separation in the second dimension for the first two components. Column set 3 had a thicker film ^{2}D phase coating, and was considered the best because of the observation of both good peak shape and separation for all compounds. The thicker film ^{2}D phase was observed to reduce the problem of peak tailing that might occur on the thin film second dimension. Note that the fungicides form an apparently correlated series of peaks in almost all cases – ie. they are not widely scattered over the 2D space. Since this occurs in all column sets, it suggests that the fungicides have similar boiling point/polarity relationships. Whilst orthogonality of separation is desirable in GC×GC, this can only arise if there are chemical/physical property differences amongst the compounds to be separated. In the present case, the separation of fungicides *per se* is neither the only, nor the main aim, but rather their separation from a matrix in which they are present. So the 2D peak positions found here are accepted at this point. In **Figure 5.6C**, two peaks **(9A and 9B)** are circled, with a ridge between them. This will be discussed further below.

Figure 5.7 shows 1DGC and GC×GC chromatograms of the fungicide standard mixture. Both methods gave 11 peaks for the nine fungicides, all with good peak shape (peak symmetry ranging from 0.97-1.10 for ^{1}As and 1.12-1.28 for ^{2}As). **Table 5.3** presents the elution order, $^{1}t_R$ and $^{2}t_R$, and A_s values of all standards on column set 3. The baseline rise that is suggested between peaks 9A and peak 9B is clear in the expanded region (**Figure 5.7A'**). The rising baseline was observed more clearly in the GC×GC chromatogram, expanded in **Figure 5.7B'**. The rising plateau starts at peak 9A and terminates at peak 9B, and is indicative of both degradation processes in the injector (giving peak 9A) and on-column degradation during the separation step (giving the baseline rise). The results from mass spectrometric detection (qMS) will be further discussed below.

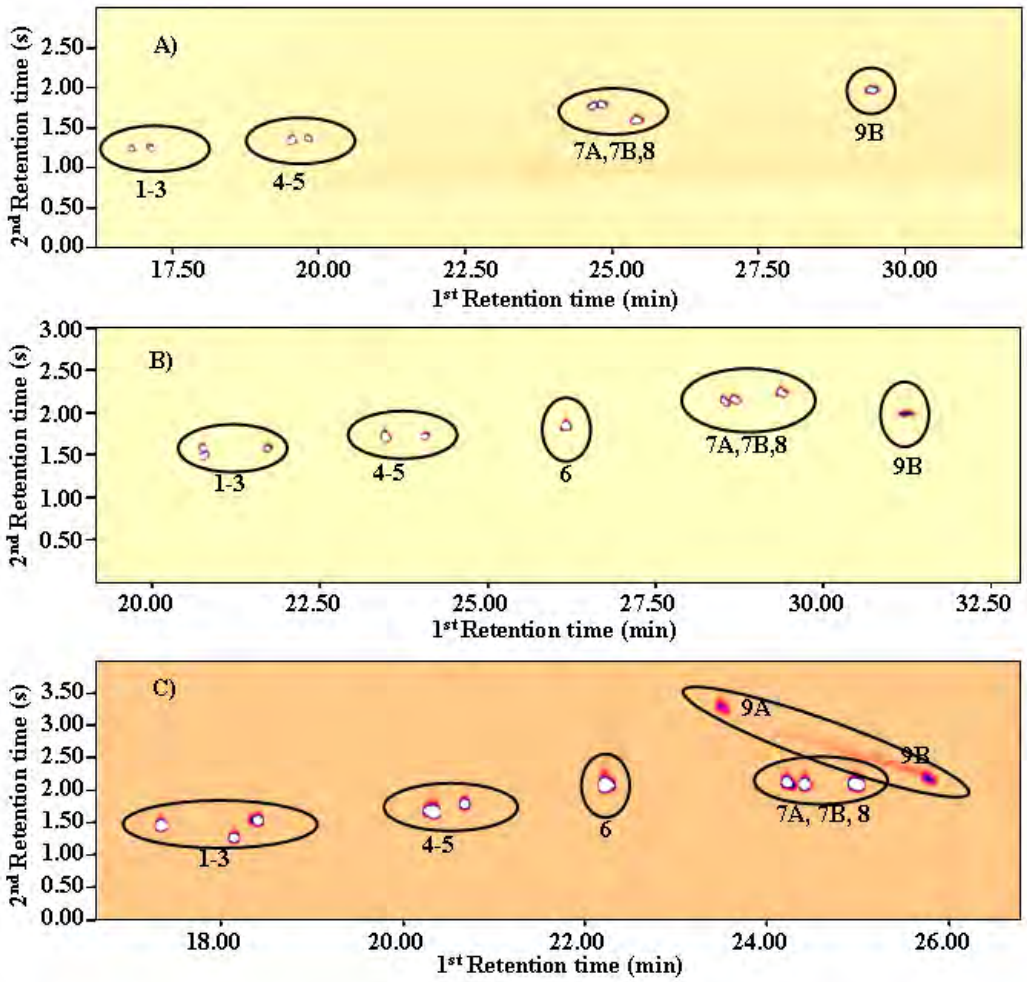

Figure 5.6: GC×GC-NPD contour plots with different column sets listed in **Table 5.1** **A** = column set 1; **B** = set 2; **C** = set 3.

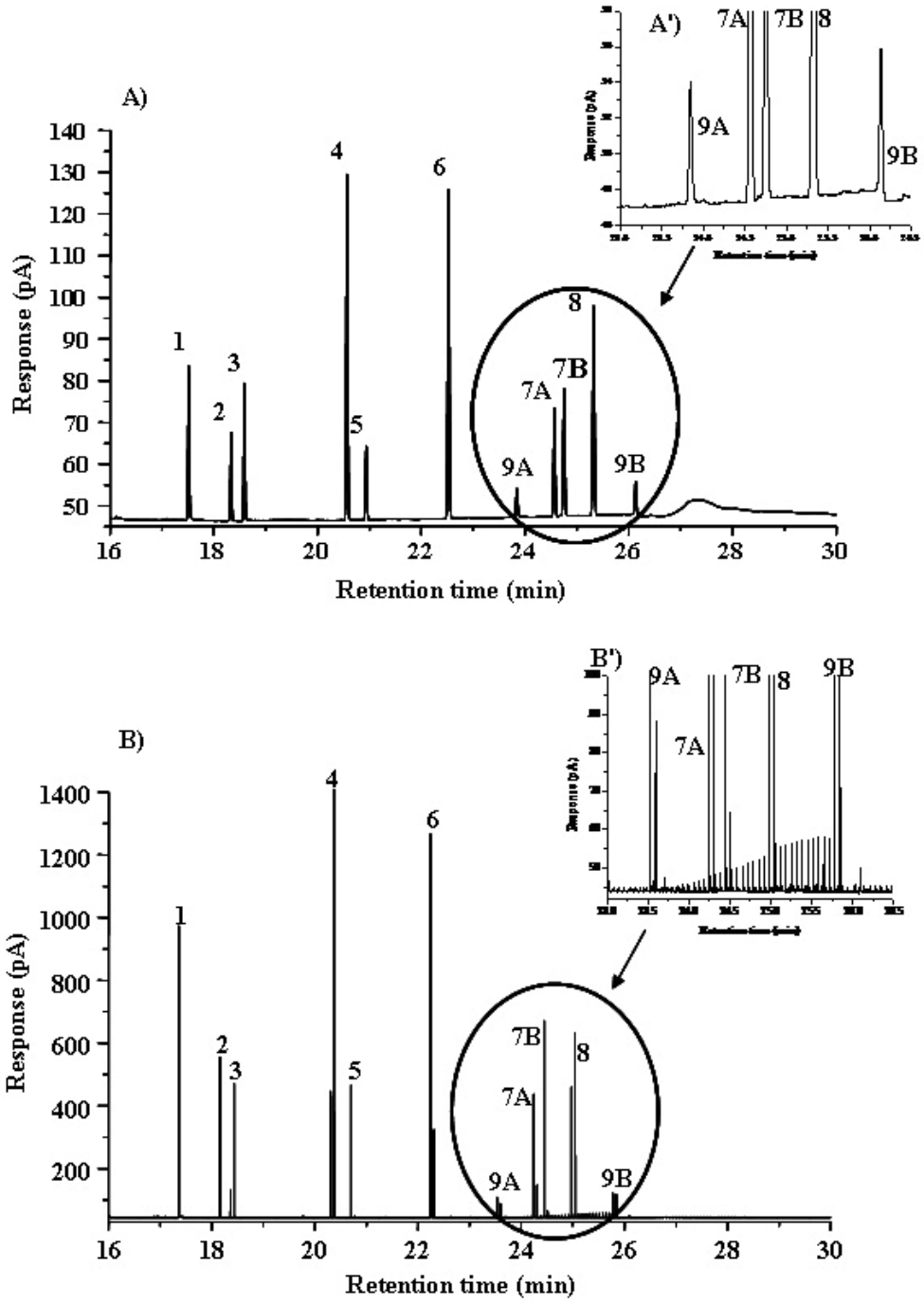

Figure 5.7: Chromatogram of nine fungicide standards with the final detector gas flows and chromatographic condition (**column set 3**). **(A)** normal GC-NPD with **(A')** expanded region of standard fungicides from peak 9A to 9B; **(B)** GC×GC-NPD with **(B')** expanded region of standard fungicides from peak 9A to 9B. Peak labels according to **Figure 5.4** structures.

Table 5.3: Data analysis of GC-NPD and GC×GC-NPD (n=3).

Compounds	^1t_R (min)	^2t_R (s)	GC-NPD				GC×GC-NPD			
			Area (pA*s)	Height (pA)	W_h (s)	^1As	∑Area (pA*s)	∑Height (pA)	W_h^* (ms)	^2As
1. Chlorothalonil	17.52	2.760	68.23	36.83	1.74	1.09	82.47	857.6	92	1.17
2. Vinclozolin	18.34	2.520	38.53	21.50	1.70	1.00	45.83	490.0	90	1.18
3. Metalaxyl	18.59	2.820	60.30	33.00	1.74	1.03	55.93	516.1	101	1.20
4. Penconazole	20.57	2.820	170.30	83.53	1.91	0.98	198.67	1896.9	100	1.19
5. Procymidone	20.94	3.060	37.87	17.70	2.00	0.99	43.57	409.2	100	1.12
6. Myclobutanil	22.53	3.360	180.20	80.53	2.13	0.98	186.30	1556.3	114	1.19
9A. Iprodione decomp. product	23.85	4.440	17.27	6.93	2.32	1.11	16.27	103.6	146	1.20
7A. Propiconazole I	24.57	3.300	60.87	26.07	2.21	1.05	62.63	516.8	115	1.20
7B. Propiconazole II	24.76	3.540	75.20	31.40	2.26	1.00	78.57	654.9	116	1.20
8. Tebuconazole	25.33	3.780	124.93	51.87	2.33	0.99	128.63	1054.0	115	1.22
9B. Iprodione	26.14	3.540	20.33	8.30	2.32	1.00	21.20	163.5	120	1.28

* Peak width at half height of the main pulse peak. Modulation period (P_M) = 4 s was used.

5.3.3 Identification and on-column degradation of fungicides

The cause of baseline rise from peak 9A to peak 9B is most likely due to on-column degradation of the fungicide (peak 9B, iprodione). The compound (9B) and the decomposition product (9A) are NPD detector sensitive species, so both contain nitrogen in their molecules. They also contain halogens, as evidenced by their ECD response (see later). The degradation process may be a thermally initiated process, occurring at high temperature in the injector (which was programmed up to 280 °C) or during the separation process. Since peak 9A appears to be the product of injector degradation, it is a relatively well-shaped, apparently single peak. Also, the long 'tail' extending from peak 9B to peak 9A suggests that peak 9A arises from a process originally from peak 9B. As iprodione (peak 9B) migrates along the column, it progressively experiences a higher column temperature, and so more degradation and higher plateau occurs. Interestingly, column sets 1 and 2 did not exhibit this effect, or at least two separate peaks for 9A and 9B were not produced. If 9B degrades to 9A in the injector, then peak 9A must be present during the subsequent chromatography step. This suggests (surprisingly) that their resolution was not achieved on column sets 1 and 2. With a long residence time in the injector during splitless injection, this will exacerbate the degradation process, and lead to more component 9A being produced.

The results of the MS identification confirmed the elution order of all standard fungicides (**Table 5.3**). **Figure 5.8** shows mass spectra of the fungicides iprodione and propiconazole. Firstly, propiconazole has two chiral centres, hence has two diastereomers which have different chemical-physical properties and may be resolved. These appear in the GC×GC plots as a close pair of peaks. Iprodione was further investigated to confirm the suspected degradation process. Mass spectra of peaks 9A and 9B (**Figure 5.8**) show that iprodione (peak 9B) is the correct iprodione compound, since it has a logical spectrum for this molecule. A small $M^{+\cdot}$ peak cluster at 329 loses 15 u to give the base peak (314 u). Peak clusters at 329, 314, 271, 244 (245), 216 and 187 have the 9:6:1 pattern consistent with 2xCl atoms. The clusters at 244/245 suggest two ion structures occur here, each with an isotope pattern for 2xCl

atoms. Note that the MS library did not have an entry that matched this compound (peak 9B), and gave no acceptable library 'hit'. Proposed iprodione decomposition product (peak 9A), had a highest mass ion in its spectrum of 244 u (for most abundant isotope). Neither ions at 329 nor 314 u were found. Interestingly, this component was well matched by the NIST library as iprodione, although **(i)** it is apparently a degradation product, and **(ii)** it bears no resemblance to the 'logical' iprodione spectrum of peak 9B. This strongly suggests that the NIST entry is not iprodione, but in fact is the degradation product.

The plateau between peaks 9A and 9B gave a series of pulsed peaks in GC×GC analysis mode; all had spectra identical to that of iprodione decomposition product, and were generated as a series of peaks when plotted as an extracted ion chromatogram (mass 244 u). Whilst on-column degradation may potentially be reduced by selection of a different phase and reduced column activity, if the process is purely thermally driven, then some degree of degradation will invariably arise. Injector based degradation can be reduced by using a lower injector temperature, on-column injection, or by using split injection (which reduces residence time in the hot injector, but also is not suited to trace analysis). Lowering the injector from 300 ^{o}C to 200 ^{o}C in 20 ^{o}C steps using the temperature programmed injection method, altered the ratio of the individual peaks for iprodione to iprodione decomposition compound from 0.13, to 0.30, 0.62, 0.88, 1.145, 1.90 and 4.42 (ie much more iprodione was degraded at the lower injector temperature of 200 ^{o}C), but the on-column degradation is still significant. This is not surprising, because as more iprodione is injected at lower injection temperature, the on-column degradation result will also increase in magnitude. In contrast, for isothermal splitless injection, in almost all cases of injector temperature from 280 ^{o}C down to 200 ^{o}C, the iprodione peak was hardly present (i.e. about 3% of the iprodione peak for 200 ^{o}C). Thus almost complete degradation accompanies splitless injection over this injector temperature range.

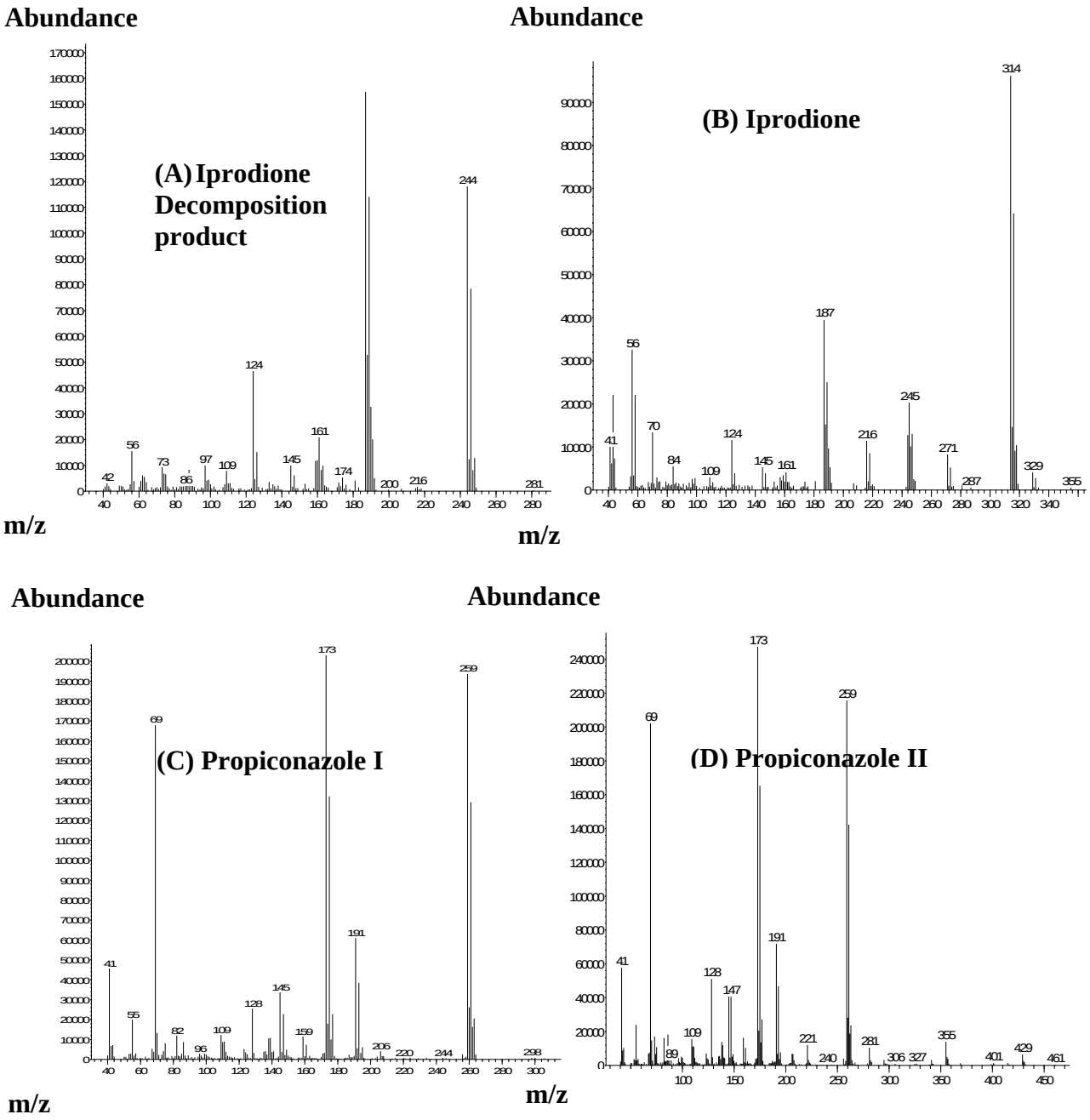

Figure 5.8: Mass spectra of selected fungicides, **(A)** iprodione decomposition product, **(B)** iprodione, **(C)** propiconazole I and **(D)** propiconazole II.

5.3.4 GC-NPD, GC×GC-NPD and validation study

GC-NPD analysis gave good peak symmetry in the range of 0.97-1.10, while GC×GC-NPD generated satisfactory peak shape, with peak symmetry in range the 1.12-1.28 (**Table 5.3**). Not surprisingly, the results show that GC×GC-NPD generated narrow second dimension peaks with a range of widths at half height from 90-120 ms, which were approximately 18-20 times narrower than peaks generated in the conventional GC-NPD analysis method. According to the mass conservation rule of peak area, the summation of peak areas of GC×GC-NPD are close to the peak area for GC-NPD analysis for a given compound. The summation of peak height response from GC×GC-NPD gives approximately 20 times larger height than that of normal GC analysis. The second aim of this section was to validate the developed method in order to apply this method to the quantitative analysis of fungicides in the presence of a real sample matrix.

5.3.4.1 Repeatability and reproducibility

Precision and accuracy of retention time are important for component identification, and thus the repeatability of the GC×GC-NPD analysis must be evaluated. Analysis of selected fungicides namely metalaxyl, procymidone, myclobutanil and iprodione at three concentration levels of 0.1, 0.5 and 1.5 $mg.L^{-1}$ was performed with n = 5 on the same day. **Table 5.4** presents results of repeatability of ^2t_R, peak area, peak height, peak width and peak symmetry at the concentration 0.5 $mg.L^{-1}$. The results show that the percentage RSD of all parameters to be less than 4%. The %RSD of the main pulsed peak of selected standard fungicides between days (3 days) of all parameters is less than 8%.

5.3.4.2 Limit of detection and limit of quantitation

Table 5.5 lists limit of detection and limit of quantitation data which are calculated experimentally as the concentration of component giving a signal equivalent to a signal-to-noise ratio of 3 and 10, respectively. It was found that the limit of detection of selected standard fungicides were in the range 28 to 74 ng.L^{-1}, while the limit of quantitation ranged from 96-246 ng.L^{-1}.

Table 5.4: Validation parameters of GC×GC-NPD developed method for fungicides analysis with concentration at 0.5 mg.L^{-1}.

Parameters	Repeatability (%)[a]				Reproducibility (%)[b]			
	Compounds				Compounds			
	1	2	3	4	1	2	3	4
$^{2}t_R$ (min)*	0.00	0.00	0.00	0.00	0.35	0.38	0.38	0.31
Peak area (pA*s)	2.61	2.11	2.84	2.77	7.13	6.45	6.42	7.60
Peak height (pA)	2.09	3.09	2.73	3.15	7.14	6.50	6.33	7.61
Peak width (ms)	3.15	2.27	0.92	1.28	2.25	1.89	1.59	2.27
Peak symmetry	1.64	2.76	2.42	0.46	2.67	1.33	3.61	2.43

* The second dimension retention time shown is the time of the main pulse peak, when modulation period 4 s was used

[a] (n=5)

[b] measurement taken on 3 different days

Compounds 1 = Metalaxyl, 2 = Procymidone, 3 = Myclobutanil, 4 = Iprodione

5.3.4.3 Calibration curves of standard fungicides

Calibration curves of the four selected fungicides as above were plotted and the linear regression slopes and R^2 values are listed in **Table 5.5**. The concentrations in the range of 1-1000 $\mu g.L^{-1}$ were plotted against the response, for both total peak area and peak height. The results show that the GC×GC-NPD method for fungicides analysis produced linear calibration curves for both total peak area and peak height. R^2 values were found to be > 0.995 except for iprodione which was observed to undergo on-column degradation so its lower value of R^2 is not unexpected. From the slope of the calibration equation, myclobutanil is the most sensitively detected fungicide in the NPD detector and iprodione gave the lowest sensitivity. **Figure 5.9** illustrates the calibration curves of the selected fungicides, for both peak area and peak height. The slope of myclobutanil is about 4x that of metalaxyl and procymidone, and this agrees with there being 4xN, 1xN and 1xN in each of these compounds respectively. Whilst iprodione has 3xN atoms, the recorded area in the single peak of iprodione does not represent the total expected area, due to the decomposition process, and so the single peak does not account for the area lost due to degradation, either in the injector or on-column. Hence the iprodione calibration curve has the lowest response (slope).

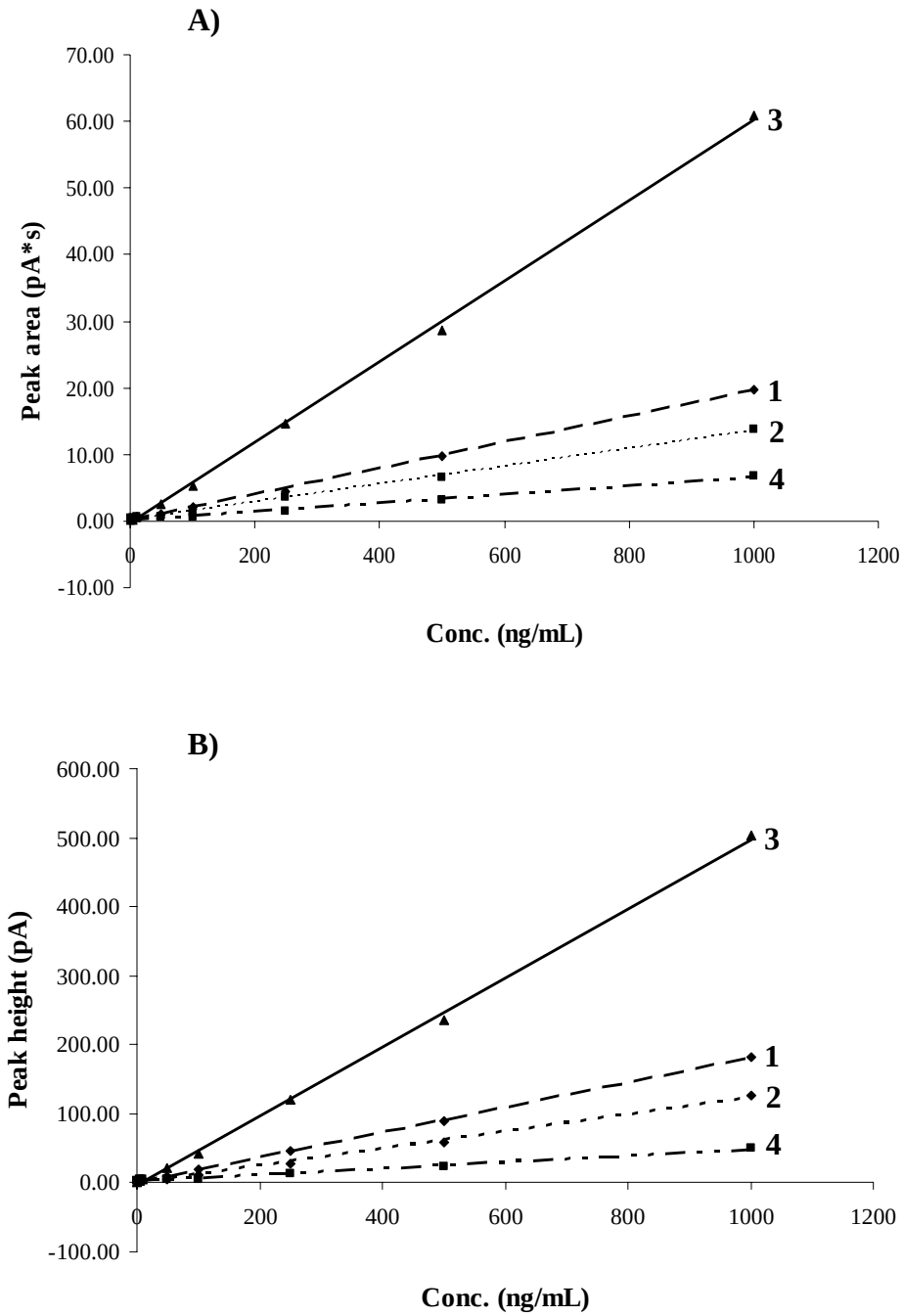

Figure 5.9: Calibration curves of selected fungicide standards using conditions as in Figure 5.7. **(A)** summed peak area (pA.s); **(B)** summed peak height (pA). **1** = metalaxyl (1×N), **2** = procymidone (1×N), **3** = myclobutanil (4×N), **4** = iprodione (3×N).

Table 5.5: Equations of peak area and peak height, R^2, LOD and LOQ of selected fungicide standards.

Comp	Conc. (μgL^{-1})	LOD[a] ($ng.L^{-1}$)	LOQ[a] ($ng.L^{-1}$)	Equation (Peak area)	R^2	Equation (Peak height)	R^2
1	1-1000	41.4000	138.0100	y = 0.019x+0.16	0.9986	y = 0.18x+1.21	0.9996
2	1-1000	73.8300	246.0900	y = 0.013x+0.15	0.9978	y = 0.12x+0.61	0.9952
3	1-1000	28.8400	96.1500	y = 0.061x-0.40	0.9990	y = 0.49x-3.41	0.9989
4	1-1000	70.9600	236.5400	y = 0.0063x+0.18	0.9932	y = 0.046x+2.51	0.9902

[a] (n=5)

y = peak area or peak height in pA.s and pA, respectively

x = concentration in $\mu g.L^{-1}$

Compounds 1 = Metalaxyl, 2 = Procymidone, 3 = Myclobutanil, 4 = Iprodione

5.3.5 Application of GC×GC-NPD in vegetable samples

The method described here was applied to the analysis of fungicides in an extract of vegetable (Brussel sprouts) samples. The purpose of the application is to gauge the effectiveness of separation of the fungicides from the matrix of the vegetable extract. **Figure 5.10** shows 1D chromatograms of standard fungicides, the blank extract, and the blank extract spiked with standard fungicides, respectively. Whilst with careful comparison, the fungicide peaks can be approximately located within the matrix background, there are many peak overlaps and the NPD analysis will be inadequately selective (in separation and detection terms) to give precise quantitation. **Figure 5.11** presents color GC×GC plots of standard fungicides, blank extract, blank extract spiked with standard iprodione and blank extract spiked with standard fungicides mixture. The results now illustrate that the fungicides are well resolved from the background matrix components. Moreover, the degradation process of iprodione is clearly shown linking peak 9A to peak 9B. Peaks are labeled in **Figure 5.11 panels**, and overlapping components that occur in ^{1}D are seen by vertically related peaks. A similar study of GC×GC-μECD is shown in **Figure 5.12**. One of the fungicides (metalaxyl) is non-halogenated, so no peak is seen for that compound. The μECD exhibits fewer peaks for the matrix, but still some significant peak overlaps can be predicted for a similar 1D sample analysis. Both NPD and μECD provide good selective detection of the respective fungicides. The μECD gives slightly broader peaks (for the same conditions) than the NPD due to the larger residence time of solute in the detector cell active volume, which has been observed in other studies of organochlorine compound analysis using GC×GC-μECD. Relative sensitivity of detection is better for μECD than for NPD.

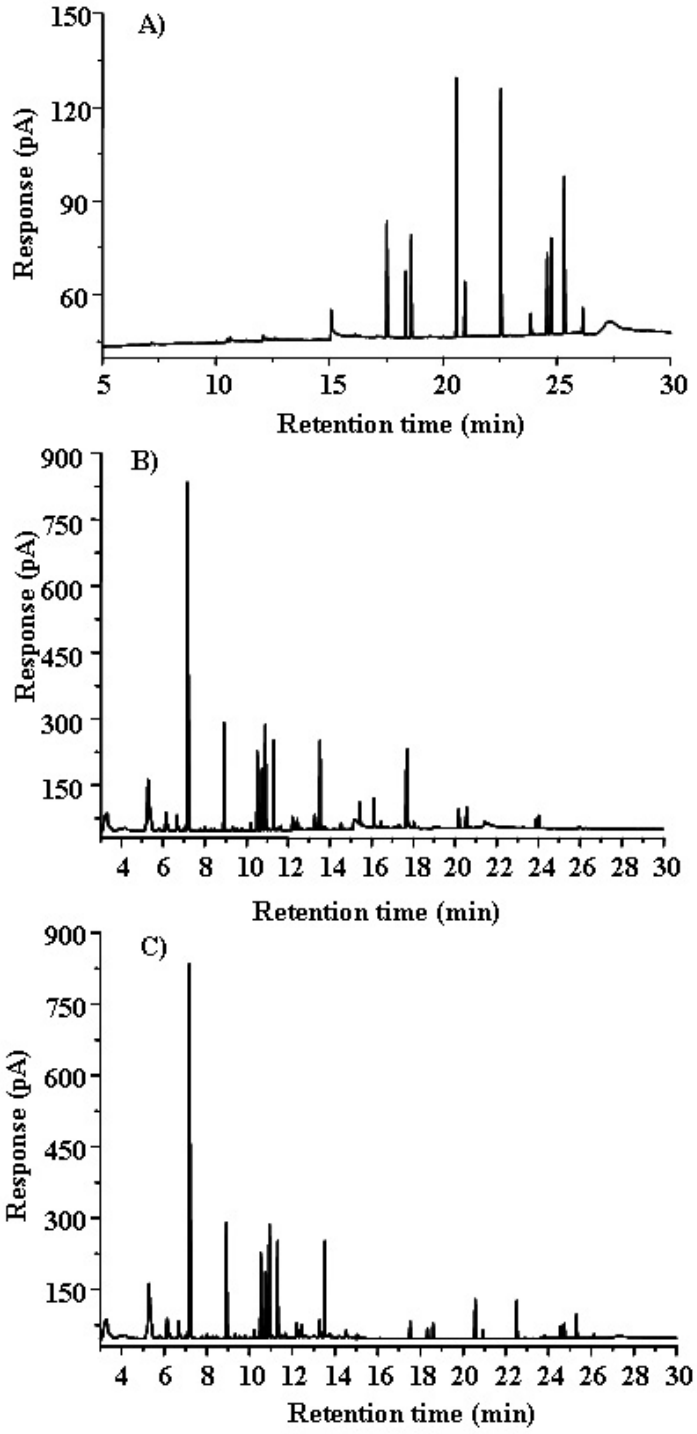

Figure 5.10: Chromatograms of single dimension GC-NPD using conditions as in Figure 5.7. **(A)** nine standard fungicides; **(B)** blank vegetable extract; **(C)** blank vegetable extract spiked with nine standard fungicides.

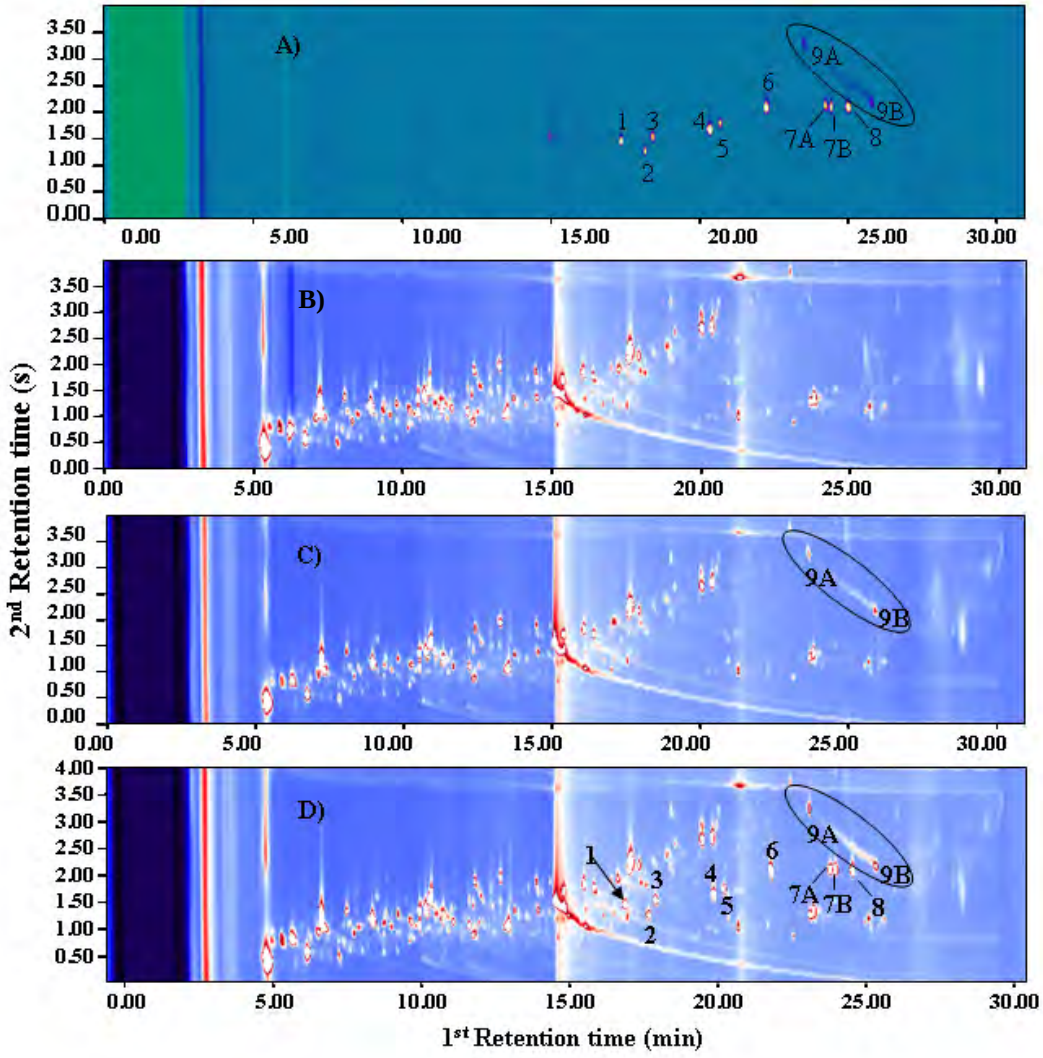

Figure 5.11: Contour plots of GC×GC-NPD using conditions as in **Figure 5.7**. **(A)** fungicide standard mixture; **(B)** blank vegetable extract; **(C)** blank vegetable extract spiked with iprodione standard; **(D)** blank vegetable extract spiked with standard fungicide mixture. Circled region shows iprodione and iprodione decomposition product peaks.

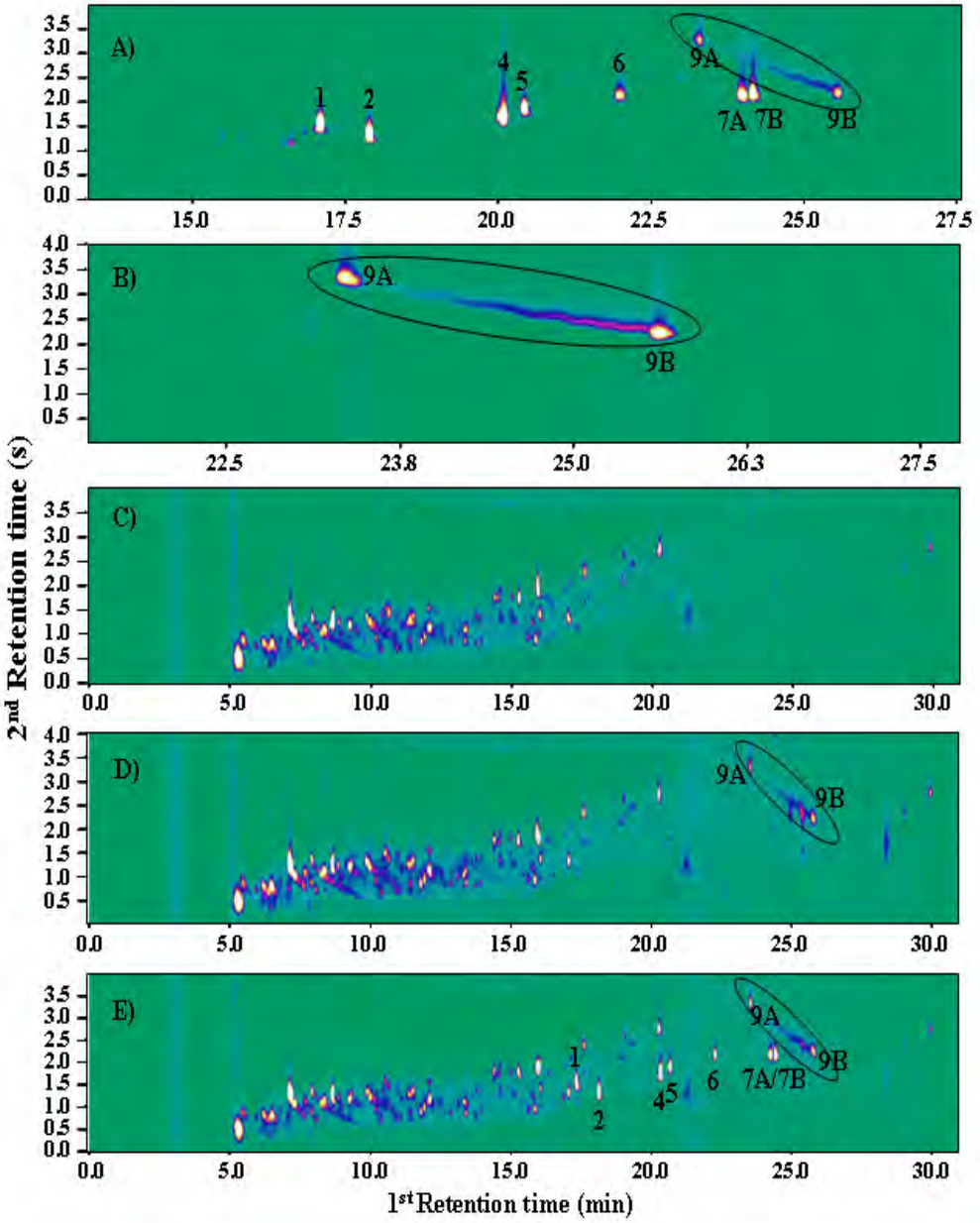

Figure 5.12: Contour plots of GC×GC-μECD using conditions as in **Figure 5.7**. **(A)** fungicide standard mixture; **(B)** standard iprodione; **(C)** blank vegetable extract; **(D)** blank vegetable extract spiked with iprodione individual standard; **(E)** blank vegetable extract spiked with standard fungicide mixture. Circled region shows iprodione and iprodione decomposition product peaks.

5.4 Conclusion

This study has demonstrated that the developed method for the determination of nitrogen-containing fungicides by using GC×GC-NPD was successful. The optimal condition of NPD detector gas flows gives good response and generally excellent peak shape for all fungicides. The non-polar/polar column set used in GC×GC, with the thicker film phase in the ^{2}D column gives symmetric, non-tailing peaks in GC×GC analysis with the NPD detector. Moreover, the capability of GC×GC-NPD to quantitatively resolve the nine fungicide standard mixture from the background matrix of a vegetable extract is illustrated. The repeatability and reproducibility of GC×GC-NPD for the nine fungicides standard allows for the confident identification of the compounds between runs, based on their peak position. Degradation of one fungicide (iprodione) was readily observed by the characteristic band response in the 2D plot, between the parent and the decomposition product. MS analysis suggests that the decomposition product is incorrectly identified by the MS library matching method as iprodione. This study shows that GC×GC-NPD has a potential for the routine analysis of fungicides in food and vegetables sample, providing a low LOD and LOQ and a good repeatability and reproducibility of peak response.

In this work, separate NPD and ECD responses were recorded. There appear to be valid reasons for use of each detector; however, considerable time-efficiency can arise if a dual detection (simultaneous) arrangement can be constructed. This development will be detailed in the next chapter.

References

[1] M.S. Klee, M.D. Williams, I. Chang, J. Murphy, J. High Resolut. Chromatogr. 22 (1999) 24.

[2] P. Korytar, P.E.G. Leonards, J. de Boer, U.A.T. Brinkman, J. Chromatogr. A 958 (2002) 203.

[3] P. Korytar, L.L.P. van Stee, P.E.G. Leonards, J. de Boer, U.A.T. Brinkman, J. Chromatogr. A 994 (2003) 179.

[4] E.M. Kristenson, P. Korytar, C. Danielsson, M. Kallio, M. Brandt, J. Makela, R.J.J. Vreuls, J. Beens, U.A.T. Brinkman, J. Chromatogr. A 1019 (2003) 65.

[5] P. Korytar, C. Danielsson, P.E.G. Leonards, P. Haglund, J. de Boer, U.A.T. Brinkman, J. Chromatogr. A 1038 (2004) 189.

[6] J. Aybar-Munoz, E. Fernandez-Gonzalez, L.E. Garcia-Ayuso, A. Gonzalez-Casado, L. Cuadros-Rodriguez, Chromatographia 61 (2005) 505.

[7] L.R. Bordajandi, L. Ramos, M.J. Gonzalez, J. Chromatogr. A 1078 (2005) 128.

[8] C. Danielsson, K. Wiberg, P. Korytar, S. Bergek, U.A.T. Brinkman, P. Haglund, J. Chromatogr. A 1086 (2005) 61.

[9] D. Ryan, P. Marriott, J. Sep. Sci. 29 (2006) 2375.

[10] C. von Muhlen, E.C. de Oliveira, P.D. Morrison, C.A. Zini, E.B. Caramao, P.J. Marriott, J. Sep. Sci. 30 (2007) 3223.

[11] L.L.P. van Stee, J. Beens, R.J.J. Vreuls, U.A.T. Brinkman, J. Chromatogr. A 1019 (2003) 89.

[12] F.C.-Y. Wang, W.K. Robbins, M.A. Greaney, J. Sep. Sci. 27 (2004) 468.

[13] J. Blomberg, T. Riemersma, M. van Zuijlen, H. Chaabani, J. Chromatogr. A 1050 (2004) 77.

[14] R. Hua, Y. Li, W. Liu, J. Zheng, H. Wei, J. Wang, X. Lu, H. Kong, G. Xu, J. Chromatogr. A 1019 (2003) 101.

[15] R. Hua, J. Wang, H. Kong, J. Liu, X. Lu, G. Xu, J. Sep. Sci. 27 (2004) 691.

[16] J. Dalluge, M. van Rijn, J. Beens, R.J.J. Vreuls, U.A.Th. Brinkman, J. Chromatogr. A 965 (2002) 207.

[17] J.-F. Focant, A. Sjodin, D.G.Jr. Patterson, Organohalogen Cpds. 60 (2003) 391.

[18] J.-F. Focant, E.J. Reiner, K. MacPherson, T. Kolic, A. Sjodin, D.G. Patterson, S.L. Reese, F.L. Dorman, J. Cochran, Talanta 63 (2004) 1231.

[19] P. Korytar, J. Parera, P. E. G. Leonards, J. de Boer, U.A.Th. Brinkman, J. Chromatogr. A 1067 (2005) 255.

[20] J. Zrostlikova, J. Hajslova, T. Cajka, J. Chromatogr. A 1019 (2003) 173.

[21] M. Navarro, Y. Pico, R. Marin, J. Manes, J. Chromatogr. A 968 (2002) 201.

[22] H.-J. Pan, W.-H. Ho, Anal. Chim. Acta 527 (2004) 61.

[23] A. Stensvand, A. Christiansen, J. Agric. Food Chem. 48 (2000) 917.

[24] M. Tsuji, N. Yoshioka, Y. Akiyama, Hyogo-kenritsu Eisei Kenkyusho Nenpo 32 (1997) 140.

[25] P.L. Patterson, J. Chromatogr. Sci. 24 (1986) 41.

[26] H. Snijders, H.-G. Janssen, C. Cramers, J. Chromatogr. A 732 (1996) 51.

[27] L. Corporation, LECO Separation Science Application Note 1.

[28] O. Belafdal, M. Bergon, J.P. Calmon, Pestic Sci. 17 (1986) 335.

[29] J. Gomez, C. Bruneau, N. Soyer, A. Brault, J. Agric. Food Chem. 30 (1982) 180.

Chapter

6

DUAL DETECTION IN COMPREHENSIVE TWO-DIMENSIONAL GAS CHROMATOGRAPHY FOR MULTI-CLASS PESTICIDE ANALYSIS (GC×GC-NPD/ECD)

This chapter has been published as, "Dual NPD/ECD Detection in Comprehensive Two-Dimensional Gas Chromatography for Multi-class Pesticide Analysis". Khummueng W., Morrison P., and Marriott P.J., J. Sep. Sci., 31(19), 3404 – 3415 (2008).

Abstract

Comprehensive two-dimensional gas chromatography (GC×GC) coupled to nitrogen-phosphorus (NPD) and electron capture (ECD) detectors has been developed as a dual detection system for multi-class pesticide analysis in vegetable sample matrices, representing a broad range of compounds with different physical and chemical properties including; 17 organochlorine pesticides (OCs), 15 organophosphorus insecticides (OPs) and 9 N-containing fungicides. The second dimension column was connected to the parallel detectors via a microfluidic-splitting valve, with an equal split ratio. The approach focuses on the selective detection of extracts of vegetable samples, to provide increased information content through simultaneous detection. Two simultaneous GC×GC plots are visualized from the dual detection system and the profiles of pure standard multi-class pesticides and spiked vegetable sample extracts demonstrated adequate separation of all pesticide standards from each other, and from the sample matrix. The efficiency of NPD and ECD modes were investigated and compared; the ECD produced broader peaks and even though high internal flows were required, the response in the ECD was still greater as measured by S/N ratio. The analytical performance of the dual detection approach, such as repeatability and reproducibility of selected pesticides were determined for further quantitative evaluation. The relative ratio of the ECD:NPD response is proposed to offer additional specificity, in addition to the $^{1}t_{R}$ and $^{2}t_{R}$ retention coordinates for identification of individual pesticides, with ratios varying from 19 to over 1000 for selected organchlorine pesticides. Results show that relative standard deviation (RSD) of the intra-day (n=5) and inter-day (3 days) measurement of the selected pesticides are less than 2.5% and 10%, respectively.

6.1 Introduction

Contamination by pesticides in the environment continues to be of concern due to their persistence and potential toxicity to human health. Persistent pesticides may be still detected in a variety of environmental compartments – sediment, soil, water, atmospheric sinks – even after their use has been restricted, and pesticide residues must be monitored in agricultural products. Pesticides are usually distributed throughout the environment in trace level, and in the presence of a high background concentration of interferences. Therefore, determination of pesticides in environmental samples is a challenge, but is of importance where (bio) accumulation may amplify such pesticides in biota. Analytical techniques used for determination of volatile pesticide residues in environmental samples are centred on gas chromatography (GC) mostly with use of a specific detector. Basically, in pesticide residue analysis specific detectors such as electron capture detection (ECD) [1-3], nitrogen-phosphorous detection (NPD) [4-7], flame photometric detection (FPD) [8], pulsed flame photometric detection (PFPD) [9] and mass spectrometry (MS) [10-12] have been used as detectors of choice. Both single and dual detection systems have been employed in a wide range of samples, due to two responses obtained in every single run. Several combinations of specific detectors including MS have been reported for this analysis, for example GC-ECD/FPD dual system for OPs and OCs pesticides analysis in medicinal plants [13], and GC-NPD/MS was performed as a new tool for forensic analyses [14]. However, GC-ECD/NPD detection is a system that has been used as a preferred configuration for all types of residue analysis [15]. In 1997 Oh-shin et al. reported a simultaneous detection and quantification method using GC-ECD/NPD for insecticides including carbaryl in drinking water [16,17]. Low LOD in the range 0.1 $ng.ml^{-1}$, and excellent linearity with R^2 = 0.998 to 1.000 were demonstrated. Sensitivity, reproducibility and simplicity demonstrated the potential of the method for the routine pesticides analysis in drinking water. Dubey and coworkers [17] determined ethylenethiourea (ETU) in food commodities by using GC-ECD/NPD system. In his study, GC-MS was used for the correctness of qualitative and quantitative results. The method was successfully applied for pesticides analysis

in fresh fruits and vegetables with recoveries of 82-92% and LOD of the technique less than 1 ng.mL^{-1}. They also found that the response ratios of both detectors for the selective derivatized ETU provide reliability for identification of the target pesticide. Thus, the further confirmation of compounds using GC-MS is often not necessary. Principally, the response ratio of compounds from two independent detectors can be used as a tool for compound identification. The ratio value used for compound identification can be calculated from response of the detector in a dual system, the so called Detector Response-Ratio (DRR) [18,19]. In 2007, Jover et al. [20] presented a modified model of Detector Response-Ratio (DRR) for a GC-ECD/NPD dual system. In his work, the DRR was redefined, slightly differently from that previous defined, as shown in **Equation (1)**.

$$DRR_x = \frac{A_{xd1}/A_{ISd1}}{A_{xd2}/A_{ISd2}} \quad (1)$$

When DRR_x is the DRR for the target analyte *x*, A_{xd1} and A_{xd2} are the peak areas obtained for *x* by use of detectors 1 and 2, and A_{ISd1} and A_{ISd2} are the peak areas obtained for the internal standard by use of detectors 1 and 2. Due to the detector response depending on the analyte concentration, therefore DRR can be considered as a function of analyte concentration. When the linearity of calibration was constructed, two calibration curves were obtained and can be expressed as in **Equation (2) and (3)**

with detector 1: $$\frac{A_{xd1}}{A_{ISd1}} = a_1 \frac{C_x}{C_{IS}} + b_1 \quad (2)$$

with detector 2: $$\frac{A_{xd2}}{A_{ISd2}} = a_2 \frac{C_x}{C_{IS}} + b_2 \quad (3)$$

Where a_1 and b_1 are the slope and ordinate of the calibration plot for detector 1, respectively a_2 and b_2 are the slope and ordinate of the calibration plot for detector 2, respectively and C_x is the concentration of analyte x. To express **Equation (1)** as a function of analyte concentration, the re-arrangement of **Equation (1)** shown in **Equation (4)** is generated.

$$DRR_x = \frac{a_1 \frac{C_x}{C_{IS}} + b_1}{a_2 \frac{C_x}{C_{IS}} + b_2} \quad (4)$$

To confirm compound identity, the experimental DRR ($DRR_{x\text{-}exp}$) for the sample will be compared with the DRR_x obtained by replacing C_x by the value of $C_{x\text{-}exp}$ calculated from results of the most sensitive detector. If $DRR_{x\text{-}exp}$ was not significantly different from DRR_x (RSD compared), thus the compound is confirmed. The utilization of DRR model in GC-ECD/NPD has been shown as an efficient method for the analysis of several classes of pesticides. However, the drawback of this technique is the possibility of false negative results due to chromatographic co-elution. The co-elution of compounds with others, or with interferences, will change the $DRR_{x\text{-}exp}$ from the $DRR_{x.}$ value. Clearly, the limitations of conventional GC, especially, lack of separation power (resolution) which is required for the separation of analytes from each other and from the sample matrix, has been shown as a difficulty arising in 1D-GC dual detection. To overcome this limitation, techniques that can provide higher separation power, selectivity and sensitivity should be applied to this task. Introduced in the early 1990s [21], comprehensive two-dimensional gas chromatography (GC×GC) has become a powerful technique for the analysis of complex samples such as petroleum products [22,23], food flavour [24,25], perfume and fragrances [26,27]. The primary characteristics of GC×GC – its high separation capacity and improvement in analyte detectability – address limitations of conventional GC [28]. The principles and implementation of this new generation of GC have been reviewed [29-31]. Flame ionisation detection (FID) is commonly employed due to its high data acquisition rate and preservation of column efficiency, whilst MS is an information rich detector for GC×GC for the analysis of complex samples. However, routine determination of environmental pollutants may demand use of highly selective and sensitive detectors. Recently, attention has been given to coupling of specific detectors such as ECD, NPD, atomic emission detector (AED), and both nitrogen and sulfur chemiluminescence detectors (NCD and SCD) with GC×GC for analysis of heteroatomic species in industrial and environmental samples.

The ECD is the more popular specific detector for GC×GC in environmental analysis primarily due to the continuing interest in organochlorine (OC) and polychlorinated biphenyl (PCB) analyses. Several research studies have reported the principles and applications of GC×GC-ECD for the analysis of halogenated compounds [32-35]. The general observation that the internal volume of the ECD causes some detector-based band broadening combined with a relatively low maximum detector acquisition rate (e.g. 50 Hz) compromises this detector's performance for GC×GC operation. The NPD has recently received attention in hyphenation with GC×GC, due to its selectivity towards both N- and P-containing compounds, and favourable features that are compatible with GC×GC have been reported [36,37]. The NPD detector geometry which was investigated by von Mühlen and colleagues [38] will be used throughout this study. Recently, Ochiai and co-workers [39] reported characterization of nanoparticles in roadside atmospheres using GC×GC-HRTOF-MS, and simultaneous detection of GC×GC coupled with NPD and quadrupole MS for thermal desorption introduction. Results showed that the NPD contour plot can serve as a marker of 15 nitrogen and/or phosphorus containing compounds complemented by information from a NIST MS library search. The common use of dual ECD/NPD screening methods for analysis of pesticide residues in food and vegetable samples in 1D-GC makes it appropriate to investigate the role of dual detection in GC×GC. High informational content and different relative sensitivities of the two different data sets within a single run are advantages derived from this detector combination. Performance and characteristics of this method such as repeatability and reproducibility were determined. To demonstrate the potential of the method as a screening technique for pesticide residues analysis, the analysis of spiked pesticides in vegetable extracts (tomato and spinach) were performed. The DRR couple has not been previously used for dual-detection ECD:NPD in GC×GC, and will be evaluated here to gauge its use for increasing the information context of GC×GC for trace residue analysis.

6.2 Experimental

6.2.1 GC×GC system

An Agilent model 6890 Gas Chromatograph (Agilent Technologies, Burwood, Australia) was used throughout this study. Injection was facilitated by a CombiPAL Focus system (CTC Analytics AG, Zwingen, Switzerland), which was serially connected to an Optic 3 high performance injector (ATAS GL International, Veldhoven, The Netherlands). In order to conduct GC×GC analysis, the Agilent 6890 GC was retrofitted with a Longitudinal Modulated Cryogenic System (LMCS) modulator from Chromatography Concepts (Doncaster, Australia). ChemStation software (Agilent) was used to instruct the electronic modulator control to commence modulation at a predefined time. The CombiPAL Focus system and Optic 3 injector were controlled using Cycle Composure version 1.5.2 and ATAS Evolution Workstation version 1.4 software, respectively.

6.2.2 Column sets

Following an initial study employing a standard 30 m ^{1}D and 1 m ^{2}D column, a combination of relatively shorter columns was used for all subsequent studies, and comprised a ^{1}D column of 18 m x 0.25 mm i.d., 0.25 μm d_f BPX5 phase (5% phenyl polysilphenylene siloxane) column, coupled to a ^{2}D column of 0.75 m x 0.15 mm i.d., 0.15 μm d_f BPX50 (50% phenyl polysilphenylene siloxane) phase, both from SGE International, Ringwood, Australia. An Agilent Technologies microfluidic splitting valve was connected to the outflow of the ^{2}D column, allowing the flow to be equally split to the two detectors via short transfer capillary lines each comprising 0.15 m x 0.10 mm i.d. deactivated fused silica tubing.

6.2.3 Chromatographic conditions

The injection method was performed in splitless mode using the Optic 3 injector; the temperature was ramped from 50 ^{o}C to 280 ^{o}C at 16 ^{o}C.s^{-1}, with a transfer time of 1 min and at a column flow rate at 0.7 mL.min^{-1}. Two GC oven temperature programs were used. The first was used for the study of system characteristics; the initial temperature was held at 50 ^{o}C for 1.0 min, ramped at 30 ^{o}C.min^{-1} to 150 ^{o}C and then ramped at 8 ^{o}C.min^{-1} to 250 ^{o}C (held for 5 min). The second was chosen as the analytical temperature program for improved analysis of multi-class pesticide standards; the initial temperature was held at 50 ^{o}C for 1.0 min, ramped at 25 ^{o}C.min^{-1} to 130 ^{o}C, then at 3 ^{o}C.min^{-1} to 240 ^{o}C then 8 ^{o}C.min^{-1} to 280 ^{o}C (held for 10 min). The modulator temperature was set at -15 ^{o}C with the modulation period (P_M) at 4 and 6 s for the first and second temperature programs, respectively. In some cases, P_M ranging from 2-5 s were tested to check for wrap-around. Dual detection was performed by using NPD and ECD detectors (Agilent Technologies). The NPD detector was operated at 320 ^{o}C with detector gas flows at 1.5, 100 and 10 mL.min^{-1} for H_2, air and N_2 make-up gas, respectively. A Blos bead, which is made of a heat and moisture resistant glass material, was used as the NPD detector bead. An extended jet and wide collector electrode were employed. A bead adjust offset of 30 pA and data acquisition rate at 100 Hz were used. The ECD detector was operated at 320 ^{o}C with N_2 make-up gas flow at 100 mL.min^{-1}. The maximum data acquisition rate of the ECD (50 Hz) was used throughout this study.

6.2.4 Analytical characteristics of the dual detection system

Selected pesticides vinclozolin, procymidone and propiconazole II were used for the study of analytical characteristics of the GC×GC-NPD/ECD system such as repeatability and reproducibility. Five injections of the same concentration of compounds were performed for the repeatability study. The injections of the same concentration of compounds over three days for the reproducibility study were carried out. Dieldrin, DDT and chlorpyrifos were used for the study of linearity of the

calibration curve, and limit of detection (LOD) of GC×GC-NPD/ECD system. The insecticide (OPs) was used as an internal standard. Five point calibration curves with internal standard were prepared over the concentration range of 0.001 to 1.0 $\mu g.L^{-1}$. Three replicates of each concentration were performed.

6.2.5 Data analysis

The GC×GC data were transformed using an in-house program and visualized as colour and/or contour plots using Transform software (Fortner Research, Virginia, USA). For data analysis, total peak area, peak height and peak width at half height were generated using ChemStation software (Agilent Technologies).

6.2.6 Standard pesticides

Selections from forty-one pesticides standard were used as the study mixture and are indicated in text and figure captions. The available standards comprised 17 OC pesticide standards from Ultra Scientific (Kingston, RI, USA; part numbers M8080), 15 OP insecticides, and 9 N-containing fungicides (provided by Primary Industries Research Victoria, Werribee, Australia). All stock solutions were diluted with pesticide grade hexane as required (compound names based on the elution order and CAS numbers are shown in **Table 6.1**).

Table 6.1: List of compound names based on elution order and CAS number of pesticide standards used in this study.

#	Compounds	CAS#	#	Compounds	CAS#
1	Dichlorvos	62-73-7	23	p,p'-DDE	72-55-9
2	Mevinphos	58-89-9	24	Penconazole	66246-88-6
3	α-BHC	7786-34-7	25	Procymidone	32809-16-8
4	Diazinon	319-84-6	26	Dieldrin	60-57-1
5	β-BHC	319-85-7	27	Endrin	72-20-8
6	γ-BHC	333415	28	Myclobutanil	88671-89-0
7	Dimethoate	1897-45-6	29	Endosulfan II	33213-65-9
8	Chlorothalonyl	319-86-8	30	p,p,-DDD	72-54-8
9	Heptachlor	76-44-8	31	Endrin aldehyde	7421-93-4
10	δ-BHC	60515	32	Parathion-ethyl	56-38-2
11	Aldrin	309-00-2	33	Endosulfan sulfate	1031-07-8
12	Heptachlor epoxide	1024-57-3	34	Iprodione degradation product	36734-19-7
13	Vinclozolin	50471-44-8	35	p,p' DDT	50-29-3
14	Chlorpyrifos-methyl	5598-13-0	36	Propiconazole I	60207-90-1
15	Parathion-methyl	298-00-0	37	Propiconazole II	60207-90-1
16	Metalaxyl	69516-34-3	38	Tebuconazole	57837-19-1
17	Fenchlorphos	299-84-3	39	Iprodione	36734-19-7
18	Endosulfan I	959-98-8	40	Methoxychlor	72-43-5
19	Fenitrothion	122145	41	Ethion	563-12-2
20	Malathion	121-75-5	42	Azinphos-methyl	86-50-0
21	Chlorpyrifos	2921882	43	Azinphos-ethyl	2642-71-9
22	Fenthion	55-38-9			

6.2.7 Sample preparation

A portion (50 g) of homogenized sample was weighed into a blender jar, with 150 mL of acetone, and blended for 5 min. The acetone extract was filtered, and transferred to a 1 L separation funnel with 650 mL of 4% Na_2SO_4 solution added. The aqueous solution was extracted by shaking with 1 x 100 mL then 2 x 50 mL portions of dichloromethane. The combined dichloromethane extracts were passed through a Na_2SO_4 drying column into a 500 mL round bottom flask. The extract was then concentrated under vacuum on a boiling water bath, with inversion into hexane, to a final volume of 10 mL. Appropriate dilution was made using pesticide grade hexane as necessary. The final extract was spiked with the multi-class pesticides standard at a level of 1.00 $mg.L^{-1}$ [40].

6.3 Results and discussion

6.3.1 GC×GC–dual detection (GC×GC- NPD/ECD) instrumental set up and feature

The challenge of pesticide residues analysis in environmental samples is to both separate individual pesticides from each other, and to separate pesticides from matrix components, at sufficiently low concentrations. Therefore, a system which offers a high selectivity, sensitivity and separation power should be sought. In this study, selective and sensitive NPD and ECD detectors were used for dual detection in GC×GC for pesticide residues analysis. **Figure 6.1** shows a diagram of the developed system. A ^{1}D column set of relatively reduced length was employed in order to lower the elution temperature (T_e) and analysis time, which required optimisation of the $^{2}t_R$ values for pesticides in the second dimension separation. The column set chosen in this system consisted of an 18 m x 0.25 mm i.d., 0.25 μm d_f low polarity column and 0.75 m x 0.15 mm i.d., 0.15 μm d_f higher polarity column. This column combination allows the use of a suitably low temperature program rate to give reasonable $^{2}t_R$ values. Flow from the second column was split via a microfluidic valve equally to two pieces of 15 cm long deactivated fused silica capillary column which terminated at each of the NPD and ECD detectors respectively, to provide simultaneous (parallel) dual detection. This arrangement of column set and the deactivated fused silica capillary columns (transfer line) resulted in an approximately 1:1 (0.35 mL.min^{-1} in each transfer line) splitting ratio to the two detectors due to passive action of the splitting valve. This approach provides more information compared to both conventional gas chromatography, and GC×GC with a single detector, as will be demonstrated below.

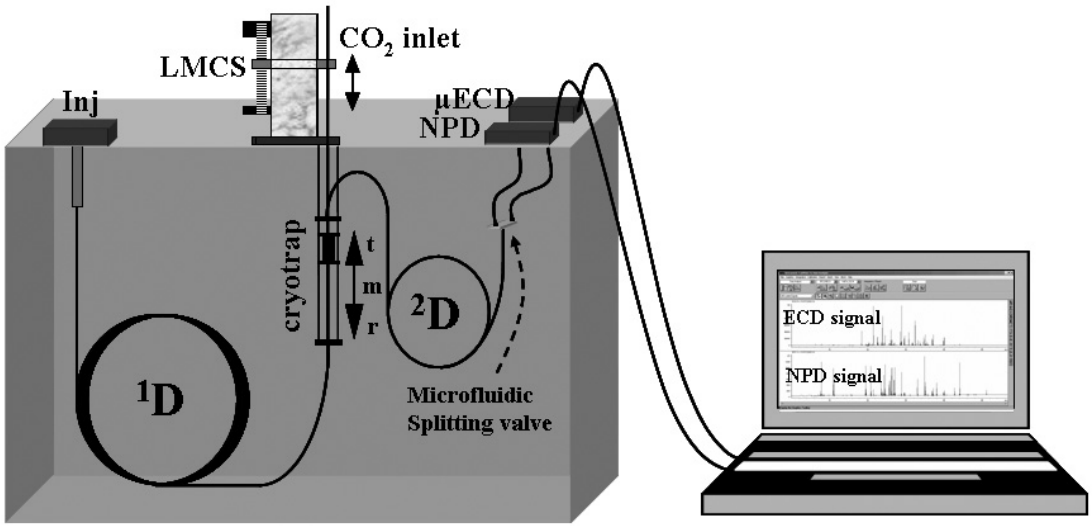

Figure 6. 1: Schematic of the GC×GC-NPD/ECD system used throughout this study. Inj = injector, LMCS = longitudinal modulated cryogenic system, ^{1}D = first dimension column, ^{2}D = second dimension column, m = cryogenic region movement, t = trap position, r = release position.

Two 2D chromatograms resulted from the parallel operation of the NPD and the ECD detector, but peak positions for individual compounds should be precisely reproduced in the plot for each detector channel. Thus the peak position of a given component will correlate in 2D space for each plot, and the relative response of each compound should be approximately indicative of the chemical nature of each compound. Thus **Figure 6.2A and 6.2B** show two 2D plots of 11 selected pesticides obtained from the GC×GC-dual detection system. These plots comprised 13 peaks, including one peak (peak 34) from the decomposition of iprodione (peak 39) and two isomers of propiconazole (peaks 36 and 37). Peaks 16 and 38 were not observed in the plot obtained from the ECD, since there are 0 and 1 Cl atoms in their molecules, respectively, consistent with a previous study [40]. Peak 21 (chlorpyrifos) appeared with a relative high sensitivity in the NPD detector compared to the ECD detector as a result of the presence of the strongly sensitive phosphorus and three chlorine atoms in the molecule. Due to the presence of phosphorus in chlorpyrifos, the NPD signal tends to exhibit tailing compared to the ECD signal; this effect is suspected due to the

interaction of P atom with the surface of the ceramic bead in the detection zone. Separate studies of P species in the NPD have not been previously reported. Similarly, peak 28 (dieldrin) gave higher relative sensitivity in the ECD detector than the NPD due to the presence of chlorine, but an absence of N and P atoms in the molecule, thus a very low signal was observed in the NPD channel. From these observations, it might be concluded that the NPD detector appears to be more selective to this series of compounds compared to ECD, which can detect all compounds that contains high electron affinity substituents such as N, S, O and halogenated atoms. Although in general, a higher sensitivity of ECD over NPD detector was observed, the ECD usually gives a broader peak shape as a result of the internal volume within the detection zone causing dispersive spreading of the peak. The relative efficiency of NPD and ECD detectors for the analysis of multi-class pesticides will be discussed later.

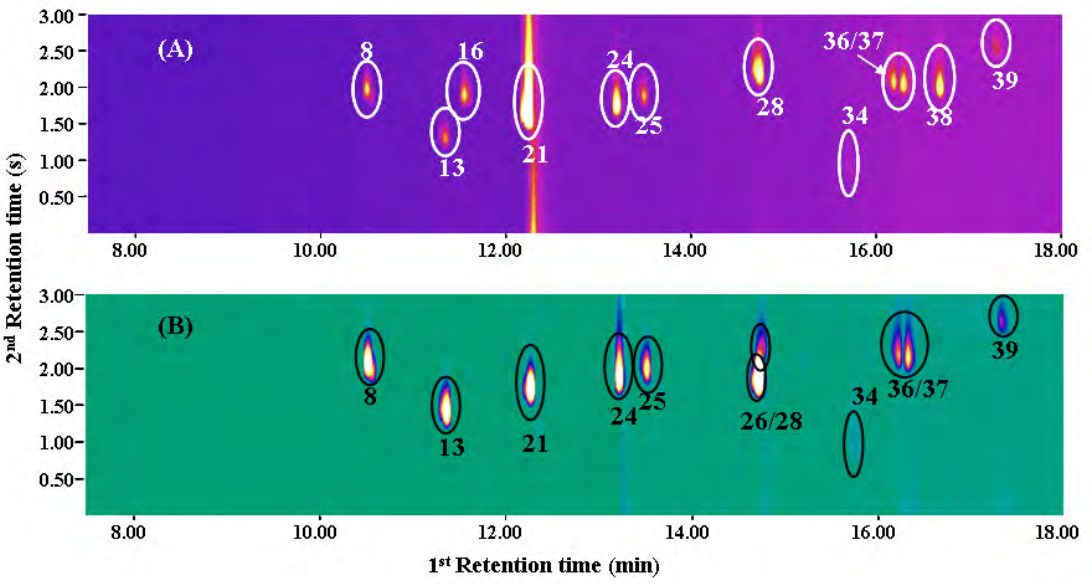

Figure 6.2: Colour plot of selected pesticides for dual detection in GC×GC. The chromatographic condition used in this study was the fast temperature program described in **Section 6.2.3**. Selected pesticides comprised 9 fungicides and one OP and 1 OC; 8. Chlorothalonil, 13. Vinclozolin, 16. Metalaxyl, 21. chlorpyrifos (OPs), 24. Penconazole, 25. Procymidone, 26. dieldrin (OCs), 28. Myclobutanil, 34. Iprodione degradation product, 36 and 37. Propiconazole (I, II), 38. Tebuconazole, 39. Iprodione compounds **(A)** Colour plot obtained from NPD detector. **(B)** Colour plot obtained from ECD detector.

As stated above, a shorter column set was employed in this study, hence, a reduction of the analysis time and elution temperature (T_e) was observed. The analysis time of the 11 pesticides used in this study was reduced by approximately 5 min when fast chromatographic conditions, described in **Section 6.2.3**, were performed, and when the typical column set (30 m ^{1}D, 1 m ^{2}D) was changed to the shorter column set (18 m ^{1}D, 0.75 m ^{2}D), respectively. The reduction in analysis time is of benefit to running costs, although a lower temperature program rate and thus longer run time were preferred for the better separation of the pesticides of interest. Therefore, for this analysis of multi-class pesticides, a lower elution temperature with approximately the same analysis time as for the typical column set was utilised. Reduction of elution temperature (T_e) from the ^{1}D to ^{2}D column may provide benefits such as; (i) better separation of the solutes from each other and from the matrix background, and (ii) better resolution of the target analytes. Generally, T_e is dependent on characteristics of the column, such as column dimension, stationary phase type, film thickness, column length and temperature ramp rate and carrier gas velocity. In GC×GC, at the lower T_e, the analytes will be delivered to the ^{2}D at a lower temperature, which increases the ^2t_R value and should increase the spread of components in the second dimension. Meanwhile, an increase in peak width of solutes in both the first and second dimension, along with the wraparound phenomena (discussed below) will become more significant. **Table 6.2** shows the elution temperature (T_e) of selected pesticides when both the typical and shorter column sets were used. At the same chromatographic condition for the GC×GC-dual system, T_e was decreased by approximately 23-30 °C. For instance, ΔT_e of chlorothalonyl and vinclozolin (peak number 8 and 13) from these columns sets were decreased by 23 °C and 24 °C, respectively.

Table 6.2: The elution temperature of selected pesticides when a typical, and a short, column set were used.

#	Compounds	Column set 1[a]		Column set 2[b]		ΔT_e (°C)
		^1t_R (min)	T_e (°C)	^1t_R (min)	T_e (°C)	
8	Chlorothalonyl	13.740	225.3	10.825	201.9	23.3
13	Vinclozolin	14.433	230.8	11.363	206.3	24. 6
16	Metalaxyl	14.661	232.6	11.622	208.3	24.3
21	Chlorpyrifos (OP)	15.408	238.6	12.300	213.8	24.9
24	Penconazole	16.428	246.8	13.261	221.4	25.3
25	Procymidone	16.742	249.3	13.550	223.8	25.5
26	Dieldrin (OC)	18.072	259.9	14.680	232.8	27.1
28	Myclobutanil	18.271	261.5	14.839	234.1	27.5
34	Iprodione degradation product	Nc[1]	Nc	Nc	Nc	Nc
36	Propiconazole I	20.198	276.9	16.245	245.3	31.6
37	Propiconazole II	20.426	278.8	16.369	246.3	32.5
38	Tebuconazole	21.161	284.6	16.749	249.3	35.3
39	Iprodione	22.150	292.6	17.475	255.2	37.4

[a] ^{1}D is BPX5 30m, 0.25 mm, i.d., 0.25 µm d_f and ^{2}D is BPX50 1m, 0.15 mm, i.d., 0.15 µm d_f

[b] ^{1}D is BPX5 18m, 0.25 mm, i.d., 0.25 µm d_f and ^{2}D is BPX50 1m, 0.15 mm, i.d., 0.15 µm d_f

[1]Nc = Not calculated

6.3.2 The efficiency of NPD and ECD detectors for multi-class pesticides analysis

In this study, the experiment investigated the effect of the microfluidic splitting valve on the dual detection system, through comparison of chromatograms obtained from single detection and dual detection modes. They were also compared for modulated and non-modulated operation. Peak widths of analytes of interest in both 1D-GC and GC×GC were determined. The results show that there are slightly different $^{1}t_R$ values and peak widths at half height (w_h) of selected pesticides when 1D-GC was performed in both single and dual detection. However, it was decided that peak area and peak height of analytes used in this study would not be compared due to the difference in selectivity of the two detectors. **Figure 6.3A to H** shows 1D-GC and GC×GC chromatograms of a selected pesticide (penconazole, peak 24) in various single and dual detection modes. **Figure 6.3A to D** is 1D-GC chromatograms obtained from four arrangements: single NPD and single ECD, then the dual detection system with NPD and ECD channels. The results show that w_h of these 1D-GC peaks were 1.875, 1.853, 1.875 and 1.987 s for each arrangement, respectively. Peak positions appear to vary slightly as the column exit is switched from the NPD to the ECD. There were only slightly different widths of these 1D-GC peaks when progressing from single to dual detection systems, hence it appears that the microfluidic splitting valve used in the dual detection system does not greatly affect peak widths of the analytes used in this study in normal GC analysis. A small measure of peak tailing can be observed. **Figure 6.3E to H** show analogous GC×GC chromatograms obtained for equivalent arrangements as above. The peak width of the biggest pulse peak (asterisked, marked *) gave w_h 99, 240, 205, 300 ms, respectively. Peak symmetry tends to suggest that the splitting valve imposes some degree of asymmetry on the peak. Best modulated peak widths were for single NPD detection (**Figure 6.3E**) i.e. in the absence of the split valve. Peak tailing is considerably more in **Figure 6.3G**. Peak tailing also appears exacerbated in **Figure 6.3H**; generally the increased peak width proposed to arise from dispersion in the ECD seems confirm. The results indicate that in GC×GC analysis, peak widths from the ECD detector

result in an increased peak width of about 1-2 fold compared to NPD. The dual detector arrangement now exhibits almost exact peak retention correspondence, so the two uncoated column segments prior to the detectors are very well matched, for example compare **Figure 6.3G and H** peak positions. Generally, response variation of NPD and ECD detection depends on the active-responding atom in the molecule, such as N, P and Cl species. All fungicides used in this study are N-containing compounds, but also most possess chlorinated groups; they not only give a good response and peak shape in NPD but also respond in the ECD detector. On the other hand, organophosphorus insecticides (OPs) give a higher response in the NPD detector compared to their relative ECD response at the same level of concentration. Tailing effects at lower concentration level in the contour plot of these compounds was increasingly observed (results not shown here). All OC pesticides have an excellent response in ECD detector but very low response in the NPD detector; this will be discussed further below.

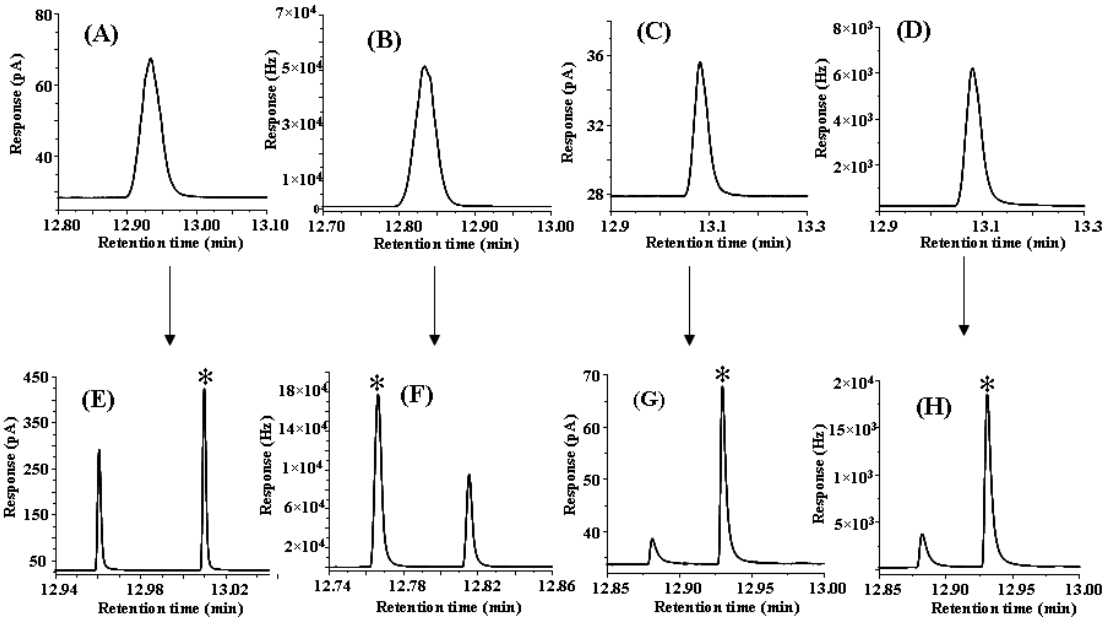

Figure 6.3: 1D-GC and GC×GC chromatograms obtained from single and dual detection. **Figure 6.3A** to **D** show 1D-GC chromatograms generated from single NPD, ECD, dual detection NPD mode and dual detection ECD mode. **Figure 6.3E** to **H** show GC×GC chromatograms obtained from single NPD, ECD, dual detection in NPD and ECD modes, respectively.

6.3.3 The effect of changing ECD detector make-up gas flow

Typically, chromatographic peaks generated in GC×GC are very narrow. Therefore, the detector data acquisition rate should be at least 50 Hz. The ECD's maximum data acquisition rate of 50 Hz makes this detector just adequate for a GC×GC system if quantitative analysis is required. Adjustment (increasing) of the make-up gas flow (N_2) means sensitivity obtained from the ECD has to be sacrificed, as the higher make up gas flow produces a better (narrower) peak shape, although accompanied by a lower sensitivity of detection. Using both the NPD and ECD as dual detectors in a GC×GC system should require an appropriate split flow to both detectors; the detector gases still must be optimised in order to optimise detector relative sensitivities, taking into account the need for minimising the ECD peak width. Here, the effect of ECD detector gas flow on the signal obtained from the NPD detector was investigated, primarily because the ECD gas flow significantly exceeds that recommended. It was of concern that an excessive flow (pressure) might cause some degree of back-pressure in the transfer line to the ECD, and so increased flow in the NPD line. The optimum NPD detector gas flow used in this study was applied from a previous study, with flows of 1.5, 100, 10 $mL.min^{-1}$ for H_2, air and N_2, respectively. The flow rate of ECD make-up gas was varied from 25 to 150 $mL.min^{-1}$. Results show different trends in metalaxyl and tebuconazole signals obtained from the NPD detector, although no specific trend is evident. **Table 6.3** shows the summation of the three biggest pulse peaks of the compounds for peak area and peak height of metalaxyl (^1t_R = 11.429 min, ^2t_R = 2.00 s) and tebuconazole (^1t_R = 16.588 min, ^2t_R = 2.10 s) for the modulated peaks, as ECD detector gas flow is varied (chromatographic conditions as stated in **Section 6.2.3**). Standard deviations (SD) for triplicate injections of the standard mixture are included**.** The metalaxyl peak increases by some 4.3% whilst terbuconazole decreases by 20% in the NPD over the range of ECD flow rate increase. If flows in each transfer line vary, it will alter the split flow (in this case, increase the flow in the NPD channel if ECD detector gas flow rate increases) to the NPD and a higher response would result. This agrees with the metalaxyl observation, but not for the terbuconazole. There may be different flow sensitivity for the response

to the two compounds in the NPD, but this has not been established. Any changes in flow in the transfer lines might be thought to vary the $^{2}t_{R}$ values of the compounds. It was found that the position of the compounds in the 2D space was the same over the change in the ECD make up gas flow from 25 to 150 mL.min^{-1}, and so there is no evidence for variation in flows in each transfer line, although the response of the compound will decrease when the higher ECD internal flow is applied due to dilution of solute within the make-up gas. An ECD make up gas flow of 100 mL.min^{-1} was chosen, which provided adequate peak shape and a reasonable sensitivity of the ECD detector.

Table 6.3: The summation of peak area and peak height of selected pesticides in NPD channel when make-up gas flow in ECD detector was varied from 25 to 150 mL.min^{-1} (NPD detector gas flow condition was 1.5, 100 and 10 mL.min^{-1}for H_2, Air and N_2, respectively).

ECD Make-up gas flow (mL.min^{-1})	NPD signal ± (SD)			
	Metalaxyl		Tebuconazole	
	Area[a] (pA*s)	Height[b] (pA)	Area[a] (pA*s)	Height[b] (pA)
25	9.85 ± (0.078)	36.55 ± (0.21)	5.63 ± (0.19)	18.40 ± (0.42)
50	9.99 ± (0.15)	37.50 ± (0.57)	5.20 ± (0.14)	17.60 ± (0.57)
75	9.679 ± (0.045)	35.70 ± (0.00)	4.91 ± (0.09)	16.50 ± (0.12)
100	9.959 ± (0.075)	37.10 ± (0.14)	4.85 ± (0.21)	16.28 ± (0.68)
125	9.98 ± (0.26)	38.67 ± (0.67)	4.40 ± (0.28)	14.05 ± (0.92)
150	10.30 ± (0.30)	40.00 ± (1.70)	4.41 ± (0.28)	14.40 ± (0.85)
Average	9.95	37.59	4.90	16.21
SD	0.2029	1.5405	0.4718	1.7181
%RSD	2.04	4.10	9.63	10.60

Standard deviation (SD) when n = 3

Metalaxyl ^1t_R = 11.429 min, ^2t_R = 2.00 s; Tebuconazole ^1t_R = 16.588 min, ^2t_R = 2.10s

[a] Summation of the three biggest pulse peaks

[b] The biggest pulse peak when P_M = 3s was performed.

6.3.4 Wrap around observation in GC×GC-dual detection system

To best preserve the first dimension separation, it is often stated that the minimum number of modulations per ^{1}D peak should be at least three to four. In terms of the modulation ratio concept (M_R) the modulation period (P_M) should be equal to about one standard deviation (σ) of the ^{1}D peak width to maintain an M_R value of about 3 to 4. Thus this specifies the modulation period in terms of peak width at base (^1w_b). However, there is no guarantee that the analyte will elute from the second dimension column within the chosen modulation period of the experiment that matches this requirement, which is a function of parameters such as column length, retention factor, and flow velocity. Analyte ^2t_R may exceed P_M such that it elutes during subsequent modulation cycles, which can cause co-elution with compounds in that modulation cycle. This leads to wrap-around, and either a shorter ^{2}D column, higher temperature ramp rate (to increase solute elution temperature) or/and a longer P_M may offer a solution to this problem. Wrap-around requires determination of the second dimension retention time (^2t_R), and there are two relatively easy methods for the prediction of analyte ^2t_R. Firstly, by using the targeted mode of analysis to collect a whole ^{1}D peak and release it at a precise time into the second dimension column, the exact ^2t_R time may be estimated. Alternatively, comparison of the position in the 2D plot for an analyte when different P_M values are used allows prediction of absolute ^2t_R ($^2t_{Rabs}$). **Figure 6.4A to D** shows contour plots of selected pesticides using the NPD detector when P_M = 2, 3, 4 and 5 s were used. The absolute ^2t_R may be calculated based on apparent ^2t_R ($^2t_{Rapp}$) using the equation for the different modulation periods that uniquely solve the expression in **Equation (5)** below;

$$^2t_{Rabs} = {}^2t_{Rapp} + nP_M \qquad (5)$$

where n is the number of modulation cycles corresponding to the extent of wrap-around of the compound: n = 0, 1, 2, 3… n = 0 means there is no wrap around in the experiment. Peak 16 (marked by a circle) in each contour plot was used

to calculate the wrap-around on this column set. For instance, in **Figure 6.4A** (P_M = 2 s) $^2t_{Rabs}$ could be 0.75, 2.75, 4.75, 6.75 … Only 4.75 s provides a reasonable solution to this time in all plots, so absolute ^2t_R ($^2t_{Rabs}$) for compound 3 = 4.75 s. Likewise, peak 28 (marked by a square) has possible times of 1.2, 2.2, 3.2, 5.2, and 7.2 s; the only time that agrees with all modulation periods is ^2t_R = 5.2 s. Thus in **Figure 6.4A**, all compounds are wrapped around 2 times, and in **Figure 6.4C**, all are wrapped around once. **Table 6.4** shows the apparent ^2t_R obtained from the NPD channel when different P_M was used. An absolute ^2t_R of each compound obtained from the estimation of the contour plot shown in **Figure 6.4A to D** are also given in this table. Dieldrin which does not respond to the NPD detector, and iprodione degradation product which gave very low response, is not displayed.

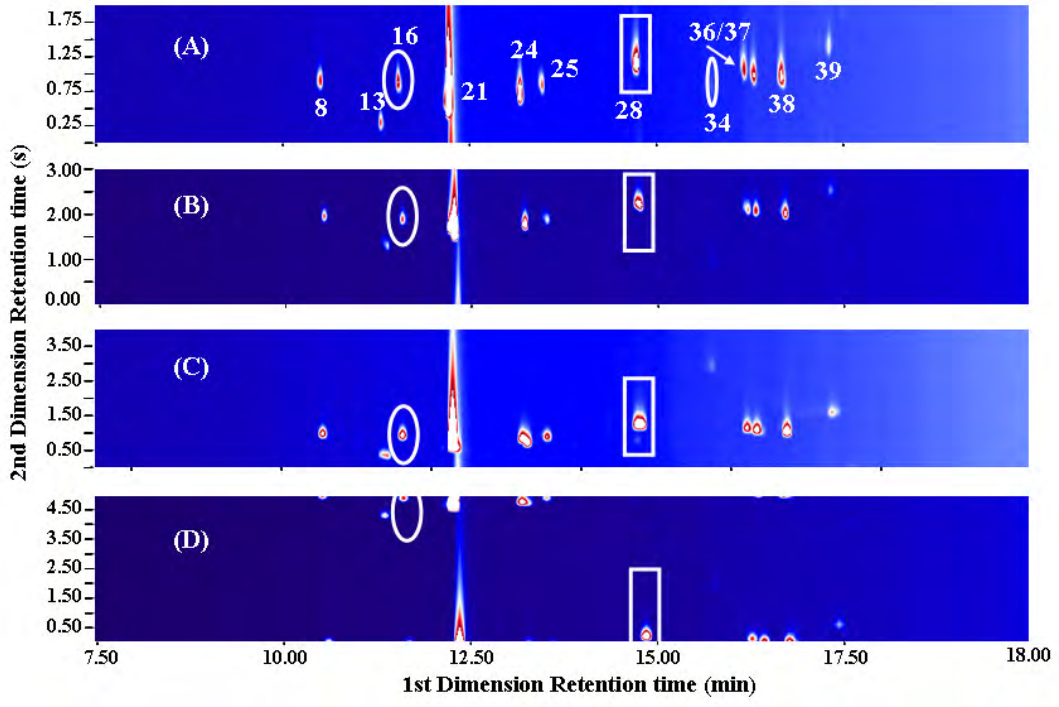

Figure 6.4: Colour plot of selected pesticides as described in **Figure 6.2** from NPD detector with fast chromatographic condition stated in **Section 6.2.3** when different P_M were used. **(A)** P_M = 2 s, **(B)** P_M = 3 s, **(C)** P_M = 4 s, **(D)** P_M = 5 s.

Table 6.4: Apparent and absolute $^{2}t_{R}$ of selected pesticides when different modulation periods (P_M) were used in GC×GC-NPD/ECD system. The signal was obtained from NPD detector and BPX5 18m, 0.25mm i.d., 0.25d_f and BPX50 0.75m, 0.15 mm i.d., 0.15 d_f column set was used.

#	Compound names	$^{1}t_{R}$ (min)	P_M (s)				Estimate Absolute $^{2}t_{R}$ ($^{2}t_{Rabs}$) (s)
			Apparent $^{2}t_{R}$ ($^{2}t_{Rapp}$) (s)				
			2	3	4	5	
8	Chlorothalonyl	10.634	1.00	2.00	1.00	5.00	**5.00**
13	Vinclozolin	11.463	0.30	1.30	0.30	4.30	**4.30**
16	Metalaxyl	11.706	0.90	1.90	0.90	4.90	**4.90**
21	Chlorpyrifos (OP)	12.386	0.60	1.60	0.60	4.60	**4.60**
24	Penconazole	13.355	0.75	1.75	0.75	4.75	**4.75**
25	Procymidone	13.650	0.85	1.85	0.85	4.85	**4.85**
26	Dieldrin (OC)	Nd[1]	Nd	Nd	Nd	Nd	**Nd**
28	Myclobutanil	14.909	1.30	2.30	1.30	0.30	**5.30**
34	Iprodione degradation product	Nc[2]	Nc	Nc	Nc	Nc	**Nc**
36	Propiconazole I	16.373	1.00	2.10	1.10	0.10	**5.10**
37	Propiconazole II	16.502	1.05	2.05	1.05	0.05	**5.05**
38	Tebuconazole	16.881	1.00	2.00	1.00	0.00	**5.00**
39	Iprodione	17.546	1.40	2.40	1.40	0.40	**5.40**

Nd[1] = Not detected

Nc[2] = Not calculated

6.3.5 Dual detection repeatability and area ratio measurements

Table 6.5 reports within day repeatability and reproducibility over 3 days for selected compounds in terms of RSD values. Peak areas are reported as the sum of the peak pulses, whereas the peak height of the largest peak only is reported. Repeatability of the order of 4-6% is seen for area and height data, whereas between days, the NPD response is larger over the successive days but smaller variation is found for the ECD response. Since the compounds here possess both ECD and NPD response, then the trivial case of an active compound towards either NPD or ECD does not arise. This case will require their position to be definitive of identity, but a compound exhibiting both NPD and ECD activity should permit their relative response to support retention in the 2D plane as an indicator of compound identity. Thus not only should peaks be in the correct location (^1t_R and ^2t_R) but they should have a response ratio for ECD:NPD that is in accord with those of standard compounds. It might be argued that if the response ratio does not agree with this, then there may be interfering peaks that amend the response in either the ECD or NPD channel. **Table 6.6** lists an example of data supporting this proposal, both within day and over 3 days. The ratios of ECD:NPD vary from a low value of about 18 for chlorpyrifos (which contains a P atom and so has an elevated NPD response compared with other compounds) to about 1000 for vinclozolin which has only one N atom and so has a suppressed NPD response. Chlorothalonil (ratio ~ 700) has 4 Cl and two C≡N groups. Ratios of the same compound are consistent across the data set. The most similar values are for those compounds (**25, 36, 37, 39**) that have 2 Cl atoms, and 3 N atoms in their structure. In the absence of interfering peaks, the key to specificity resides in both 2D position and response ratio, and in the GC×GC experiment, peak position should correspond to identification. **Figure 6.5** shows chemical structures of selected pesticides used to the response ratio calculation. Clearly, good agreement between chemical structure of the selected pesticides and of the response ratio was apparent. **Figure 6.6** shows a flow diagram of the role of dual detection in GC×GC, to provide identification based on the incremental criteria of ^1t_R,

then $^{2}t_{R}$, and finally DRR correlation, under the same chromatographic condition. $^{1}t_{R}$ and $^{2}t_{R}$ of a target compound in both channels of the dual detection would normally be used for compound identification. If $^{1}t_{R}$ and $^{2}t_{R}$ are both at the same position as the standard compound, then the identification of the compound is tentatively correct. The DRR value augments retention as an additional tool for compound identification, obtained directly from each detector if the dual detection is in the simultaneous mode. However, the IS is necessary for signal correction in each detector if the system is not connected in a parallel/simultaneous manner. As stated above, false negative signals can cause an incorrect DRR value; one might propose that MS analysis (even in SIM mode for trace nalysis) might then be performed to provide further identification power.

Table 6.5: Repeatability and reproducibility of the GC×GC-NPD/μECD system.

Comp.	Repeatability[a] (%RSD)						Reproducibility[b] (%RSD)					
	Peak width[c] (s)		Peak Area[c] (pA*s)		Peak Height[e] (pA)		Peak width (s)		Peak Area (pA*s)		Peak Height (pA)	
	NPD	ECD	NPD	ECD	NPD	ECD	NPD	ECD	NPD	ECD	NPD	ECD
13	0.80	1.72	4.39	4.65	5.00	4.66	1.00	0.84	6.77	0.87	6.63	1.18
25	1.32	1.35	4.77	4.84	4.97	4.83	1.53	0.36	7.26	1.43	6.83	1.42
37	1.67	3.09	4.59	6.01	4.83	5.61	2.82	7.41	8.54	2.44	10.52	7.90

Compound #13 = Vinclozolin

Compound #25 = Procymidone

Compound #37 = Propiconazole II

[a] n= 5

[b] n= 3 days

[c] Peak width at half height of a main pulse peak of compound from GC×GC-dual detection

[d] The summation of peak area of three biggest pulse of compound from GC×GC-dual detection

[e] Total peak height of main pulse peak of compound from GC×GC-dual detection

Table 6.6: Repeatability of area ratio from ECD and NPD channels. (n=5)

Peak #	Compounds	Peak Area Ratio ECD:NPD					Average	SD	% RSD
		1	2	3	4	5			
8	Chlorothalonil	656	676	698	736	729	699	34	4.9
13	Vinclozolin	957	909	1004	1024	1029	985	51	5.2
21	Chlorpyrifos	16	17	18	19	19	18	1.0	5.8
24	Penconazole	245	252	259	258	258	255	6	2.4
25	Procymidone	387	386	396	407	412	398	12	2.9
26	Dieldrin	586	581	619	628	630	609	23	3.8
36	Propiconazole I	187	183	201	204	204	196	10	5.2
37	Propiconazole II	200	205	206	213	210	207	5.3	2.6
39	Iprodione	217	231	233	239	241	232	9.2	3.9

Reproducibility of area ratio from ECD and NPD channel over 3 days

Peak #	Compounds	Peak Area Ratio ECD:NPD			Average	SD	%RSD
		Day #1	Day #2	Day #3			
8	Chlorothalonil	786	699	669	718	61	8.5
13	Vinclozolin	1102	985	990	1026	67	6.5
21	Chlorpyrifos	19.6	17.8	18.7	18.7	0.9	4.8
24	Penconazole	281	255	250	262	17	6.4
25	Procymidone	439	398	395	411	25	6.1
26	Dieldrin	654	609	655	639	26	4.1
36	Propiconazole I	213	196	197	202	9.6	4.8
37	Propiconazole II	230	207	209	215	13	6.1
39	Iprodione	261	232	230	241	17	7.1

8

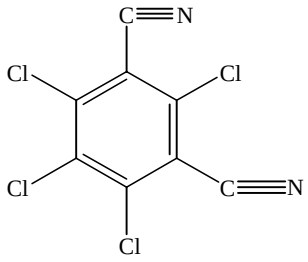

Chlorothalonil (MW = 266.0)

13

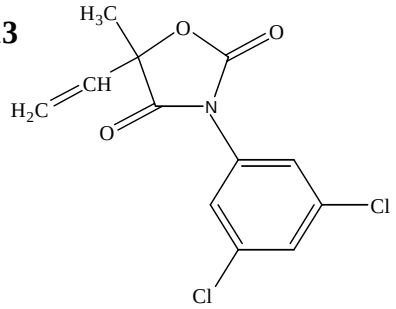

Vinclozolin (MW = 285.0)

21

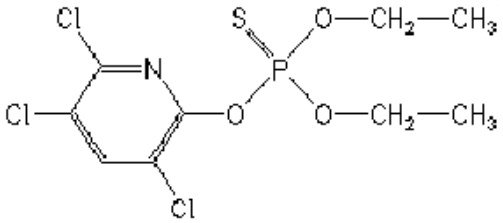

Chlorpyrifos (MW 348.93)

24

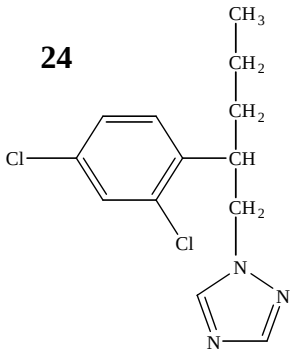

Penconazole (MW = 284.0)

25

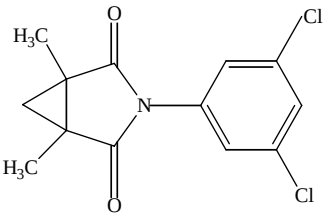

Procymidone (MW = 283.02)

26

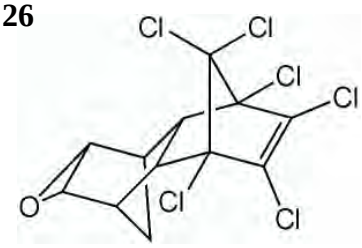

Dieldrin (MW = 377.87)

36, 37

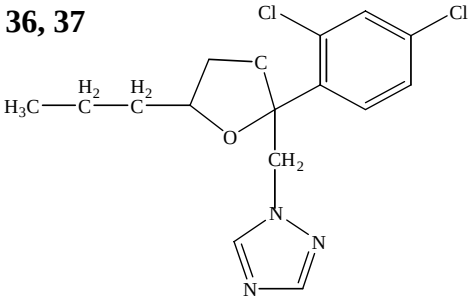

Propiconazole I and II (MW = 341.07)

39

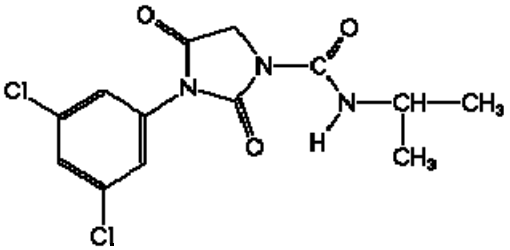

Iprodione (MW = 329.03)

Figure 6.5: Chemical structure of pesticides standard used for comparison of signal ratio of ECD:NPD detector. N, P, S and Cl in each molecule correspond to ratio of ECD:NPD.

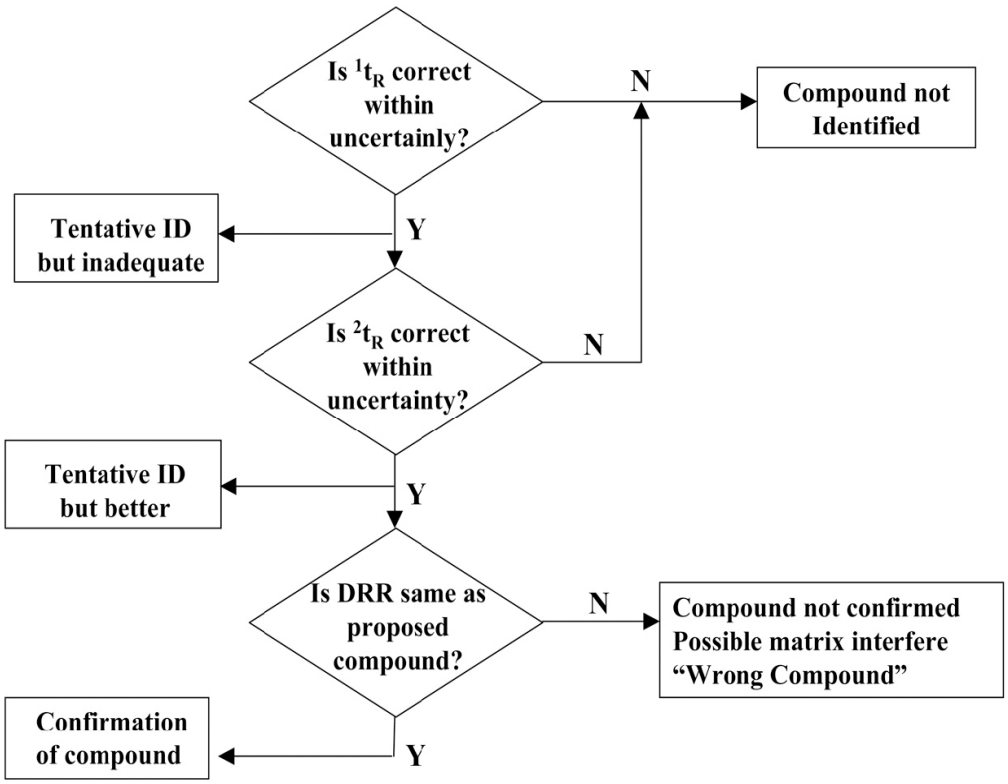

Figure 6.6: Flow diagram of progressive roles of ^1t_R, ^2t_R and DRR measures in GC×GC-dual detection for compound identification.

6.3.6 Analytical characteristics of GC×GC-dual detection

In this study, the analytical performance of the developed method for quantitation aspect such as linearity and limit of detection were evaluated. Five point calibration curves with an internal standard were prepared in the concentration range of 1-1000 µg.L^{-1} of each standard and 10 µg.L^{-1} for the internal standard. Each concentration level was injected in triplicate into the dual system. The main pulse peaks of each compound were summed (both peak area and peak height) and the ratio of each standard to internal standard was used to construct the calibration curves. Detection limits were also calculated based on the lowest concentration level of the standard that can be detected. The lowest concentration that gave a signal three times larger than the standard deviation of the background noise was considered for the calculation of limit of detection of the technique. Therefore, the LOD = 3xSD of the

signal of the lowest concentration. Linear regression, correlation coefficient (R^2) and limit of detection (LOD) of selected pesticides from NPD and EDC detector are given in **Table 6.7.** The results suggest that good linearity and trace detection is possible for N- and P- containing compounds by using GC×GC-dual detection developed in this study.

Table 6.7: Linear regression and R^2 of the selected pesticides using GC×GC-dual detection.

NPD Detector

Comp.	Linearity range ($\mu g.L^{-1}$)	Linear Regression (Peak Area[a] ratio)	R^2	Linear Regression (Peak Height[b] ratio)	R^2	LOD[a] ($\mu g.L^{-1}$)
21	1-1000	y = 0.0008x + 0.0081	0.9972	y = 0.0013x - 0.0151	0.9985	0.0200
26	1-1000	y = 0.0006x + 0.0066	0.9931	y = 0.0009x + 0.0034	0.9945	0.3900
35	5-1000	y = 0.0007x - 0.0047	0.9647	y = 0.0011x - 0.011	0.9982	0.5400

ECD Detector

Comp.	Linearity range ($\mu g.L^{-1}$)	Linear Regression (Peak Area[a] ratio)	R^2	Linear Regression (Peak Height[b] ratio)	R^2	LOD[a] ($\mu g.L^{-1}$)
21	1-1000	y = 0.0008x + 0.0161	0.9915	y = 0.0011x + 0.0062	0.9967	0.0160
26	1-1000	y = 0.0026x + 0.0599	0.9923	y = 0.0039x + 0.0889	0.9918	0.0167
35	1-1000	y = 0.0017x + 0.0034	0.9964	y = 0.0026x + 0.0093	0.9961	0.0680

LOD calculated based on the summation of peak height

Compound # 21 is chlorpyrifos

Compound # 26 is dieldrin

Compound # 35 is p,p'DDT

[a] The summation of peak area of the three biggest pulses of the compound.

[b] Peak height of the biggest pulse peak of compound

6.3.7 GC×GC-dual detection method development for multi-class pesticides analysis

The analysis of pesticide residues should be improved if the separation method is required to provide separation of the pesticides of interest from each other, as well as separate them from matrix components. In this study, optimisation of GC×GC with dual detection aims to achieve the best separation of a broad range of pesticides which might co-elute in conventional GC, although some of them might not normally be analysed together. Several GC conditions were trialled to enhance resolution of the target analytes (detailed results not shown here). A low temperature program rate for GC×GC-dual detection was chosen in order to minimise the co-elution of the pesticides. Better resolution of pesticides from each other was observed at slower temperature ramp rates and slower column flow rate. A modulation period of 6 s was used to minimise wrap-around of the analytes (see above). Figure 6.7A and B show separate contour plots of fungicides and OP standards using the NPD detector channel under optimum conditions (Section 6.2.3). OC pesticides gave a very small signal in the NPD detector, thus a contour plot of OC pesticides is not shown. On the other hand, results of the three classes of pesticides standards – fungicides, OPs and OCs – using the ECD detector channel are shown in Figure 6.7C to E respectively. All classes of pesticides gave relatively good response in the ECD detector. In general, the results show that separation of all pesticides was achieved. For instance, the pair of peaks (4 and 5) marked in the circle illustrated the power of separation of the developed method for the separation of peaks in the 2D space, which would otherwise co-elute in ^{1}D Figure 6.8B and D show profiles of pesticide standard mixtures used in this study obtained from NPD and ECD when the optimum separation condition was employed (Section 6.2.3). The results show that the ECD detector responded to most of the pesticides while as expected the NPD detector responded to only N- and P-containing compounds. At the concentration level of 1.00 $\mu g.L^{-1}$ a higher sensitivity was observed with the ECD detector. However, because of a larger internal volume of the detector for the ECD, increased overlap of the pesticide peaks was also observed for this detector. Note that there are many instances

in the ECD result where no response is given in the analogous non-modulated chromatogram, but give clearly defined peaks in GC×GC mode. This is attributed to the improved sensitivity of detection response in GC×GC.

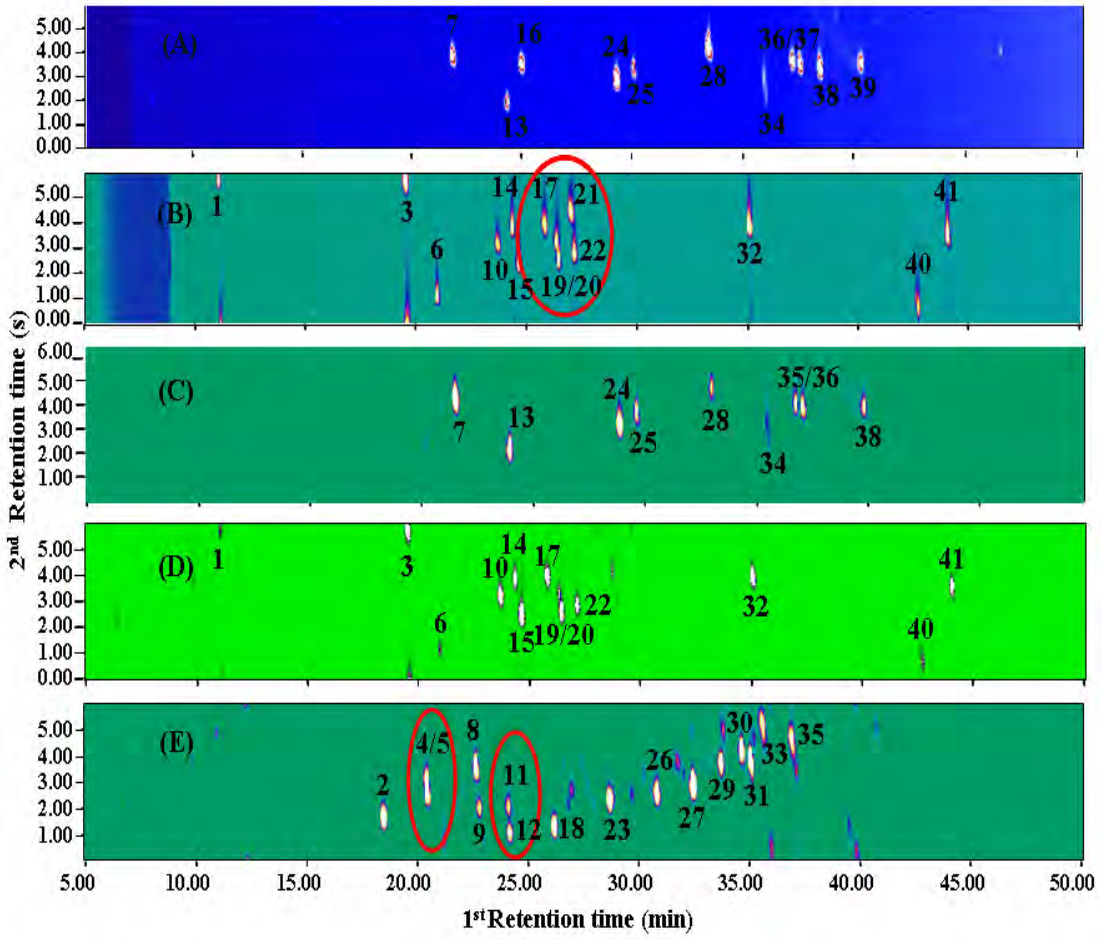

Figure 6.7: Colour plot of fungicides, OP and OC pesticides obtained from GC×GC dual detection when ~ optimum chromatographic condition described in **Section 6.2.3** and P_M = 6 s were used. **(A)** Fungicide standards from NPD detector. **(B)** OP standard from NPD detector. **(C)** Fungicide standards from ECD detector. **(D)** OP standard from ECD detector. **(E)** OC standards from ECD detector.

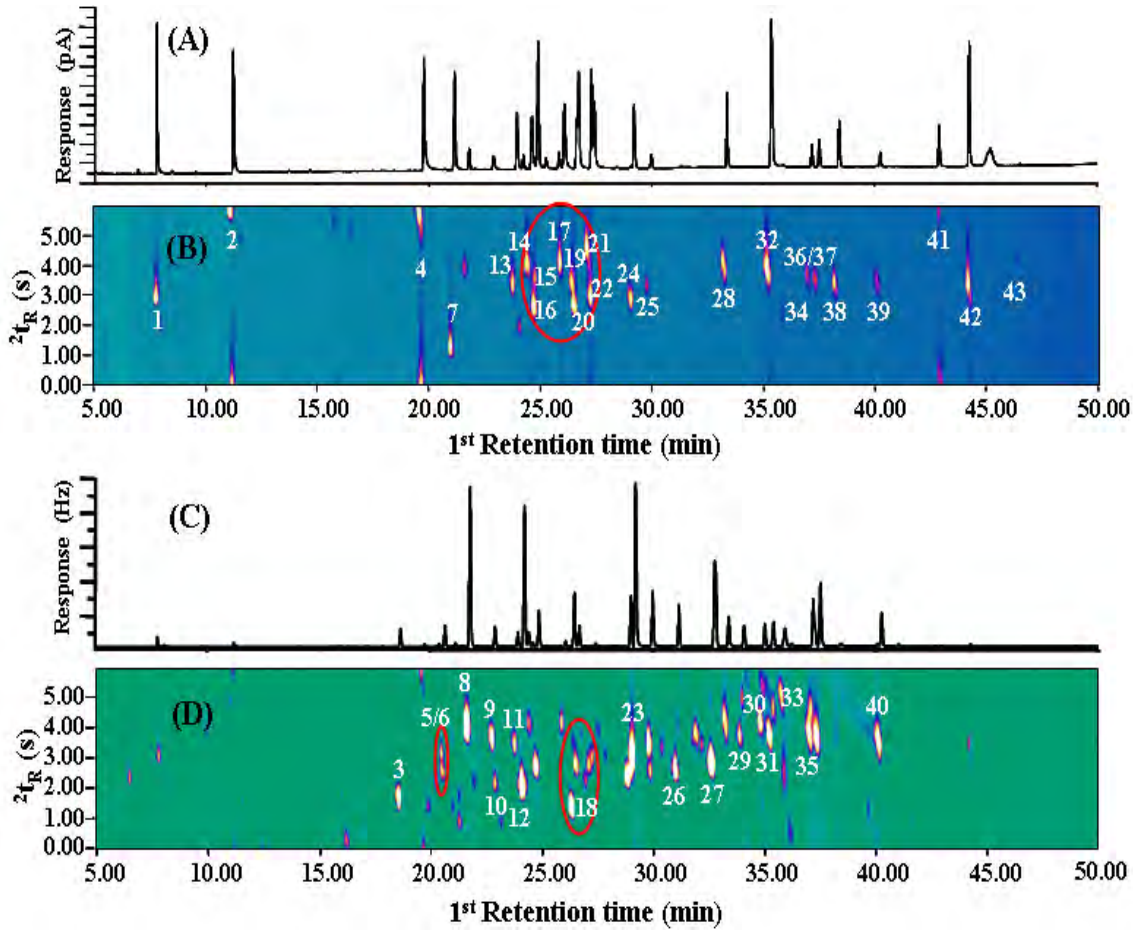

Figure 6.8: Colour plot of multi-class pesticide standard mixture from GC×GC dual detection when ~ optimum chromatographic condition described in **Section 6.2.3** and P_M = 6 s were used. **(A)** 1D-GC chromatogram of multi-class pesticide standard mixture obtained from NPD detector. **(B)** Colour plot of multi-class pesticide standard mixture obtained from NPD detector. **(C)** 1D-GC chromatogram of multi-class pesticide standard mixture obtained from ECD detector. **(D)** Colour plot of multi-class pesticide standard mixture obtained from ECD detector.

6.3.8 The application of dual detection to analysis of pesticides in vegetable samples.

The optimum GC×GC-dual detection method was applied to screening of the pesticide residues in vegetable samples. Several co-eluting peaks observed in ^{1}D chromatograms were separated in the second dimension plane, making the analytical results more reliable. In order to study the effect of matrix compounds, fresh spinach was extracted according to the method described in Section 6.2.7. Greater complexity with respect to matrix components in the spinach extract was observed. Figure 6.9A and B are the profiles of blank spinach extract and blank spinach extract spiked with the standard mixture obtained with the NPD detector. There are also a small number of compounds to which this detector responds in this vegetable extract. The profile from the ECD detector shows more volatile compounds that respond to the ECD detector. Results are shown in Figure 6.9C and D. There are some matrix components from the spinach extract which will co-elute with the standard mixture in ^{1}D analysis. However, many of them were separated well from the pesticides in the 2D space. Note that due to complexity of the matrix, and the component standards, only a few peak assignments are given in this figure, related to the components for which DRR values are recorded. **Table 6.8** presents DRR values in a slightly modified manner to those in **Table 6.6**, being ratioed against peak 24 (penconazole) for which data indicated it to be relatively non-interfered. In this case, we essentially use this as a ‘pseudo’-IS. Also, data for **Tables 6.6 and 6.8** were obtained under different chromatographic conditions (faster versus slower), and detector settings. Comparative data for results from **Figure 6.8 D and B** (ECD/NPD) and **Figure 6.9 D and B** (ECD/NPD) in **Table 6.8** seem to be quite consistent. We note that (i) peaks 13, 21, 36 and 37 give similar DRR results, which we take to confirm their purity; (ii) peak 25 has a much larger DRR against peak 24 and suggests that it exhibits positive interference in the extract, to produce a false negative result (the DRR is incorrect, so we would suspect it to be not confirmed); and (iii) the iprodione result (peak 39) differs in magnitude of DRR which may be a consequence of the decomposition of this component as observed elsewhere.

Table 6.8 Detector response ratio (DRR) values of selected pesticides in spinach extract sample matrix

Peak no.	Compound names	Peak area ratio ECD/NPD *versus* penconazole area ratio	
		DRR value of pure selected pesticides standard [a]	**DRR value of selected pesticides in spinach sample matrix [b]**
13	Vinclozolin	0.092	0.083
21	Chlorpyrifos	0.049	0.034
24	Penconazole	1.00	1.00
25	Procymidone	1.63	3.22
36	Propiconazole I	0.79	0.79
37	Propiconazole II	0.91	0.91
39	Iprodione	0.85	1.12

Slower chromatography conditions (**Section 6.2.3**) were used for this analysis.

[a] Pure standard mixture at 2.00 µg/mL.

[b] Spinach extract spiked with standard mixture at 1.78 µg/mL

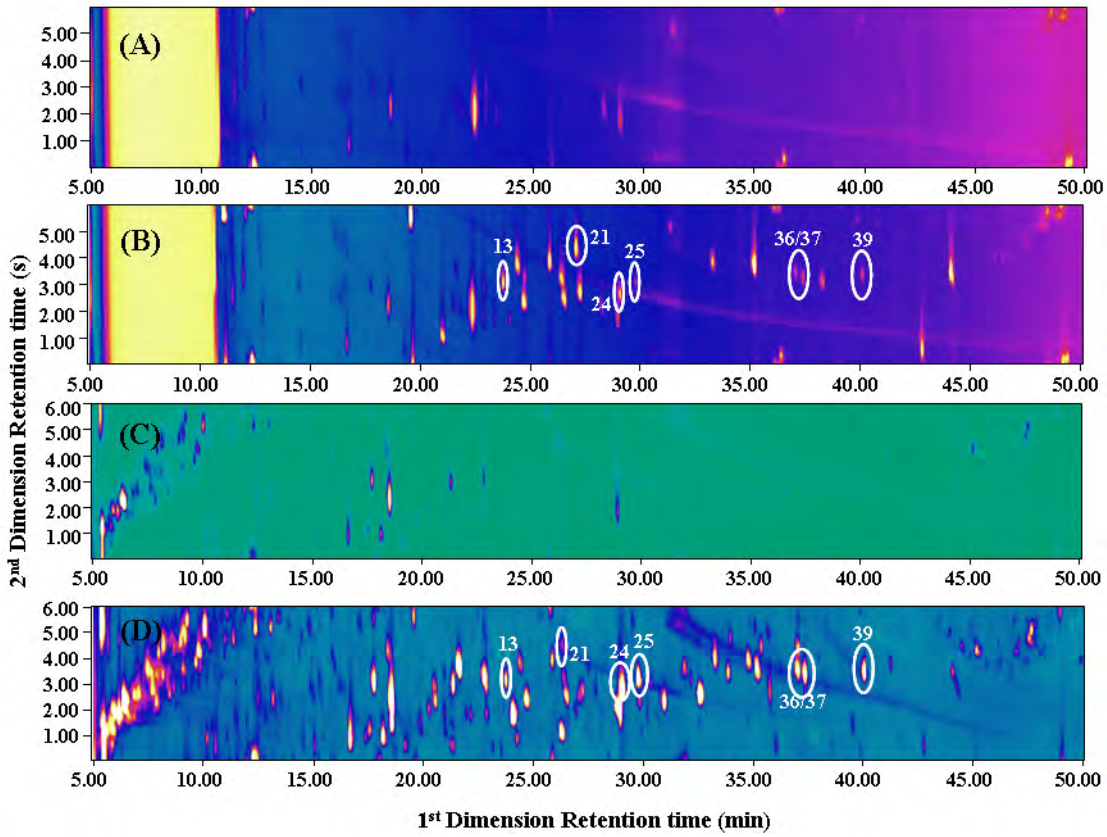

Figure 6.9: Colour plot of blank spinach extract and blank spinach extract spiked with pesticide standard mixture using GC×GC dual detection when optimum chromatographic condition described in **Section 6.2.3** and P_M = 6 s were used. **(A)** Blank spinach extract obtained from NPD detector. **(B)** Blank spinach extract spiked with pesticide standard mixture obtained from NPD detector. **(C)** Blank spinach extract obtained from ECD detector. **(D)** Blank spinach extract spiked with pesticide standard mixture obtained from ECD detector.

6.4 Conclusion

The dual/simultaneous detection by using parallel ECD and NPD detectors within a single analysis was investigated for GC×GC operation. A broad range of pesticides and the other organohalogen substances in environmental samples, including N- and P-containing compounds, can be detected simultaneously. The method provides increased information content, greater selectivity and improved sensitivity for all pesticides over conventional GC, and also GC×GC with either of the single detectors. A metric based on bidimensional retention positions combined with the ratio of ECD to NPD response, termed as the detector response ratio, DRR, is proposed to provide a useful basis upon which to confirm peak purity i.e. especially in the absence of interfering peaks in the 2-D space. Since GC×GC has an acknowledged improved separation power, this should make the DRR a more useful measure for identification than an equivalent ratio in single dimension GC. The application of this method to screening analysis of multiclass pesticides in vegetable samples was shown to be effective. We can propose (not tested here) that similar detector response ratios might also be equally useful. For instance, the combination of FID and ECD is not a dual detector arrangement of choice for PCBs analysis due to the different of detector mechanism or relative response magnitude. The ECD may give a large peak for a residue that has little FID response. But otherwise it should be valid to develop a DRR for the FID/ECD arrangement, which also has the ability to provide additional identification power. Thus the FID will respond more to the C-H content, whereas the ECD will respond more to the halogen content. In 2D GC×GC space where PCBs locate in a ‘roof-tile’ type arrangement, the ECD/FID DRR can be tested to determine (i) if there is a correlation between the numbers of chlorine substituent and similarity of the DRR value, and (ii) if there is a structural moderation of the DRR value that is sensitive to the arrangement of chlorines about the PCB molecule.

References

[1] A. Colume, S. Cardenas, M. Gallego, M. Valcarcel, J. Chromatogr. A 882 (2000) 193.

[2] M. Barriada-Pereira, E. Concha-Grana, M.J. Gonzalez-Castro, S. Muniategui-Lorenzo, P. Lopez-Mahia, D. Prada-Rodriguez, E. Fernandez-Fernandez, J. Chromatogr. A 1008 (2003) 115.

[3] L. Cai, J. Xing, L. Dong, C. Wu, J. Chromatogr. A 1015 (2003) 11.

[4] H. Sabik, R. Jeannot, J. Chromatogr. A 818 (1998) 197.

[5] J. Oliva, A. Barba, N. Vela, F. Melendreras, S. Navarro, J. Chromatogr. A 882 (2000) 213.

[6] H. Berrada, G. Font, J.C. Molto, J. Chromatogr. A 1042 (2004) 9.

[7] E. Ballesteros, M.J. Parrado, J. Chromatogr. A 1029 (2004) 267.

[8] K. Patel, R.J. Fussell, R. Macarthur, D.M. Goodall, B.J. Keely, J. Chromatogr. A 1046 (2004) 225.

[9] J. Zrostlikova, S. J. Lehotay, J. Hajslova, J. Sep. Sci. 25 (2002) 527.

[10] K. Patel, R.J. Fussell, M. Hetmanski, D.M. Goodall, B.J. Keely, J. Chromatogr. A 1068 (2005) 289.

[11] A. Garrido Frenich, J.L. Martinez Vidal, A.D. Cruz Sicilia, M.J. Gonzalez Rodriguez, P. Plaza Bolanos, Anal. Chem. Acta. 558 (2006) 42.

[12] J-H. Wang, Y-B. Zhang, X-L. Wang, J. Sep. Sci. 29 (2006) 2330.

[13] V.G. Zuin, J.H. Yariwake, C. Bicchi, J. Chromatogr. A 985 (2003) 159.

[14] B. Aebi, W. Bernhard, Forensic Sci. Int. 102 (1999) 91.

[15] Y. Gaillard, J.-P. Gay-Montchamp, M. Ollagnier, J. Chromatogr., Biomed. Appl. 622 (1993) 197.

[16] Y.-S. Oh-Shin, M. Ko, H.-S. Shin, J. Chromatogr. A 769 (1997) 285.

[17] J.K. Dubey, T. Heberer, H.-J. Stan, J. Chromatogr. A 765 (1997) 31.

[18] C. Bicchi, A.D. Amato, M. Orlandin, J. High Resol. Chromatogr. 17 (1994) 335.

[19] C. Bicchi, A.D. Amato, A. Binello, J. High Resol. Chromatogr. 19 (1996) 80.

[20] E. Jover, A. Gomez-Gutierrez, J.M. Bayona, Chromatographia 66 (2007) 75.

[21] Z. Liu, J.B. Phillips, J. Chromatogr. Sci. 29 (1991) 227.

[22] J. Blomberg, P.J. Schoenmakers, J. Beens, R. Tijssen, J. High Resol. Chromatogr. 20 (1997) 539.

[23] C. Vendeuvre, F. Bertoncini, L. Duval, J-L. Duplan, D. Thiebaut, M-C. Hennion, J. Chromatogr. A 1056 (2004) 155.

[24] M. M. Adahchour, J. J. Beens, R. J. J. Vreuls, A. M. Batenburg, E. A. E. Rosing, U. A. Th. Brinkman, Chromatographia 55 (2002) 361.

[25] M. Adahchour, L.L.P. Van Stee, J. Beens, R.J.J. Vreuls, A.M. Batenburg, U. A. Th. Brinkman, J. Chromatogr. A 1019 (2003) 157.

[26] L. Mondello, A. Casilli, P.Q. Tranchida, G. Dugo, P. Dugo, J. Chromatogr. A 1067 (2005) 235.

[27] C. Cordero, C. Bicchi, D. Joulain, P. Rubiolo, J. Chromatogr. A 1150 (2007) 37.

[28] J. Beens, U.A.T. Brinkman, Anal. Bioanal. Chem. 378 (2004) 1939.

[29] P. Marriott, R. Shellie, Trends Anal. Chem. 21 (2002) 573.

[30] M. Adahchour, J. Beens, R. J. J. Vreuls, U. A. Th. Brinkman, Trends Anal. Chem. 25 (2006) 438.

[31] M. Adahchour, J. Beens, R. J. J. Vreuls, U. A. Th. Brinkman, Trends Anal. Chem. 25 (2006) 540.

[32] L.R. Bordajandi, L. Ramos, M.J. Gonzalez, J. Chromatogr. A 1125 (2006) 220.

[33] P. Korytar, C. Danielsson, P.E.G. Leonards, P. Haglund, J. de Boer, U.A.T. Brinkman, J. Chromatogr. A 1038 (2004) 189.

[34] P. Korytar, L.L.P. van Stee, P.E.G. Leonards, J. de Boer, U.A.T. Brinkman, J. Chromatogr. A 994 (2003) 179.

[35] E.M. Kristenson, P. Korytar, C. Danielsson, M. Kallio, M. Brandt, J. Makela, R.J.J. Vreuls, J. Beens, U.A.T. Brinkman, J. Chromatogr. A 1019 (2003) 65.

[36] D. Ryan, P. Marriott, J. Sep. Sci. 29 (2006) 2375.

[37] D. Ryan, P. Watkins, J. Smith, M. Allen, P. Marriott, J. Sep. Sci. 28 (2005) 1075.

[38] C. von Muhlen, E. C. de Oliveira, P.D. Morrison, C. A. Zini, E. B. Caramao, P.J. Marriott, J. Sep. Sci. (submitted for publication).

[39] N. Ochiai, T. Ieda, K. Sasamoto, A. Fushimi, S. Hasegawa, K. Tanabe, S. Kobayashi, J. Chromatogr. A 1150 (2007) 13.

[40] W. Khummueng, C. Trenerry, G. Rose, P.J. Marriott, J. Chromatogr. A 1131 (2006) 203.

Chapter

7

COMPREHENSIVE TWO-DIMENSIONAL GAS CHROMATOGRAPHY FOR THE ANALYSIS OF POLYCHLORINATED BIPHENYLS IN ENVIRONMENTAL SAMPLES

Abstract

In this chapter, applications of comprehensive two-dimensional gas chromatography (GC×GC) for polychlorinated biphenyls (PCBs) analysis will be presented. A Longitudinal Modulated Cryogenic System (LMCS) was used to modulate and transfer the targeted analytes from ^{1}D to ^{2}D for further separation. Several temperature programs have been optimized to achieve the best separation of the PCBs mixture and soil sample extracts. The results show that peak intensity and peak resolution improvement was observed compared to those obtained in 1D-GC. The separation of PCBs provided by 1D-GC can be significantly enhanced by using GC×GC-μECD. Even in the absence of coupling to mass spectrometric detection (qMS and TOFMS), group-type separation of PCBs mixture was observed by using GC×GC-μECD. This is a useful aspect of the separation arising from GC×GC when the separation and identification of the individual standard is time consuming or the standard mixture do not exist. To demonstrate the potential of the developed GC×GC-μECD method, soil extracts which were suspected to contain high levels of PCBs were analysed as an application. High peak intensity and similar peak pattern as obtained in Aroclors 1260 standard mixture were found in all cases.

7.1 Introduction to Polychlorinated Biphenyl (PCBs)

The polychlorinated biphenyls (PCBs) is a family of organic compounds which contain 1 to 10 chlorine atoms attached to the biphenyl molecule. A general formula and structure of PCBs is presented in **Figure 7.1**. Basically, the number and distribution of chlorine atoms on the biphenyl molecule indicate their toxicity and determine the PCBs nomenclature. There are 209 PCB congeners, and their abiquity causes contamination in every compartment of the environment world-wide. They have been classified as Persistent Organic Pollutants (POPs) by the United Nations Environment Programme (UNEP) under the Stockholm Convention on POPs in 1997 [1]. The 209 PCBs are manmade and there are no natural sources. They normally enter into the environment as a result of human activities. As a consequence of concern of PCBs persistency in the environment, and toxicity effects to human health, most of their uses have been banned since the late 1970s and production ended in the United States in 1997. However, they remain one of chemical classes that pose concern to humans especially as they are considered as carcinogenic in the human, and monitoring of PCBs is an ongoing requirement. Uptake of PCBs into human and/or animal is via contact with the contaminated PCBs such as by eating contaminated food, breathing contaminated air or through contact with contaminated water or soil. Moreover, due to their lipophilicity PCBs can be accumulated in body tissue which contain high levels of lipid and fats, and can remain for a long period of time.

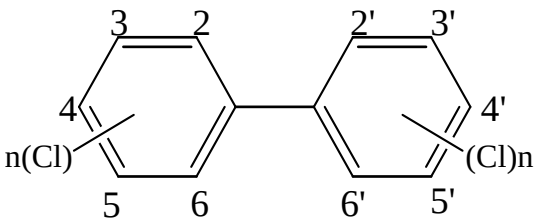

Figure 7.1: General formula and structure of PCBs [2].

Molecular weights of PCBs range from 188.7 for $C_{12}H_9Cl$ to 498.7 for $C_{12}Cl_{10}$. Most of them are colourless, odourless, of low water solubility, but highly soluble in all non-polar solvents, oils and fats, have low vapour pressure, are chemically stable, high heat capacity and low flammability. Due to their high thermodynamic stability, all degradation mechanisms are generally difficult and very slow. However, PCB physical and chemical properties vary widely across the class. Numerous applications of PCBs including; cooling and insulating fluids for industrial transformers, capacitors and stabilizing additives in flexible PVC coatings of electrical wiring electronic components, flame-retardants, inks, adhesives, dyes, paints, plasticizers and fluorescent lighting fixtures, etc.

The commercial production of PCBs comprises various mixtures of components under various trade names such as Aroclor, Auxol, Clorinal, Delor, Pyroclor, etc [2]. However, commercial mixtures called “Aroclor” will be used in this study; Aroclors are named according to a 4 digit code. The first two digits refer to the number of carbon atoms in biphenyls molecule (for PCBs is 12 carbon atoms) the second two digits generally indicate the percentage of chlorine (by weight) in the mixture, thus Aroclor 1242 contain 42% chlorine by weight, for instance. An exception is Aroclor 1016 which also has 12 carbon atoms and 42% of chlorine as in Aroclor 1242. A greater percentage of chlorine in the mixtures is indicative of more toxicity and persistency.

The 209 PCB congeners can be grouped in ten homolog groups based on their number of chlorine atoms on the biphenyl molecule. The PCB homolog subcategories comprise PCBs congeners which have an equal number of chlorine substituents. For instance, hexachlorobiphenyl homolog contains all PCBs congeners which have six chlorine atoms in their molecule although in a different arrangement. **Table 7.1** shows PCB congeners contained in each homolog grouping.

Table 7.1: Number of congeners in each PCB homolog group[2].

PCBs homolog	**Cl substituents**	**Number of PCB congeners**
Monochlorobiphenyl	1	3
Dichlorobiphenyl	2	12
Trichlorobiphenyl	3	24
Tetrachlorobiphenyl	4	42
Pentachlorobiphenyl	5	46
Hexachlorobiphenyl	6	42
Heptachlorobiphenyl	7	24
Octachlorobiphenyl	8	12
Nonachlorobiphenyl	9	3
Decachlorobiphenyl	10	1

In these study two PCB commercial mixtures, Aroclor 1248 and Aroclor 1260 were used to demonstrate the potential of the separation power of the GC×GC technique. **Figure 7.2** shows a correlation of congener number *vs* mass% of congeners contained in Aroclor 1248 and 1260.

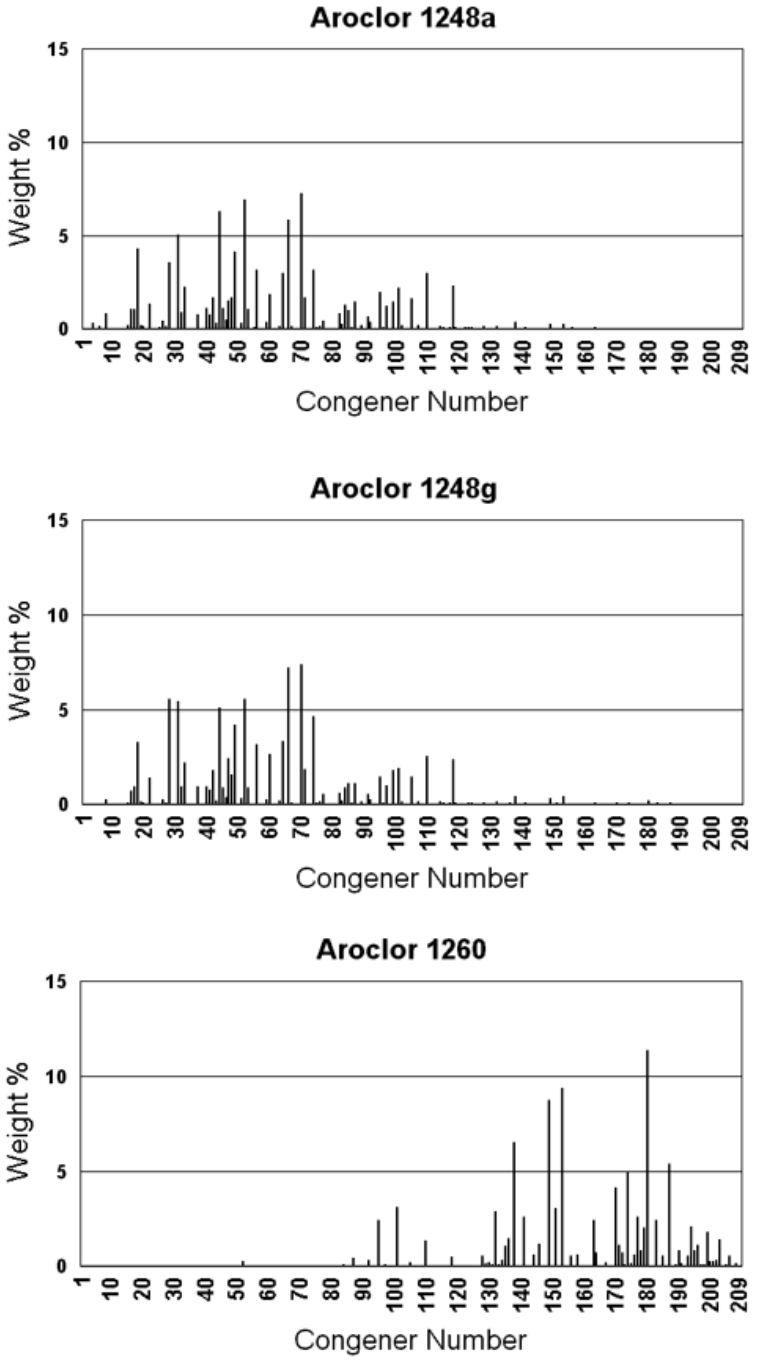

Figure 7.2: Plot of congener number vs relative mass abundance of Aroclor 1248 and 1260 composition [3].

7.2 The analytical methods for the determination of PCBs in environmental samples

Polychlorinated biphenyl (PCBs), polychlorinated dibenzo-p-dioxin (PCDDs), polychlorinated dibenzofurans (PCDFs) and organochlorinated pesticides are included in the list of target compounds in environmental analysis, due to their persistency and toxicity. Analytical approaches for measurement of PCBs have been increasing since they were first found in the environment. Methods to investigate contamination of PCB congeners in food and environmental samples have been reported elsewhere [4-7]. Generally, the analytical methods for PCB determination include an extraction process followed by clean-up steps, and instrumental analysis. Most instrumental analyses as used for PCB congeners in complex samples are centred on chromatographic technique, for instance, gas chromatographic techniques with an element specific detector, especially the electron-capture detector (ECD) followed by mass spectrometric detection (qMS and TOFMS) for the confirmation [8-10], and liquid chromatography coupled with mass spectrometric detection (LC-MS) [11-14]. Gas chromatography with the electron capture detector (GC-ECD) is apparently the most popular method for the analysis of organohalogenated compound in all sample types. However, individual congener separation can not be achieved by using normal GC-ECD due to the possibility of coelution of the other PCB congeners, and the interference of the sample matrix.

Recently, several researchers have attempted to separate and determine PCBs by using the powerful technique of comprehensive two-dimensional gas chromatography (GC×GC). A relevant review of environmental toxicant analysis by using MDGC and GC×GC has been published by Marriott et al. [15]. The GC×GC technique has been applied for the analysis of halogenated complex mixture in a variety of samples. Electron-capture detection is normally coupled with this technique since it can provide sensitivity, selectivity and fast data acquisition rate for PCBs at trace level. The modification from regular ECD to μECD, partially solved peak broadening problems and provides sufficient data points to reconstruct the chromatogram obtained from the ECD detector. GC×GC-μECD not only improves

the separation of PCBs from each other and from the matrix background but can also provide group-type or ordered structure separations. This will be useful for compound classifications in complex samples. Much attention has been devoted to the separation of PCB congeners by using this technique. Up till now, there are number of publications which have been reported in this area, summarised below;

In 2001 Harju et al. [16] reported the analysis of atropisomeric PCBs using a dual oven GC×GC-μECD system with a narrow bore β-cyclodextrin −liquid crystal column set. The results showed that six out of nine atropisomeric PCBs used in this study can be resolved and two can be partially separated from co-eluting congeners in a mixture of 144 congeners. Chiral resolution of the enantiomeric pairs ranged from 0.6 to 2.0. Subsequently, a shape selective column set for the analysis of toxic PCBs using the GC×GC technique was reported by Haglund et al. in the same year [17]. Atropisomeric shape of PCB molecules depend on substitution in the ortho-position. The non-ortho- substituted PCBs more easily adopt a planar configuration than other congeners. According to the rotational energy barriers, the decrease of the energy is in the order of non-ortho- < mono-ortho- < di-ortho- << tri-ortho < tetra-ortho, respectively. In this study, the set-up with the more selective (liquid crystal) column as the first column allows the system to fully exploit the shape selectivity. A number of toxic planar PCBs used in this study, including PCB number 77, 105, 118, 126, 156 and 169, were successfully separated from the other PCB congeners present in technical PCB formulations.

In 2002, Korytar et al. reported [18] high-resolution separation of PCBs using GC×GC-μECD. The 12 toxic non- and mono-ortho CBs were target analytes in this study. A selection of column sets and optimisation of the temperature program were investigated. The results show a complete separation of all 12 priority CBs was achieved with two column sets, HP-1-HT-8 and HP-1-SupelcoWax-10.

In 2003, Harju et al. [19] reported the separation of 209 PCBs using GC×GC-μECD. Five different polar ^{2}D columns connected to DB-XLB as ^{1}D were investigated. The results show that 176 and 181 out of 209 PCB congeners were separated at R_s > 0.5 on the column combination of DB-XLB/SP-2340 (biscyanopropyl siloxane) and DB-XLB/LC-50 (smectic liquid crystal), respectively.

The preferred column combination, with a long first and second column was applied for the monitoring of CBs in grey seal blubber. In addition, the study suggests that lower oven temperature ramp rate, μECD detector, are the preferred combination approach for PCBs and related compounds in complex sample analysis.

In 2004, Focant et al. [20] improved the separation of 209 PCBs using GC×GC-TOFMS. In this work, four column combinations based on thermally stable phases were employed. The results show that HT-8 (50 m x 0.22 mm i.d. x 0.25μm d_f) and BPX50 (2.5 m x 0.10 mm i.d. x 0.10 μm d_f) column set produced the best separation, achieving separation of 192 out of 209 PCB congeners in 146 min (1.3 analytes/min).

Publications reporting PCBs using GC×GC technique are summarised in **Table 7.2**.

Table 7.2: Applications of PCBs and related compounds using GC×GC technique.

Year	Analytes and Sample	Research goals	Detector	Ref.
2002	PAHs and PCBs in sediment	Development of a novel cryogenic modulator for GC×GC analysis	FID and ECD	[21]
2003	Technical toxaphene	To achieve high separation of toxaphene and obtain ordered structure chromatogram	ECD and TOF-MS	[22]
2003	PCBs in grey seals	To optimise the analysis for chiral CBs (atropisomeric and planar PCBs and their enantiomeric fraction) in standard mixtures and grey seal samples	ECD	[23]
2003	Pesticide residues in fruit	To evaluate GC×GC-TOFMS method for trace ($\leq$0.01 $mg.kg^{-1}$) qualification and quantification analysis of pesticide residues in fruit matrices	TOF-MS	[24]
2004	PCDDs, PCDFs and non-ortho-PCBs	Measurement of dioxins and PCBs in various environmental and biological matrices using GC×GC-ID-TOFMS	ID-TOFMS	[25]
2005	19 chirals PCBs in food samples	Analysis chiral PCBs based on β-cyclodextrin capillary columns and to evaluate the potential of MDGC and GC×GC techniques to solve coelution problems when analysing food samples	ECD	[26]
2005	PCBs in sludge	To select an appropriate extraction method and demonstrate the potential of GC×GC for dirty extract analysis	ECD	[27]
2005	Chiral PCBs in food samples	To optimise three chiral column sets for the determination of chiral PCBs in fatty food samples	ECD	[28]
2005	Dioxins and PCBs in foodstuffs	To develop and test GC×GC-IDTOFMS method for the measurement of dioxins and PCBs in foodstuffs, and compare with other methods	IDTOFMS	[29]

Table 7.2 Applications of PCBs and related compounds using GC×GC technique. (Continued)

Year	Analytes and Sample	Research goals	Detector	Ref.
2005	PCDDs, PCDFs and 12 WHO-PCBs	To validate the procedure for quantitative analysis of PCDD/Fs and 12 WHO-PCBs in food samples	ECD	[30]
2007	PCBs and PBDEs	To evaluate MDGC, and GC×GC techniques for the analysis of PBDEs and PCBs in breast milk samples	ECD	[31]
2008	Multiple pesticide residues	To determine multiple pesticide residues in various tea samples by using head-space SPME with GC×GC-TOFMS	TOFMS	[32]
2008	Organohalogenated pollutants	To evaluate a screening method for the separation of eight classes of environmentally toxic POPs	ECD	[33]
2008	Pesticides	To apply GC×GC-TOFMS for qualitative and quantitative determination of pesticide residues and contaminants in animal feed	TOFMS	[34]

7.3 Group-types separation concept for PCBs analysis

Next to useful peak capacity gain, the power of additional separation and peak intensity increase, the group-type or ordered structure separation is another advantage that can be obtained from GC×GC analysis. Group-type separation is a fundamental requirement for correlating the complex compound suite with their physical and chemical properties, and highly organised patterns can be observed in the two dimensional contour plot [35]. The compounds that belong to the same homologous family will be aligned such as to form straight lines according to their boiling point and polarity in the 2D separation space. This is an important aspect of GC×GC, especially for complex sample analysis, due to a rapid preliminary classification and recognition which is possible. This permits fingerprint recognition of the analytes to

be obtained. For example, since the number of compounds in oils is enormous, group-type separation provides a simple and fast way to classify different chemical fraction with in oil. In addition, not only can petrochemical samples form group-type separation utilising GC×GC techniques but natural fats and oils [36] and chlorinated compounds can also produce group-type separation. It is to be expected that as research in GC×GC continues, many further applications will reveal useful structure-retention relationship. Recently, group separation has been reported as a useful approach for PCBs analysis by Korytar et al.[37]. **Figure 7.3** illustrates group- type separation of Aroclor 1260 when the optimum chromatographic condition (**Section 7.5.3**) was applied. A polychlorinated biphenyl mixture was separated in bands based on number of chlorine substituents on their molecule. Each band of the compounds was approximately aligned in a straight line (the solid lines indicate the group separation revealed for the Aroclor 1260 mixture) from the lower boiling point, lower polarity to the higher boiling point, higher polarity (when an “orthogonal” column set was employed). From the figure, each band represents a homologous group of PCB congeners which contain Cl atoms from **n** atom to **n+5** atoms, hence the greater number of Cl substituent groups were generally retained longer in the first dimension. It is important to note that confirmation is needed to identify the individual PCB congeners in each group. However, in this study confirmation using mass spectrometric detection (qMS and TOFMS) was not used. A more appropriate confirmation would be injecting individual congener to identify their unique position in 2D space. **Figure 7.3** shows group-type separation obtained from the separation of Aroclor 1260 using GC×GC-μECD in this study (**see later**).

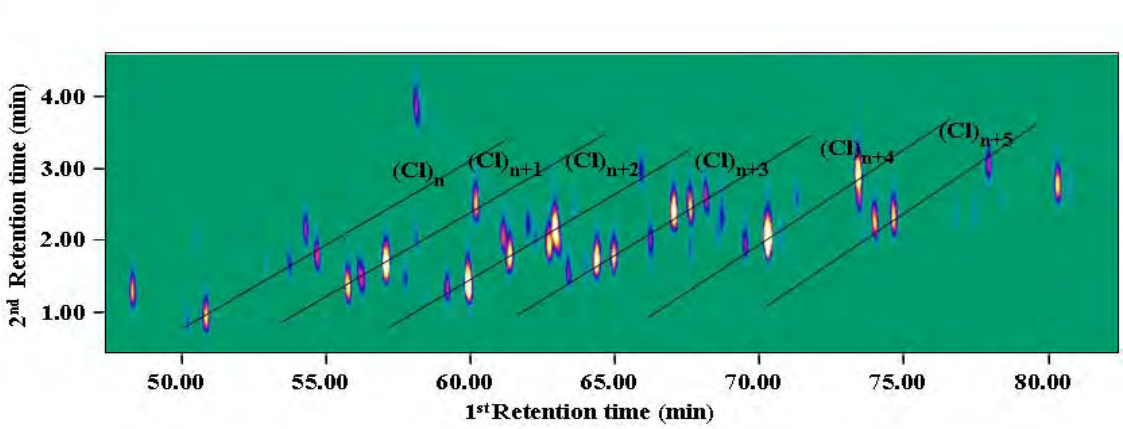

Figure 7.3: Contour plot of PCB congener separation by using GC×GC-µECD. The distribution of group-type PCBs based on their number of chlorine substituents is shown (from the present work; refer to **Section 7.5.3**)

In this chapter, the experiment was divided into two parts. The first part was the separation of Aroclor 1248 by using GC×GC-FID. This experiment and interpretation aimed to illustrate the potential of GC×GC-FID for Aroclor 1248 analysis over conventional GC, since the FID detector does not usually provide good selectivity and sensitivity for PCBs analysis. In the second part, GC×GC coupled with µECD detector was employed for the analysis of PCBs congeners (Aroclor 1260). Several oven temperature programs were tested to achieve the best separation for both individual and group type-separation. Group-type separation was accomplished when the optimum chromatographic condition was performed. To demonstrate the potential of the developed method, the analysis of highly PCB contaminated soil extracts was carried out.

7.4 Experimental; Aroclor 1248 analysis

7.4.1 Gas Chromatographic system

An Agilent 6890 Gas Chromatograph (Agilent Technologies, Palo Alto, CA, USA) was used throughout this study. To conduct GC×GC analysis, the 6890 GC system was retrofitted with a Longitudinally Modulated Cryogenic System (LMCS) from Chromatography Concepts (Doncaster, Australia). HP Chemstation software (Agilent Technologies) was used to instruct the electronic modulator control to commence the modulation at a predefined time.

7.4.2 Column sets

First dimension column (^{1}D) was a30 m x 0.25 mm i.d., 0.25 μm d_f BPX5 phase column (SGE International, Ringwood, Australia). The second dimension column (^{2}D) comprised of a 6 m x 0.1 mm i.d., 0.1 μm d_f of HT-8 (8% phenyl (equiv.) polycarborane-siloxane) coated column (SGE International, Ringwood, Australia).

7.4.3 Standards

The commercial mixture of Polychlorinated Biphenyls (PCBs) standards (Aroclors 1248) was used in this study. The stock solution was diluted with pesticide grade hexane at an appropriate concentration.

7.4.4 Chromatographic conditions

In this study, the injection of GC×GC system was performed in the split mode. The inlet temperature was at 250 °C, split ratio of 50:1 and split flow at 50 mL.min^{-1} were used throughout this study. The GC oven temperature program used in the study was held at 50 ^{o}C for 2.0 min, ramped at 30 ^{o}C.min^{-1} to 210 ^{o}C and then ramped at 1 ^{o}C.min^{-1} to 250 ^{o}C. The total analysis runtime was 47.33 min. The

carrier gas was hydrogen, supplied at a constant flow of 1.00 mL.min^{-1}. LMCS temperature was set at -20 ^{o}C with the modulation period (P_M) at 3 s. The FID detector was operated at 300 ^{o}C, with hydrogen and make up flow (N_2) 30 mL.min^{-1}. The data acquisition rate was at 100 Hz.

7.5 Experimental; Aroclor 1260 analysis

7.5.1 Instrumentation

An Agilent 6890 Gas Chromatograph was used throughout this study. Injection was facilitated by the CombiPAL Focus system (CTC Analytics AG, Zwingen, Switzerland), which was serially connected to an Optic 3 high performance injector (ATAS GL International, Veldhoven, The Netherlands). In order to conduct GC×GC analysis, the Agilent 6890 GC was retrofitted with the LMCS from Chromatography Concepts (Doncaster, Australia). HP Chemstation Software (Agilent Technologies) was used to control the GC instrument and instruct the electronic modulator control to commence the modulation at a predefined time. The CombiPAL Focus system and Optic 3 injector were controlled using Cycle Composure version 1.5.2 and ATAS Evolution Workstation version 1.2 software, respectively.

7.5.2 Column sets

The column set used in this experiment comprised a 30 m x 0.25 mm i.d., 0.5 μm d_f BPX5 phase column (SGE International, Ringwood, Australia) and 1.0 m x 0.15 mm i.d., 0.15 μm d_f BPX50 (50% phenyl siloxane) coated column (SGE International, Ringwood, Australia).

7.5.3 Chromatographic conditions

Injection to the GC×GC system was performed in splitless mode using the Optic 3 injector where the temperature was ramped from 70 ^{o}C to 280 ^{o}C at 10 ^{o}C.s^{-1}, with transfer time of 1 min. The GC oven temperature used in this study was held at 70 ^{o}C for 2.0 min, and then ramped at 5 ^{o}C.min^{-1} to 160 ^{o}C. The second ramp was set at 1.5 ^{o}C.min^{-1} to 250 hold for 15 min, and 20 ^{o}C.min^{-1} to 300 ^{o}C hold for 3 min to clean the column. The modulation process was started at 19.96 min to 90.00 min with the modulation period (P_M) at 5 s. The μECD detector was operated at 330 ^{o}C, with the optimum condition for make-up gas at 100 mL.min^{-1}. All data were collected at an acquisition rate of 50 Hz.

7.5.4 Data analysis

GC×GC data were transformed using an in-house program and visualized as contour plots and/or colour plot using transform software (Fortner, Research, Virginia, USA).

7.5.5 Standards

A polychlorinated biphenyls (PCBs) mixture (Aroclor1260) was used throughout this study as a standard. The stock solution was diluted with pesticide grade hexane at 1.00 mg.L^{-1}. Soils samples extract were provided from co-laboratory, Melbourne , Australia.

7.6 Results and discussion

7.6.1 The separation of Aroclor 1248 using GC×GC-FID

In this study, several GC×GC chromatographic conditions have been optimized for the separation of standard PCBs mixture (Aroclor 1248). The optimum condition used for this analysis was found to be as follows; initial temperature was held at 50 ^{o}C for 2.0 min, followed by ramping at 30 ^{o}C.min^{-1} to 210 ^{o}C, and then ramped at 1 ^{o}C.min^{-1} to 250 ^{o}C. It is important to note that 6.0 m HT-8 Fast PCBs column was employed as a second dimension column in this study, which would cause peak broadening and wrap around for the analysis. However, an excellent separation was achieved, as well as the intensity of the congeners being enhanced compared to those obtained from 1D-GC-FID analysis. **Figure 7.4A** shows the 1D-GC-FID chromatogram of Aroclor 1248. From the figure, regions marked X and Y are presented as co-elution regions of PCB congeners, and these were suspected to contain approximately 3 and 4 peaks, respectively. The intensity of three suspect peaks in area X were measured at about 2, 6 and 4 pA, respectively. Whilst, the biggest peak in area Y measured approximately 2 pA and the small peaks had responses of about 1 pA. **Figure 7.4B** shows the raw GC×GC chromatogram of Aroclor 1248, including the X and Y regions. As can be seen in the figure, peak intensity of the interested peaks (X and Y) was increased. The intensity increased approximately 10 to 20 times and even though FID is not an appropriate detector for the analysis of halogenated compounds, PCBs or chlorinated compounds in this case. It is interesting to contemplate if the added sensitivity might make the FID more useful in GC×GC mode compared to its use for 1D mode.

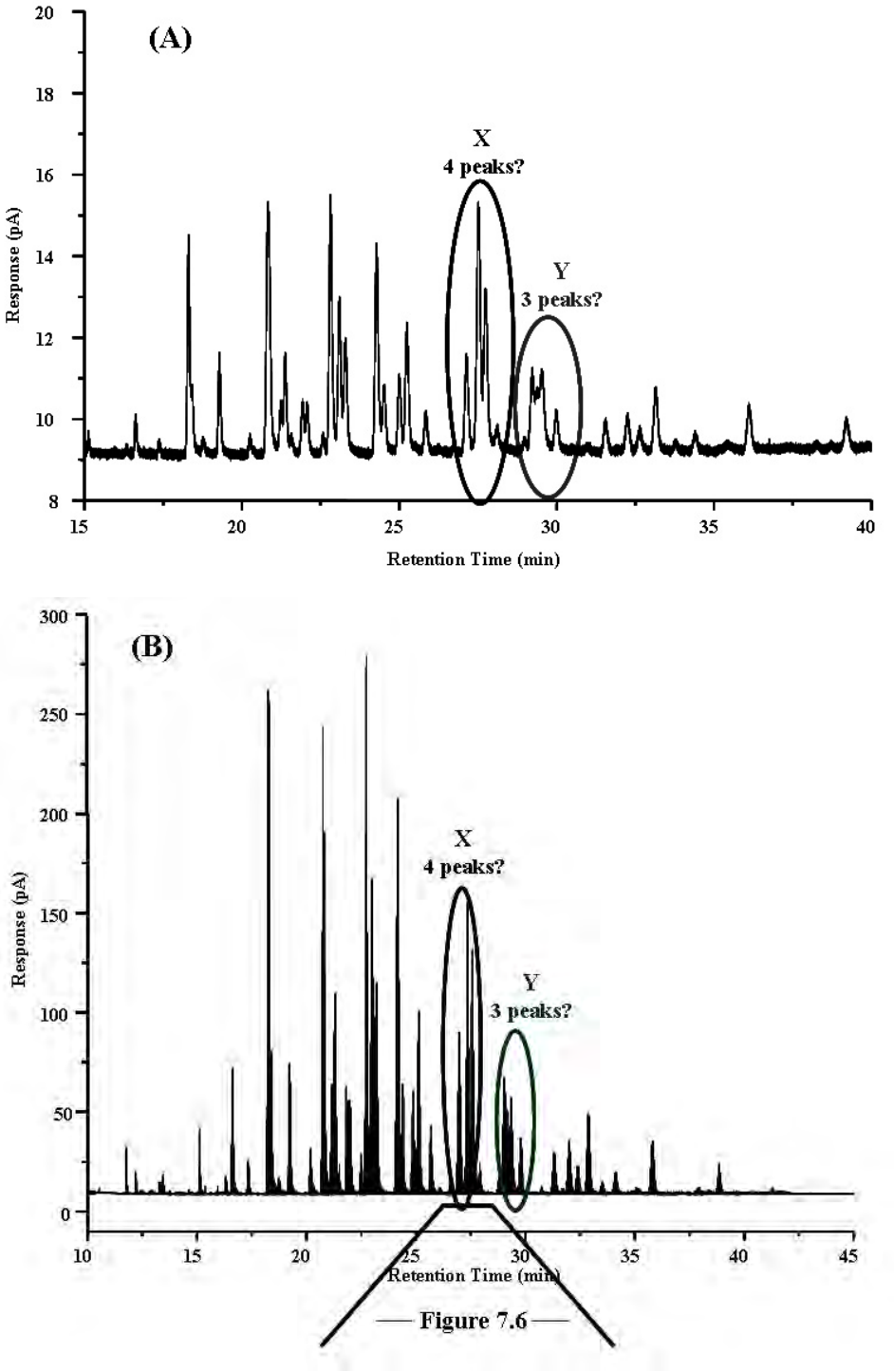

Figure 7.4: Chromatogram of Aroclor 1248. **(A)** 1D-GC-FID chromatogram of Aroclor 1248, **X** and **Y** are marked an as a region to demonstrate the potential of the GC×GC-FID analysis. **(B)** Raw GC×GC chromatogram of Aroclor 1248 with the region **X** and **Y**, when GC×GC-FID was performed. Note that the same solution and injection condition was used for **(A)** and **(B)**.

It is acknowledged that resolution and signal-to-noise ratio enhancement is an advantage of GC×GC over 1D-GC analysis. For Aroclor 1248 analysis using GC×GC-FID in this study, it is important to highlight the separation of congeners in region X. **Figure 7.5** shows the raw GC×GC chromatogram of an expanded region marked X shown in **Figure 7.4B**. As can be seen from the chromatogram, four peaks in X area are now displayed. Obviously, there is a small peak (marked *) completely co-eluted with the biggest one (marked #) in the area. This result can not be observed in 1D-GC due to insufficient efficiency to separate these peaks from each other. The separation of these four peaks is now significantly improved and base-line separation of the congeners was also achieved.

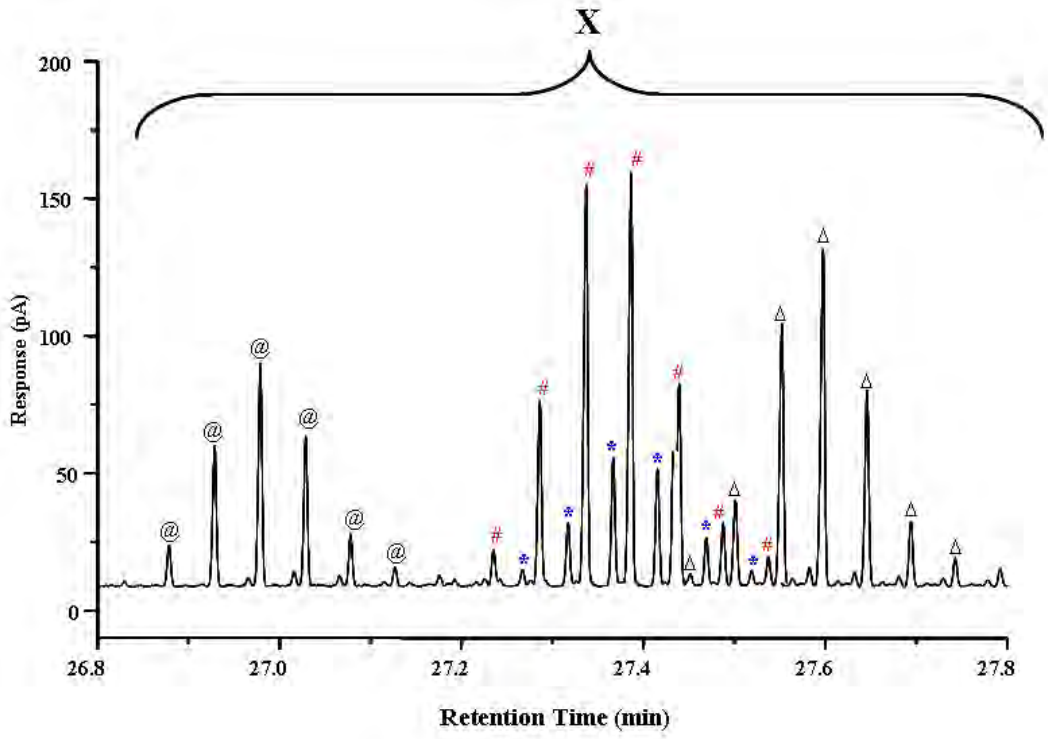

Figure 7.5: Raw 2D-GC chromatogram of expanded region of area **X** in **Figure 7.4**.

The result obtained from GC×GC analysis may be visualised in the "bird's eyes view" pattern or contour plot. **Figure 7.6A** shows the raw GC×GC chromatogram of Aroclor 1248 with each individual peak labelled numerically based on their elution order. This raw chromatogram can be transformed to the contour plot which will be discussed below. A **K** line was sketched straight through the chromatogram to mark the intensity level of peaks for further data manipulation and presentation. All congeners which have intensity higher than the **K** line will be displayed in the contour plot as shown in **Figure 7.6B**. Again in this figure, peaks were labelled with the number that relates to the raw chromatogram. In this contour plot a group of congeners which is marked in red circle are congener in region X. The superior separation is shown, peak numbers **25** and **26** which completely co-eluted in 1D-GC are now separated in the 2D space with $^{2}t_{R}$ about 1.00 and 2.10 s, respectively. The successful separation of Aroclor 1248 by using FID detector and a longer ^{2}D column is now apparent. This advantage of the GC×GC technique will benefit accurate peak assignment and quantification purposes for complex samples analysis.

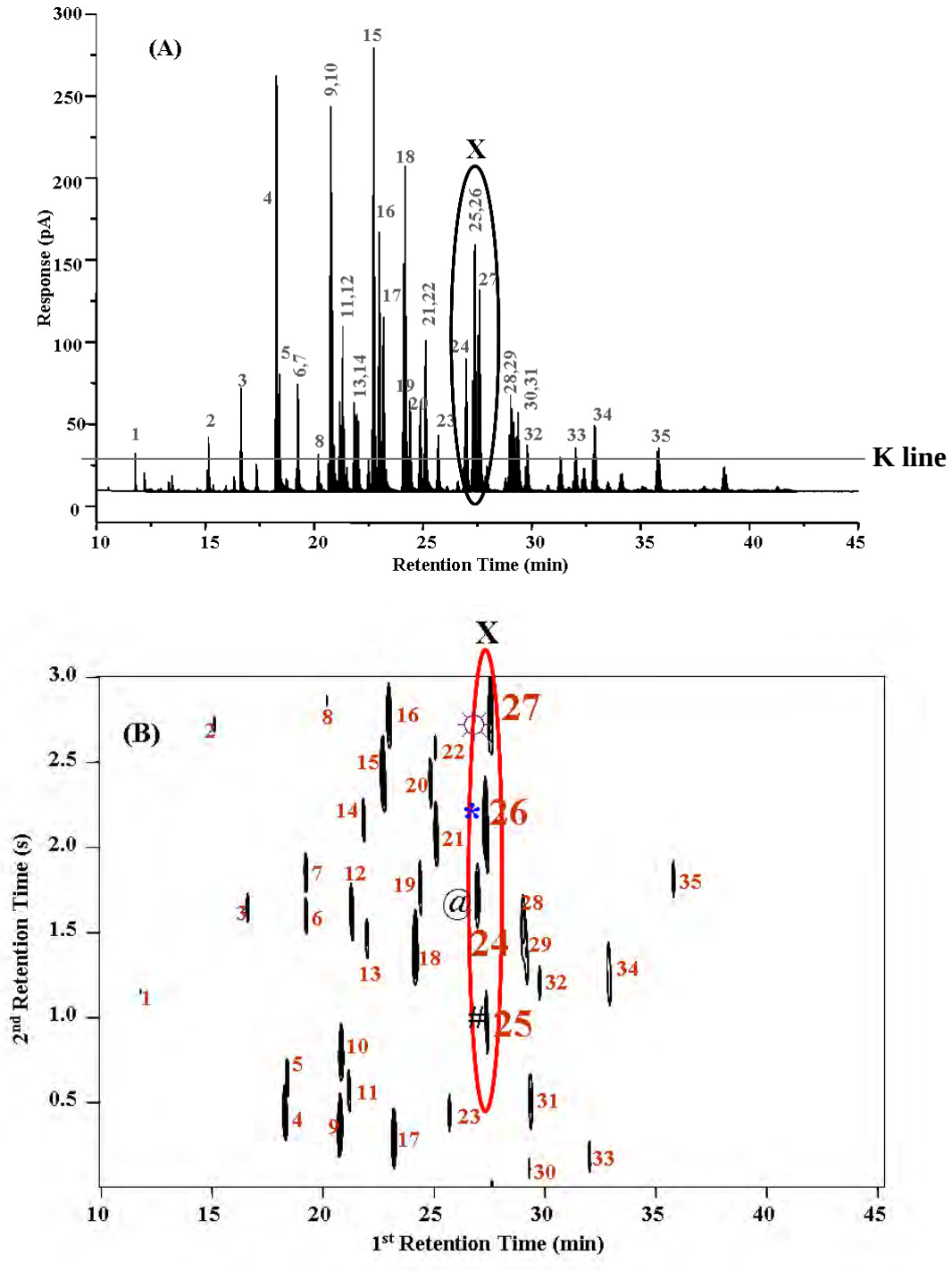

Figure 7.6: (A) Raw 2D-GC chromatogram of the analysis of Aroclor 1248. Each individual congener which has intensity higher than the red line was marked with number based on their elution order. **(B)** Contour plot of the Aroclor 1248, all peaks in this contour plot have intensity higher than the red line in **(A).** This means the lowest contour level here is approximately 30 pA.

7.6.2 The separation of Aroclor 1260 by using GC×GC-μECD

Since, GC×GC can generate narrow chromatographic peaks (typically 50-500 ms at base) the detection system applied has to be fast enough to provide sufficient data points per chromatographic peak to reconstruct the chromatogram properly. Recently, a new generation of ECD detector called micro-ECD (μECD) with a smaller internal volume size of 150 μL (10 times smaller than the previous model) was introduced. The sampling rate up to 50 Hz makes it suitable for GC×GC analysis. Up till now, GC×GC-μECD appears to be a promising approach for PCBs analysis. It has been proven as a technique of choice for the analysis of halogenated compounds in a wide range of samples. Over 30 research works demonstrating the state- of-art for PCBs analysis using this technique have been reported (**Table 7.2)**.

Here, GC×GC-μECD was optimised for the analysis of PCBs in soil samples. The main goal of this study is to achieve the best separation and obtain group separation of PCB congeners in Aroclor 1260 mixture and apply the method for soil analysis. The preliminary temperature program shows that the fast temperature program and ramp rate cause congeners to co-elute. Therefore, the GC×GC-μECD system has been optimised by carefully tuning to a lower oven temperature program and ramp rate. Meanwhile, the modulation period (P_M = 4, 5, 6s) was also optimised to reduce wrap around. **Table 7.3** shows oven temperature programs, detection conditions and P_M used in this study. The best result was obtained when a lower temperature program and a slower ramp rate was used, but not all congeners were resolved. Therefore, **condition #7** in **Table 7.3** was chosen with an acceptable analysis time. Similar results were observed in most cases of temperature programs used, thus only three results are shown in this Chapter. Clearly, group separation of PCB congeners was achieved, when the optimum condition was performed. However, to enhance the identification, a further confirmation using mass spectrometric detection and individual congener injection is strongly recommended.

Table 7. 3: Chromatographic and detection conditions for the separation of PCB 1260 used in this study.

#	**Make up gas flow ($mL.min^{-1}$)**	**P_M (s)**	**Chromatographic conditions**
1	60	4	70 °C hold for 1 min, 30 $°C.min^{-1}$ to 160 °C and 3 $°C.min^{-1}$ to 280 °C hold for 6 min
2*	**80**	**4**	**70 °C hold for 1 min, 30 $°C.min^{-1}$ to 160 °C and 3 $°C.min^{-1}$ to 280 °C hold for 6 min**
3	80	6	70 °C hold for 2 min, 30 $°C.min^{-1}$ to 200 °C and 1.5 $°C.min^{-1}$ to 270 °C hold for 10 min
4	80	5	70 °C hold for 2 min, 30 $°C.min^{-1}$ to 200 °C and 1.5 $°C.min^{-1}$ to 270 °C hold for 10 min
5*	**80**	**5**	**90 °C hold for 2 min, 30 $°C.min^{-1}$ to 200 °C and 1.5 $°C.min^{-1}$ to 250 °C hold for 10 min**
6	100	5	90 °C hold for 2 min, 30 $°C.min^{-1}$ to 200 °C and 1.5 $°C.min^{-1}$ to 250 °C hold for 10 min
7*	**100**	**5**	**70 °C hold for 2 min, 5 $°C.min^{-1}$ to 160 °C and 1.5 $°C.min^{-1}$ to 250 °C hold for 15 min, then ramp up at 20 $°C.min^{-1}$ to 300 °C and hold for 3 min**

***** Chromatographic condition used for examples in this chapter

Figure 7.7 shows a 1D-GC chromatogram and colour plot of Aroclor 1260 when chromatographic condition #2 in **Table 7.3** was employed. Fairly good separation of the individual congeners and homologs were observed. In the figure, congeners in Aroclor 1260 show a hint that they may be separated in a line based on Cl substituents. However, to achieve better separation, a slower temperature program, longer P_M and higher make-up gas flow were considered.

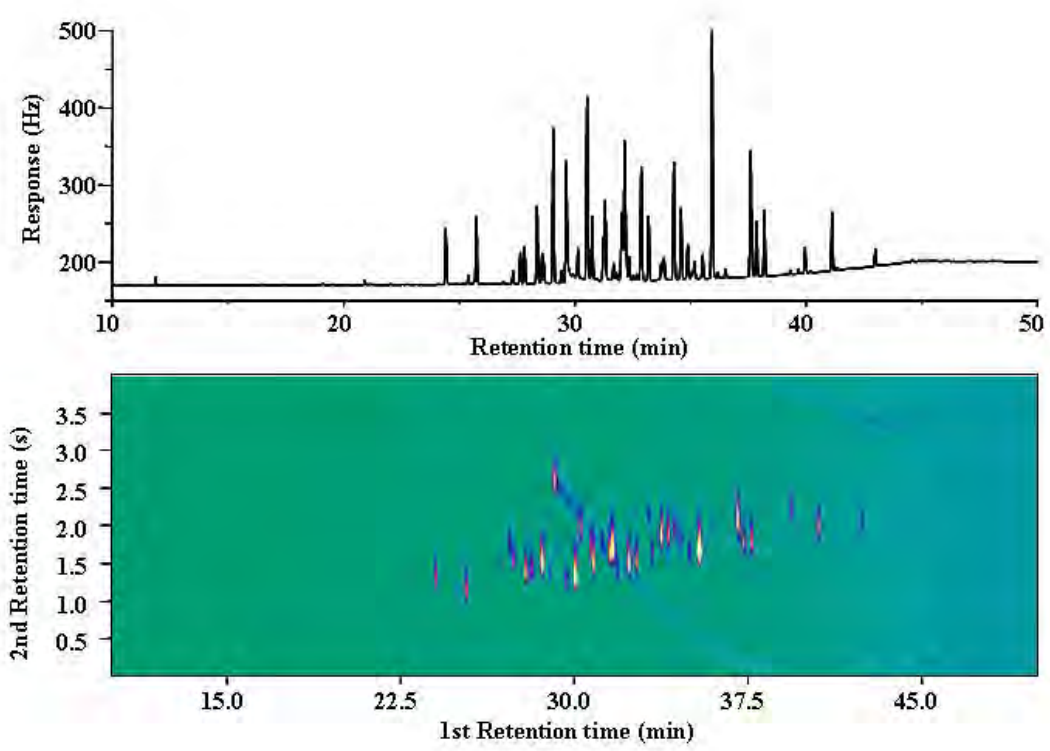

Figure 7.7: 1D-GC chromatogram and colour plot of Aroclor 1260 mixture, when a non-polar-polar column set and chromatographic condition #2 shown in **Table 7.3** was used. In this experiment P_M = 4 s was performed.

Figure 7.8 shows the result obtained from chromatographic condition #5 as shown in **Table 7.3**. In this experiment a lower temperature program and a slower ramp rate were used in order to achieve both separation of the individual congeners and homolog in the mixture. P_M = 5 s was used to minimise wrap around phenomena. The parallel groups of compounds are now separated from each other. However, the steep alignment of the congener's homolog was observed and this might be caused by a higher initial temperature and a faster temperature ramp rate in the first step. Thus, a lower initial temperature and a slower first ramp rate will be taken into account.

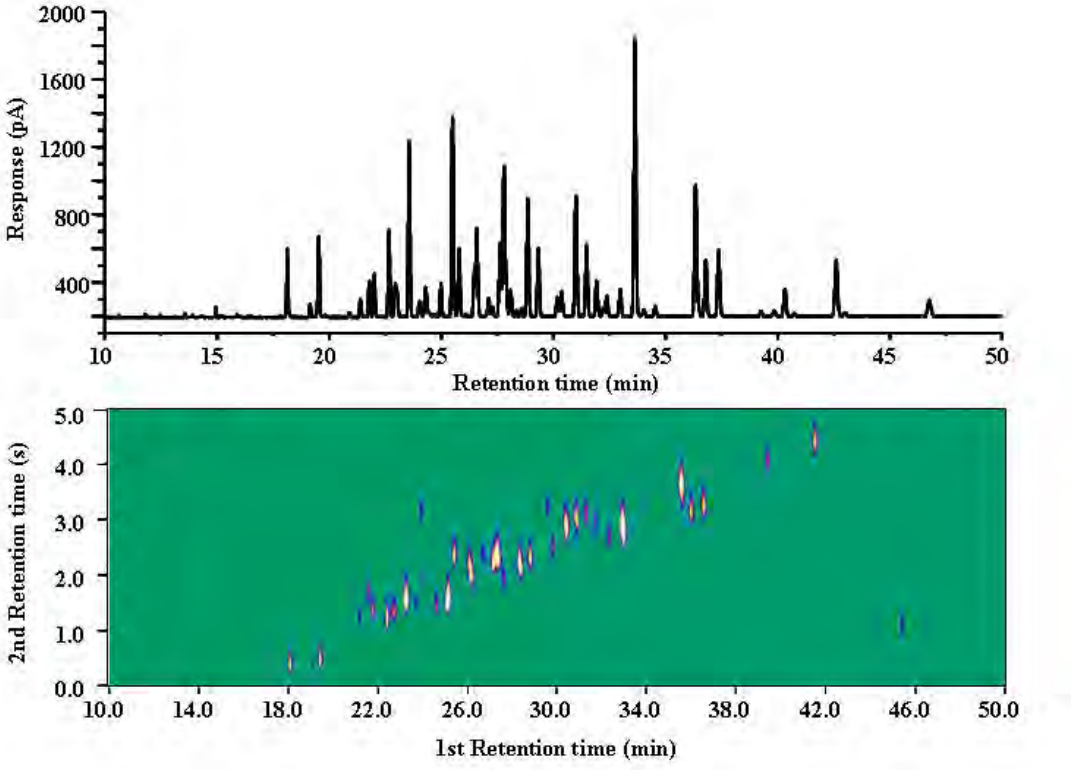

Figure 7. 8: 1D-GC chromatogram and colour plot of Aroclor 1260 mixture, when a non-polar-polar column set and chromatographic condition #5 shown in **Table 7.3** was used. GC×GC with P_M = 5 s was performed.

Figure 7.9 shows the result obtained from condition #7 (**Table 7.3**). This condition was chosen as an optimum condition and used through out the remainder of this study. In this condition the slower first and second temperature ramp rate were utilised in order to obtain the group separation of the congeners contained in Aroclor 1260. P_M = 5 s and higher ECD make up gas flow at 100 $mL.min^{-1}$ were used. The results show that congeners contained in the mixture were separated into groups. A good distribution and separation between individual congeners and homologs were achieved. Congeners with the same numbers of Cl groups were aligned in a line; each line represents a group of congeners which belong to the same homolog. Also in this condition the final temperature was set to 300°C to clean up the column. To demonstrate the potential of the method as a screening method for PCB congeners in environmental samples, soil extracts were investigated as an application (see below).

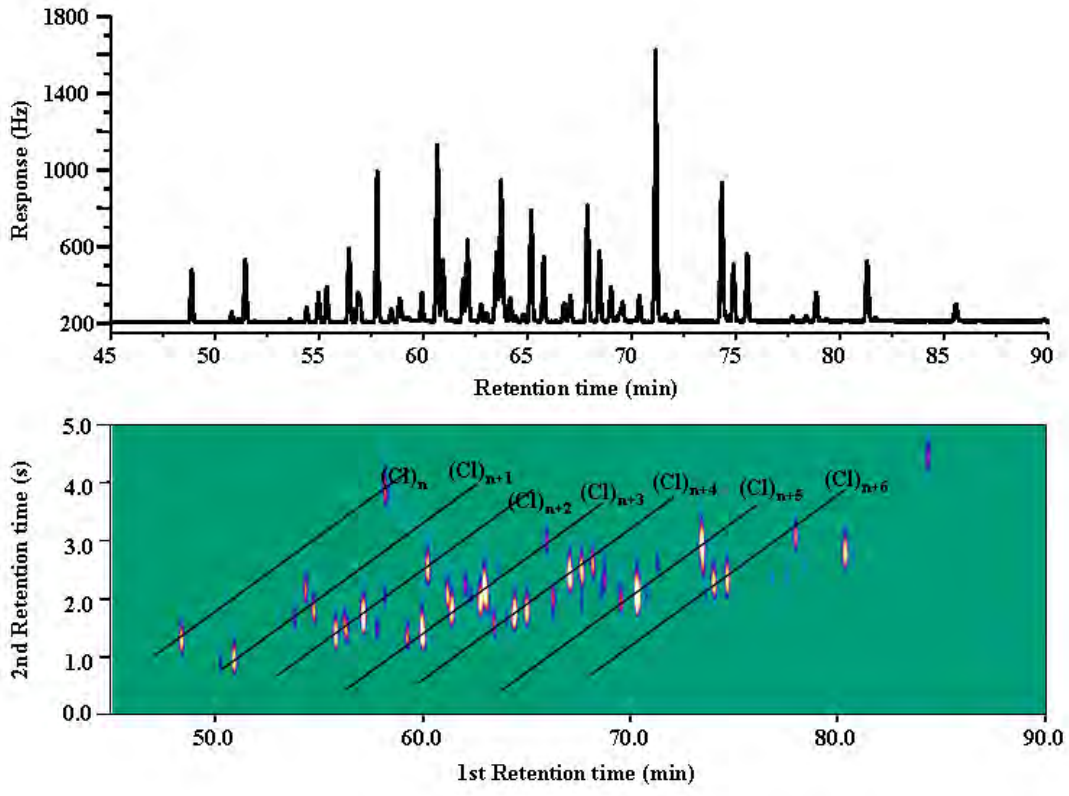

Figure 7.9: 1D-GC chromatogram and colour plot of Aroclor 1260 mixture, when a non-polar-polar column set was used. The optimum chromatographic condition (condition #7) shown in **Table 7.3** and P_M = 5 s were performed.

7.6.3 Application of GC×GC-μECD for the analysis of PCBs congeners in contaminated soil.

It can be see that the PCB congeners contained in Aroclor 1260 are nicely distributed over the 2D space. Thus, the optimum GC×GC condition developed in this study was applied for the analysis of PCBs congeners in suspected contaminated soil samples. The pattern and the group recognition of PCB congeners observed in this study were used for preliminary classification of congener found in soil samples. As expected, group separation of the congeners was achieved. High levels of PCB contamination in soil sample were found in all cases. A similar pattern of chromatogram as in Aroclor 1260 standard mixture was obtained. **Figure 7.10** shows 1D-GC chromatogram and colour plot of two cases of soil samples. The results illustrated that GC×GC-μECD with the low temperature program and ramp rate have sufficient efficiency to separate PCBs congeners into groups.

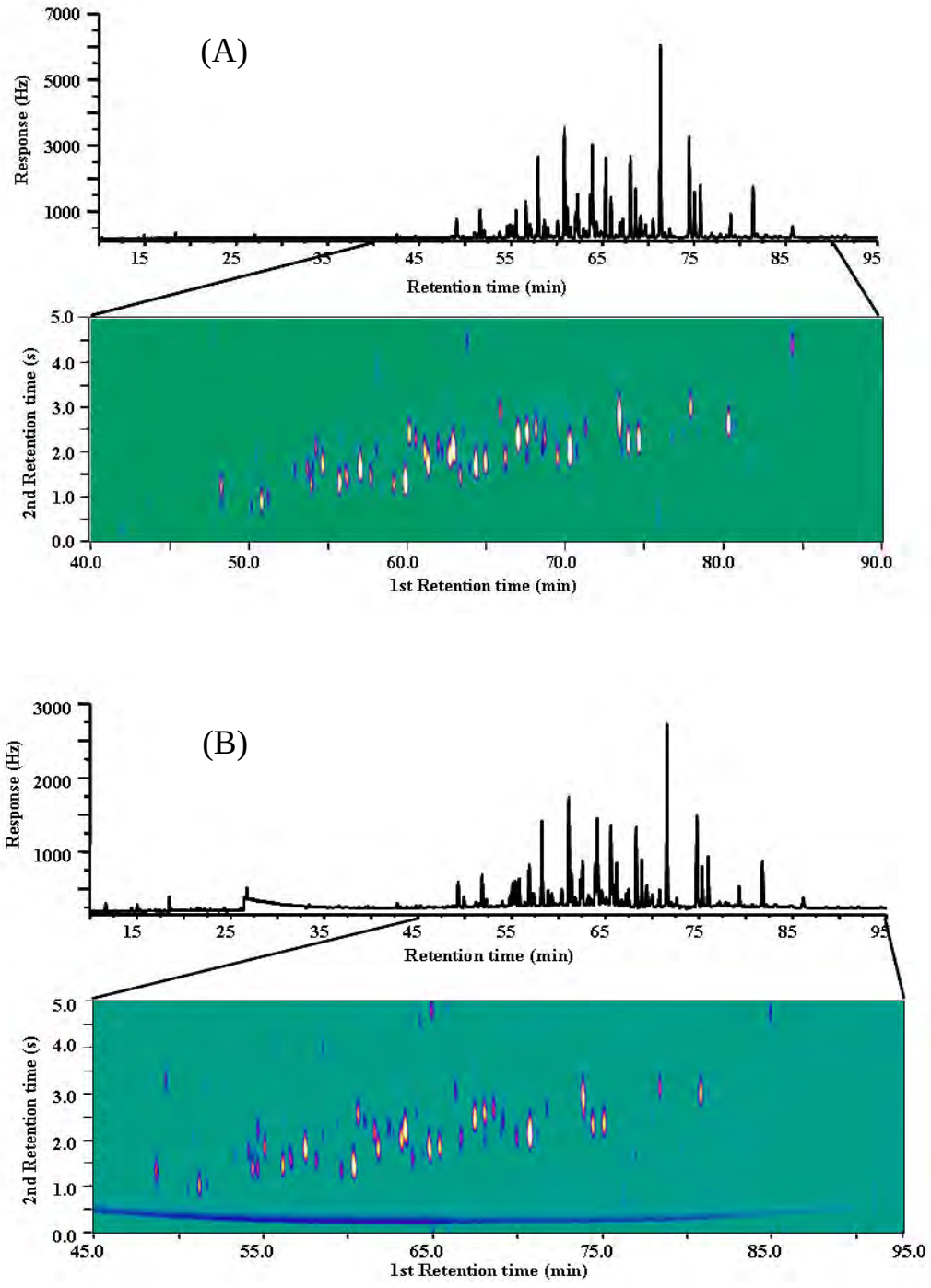

Figure 7.10: 1D-GC chromatogram and contour plot of PCBs congener contaminated in soil samples **(A)** soil extract case**1 (B)** soil extract case**2**.

7.7 Conclusion

In this study, the optimisation of GC×GC-FID and GC×GC-μECD for PCBs analysis was evaluated. A good separation and peak intensity increase was obtained in GC×GC-FID analysis. GC×GC-μECD analysis, once properly optimised, can provide a fast and easy method for the screening of PCB congeners in environmental samples. The method was simplified by using the non-polar-polar column set (orthogonal column set), and properly tuning the oven temperature program and ramp rate. The results show that decreasing temperature program rate generally gives improvement in separation within and between congeners of different Cl number contained in PCBs mixture. Group separation of Aroclor 1260 makes it easy to recognise congeners directly from the 2D space, when the optimum chromatographic condition was performed. This would be another advantage to highlight for halogenated compounds analysis by using GC×GC-μECD. The number of groups separated with high intensity was observed for the analysis of soil samples. However, mass spectrometric detection should be applied for further analysis of PCB mixtures when improved identification and confirmation is required.

References

[1] United Nations Environment Programme (UNEP), (http://www.chem.unep.ch/pops/.).

[2] US Environmental Protection Agency, (http://www.epa.gov/toxteam/pcbid/defs.htm).

[3] Us Environmental Protection Agency, (http://www.epa.gov/pcb/pubs/aroclorplots.pdf).

[4] S.-H. Jeong, J.-H. Cho, J.-M. Park, M.S. Denison, J. Anal. Toxicol. 29 (2005) 156.

[5] S. Centi, E. Silva, S. Laschi, I. Palchetti, M. Mascini, Anal. Chim. Acta 594 (2007) 9.

[6] H. Liu, Q. Zhou, Y. Wang, Q. Zhang, Z. Cai, G. Jiang, Environment Int. 34 (2008) 67.

[7] K. Srogi, Environmental Chemistry Letters 6 (2008) 1.

[8] S.P.J. van Leeuwen, J. de Boer, J. Chromatogr. A 1186 (2008) 161.

[9] P. Haglund, P. Korytar, C. Danielsson, J. Diaz, K. Wiberg, P. Leonards, U.A.T. Brinkman, J. Boer, Anal. Biochem. 390 (2008) 1815.

[10] J.W. Cochran, J. Chromatogr. Sci. 40 (2002) 254.

[11] F. Otto, G. Leupold, H. Parlar, R. Rosemann, M. Bahadir, H. Hopf, Anal. Chem. 70 (1998) 2831.

[12] L. Sun, H.K. Lee, J. Sep. Sci. 25 (2002) 67.

[13] K. Lundgren, B. van Bavel, M. Tysklind, J. Chromatogr. A 962 (2002) 79.

[14] R.J. Letcher, H.X. Li, S.G. Chu, J. Anal. Toxicol. 29 (2005) 209.

[15] P.J. Marriott, P. Haglund, R.C.Y. Ong, Clin. Chim. Acta 328 (2003) 1.

[16] M. Harju, P. Haglund, J. Microcolumn Sep. 13 (2001) 300.

[17] P. Haglund, M. Harju, R. Ong, P.J. Marriott, J. Microcolumn Sep. 13 (2001) 306.

[18] P. Korytar, P.E.G. Leonards, J. de Boer, U.A.T. Brinkman, J. Chromatogr. A 958 (2002) 203.

[19] M. Harju, C. Danielsson, P. Haglund, J. Chromatogr. A 1019 (2003) 111.

[20] J.-F. Focant, A. Sjodin, D.G. Patterson, Jr., J. Chromatogr. A 1040 (2004) 227.

[21] T. Hyoetylaeinen, M. Kallio, K. Hartonen, M. Jussila, S. Palonen, M.-L. Riekkola, Anal. Chem. 74 (2002) 4441.

[22] P. Korytar, L.L.P. van Stee, P.E.G. Leonards, J. de Boer, U.A.T. Brinkman, J. Chromatogr. A 994 (2003) 179.

[23] M. Harju, A. Bergman, M. Olsson, A. Roos, P. Haglund, J. Chromatogr. A 1019 (2003) 127.

[24] J. Zrostlikova, J. Hajslova, T. Cajka, J. Chromatogr. A 1019 (2003) 173.

[25] J.-F. Focant, E.J. Reiner, K. MacPherson, T. Kolic, A. Sjodin, D.G. Patterson, S.L. Reese, F.L. Dorman, J. Cochran, Talanta 63 (2004) 1231.

[26] L.R. Bordajandi, P. Korytar, J. de Boer, M.J. Gonzalez, J. Sep. Sci. 28 (2005) 163.

[27] E.M. Kristenson, H.C. Neidig, R.J.J. Vreuls, Brinkman U. A. T., J. Sep. Sci. 28 (2005) 1121.

[28] L.R. Bordajandi, L. Ramos, M.J. Gonzalez, J. Chromatogr. A 1078 (2005) 128.

[29] J.-F. Focant, G. Eppe, M.-L. Scippo, A.-C. Massart, C. Pirard, G. Maghuin-Rogister, E. De Pauw, J. Chromatogr. A 1086 (2005) 45.

[30] C. Danielsson, K. Wiberg, P. Korytar, S. Bergek, U.A.T. Brinkman, P. Haglund, J. Chromatogr. A 1086 (2005) 61.

[31] B. Gomara, L.R. Bordajandi, M.J. Gonzalez, J. Sep. Sci. 30 (2007) 1920.

[32] J. Schurek, T. Portoles, J. Hajslova, K. Riddellova, F. Hernandez, Anal. Chim. Acta 611 (2008) 163.

[33] L.R. Bordajandi, J.J. Ramos, J. Sanz, M.J. Gonzalez, L. Ramos, J. Chromatogr. A 1186 (2008) 312.

[34] M.K. van der Lee, G. van der Weg, W.A. Traag, H.G.J. Mol, J. Chromatogr. A 1186 (2008) 325.

[35] P.J. Schoenmakers, J.L.M.M. Oomen, J. Blomberg, W. Genuit, G. van Velzen, J. Chromatogr. A 892 (2000) 29.

[36] L. Mondello, A. Casilli, P.Q. Tranchida, P. Dugo, G. Dugo, J. Chromatogr. A 1019 (2003) 187.

[37] P. Korytar, P.E.G. Leonards, J. de Boer, U.A.T. Brinkman, J. Chromatogr. A 1086 (2005) 29.

Chapter

8

THESIS CONCLUSION AND RECOMMENDATION
FOR FUTURE RESEARCH DIRECTIONS

8.1 Thesis Conclusion

Comprehensive two-dimensional gas chromatography (GC×GC) has been acknowledged as a powerful technique for monitoring analytes in complex samples. The technique has been successfully applied for the identification of compounds in wide range of samples. The principles and instrumentations have been developed and well understood. GC×GC system is now commercially available with robust technical implementation and user-friendly feature. The increase of sensitivity, separation power, selectivity and group type separation ability which can be obtained in GC×GC analysis; demonstrated the advantages of GC×GC technique over 1D-GC and MDGC. Additionally, GC×GC also plays an important role in quantitative analysis of target analytes in samples. However, the lack of automatic summation of peak area and peak height of the pulsed peak is shown to be a difficulty when applying GC×GC as a routine technique. Several researchers are now developing programs to manage the large amount of the data generated from the GC×GC system. However, the replacement by GC×GC over conventional GC as a routine analysis method may soon be reality. Sample-to-sample comparison for GC×GC data and appropriate chemometric software will be an important tool for future research.

In this study, the knowledge of fundamentals and applications of GC×GC have been gained. Element selective detectors used for GC×GC system were studied and reviewed, especially NPD and ECD detectors. Detectors for GC×GC must be fast enough to acquire sufficient data points to ensure proper reconstructing of the chromatogram. Therefore, a perfect detector for GC×GC should have a small internal volume, short rise time and high data acquisition rate. GC×GC detector selection is dependent on research aims, and the nature of analytes and sample matrix. It is interesting to add that, attention to coupling mass spectrometric detectors to GC×GC has been a general goal. Much more information content, higher resolution and identification make both TOFMS and qMS powerful detectors for GC×GC system. Information content arises from both the GC domain (better separation) and MS domain (accurate peak identity though library comparison). Therefore, it is very

important to note that an overview of qMS and TOFMS (including accurate mass MS) for the analysis of the samples used in this study should be done in further study.

GC×GC coupled with selective detection has received attention as a powerful technique for toxicants analysis. Numerous applications of the analysis of environmental pollutants such as PCBs, PCDDs, PCDFs, PAHs and their related compounds including pesticide residues have been reported so far. GC×GC coupled with ECD and/or NPD has quickly achieved the status as the most powerful technique in the analysis of organohalogenated compounds and other pollutants in environmental samples. In this study, GC×GC coupled with ECD or NPD detectors in single detection mode were used throughout for the analysis of organohalogenated compounds and N- and P-containing compounds, respectively. GC×GC coupled with both ECD and NPD as a dual detection system show that it is an excellent technique for trace analysis for a wide range of residue analysis.

The modulator used in GC×GC technique is considered an essential part of the technique. Up to the present day, much attention still has been devoted to modulator development. In this thesis, the modulation ratio (M_R) concept was exploited and defined as a ratio of 4 times the first column peak standard deviation (4σ) divided by modulation period (P_M), or 1.6985 times half height width of the peak divided by P_M. The modulation ratio was proposed to simplify the choice of sampling rate during modulation in an effective way. The use of M_R benefits experimental set up and potentially also quantification. Additionally, it can point to parameters which should be considered before a GC×GC experiment is performed. However, M_R is also affected by modulation phase and temperature program. Therefore, a further study of M_R in GC×GC should focus on these effects. M_R for both Gaussian and tailing peaks were studied in this thesis. A quantitative analysis model based on M_R was reported recently. The optimization of M_R for temperature programmed analysis of complex samples might be performed in order to maintain M_R value to the “magic number” of 3 to 4 during the analysis, however, this may be difficult to realize in a practical sense.

Cryogenic loop modulation methods developed in this study are novel, and extend the applicability of the LMCS modulator for modulation processes. Two

geometries of LMCS were proposed and compared to the regular straight-through type which is normally used as the routine operation mode in most laboratories. The incoming effluent from ^{1}D will be separated from later effluent zones, whilst the former is transferred to ^{2}D in the modulation process. Cryogenic loop modulators type 1 and 2 were established and developed with different loop shapes. Loop type 1 produces a broader peak shape compared to the other types, and regular type. The slower modulator movement explains peak broadening in cryogenic loop type 1. However, a new version of LMCS modulator provides a solution to peak broadening in loop type 1 due to fast movement in both up and down directions. Not only GC×GC targeted mode can be performed with the loop system but better results are also obtained in the comprehensive mode, especially for loop type 2. The success of analysis of OCs pesticides standards in this study shows that cryogenic loop modulation would benefit the analysis of toxicants in complex samples.

Comprehensive two-dimensional gas chromatography coupled with a Nitrogen Phosphorus Detector (NPD) was applied as a tool for the analysis of trace nitrogen containing fungicides in vegetable samples. The NPD detector is one of the most useful selective detectors for the analysis of nitrogen-containing compounds. In this study the modified NPD detector with an extended jet and a standard collector was used for improved peak intensity and peak shape. This is an example of the flexibility and optimization of detectors used for GC×GC, showing that better results can be obtained when a modified NPD was employed. GC×GC-NPD demonstrated the superior separation of nine fungicides of interest from each other, and from sample matrix. Additionally, quantitative aspects such as linearity, repeatability, reproducibility and limit of detection of GC×GC-NPD technique were validated in this study. The study illustrated that GC×GC coupled with NPD is advancement for detector technology development for the GC×GC technique.

Dual detection employing NPD and ECD was also developed in this study. GC×GC-NPD/ECD has a potential for analysis of a wide range of pesticide residues in vegetable samples. Two chromatographic results can be obtained from the dual system within one analysis run. Cleary, this method is appropriate as a screening method in residue analysis. It is interesting to add that the Detection Response Ratio

(DRR) of the signal obtained from NPD and ECD detectors show benefits for compound identity. The DRR of compounds from NPD and ECD is unique and is specific to chemical properties of compounds which will be useful for compound identification. The study shows that GC×GC coupled with two selective detectors (NPD and ECD) for pesticides analysis, and exploiting the DRR concept, provides additional compound identity or characteristics depending on the number of halogenated atoms and N- or P-groups contained in their molecule. This may make compound identification using mass spectrometry detection not necessary in some cases. This demonstrated various advantages of GC×GC-dual detection over 1D-GC and GC×GC with single detection.

Group type separation is an intriguing phenomenon, and useful for very complex analysis when individual structured separations can not be identified or in cases where standards of an analyte of interest does not exist. Compounds in the sample matrix can be classified according to a structure/retention relation. Compounds in the same homologous series will be aligned in the contour plot obtained from GC×GC analysis, where the class of compounds can be ideally recognized. Petroleum is a most complex sample that benefits from the GC×GC technique. However, not only petroleum samples reveal group type separation, but fatty acids and polychlorinated biphenyls (PCBs) also exhibit this behavior.

In this study, Aroclor 1248 and 1260 were analysed using GC×GC-FID and GC×GC-ECD, respectively. Even though, FID is not an appropriate detector for PCBs analysis (at least for 1D-GC) the significant signal-to-noise ratio increase obtained from GC×GC-FID analysis is better compared to 1D-GC-FID analysis. On the other hand, group type separation of Aroclor 1260 with high signal response was achieved when GC×GC-ECD was utilized. The developed method was applied to the analysis of suspected PCBs contaminated soil samples and similar peak patterns as obtained in Aroclor 1260 was observed. The successful optimization for this separation shows that GC×GC-ECD is the technique of choice for this type of analysis. However, the coupling of mass spectrometric detection (qMS and TOFMS) with GC×GC should be of concern. The high scanning speed of TOFMS is satisfactory for the narrow peaks that emerge from the GC×GC system. It has been established as the most powerful

technique for the separation of complex samples. The rapidly increasing numbers of successful applications of GC×GC-TOFMS reported to date, confirm the effectiveness of the technique. Obviously, GC×GC-TOFMS will be a further important technology due to access to supporting MS identification data. This technique offers an attractive alternative for performing trace analysis for chromatographers, and it will undoubtedly be expanded even more in the following years.

8.2 Recommended future research directions

From this research work, recommended future research directions can be suggested as outlined below;

1. Recently, a number of specific detectors such as ECD, NPD, NCD, SCD and AED have been used as detectors in GC×GC systems. High selectivity, sensitivity and relatively fast data acquisition rates (at least 50 Hz) are major aspects of all these detectors. GC×GC coupled with specific detectors have individual characteristics for particular analyses. For instance, GC×GC-ECD is the technique of choice for halogenated compounds. GC×GC-NPD is very useful technique for the analysis of N- and P- containing compounds, etc. In this research work, the NPD detector from the manufacturer was modified and used as a detector for GC×GC in the analysis of N-containing fungicides in vegetable samples. Improved sensitivity, selectivity, separation power and less tailing effects were achieved. Due to GC×GC-NPD being a relatively new technique, thus, it would be beneficial for the analysis of N- and P-containing compounds (e.g. amino acids, organic amines, drugs and N-PAHs) in a wide range of samples such as petrochemical, foods and biological samples and these areas need to be tested.

Additionally, the analysis of component of petroleum, petrochemicals, pharmaceuticals, and food safety industries is now focused on the determination of S- or P- containing compounds. The Flame Photometric Detector (FPD) is a suitable detector of the determination of S- or P-containing compounds especially in trace level analysis. FPD coupled to GC×GC system would greatly benefit both petroleum and environmental analysis. However, FPD has not yet been coupled to GC×GC

systems; thus, its data acquisition rate, applications, and optimization need to be evaluated.

2. Modulation Ratio (M_R) is the new terminology that has been defined in the present work and now the concept has been extended and used in further GC×GC research. For example, Seeley and co-workers [1] used the M_R concept for the determination of the correct choice of P_M to minimize the inconsistent transfer of the fraction of the peaks from the first column to the second column in the "Microfluidic Dean's Switch" modulator. Amador-Munoz and Marriott [2], reported a model of quantitative analysis based on the M_R concept using GC×GC. The model uses either the 2 or 3 major modulated peaks of compounds for quantitative analysis. The developed model was applied for the analysis of PAH using deuterated PAH internal standards. The approach offers a simplified and relative robust quantitative analysis method for GC×GC. Clearly, the M_R concept was proposed to be relevant for setting the P_M value used in GC×GC analysis and for simplified quantitative GC×GC analysis. The next step in the M_R study can be focussed on the optimisation of M_R value during the analysis. This would benefit quantitative features of GC×GC and minimise wrap around phenomena during the analysis (i.e. variable P_M during analysis to achieve best value of M_R)

3. Nowadays, qMS and TOFMS are the most important detectors for GC×GC analysis. The need for identification of the compounds in complex samples such as petroleum samples is fulfilled by the high accuracy identification afforded by TOFMS. The analysis of POPs, PCBs, pesticides and all toxicants in environmental samples should now employ GC×GC-TOFMS as a determination technique. The advantages of this approach such as high accuracy, high speed, and highly precise mass spectral matching, make TOFMS important for further investigation in this research work. Although the usefulness of MS identification is understood, it needs to be stated that if peaks are fully resolved then the role of MS is not as critical as in 1D-GC where overlapping peaks often require mass spectral deconvolution. The one technology that needs further evaluating, however, is accurate mass MS, and this should be tested for pesticides in the future.

4. The concept of DRR should be further developed to test its utility for improved identification when combined with $^{1}t_R$ and $^{2}t_R$ peak position. The information power provided by such approaches can then be contrasted with MS detection. A wider range of standards needs to be tested, a more informed correlation of structure with DRR for this expanded set of compounds, and understanding of how much variation can be tolerated in the DRR value in order to still give good identification. It can be speculated that DRR may also be useful for e.g. ECD/FID, and this needs to be tested for compounds in pesticide analysis.

References

[1] J.V. Seeley, N.J. Micyus, S.V. Bandurski, S.K. Seeley, J.D. McCurry, Anal. Chem. 79 (2007) 1840.

[2] O. Amador-Munoz, P.J. Marriott, J. Chromatogr. A 1184 (2008) 323.